ÉCOLE POLYTECHNIQUE DE BRUXELLES
UNIVERSITÉ LIBRE DE BRUXELLES

Ultra-fast Line Protection Relay Algorithm Based on a Gamma Model of Line

Thesis submitted by Neriton HOXHA
in fulfilment of the requirements of the PhD Degree in Engineering and Technology ("Docteur en Sciences de l'Ingénieur et Technologie")
Academic year 2019-2020

Supervisor: Professor Pierre HENNEAUX

Co-supervisor: Professor Jean-Claude MAUN

Department of Bio, Electro and Mechanical Systems

Thesis jury:

Michel KINNAERT (Université libre de Bruxelles, Chair)
Benjamin GENET (Université libre de Bruxelles / Elia, Secretary)
Pierre HENNEAUX (Université libre de Bruxelles, Promoter)
Marc PETIT (CentraleSupélec)
Willem LETERME (KULeuven)
Cezary DZIENIS (Siemens AG)

SIEMENS

Abstract

The relay protections of the transmission lines play a fundamental role in the electrical power systems. They permit to ensure the security and the reliability of the electricity transmission from the generators to the final consumers. The objective of a relay protection is to provide a corrective action as quickly as possible when an abnormal condition of the power system is detected. The quickness of the response permits to limit the stress on the equipments of the power system and the consumers, to ensure the security of the people, to improve the power quality and to maintain the stability of the power system.

The protective relaying systems have evolved a lot since their first implementation in the 1900's. However, the electrical power systems are in constant evolution and the reliability of the protective relaying systems becomes more and more challenging. The three main characteristics of the relay protections which are security, dependability and speed must be continuously improved to achieve these objectives. The major relay protections implemented nowadays are based on frequency-domain methods. These methods are intrinsically limited in speed by the phasor estimation of the voltage and current signals. More recent methods based on incremental quantities permitted to break this limitation by working directly in time-domain. Despite the speed of these methods, the dependability is usually limited in order to ensure the security.

In this work, it is proposed to develop a time-domain ultra-fast non-pilot distance protection based on a Γ model of line to improve the security, the dependability and the speed, even for long lines and weak power systems. This protection is composed of a loop selection element, a directional element and a distance element. The target tripping time is 4 ms or less.

Acknowledgements

I was working as a consultant in engineering during four years when I decided to give a new direction to my career. I contacted my former professor in electro-technical field, Prof. Jean-Claude Maun, who was also the chief of the Energy department. This work is specially dedicated to Prof. Jean-Claude Maun who passed away a few months before the end of my PhD thesis. Prof. Jean-Claude Maun gave me the chance to work as researcher in the Université libre de Bruxelles. I had the great opportunity to benefit from his great experience in the field of relaying systems. He gave me a lot of helpful suggestions and solutions. We had the opportunity to exchange a lot during our frequent travels for meetings at Berlin. He followed my work very closely during four years, even after the beginning of his retirement, and until a few days before his passing. I would like to extent all my gratitude to Prof. Jean-Claude Maun and to extend sincere condolences to his family.

I would also like to thank Prof. Pierre Henneaux who had the difficult task to take the role of the supervisor in a very short time. During the last months of this work, Prof. Henneaux reviewed my entire thesis and suggested me a lot of possible improvements that permitted me to finish my thesis under proper conditions.

This work was a collaboration between the BEAMS department of ULB and the development department of Siemens AG. During four years we had several meetings where very interesting discussions took place. I would like to thank all the members of the Siemens team involved in this project and more particularly M. Matthias Kereit who was in charge of the coordination between the ULB and Siemens.

I would also like to thank all the people who gave me the courage and the motivation all along this very good experience. All my gratitude to my family, my friends and my colleagues.

Contents

List of Figures

Nomenclature

Abbreviations

ADC	Analog to Digital Converter
ALF	Accuracy Limit Factor
ARV	Average Rectified Values
BLUE	Best Linear Unbiased Estimators
CCVT	Coupling Capacitive Voltage Transformer
CFCT	Critical Fault Clearing Time
CI	Confidence Interval
CIC	Cascaded Integrator Comb
CT	Current Transformer
DERs	Distributed Energy Resources
EMTP	Electro-Magnetic Transients Program
FCT	Fault Clearing Time
FIR	Finite Impulse Response
HC	Heteroscedasticity-Consistent
IIR	Infinite Impulse Response
KCL	Kirchoff's Current Laws
KVL	Kirchoff's Voltage Laws
MSE	Mean Squared Error
NMSE	Normalized Mean Squared Error

OLS	Ordinary Least-Squares
RLS	Recursive Least-Squares
RSS	Residual Sum of Squares
SCD	Standard Class Designation
SIR	Source Impedance Ratio
SVD	Singular Value Decomposition
ULM	Universal Line Model
VT	Voltage Transformer

Symbols

α	Attenuation constant of a transmission line
β	Phase constant of a transmission line
ΔI	Incremental current
ΔI_Z	Incremental replica current
ΔV	Incremental voltage
δ	Delta factor for the initialisation of an RLS method
γ	Propagation constant of a transmission line
λ	Forgetting factor of an RLS method
τ_K	Corrective time constant of the transformers
c_l'	$0.5 \cdot c_l$
c_l^*	Adapted capacitance: $0.4 \cdot c_l$
c_l	Capacitance per length of the line
c_+	Positive or direct sequence capacitance per length of the line
c_-	Negative or reverse sequence capacitance per length of the line
c_0	Zero sequence capacitance per length of the line
c_α	Alpha sequence capacitance per length of the line

c_β	Beta sequence capacitance per length of the line
d_{thres}	Distance threshold for inductance convergence testing
e_{rel}	Relative error of the identified distance to fault (%)
e_{tot}	Error of the identified distance to fault compared to the total line length (%)
F_S	Sampling rate of the simulation tool
f_{algo}	Sampling rate of the ultra-fast distance protection algorithms
g_l	Conductance per length of the line
I_0	Zero sequence current of the Clarke symmetrical components system
I_α	Alpha sequence current of the Clarke symmetrical components system
I_β	Beta sequence current of the Clarke symmetrical components system
I_p	Pre-fault current
k_{CLM}	Mutual capacitance-inductance compensation factor for a phase-to-ground fault
k_{CL}	Capacitance-Inductance compensation factor for a phase-to-ground fault
k_{CRM}	Mutual capacitance-resistance compensation factor for a phase-to-ground fault
k_{CR}	Capacitance-Resistance compensation factor for a phase-to-ground fault
k_{LM}	Mutual inductance compensation factor for a phase-to-ground fault
k_L	Inductance compensation factor for a phase-to-ground fault
k_{RM}	Mutual resistance compensation factor for a phase-to-ground fault
k_R	Resistance compensation factor for a phase-to-ground fault
l_l	Inductance per length of the line
l_+	Positive or direct sequence inductance per length of the line
l_-	Negative or reverse sequence inductance per length of the line
l_0	Zero sequence inductance per length of the line
l_α	Alpha sequence inductance per length of the line

l_β	Beta sequence inductance per length of the line
l_{m0}	Zero sequence mutual inductance per length of the line
$m_{secured}$	Secured distance to fault
$m_{setting}$	Protected zone 1 by the fast distance algorithm
N_S	Number of successive samples for inductance convergence testing
R_f	Fault resistance
r_l	Resistance per length of the line
r_+	Positive or direct sequence resistance per length of the line
r_-	Negative or reverse sequence resistance per length of the line
r_0	Zero sequence resistance per length of the line
r_α	Alpha sequence resistance per length of the line
r_β	Beta sequence resistance per length of the line
r_{m0}	Zero sequence mutual resistance per length of the line
$R_{setting}$	Resistance of the transmission line at the end of the protected zone
R_{thres}	Maximum fault resistance
SF_{CI}	Security factor for the confidence interval
v	Wave velocity of a transmission line
V_0	Zero sequence voltage of the Clarke symmetrical components system
V_α	Alpha sequence voltage of the Clarke symmetrical components system
V_β	Beta sequence voltage of the Clarke symmetrical components system
V_p	Pre-fault voltage
W_{min}	Minimum window length of the fast distance element algorithm
Z_0	Characteristic impedance of a lossless transmission line
Z_C	Characteristic impedance of a transmission line
m	Distance to fault (km)

Chapter 1

Introduction

1.1 Context and motivation

The evolution of the electrical power systems has pushed the transmission lines to operate close to their operating limits. This evolution was motivated by different factors like the increase of the global demand [1], the liberalization of the electricity market, the cost considerations and the environmental impact. One of the main characteristics of Smart Grids is the high level of penetration of Distributed Energy Resources (DERs) [2]. It introduces new challenges because the DERs may be of different sizes and types, and may be connected at all different levels of the electric power system – transmission, distribution and low voltage. The presence of the DERs may impact the stability of an electrical power system [3] but also directly the distance protection settings (i.e., it impacts the Source Impedance Ratio (SIR)[1]) [4].

These evolutions impact the reliability of the protective relaying systems which becomes more and more challenging. The power quality, the power stability, the security aspects and the stress level on the power equipments may become unsuitable if the protection of the transmission lines is not adapted to take into account the recent implementations in the power systems. Indeed, the transmission line is a fundamental part of the electric power system which must supply the electricity to the consumers with a high level of reliability. Any perturbation in the electrical power system may have an important impact on the stability of the network. The protective relay must response to an abnormal condition on the power system as quickly as possible in order to limit the stress on the equipments of the power system and the consumers, to ensure the security of the people and to maintain the stability of the power system.

One of the solutions to decrease the different impacts mentioned above is the reduction of the Fault Clearing Time (FCT), defined as the time interval between the fault inception

[1] the SIR of a line is defined as the ratio of the impedance of the source to the impedance of the line. The impedance of the source is the equivalent impedance of all the elements behind the line (voltage source, transformers, transmission lines, etc.)

and the fault clearance [5]. A short-circuit current creates thermal and mechanical effects on the conductors and the equipments of the power system [6]. A FCT reduction would permit to reduce the stress on the different components and thereby to increase their lifespan. The power quality and the power stability are two important criteria for an electrical power system. They impact both the power system itself and the final users. The power quality includes several aspects like the current, the voltage and the frequency characteristics against a set of reference technical parameters [7]. As explained in [8] one of the major problem related to a poor power quality is the voltage sag. During a short-circuit the voltage decreases and it may impact dramatically some devices. It may lead to the shut-down of equipments or process that are very sensitive to the voltage variation. The power quality can be improved by decreasing the FCT. The stability of a system is its ability to return to its normal or stable condition after being perturbed [9]. For an electrical power system it is related to its ability to maintain the synchronism of the generators. The power stability is characterized by a transfer power function as illustrated by Fig. 1.1 where the maximum transmittable active power in a transmission line is defined by a maximum power angle δ_{cri} beyond which the synchronism may be lost. The maximum time during which a disturbance can be applied without the system losing its stability is defined as the Critical Fault Clearing Time (CFCT) [10]. The power stability may be improved by reducing the power transfer of the system or by constructing a new transmission line. The first solution will limit the load that can be connected to the power system while the second will increase the total cost. Alternative solutions to improve the power stability are the re-dispatching or the reduction of the FCT to ensure that this last is lower than the CFCT. The FCT is composed essentially by the operating time of the relay to detect the fault (algorithm time) and the time for the breakers to interrupt the current. The scope of a line protection relay algorithm is related to the first part of the FCT.

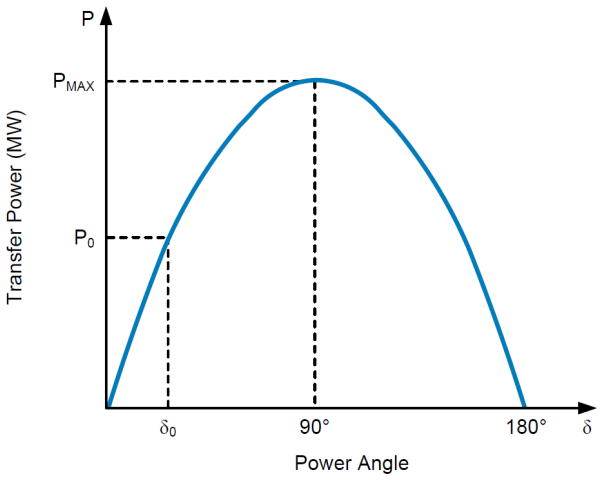

Figure 1.1: Power system transfer capability [8]

The reduction of the FCT must be achieved while respecting the reliability of the process. In the field of relaying the reliability implies dependability and security. The dependability is the measure of the certainty that the relays will operate correctly for all the faults for which they are designed to operate and the security is the measure of the certainty that the relays will not operate incorrectly for any fault [11]. The first protective relaying systems were developed in the early years of 1900. For more than 100 years this area has undergone many changes in relays principles as well as in their technologies. The first relays began as electromechanical devices. The development of semiconductors led to the solid-state relays[2] in the 1940's [12]. Finally, the recent protections are implemented on microprocessors since the 1980's [12]. Fig. 1.2 shows the evolution of the use of the different generations of relay.

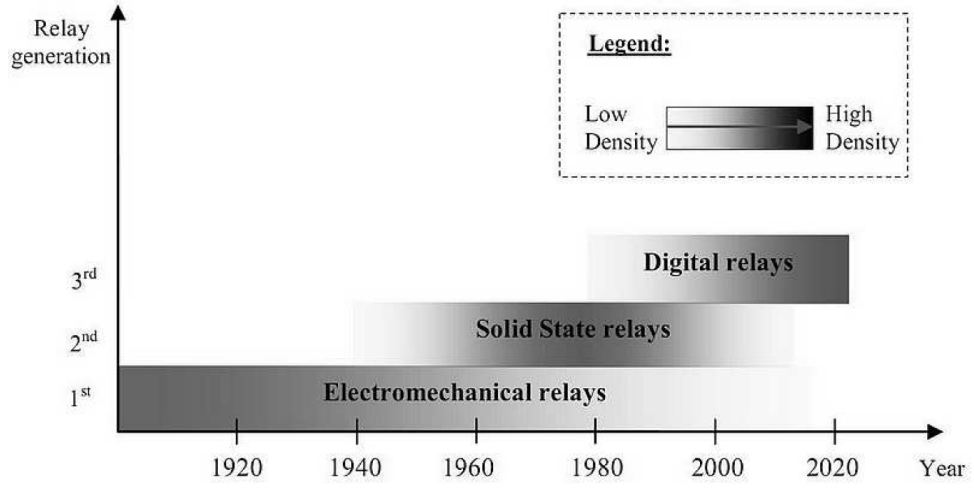

Figure 1.2: The different eras of protective relays [12]

The operating principles of relays have also evolved a lot during the last decades. The first distance relays appeared in the 1920's in the form of impedance (R-X diagram) [12]. The major protective relays principles are based on the fundamental (steady-state) frequency components evaluation of the voltage and the current. It is a frequency-domain method involving the estimation of the voltage and current phasors. The major limitation of the frequency-domain approach is the speed of the phasor estimation algorithms. This signal-based approach implies theoretically a full-cycle data window. In practice, the impedance-based protective relays operate in one to one-and-a-half cycles (20 ms to 30 ms for a 50 Hz power system) [13]. Some fast methods of phasors estimation permit to use only a half-cycle window but they have a lower accuracy and dependability [13]. The introduction of the concept of incremental quantities[3] in the protective relays algorithms [14] has permitted to implement the so-called ultra-high-speed protections [13], [15]. The

[2]also called static relays because they did not contain a moving part

[3]the incremental quantities are the voltage and current signals of an equivalent fault network obtained by removing the pre-fault conditions (see Chapter 9)

term of ultra-high-speed is considered to be operation in 4 ms or less [11]. However, these methods assume that the power system (voltage sources and transmission lines) may be represented by a simple RL model. This assumption may impact directly the speed, the dependability and the security of the protective relays as it will be shown in this work.

The performances of the ultra-high-speed distance protection developed by Schweitzer Engineering Laboratories (SEL) are shown in [13]. This method is based on the incremental quantities mentioned above and assumes the simple RL transmission line model. Table 1.1 summarized some pertinent results obtained with the ultra-fast distant element implemented by SEL using real-world power system data. It permits to highlight the following conclusions:

- the tripping times are very fast for all the tested close-in faults.
- for some fault inception angles, the tripping times may be too high even for a line of only 56 km faulted at its middle (case 2). It will be shown in Chapter 9 that the methods based on incremental quantities may be a lot impacted by the fault inception angle.
- the dependability of this method is limited close to the setting zone (case 5). The security margins are higher in order to avoid over-reaching but the dependability decreases.
- this method based on the RL model is efficient only for very strong power systems. Indeed, all the tests performed in [13] involved very small SIR (lower than 1).

Case	**Line length (km)**	**SIR**	**Fault position (pu)**	**Setting zone (pu)**	**Tripping time (ms)**
1	56	0.33	0.55	0.86	4
2	56	0.42	0.53	0.86	6.9
3	92	0.64	0.01	0.76	2.6
4	159	0.13	0.18	0.85	2.8
5	159	0.18	0.82	0.85	-

Table 1.1: Performances of the ultra-fast distance element TD21 developed by SEL

In this context of the challenging evolution of the electrical power systems and the limitations of the existing protective relay methods, this work proposes a new ultra-fast protection relay algorithm in the time-domain based on a Γ (Gamma) model of line. This work has been done in a close cooperation with the development department of Siemens.

1.2 Objectives

The objective of this work is to develop an **ultra-high-speed non-pilot**[4] **distance protection algorithm** to protect the transmission lines. The target tripping time is therefore **4 ms** or less. The second objective of this work is to **improve the dependability** of the ultra-high-speed distance protection while **guaranteeing the security**. The voltage level of the majority of the transmission line in Europe is 220 kV and 380-400 kV. Most of the transmission lines in Europe are shorter than 100 km [16]. In Belgium for example the longest transmission line has a length of 104.4 km [17]. In this work the target line length to protect is set at **100 km**.

The performances evaluation of the algorithm implemented in this work were done using test cases obtained by simulation. Another objective was to take into account the effects and the limitations of an existing hardware developed by Siemens AG. In this context the complete data acquisition system was simulated. The first constraint coming from the existing hardware is the sampling rate f_{algo} to use for the algorithms. This last is set at **8 kHz**.

The frequency-domain methods are intrinsically limited in response time by the need of a filtering process to estimate the voltage and current phasors. The algorithms proposed in this work are developed in the **time-domain**. The distance relay is characterized by a setting zone (or zone of distance) which delimit the maximum distance to fault from the relay location. In practice a distance protection cannot precisely operate until this setting zone. An under-reaching[5] or an over-reaching[6] should be accepted. These two opposed concepts are respectively related to the dependability and the security of the protection. The security of the ultra-high-speed algorithm is usually favoured to the detriment of the dependability. The improvement of the dependability and the security of the protection may be achieved by implementing an algorithm based on a **more accurate model of transmission line** than the simple RL.

A complete distance protection includes 4 different elements: first, the fault detection element which aims to detect an abnormal situation in the transmission line and to initiate the rest of the chain. This element must therefore operate as fast as possible; secondly, the loop selection element must identify the faulted loops among the ten possible types of fault (phase-to-ground fault, phase-to-phase fault, three-phase fault, etc.). If the distance to fault is estimated from a healthy loop it may lead to a wrong operation (under-reaching or over-reaching). The third element is the directional element which detects the fault direction (before or after the relay location). Only the forward faults should be tripped by the distance protection. Finally, the distance element identifies the distance to fault

[4] the tripping decision is based only on the local measurements at the relay location (in contrast with the pilot relays which require a communication channel)

[5] it refers to a missed operation of the distance relay for a fault located inside the setting zone

[6] it refers to an unwanted operation of the distance relay for a fault located after the setting zone

and gives the tripping signal to the circuit breakers if the fault is seen inside a defined setting zone. The developments done in this thesis are mainly focused on the distance element which requires a high level of accuracy. For the directional and the loop selection elements, a review of the existing ultra-fast methods is done to test their performances, to highlight the limitations and to propose some improvements. The fault detection element was not studied in this work because it has been accepted that the existing methods are sufficient to give a fast and secure fault detection [18].

1.3 Major contributions of this work

In this PhD thesis an ultra-high-speed distance protection algorithm is developed. The major contributions of this work are related to the distance element algorithm:

- implementation of a Γ model of transmission line for an ultra-high-speed distance protection in the time-domain thanks to a Linear Recursive Least-Squares Estimation method.
- improvement of the frequency behaviour of the Γ model until the first resonance frequency of a distributed parameters model of line.
- the use of the integral form of the equation representing the model of a line in order to limit the impact of a noisy signal.
- inclusion of a simple model of the voltage and the current transformers in the model of the transmission line.
- the use of a residual analysis to ensure the security of the method and to improve its dependability.

1.4 Thesis outline

Chapter 2 presents the different models of transmission lines, from the very simple (lumped parameters RL model) to the most accurate (distributed frequency-dependent parameters). A comparison of their frequency behaviour is made. Chapter 3 represents the major contribution of this work. The ultra-high-speed distance algorithm based on a Γ model of line is implemented. The classic Γ model of line is also adapted in order to improve its frequency behaviour. Chapter 4 shows the mathematical concepts related to the Least-Squares estimation method to ensure the security of the distance element algorithm. Moreover, a Recursive Least-Squares method is implemented to improve the performances of the method in term of computational loads. In Chapters 5 and 6, the distance algorithm is extended to a three-phase power system with the use of the Clarke

transform. The different types of fault are treated. In Chapter 7, a complete data acquisition process based on an existing hardware is simulated. It permits mainly to highlight the effects, usually neglected, of the voltage and the current transformers on a time-domain algorithm. Chapter 8 presents the security criteria implemented for the distance element algorithm. Chapters 9 and 10 present the existing ultra-fast methods for the directional element and the loop selection element respectively. The performances, the limitations and some proposals for improvement are provided. Chapter 11 presents the performances of the complete distance protection. Finally, Chapter 12 presents the main conclusions and recommendations for future works. Table 1.2 shows the summary of the objectives and the contributions of the different chapters of the thesis.

Chapter n°	**Objectives**	**Contributions**
2	- Present and compare the different models of transmission line	- Frequency behaviour of the models of transmission line
3	- Develop an ultra-fast time-domain distance element algorithm	- Faulted line parameters identification with a Linear Least-Squares method - Linearisation of the Γ model - Improvement of the Γ model - Impact of the SIR
4	- Mathematical analysis of the Linear Least-Squares method and its assumptions	- Condition number impact - Development of a Recursive Linear Least-Squares method - Residual analysis and confidence interval
5	- Generalization of the identification method for a three-phase transmission line model	- Decoupled three-phase Γ model using the Clarke transform
6	- Study the different types of fault - Extend the method for parallel transmission lines	- Calculation of the different compensation factors for a phase-to-ground fault with a Γ model - Analysis of the transfer function instabilities of the Γ model in the case of a phase-to-ground fault

7	- Simulate the existing data acquisition process and study the impact of the different components	- Adaptation of the identification algorithm to take into account the model of a current and a voltage transformer - Presence of a new parameter to identify linked to the signals of the primary side of the transformers
8	- Implementation of blocking methods to avoid over-reaching while maximizing the dependability	- Convergence criteria of the identified parameters of the line - Secured distance to fault based on a residual analysis (confidence interval and normalized mean squared error)
9	- Develop an ultra-fast time-domain directional element algorithm	- Performances and limitations of existing methods
10	- Develop an ultra-fast time-domain loop selection element algorithm	- Improvement and validation of the Siemens method based on incremental quantities
11	- Validation and performances evaluation of the complete distance protection	- Big database of tests (simulations) - Methods validation for distance and loop selection element - Adaptive convergence criteria to increase the speed of the distance element algorithm

Table 1.2: Summary of the thesis outline

Chapter 2

Overhead transmission line models

2.1 Introduction

The classical impedance-based distance protections assume an RL transmission line model. The complex impedance of the line may be found by applying a filtering method to estimate the voltage and the current phasors. This signal-based approach implies a full-cycle data window. In some particular cases, a half-cycle data window can be used for the phasors estimation. The phasors estimation methods are therefore limited in response time.

Recent works performed in the time domain have led to faster distance protections. These protective relaying's are based on the incremental quantities [13], [15]. However, as for the impedance-based methods, the current algorithms represent the transmission lines by a simple RL model that is only valid for short lines or narrow frequency range for long lines. It implies the use of a low-pass filter that eliminates the high frequencies. The specifications of the low-pass filter needed to eliminate the high frequencies may be such that it could introduce a significant extra-delay in the algorithm response time [19].

One of the solutions proposed in this thesis to improve the performances of the ultra-fast distance protection is to implement an algorithm based on a more accurate model of line. In this chapter the different models of overhead transmission lines are presented. The lumped and the distributed parameters models of line will be presented in Section 2.2 and 2.3 respectively. In Section 2.4 the frequency behaviour of the different models will be analysed in order to define the frequency range in which both simulated and identification models fit for different line length. Indeed, a clear distinction must be made between:

- the model used for the simulation. This is the model implemented in the simulation tool (EMTP). The accuracy of this model will ensure an ideal correlation between the results obtained by simulation and by a real-world power system network.

- the model used for the distance protection algorithms, which is the physical background associated to the mathematical methods. The accuracy of this model will

reduce the numerical and mathematical errors of the algorithms.

The lumped and the distributed parameters transmission line models will be studied. For the sake of clarity all the models described in this chapter refer to a single-phase transmission line. The generalization to a three-phase model is done in Chapter 5. Fig. 2.1 summarizes all the models studied in this chapter.

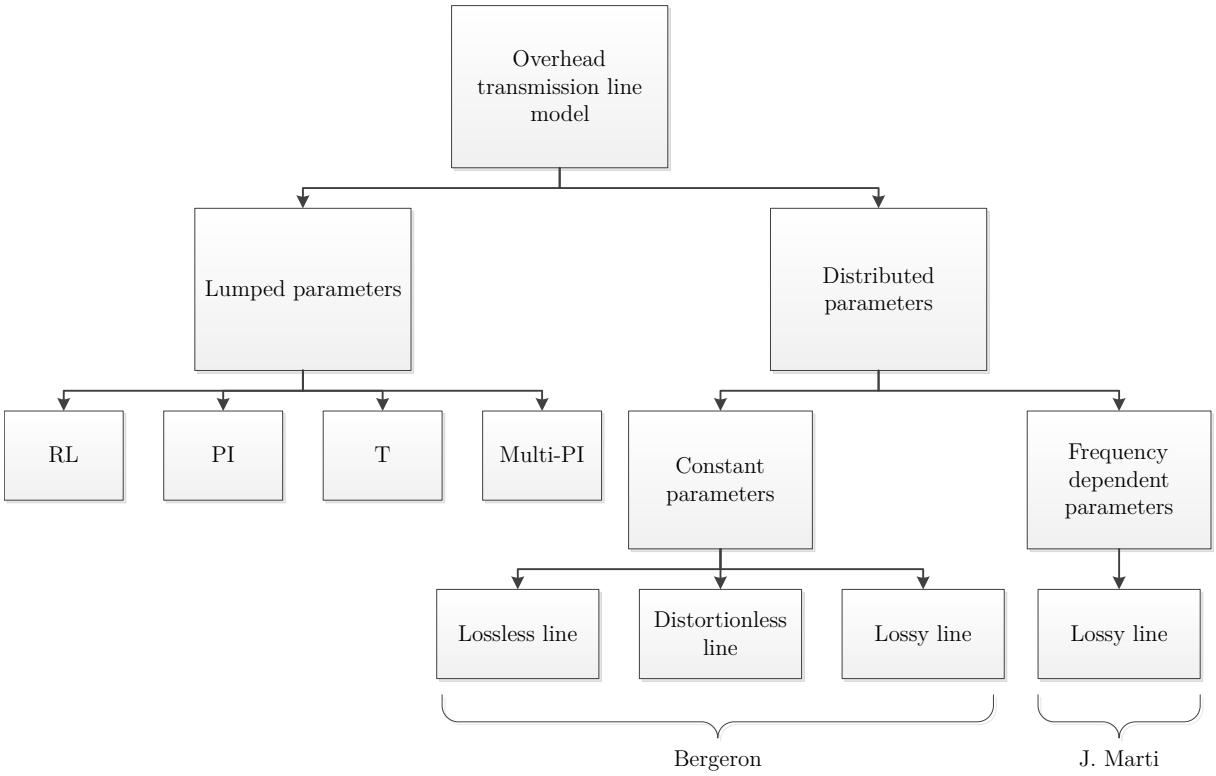

Figure 2.1: Overhead transmission line models

2.2 Lumped parameters

The lumped parameters models assume that the different parameters along the line can be replaced by lumped elements which represent the total impedance of the line. These models are accurate enough only for steady-state studies or short lines. They do not take into account the electromagnetic propagation phenomena. Moreover, the frequency dependence[1] of the parameters is generally not included in these models. There are some improvements performed during the last decades to include this frequency dependence in the lumped parameters models [20], [21]. However these methods based on cascade of lumped elements are not adapted for a fast algorithm because of their complexity [22].

[1]the parameters of an actual transmission line like the resistance and the inductance vary with the frequency due to some phenomena like the skin effect (see Section 2.3.2)

2.2.1 RL model

The RL model is the simplest model used for the transmission lines. The line is considered as a resistance, to represent the Joule losses, in series with an inductance (Fig. 2.2). Due to the simplicity of its implementation, it is the most used in the power system protections for classical relays [11] and high-speed relays [23]. The currents flowing through the capacitances of the line can be neglected for the fault conditions because the short-circuit current magnitudes are high. However, this model is only valid for relatively short lines or for very low frequencies because it does not permit to represent accurately the high frequencies as it will be shown in Section 2.4.

Figure 2.2: RL line model

2.2.2 RLC PI model

To study accurately the long lines and/or to increase the frequency range of the algorithm, it is necessary to take into account the capacitive effects of the transmission line. Two lumped capacitors may be placed at both ends of the RL model as shown in Fig. 2.3. This model is more accurate for longer lines than the RL model both for steady-state and for transient study. An alternative solution is to place a single capacitor at the middle of the line (RLC T model). However, as it will be shown in Section 3.2.3, the transfer function of a T model is more complex (there is one more electrical node) while it does not improve the frequency behaviour compared to the π model of line.

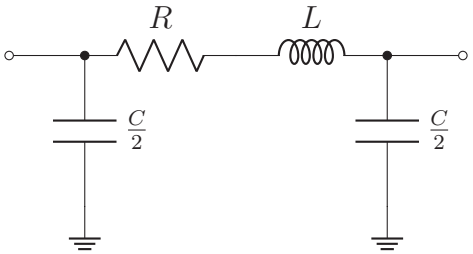

Figure 2.3: RLC π line model

2.2.3 Multi-PI model

The actual parameters of a true transmission line are not lumped but are distributed. When the line parameters cannot be considered as lumped any more because of the

distributed capacitive effects, it is possible to represent the line by a succession of π sections in cascade. The more π sections in the model, the closer the behaviour of the line to an actual line. The multi-π model deals better with non steady-state cases or with solutions over a wide range of frequencies.

2.3 Distributed parameters

As mentioned before the actual parameters of a true transmission line are distributed. Moreover, these parameters are not constant but function of the frequency. For a steady-state analysis the lumped parameters are accurate enough in many applications. However, for transient analysis the travelling time of the electromagnetic waves has to be taken into account. Travelling waves solutions are much faster and better suited for computers than cascaded π-circuit [24, page 57]. Consider a single dimension line segment Δx represented by the parameters $r_l\Delta x$, $g_l\Delta x$, $l_l\Delta x$ and $c_l\Delta x$ as shown in Fig. 2.4 where r_l, l_l, g_l and c_l are respectively the resistance, the inductance, the conductance and the capacitance per length of the line.

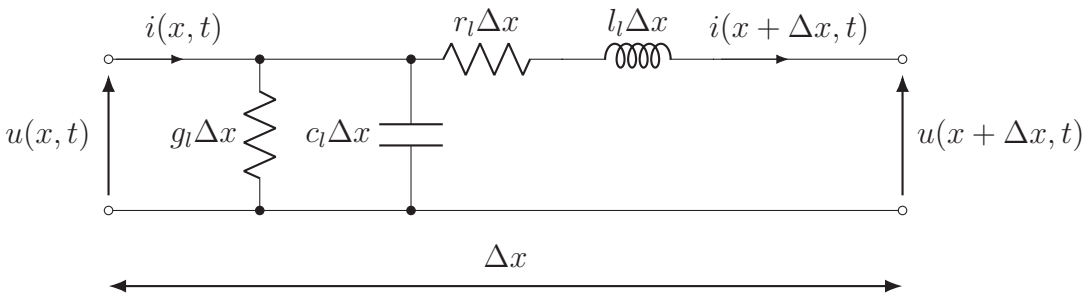

Figure 2.4: Segment of a transmission line with distributed parameters

The transmission lines with distributed parameters are using the travelling waves solution following the telegraph equations. In Laplace domain the equations are given by (2.1) and (2.2) [25]:

$$\frac{\partial^2 u(x,s)}{\partial x^2} = \gamma(s)^2 u(x,s) \tag{2.1}$$

$$\frac{\partial^2 i(x,s)}{\partial x^2} = \gamma(s)^2 i(x,s) \tag{2.2}$$

where s is the Laplace operator and where the propagation constant $\gamma(s)$ is given by:

$$\gamma(s) = \sqrt{r_l g_l + (r_l c_l + g_l l_l)s + l_l c_l s^2} = \frac{1}{v}\sqrt{(s+\alpha)^2 - \beta^2} \tag{2.3}$$

and

$$\alpha = \frac{1}{2}[(r_l/l_l) + (g_l/c_l)] \qquad \text{is the attenuation constant} \tag{2.4}$$

$$\beta = \frac{1}{2}[(r_l/l_l) - (g_l/c_l)] \qquad \text{is the phase constant} \tag{2.5}$$

$$Z_C = \sqrt{\frac{sl_l + r_l}{sc_l + g_l}} \qquad \text{is the characteristic impedance} \tag{2.6}$$

$$v = \sqrt{(1/l_l c_l)} \qquad \text{is the wave velocity} \tag{2.7}$$

The solutions for the travelling waves can be found analytically but may be very complex. Some assumptions have to be made to find simpler travelling waves solutions in the temporal domain. In EMTP software, two resolution methods are implemented: the Bergeron's method for constant parameters of line and the J. Marti's method for frequency-dependent parameters of line. These methods are widely used in the literature for overhead transmission lines with distributed parameters.

2.3.1 Bergeron model

The Bergeron model of line is used for constant distributed parameters. This model permits to find a solution of the problem (2.1) and (2.2) that depends only on the "*history vectors*"[2] [24]. This makes the Bergeron's model very easy to implement in a computer program. However, some assumptions have to be made to obtain this kind of solutions. A solution can be derived easily for a lossless or a distortion-less[3] line.

Lossless line

For a lossless line the assumptions used to solve this problem are:

- no resistance r_l and conductance g_l.

- the inductance l_l and the capacitance c_l are distributed along the line.

It leads to the following simplifications:

$$\gamma(s) = s/v \tag{2.8}$$

$$Z_C = Z_0 = \sqrt{\frac{l_l}{c_l}} \tag{2.9}$$

Equations (2.1) and (2.2) become in the temporal domain:

[2] vectors of the current and the voltage composed only by the values from the past (previous samples)

[3] it is assumed that the Heaviside condition is respected: $r_l/l_l = g_l/c_l$. This model is seldom used in practice [24, page 69] and will not be studied in this thesis because the actual transmission lines are not distortion-less

$$\frac{\partial^2 u(x,t)}{\partial x^2} = \frac{1}{v^2}\frac{\partial^2 u(x,t)}{\partial t^2} \tag{2.10}$$

and

$$\frac{\partial^2 i(x,t)}{\partial x^2} = \frac{1}{v^2}\frac{\partial^2 i(x,t)}{\partial t^2} \tag{2.11}$$

for which the general solutions are given by d'Alembert's formula [26]:

$$u(x,t) = Z_0(f_1(x-vt) - f_2(x+vt)) \tag{2.12}$$

$$i(x,t) = f_1(x-vt) + f_2(x+vt) \tag{2.13}$$

where f_1 and f_2 are arbitrary functions. There is a forward and a backward wave for the voltage and the current. By Multiplying (2.13) by Z_0 and adding it to or subtracting it from (2.12), it gives:

$$u(x,t) + Z_0 i(x,t) = 2Z_0 f_1(x-vt) \tag{2.14}$$

$$u(x,t) - Z_0 i(x,t) = -2Z_0 f_1(x+vt) \tag{2.15}$$

Note that $u(x,t) + Z_0 i(x,t)$ is constant when $x - vt$ is constant and $u(x,t) - Z_0 i(x,t)$ is constant when $x + vt$ is constant. If the travel time to get from one end **S** of the line to the other end **R** is $\tau = L/v = L\sqrt{l_l c_l}$ (where L is the line length), then the expression $u(x,t) + Z_0 i(x,t)$ is equal at node **S** and time $t - \tau$ and at node **R** and time t. After some re-arrangements it finally leads to:

$$i_{S,R}(t) = \frac{u_S(t)}{Z_0} + i_S(t-\tau) \tag{2.16}$$

$$i_{R,S}(t) = \frac{u_R(t)}{Z_0} + i_R(t-\tau) \tag{2.17}$$

where:

$$i_S(t-\tau) = -\frac{1}{Z_0}u_R(t-\tau) - i_{R,S}(t-\tau) \tag{2.18}$$

and

$$i_R(t-\tau) = -\frac{1}{Z_0}u_S(t-\tau) - i_{S,R}(t-\tau) \tag{2.19}$$

are the "*history vectors*" because they are composed only by the values from the past. $i_{S,R}$ is the current flowing from **S** to **R** and $i_{R,S}$ is the current flowing in the opposite

direction. The complete development of the Bergeron lossless line model can be found in [27, pages 140-141].

Lossy line

The actual transmission lines are not lossless. If the losses are considered it is impossible to find a temporal solution directly from the travelling waves equations. However, the losses can be included by placing lumped resistances in three places as shown in Fig. 2.5. This simplification is accurate enough if $R/4 << Z_0$ where R is the total line resistance [24, page 49]. The temporal equations of the lossy Bergeron model of line are available in [28], [29].

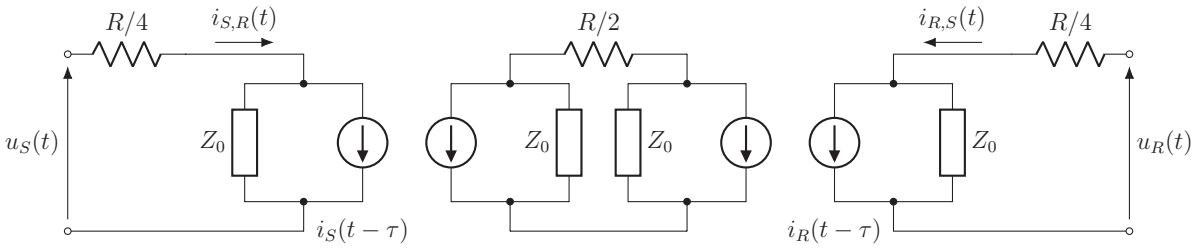

Figure 2.5: Bergeron model for lossy lines

2.3.2 J. Marti model

The J. Marti model developed by J. R. Marti in [30] is an efficient model that permitted to take into account the frequency dependence of the distributed parameters of the transmission lines. On actual overhead lines the parameters are not constant but function of frequency due to the skin effect. The self and the mutual impedances of an overhead transmission line can be expressed as follows [6]:

$$Z_{ii} = \left[R_{i(c)} + j\omega L_{i(c)}\right] + j\omega L_{i(g)} + \left[R_{i(e)} + j\omega L_{i(e)}\right] \Omega/km \tag{2.20}$$

and

$$Z_{ij} = j\omega L_{ij(g)} + \left[R_{ij(e)} + j\omega L_{ij(e)}\right] \Omega/km \tag{2.21}$$

where subscript c represents the contribution of the conductors to the resistance and the internal inductance, g represents the contribution of the conductors to the inductance due to the geometry (external inductance) and e represents correction terms to the resistance and inductance due to the contribution of the earth return path. Indeed, as the ground is used as earth return path its effect must be also considered. The skin effect may therefore impact the contributions on the impedance due to both conductors and earth return path.

Fig. 2.6 coming from [24] shows the variation of the zero and the positive resistance and inductance with the frequency. The positive inductance and resistance remain more or less constant until about 1 kHz. However, the zero components vary very much at low-frequencies due to the skin effects in the earth return path. The zero sequence parameters have an impact on parameters identification in the case of a phase-to-ground fault as it will be shown in Chapter 5. The capacitance is not represented in this figure because it can be considered as constant until about 100 kHz [24, pages 14-15].

As the line parameters are frequency-dependent, it is not possible to find a solution directly in the time domain (even for a lossless case). This model approximates the characteristic admittance and the propagation constant by rational functions in the frequency domain. The temporal domain solution is then given by the use of an inverse Fourier transform.

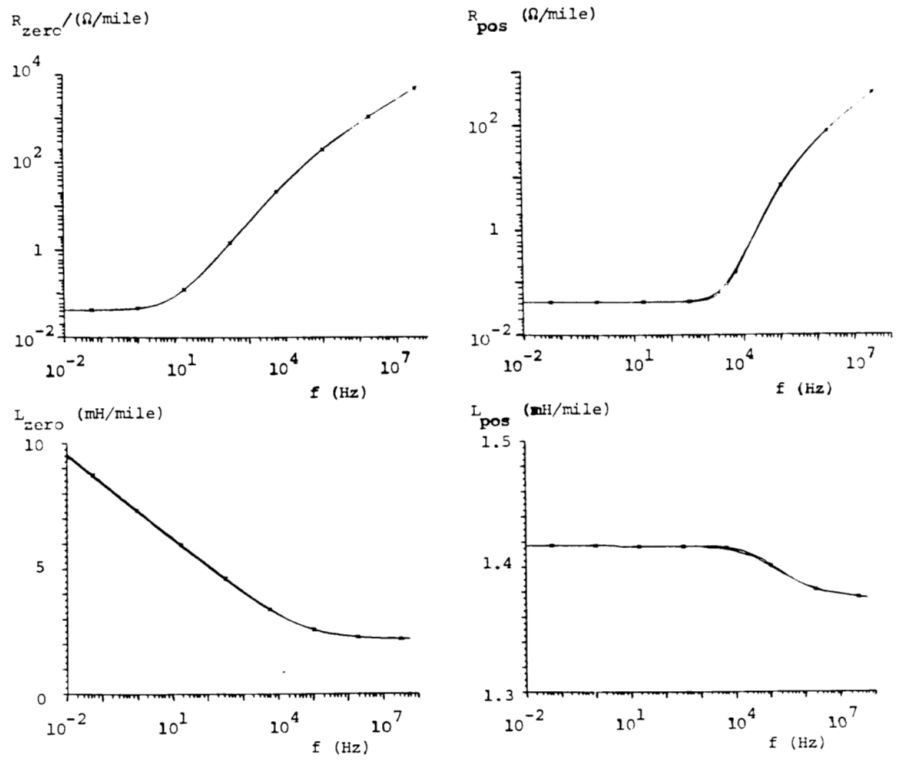

Figure 2.6: Frequency-dependent line parameters [24]

Other frequency-dependent transmission line models have been developed in the literature. For example, the Universal Line Model (ULM) [31] does not assume constant transformation matrices (which may be source of errors) unlike the J. Marti model. However, as explained in [32], [33] both models gives comparable results in many cases despite an additional complexity of the ULM model. Moreover, it will be shown in Section 2.4.2 that the Bergeron model of line would be sufficient. For these reasons, only one frequency-dependent model (J. Marti) is presented in this thesis.

2.4 Frequency response comparison of the models

In this section the frequency behaviour of the different models will be compared. The fast distance element implemented in this project is based on the faulted line parameters identification. As it will be explained in Chapter 3, the model of line used for the identification must fit the model of line used for the simulation in a defined frequency range. The distributed models will be used as reference model because they better represent the actual parameters of a true transmission line for transient phenomena. The lumped parameters models will be compared to a Bergeron model in order to define a frequency range in which both models fit. This analysis will be done by the use of Bode's curves of the transfer function of the lines. The transfer function of the faulted line is simply the ratio between the voltage and the current at the relay location given by (2.22).

$$H(j\omega) = \frac{V_R(j\omega)}{I_R(j\omega)} \tag{2.22}$$

Fig. 2.7 shows the circuit used to obtain the Bode's curves. The dotted elements represent the external network that has no impact on the evaluation of the transfer function of the faulted line. The line parameters corresponding to a typical 220 kV overhead transmission line extracted from [34] are $r_l = 0.058\ \Omega$/km, $l_l = 0.955$ mH/km and $c_l = 0.0124\ \mu$F/km.

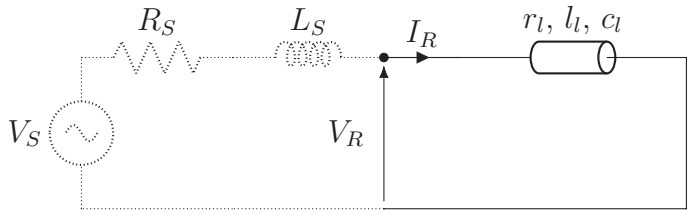

Figure 2.7: Simulation of a faulted line for Bode's curves generation

2.4.1 Bode's curves

A frequency scan is applied on the circuit shown in Fig. 2.7 to obtain the steady-state voltage and current at the relay location for each frequency. The objective is to check the frequency range in which the reference model (Bergeron) fits the lumped parameters models. The Bode's curves are obtained for a short transmission line in Fig. 2.8 and for a long transmission lines in Fig. 2.9. As expected the lumped parameters models fit the Bergeron model in a wider range of frequencies for short lines than for long lines. It also appears that some resonance frequencies may be present in the transfer function of the models including the capacitance. The following conclusions can be drawn:

- the RL model does not include a resonance peak. It must be filtered up to a few hundreds Hz in order to fit the true behaviour of a line.

- the resonance frequency of the π model differs from the first resonance peak of the Bergeron model. An adapted π model can be developed to improve its frequency behaviour until the first resonance peak of the Bergeron model. The adapted π model does not split equally the capacitance between the two ends of the line. As shown in Fig. 2.8 and 2.9 the resonance peak is well approximated thanks to this adapted model. The correction factor used will be explained in Chapter 3.

- a multi-π model of 10 sections approximates well the Bergeron model up to a few thousands Hz.

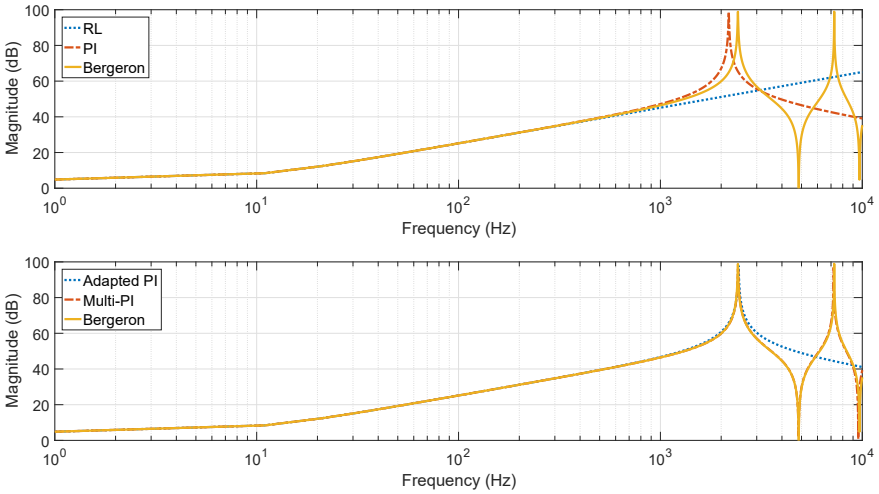

Figure 2.8: Bode's curves of the transfer function of single-phase models of line of 30 km

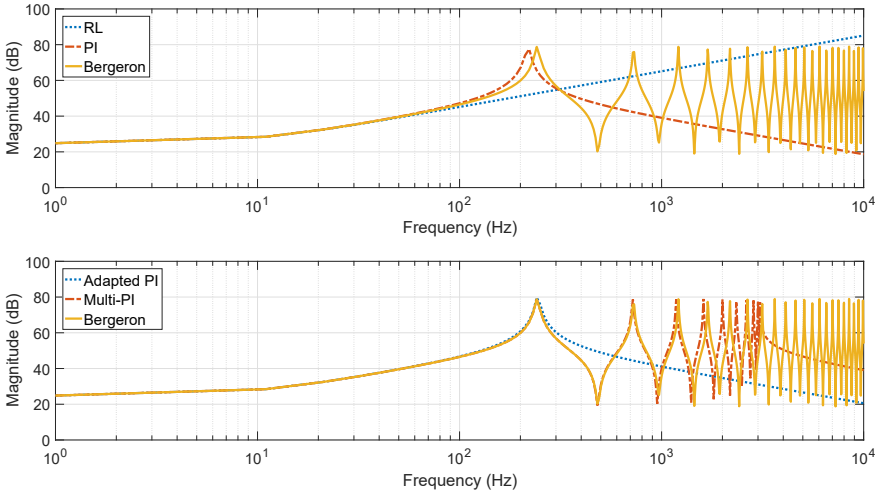

Figure 2.9: Bode's curves of the transfer function of single-phase models of line of 300 km

This kind of analysis should be made for all the line lengths in order to set the filtering frequency. Indeed, a low-pass filter must be used for the ultra-fast distance element algorithm to keep only the frequency range in which the simulated model of line fits the identification model implemented in the algorithm. It is also important that this frequency range is as wide as possible in order to keep the maximum of transient information. It will be shown in Chapter 3 that the multi-π model has a too complex transfer function to be used as an identification model. The filtering frequency will be fixed by the frequency at which the adapted π and the RL models begin to differ too much from the Bergeron model.

Assuming a threshold of 3 dB of difference between both models. The corresponding filtering frequency will be the maximum frequency at which the models differs from the Bergeron model of less than 3 dB. Fig. 2.10 shows the results.

In Fig. 2.10 three different frequencies are represented: 1000 Hz, 500 Hz and 300 Hz. The hatched regions represent the maximum line length possible to achieve with the three filtering frequencies for the two models of line and for the defined threshold difference of 3 dB. As expected the adapted π model of line permits to achieve longer line than the RL model for a given filtering frequency. For a short line both models are valid with a cut-off frequency of 1 kHz. For a long line the adapted π model is more suitable. Finally, for a very long line only the adapted π model can be used if the the cut-off frequency is decreased.

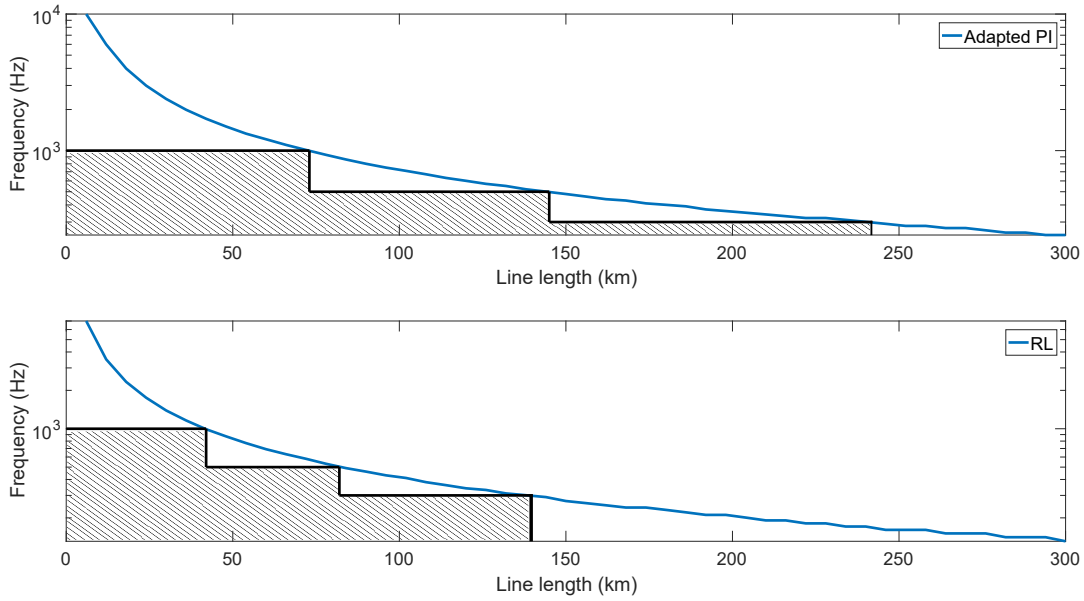

Figure 2.10: Maximum frequencies at which adapted π and RL models differ from the Bergeron model for less than 3 dB for different line lengths

Table 2.1 summarizes the filtering frequency that must be used for the distance element algorithm according to the line length.

Filtering frequency	Max. length RLC	Max. length RL
1000 Hz	75 km	45 km
500 Hz	145 km	80 km
300 Hz	240 km	140 km

Table 2.1: Maximum line length for adapted π and RL model for different filtering frequencies

2.4.2 J. Marti model

In the previous section it has been assumed that the reference model of line is represented by a Bergeron model. This choice has been motivated by the fact that the implementation of this model in an EMTP software is simpler. Indeed, the construction of the curves of the different parameters of the line against the frequency requires more information about the complete line and tower topology than for the Bergeron model. In this section a comparison between the transfer function of a Bergeron model and a J. Marti model will be made in order to ensure that both models fit until the first resonance frequency.

For the J. Marti model of line it is more relevant to analyse a three-phase model of line. A phase-to-phase or a three-phase fault involves only the positive sequence line parameters while a phase-to-ground fault involves both positive and zero sequence line parameters. As the frequency dependence is more significant for the zero sequence (see Fig. 2.6), the phase-to-ground fault should be more impacted. Fig. 2.11 compares the Bode's curves of the transfer function of a three-phase Bergeron and J. Marti model of 100 km. The transfer functions represented in these figures correspond to the line parameters identified by the RLC identification method as explained in Appendix A. Note that in this thesis the Clarke transformation is used to study a three-phase system. This transformation leads to the α, β and 0 sequence components. The following conclusions can be made:

- for the phase-to-phase fault on the top of the figure the two transfer functions are similar until a few kHz. The use of the Bergeron model as reference is therefore justified in this case.

- for the phase-to-ground fault on the bottom the two transfer functions are very close until the first resonance frequency.

- however, for the phase-to-ground fault a distortion appears before the resonance frequency. This phenomenon is not linked to the model of line used but is due to the series circuit formed by the α and the 0 sequence network. This phenomenon will be analysed deeply in Section 6.6.

- for the higher frequencies the matching is no longer met. It is therefore necessary to filter the frequencies higher than the first resonance frequency if the Bergeron model is used as a reference for the simulation.

- finally, there is also a difference for the very low frequencies (below 10 Hz). For the Bergeron model the positive sequence of the resistive parameter is $r_l = 0.0588$ Ω/km. This parameter is constant for all the frequencies. For the J. Marti model the positive sequence of the resistive parameter is $r_l = 0.0581$ Ω/km at 50 Hz and $r_l = 0.0398$ Ω/km at 0.1 Hz. However, the accuracy of the J. Marti model for the very low frequencies is not totally reliable because this model presents unstable behaviour for low frequencies [35], [36].

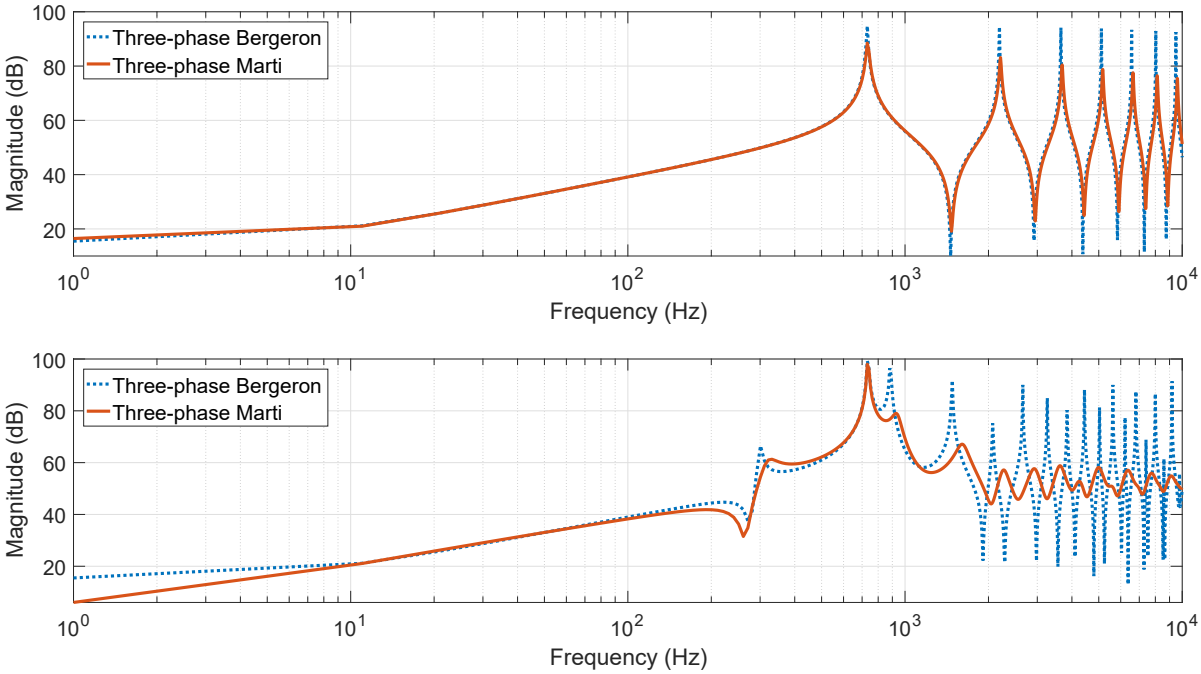

Figure 2.11: Bode's curves comparison for a phase-to-phase fault above and a phase-to-ground fault below between a Bergeron and a J. Marti line of 100 km

2.5 Conclusions

In this chapter the different models of line have been presented and their frequency behaviour has been studied. From the very simple RL model to the most accurate J. Marti model. It appeared that it is necessary to improve the model of line usually implemented in the existing protection algorithm in order to increase the frequency range in which the actual transmission line and the model used for the algorithm fit. This improvement would

permit to protect longer lines without increasing too much the filtering specifications and therefore the possible extra-delays.

The Bergeron model was chosen as the reference model to represent a real-world overhead transmission line because this model is easier to implement for a large database of tests. It was shown that this model is quite similar to the J. Marti model until the first resonance frequency. The higher frequencies should be removed by a low-pass filter. The comparison of the performances of both models will be done in Chapter 6.

In the next chapter a distance element algorithm based on a transmission line parameters identification will be implemented and validated.

Chapter 3

Line parameters identification method

3.1 Introduction

The purpose of this chapter is to construct a distance element algorithm for the ultra-fast distance protection relay. The distance to fault can be deduced from the parameters of the faulted transmission line as in classical relay. In Section 3.2 the transfer function of the different transmission line models presented in the previous chapter will be calculated. In Section 3.3 the adapted π model of line will be developed. It will lead to a correction factor for the capacitance of the line. The time-domain equations will be deduced from these transfer functions for the selected model in Section 3.4. The parameters of the faulted line will be estimated with a linear least-squares method which will be deeply detailed in Chapter 4. Firstly, in Section 3.5 all the identification methods implemented will be validated with a perfect simulation model corresponding exactly to the identification model. In Section 3.6 it will be shown that the SIR has an important impact on the high frequencies appearing in the voltage and the current signals of the faulted line. This study will be useful to understand the results obtained for a more complex model of line for different SIR values. In Section 3.7 the distance element algorithm will be tested with a more accurate transmission line model corresponding to a distributed parameters model. Finally, the impact of the fault resistance on the identified distance to fault will be treated in Section 3.8.

3.2 Transfer function

It is necessary to obtain the transfer function of the different transmission line models in the frequency domain. The transfer function is defined as the ratio of the voltage to the current at the relay location. The distributed parameters models of line are solution

of the problem given by (2.1) and (2.2). A distributed model can be represented as an infinite cascade of π-sections. It is also possible to find the time-domain equations of the Bergeron model directly from the travelling waves theory as it was done in [29]. However, this method implies the use of a very high sampling rate (a few MHz). In this project the sampling rate of the algorithm is fixed to only 8 kHz as explained in Chapter 1. Other methods in the frequency domain have been developed for a single-ended distance algorithm based on the Bergeron model [37], [38]. However, as explained in Chapter 2, the frequency domain approach is limited in response time by the filtering process. It is thus impossible to construct a simple transfer function for the distributed parameters models of line adapted to an on-line fast distance protection algorithm. The Bergeron model will be used as reference to represent the real-world transmission line. The lumped parameters models will be used for the least-squares identification algorithm. The implementation of the identification method will be done for a single-phase circuit. The generalization to the three-phase lines will be treated in Chapter 5. Moreover, the assumption of a bolted short-circuit (zero fault resistance) will be made to simplify the development of the method. The impact of the fault resistance will be discussed in Section 3.8.

3.2.1 RL line

The transfer function of an RL circuit is straightforward because there are only series line impedance. The transfer function is simply the impedance of the line as shown in Fig. 3.1 and is given by (3.1).

$$H_{RL}(j\omega) = \frac{V_R(j\omega)}{I_R(j\omega)} = mr_l + j\omega ml_l \tag{3.1}$$

where m is the distance to fault (km). The dotted elements represent the external network which does not impact the transfer function of the line.

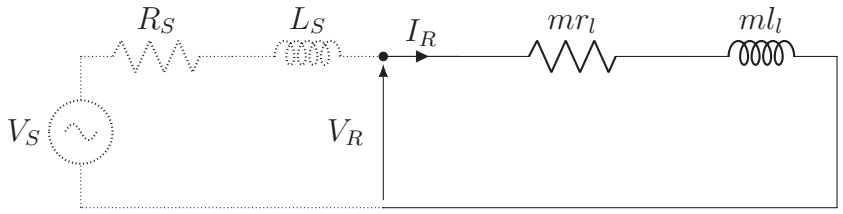

Figure 3.1: RL model of a faulted line

3.2.2 RLC PI line

Fig. 3.2 shows a classical π model of line with a simple model of generator connected at both ends.

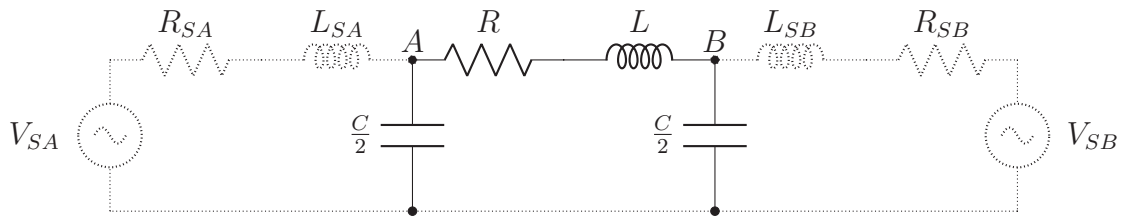

Figure 3.2: π model of line with a voltage source connected at both ends

When a bolted fault appears on the line between the nodes A and B at a distance m from the beginning, the line can be split in two parts: a faulted part shown in Fig. 3.3 which is the left part of the line; and a right part of the same line which does not have any impact on the equations as the fault is a bolted short-circuit. Fig. 3.3 represents the so-called Γ model of line [39]. Note that in the usual form of the Γ model of line all the capacitance of the line is put at one extremity. In this project the denomination of Γ model is related to a half branch of the π model.

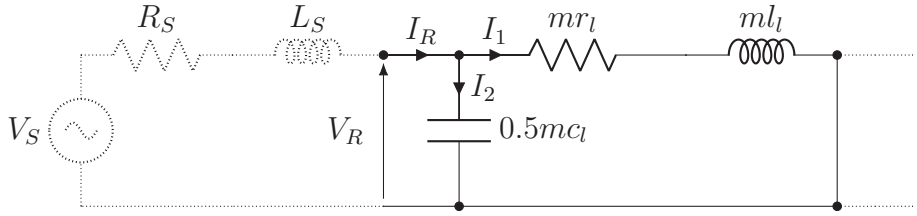

Figure 3.3: Γ model of a faulted line

There are 2 closed circuits that give 2 equations regarding the Kirchoff's Voltage Laws (KVL) and 1 regarding to the Kirchoff's Current Laws (KCL). After introducing $c_l' = 0.5 \cdot c_l$, it leads to:

$$\begin{cases} V_S - R_S I_R - j\omega L_S I_R - \dfrac{1}{j\omega m c_l'} I_2 = 0 & (3.2) \\ \dfrac{1}{j\omega m c_l'} I_2 - m r_l I_1 - j\omega m l_l I_1 = 0 & (3.3) \\ I_R = I_1 + I_2 & (3.4) \end{cases}$$

Using the relation:

$$V_R = V_S - R_S I_R - j\omega L_S I_R \tag{3.5}$$

the transfer function is finally given by:

$$H_{RLC\ PI}(j\omega) = \frac{V_R(j\omega)}{I_R(j\omega)} = \frac{j\omega m l_l + m r_l}{(j\omega)^2 m c_l' m l_l + j\omega m c_l' m r_l + 1} \tag{3.6}$$

In Section 2.4 it was shown that the π model of line cannot fit a distributed parameters

model in a wide frequency range for the very long lines. To improve the fitting it is necessary to use more than one π-section (multi-π model of line). An alternative solution is to adapt the transfer function of the π model in order to improve the fitting until the first resonance frequency. Fig. 3.4 shows that this improvement can be achieved by taking a lower value of the capacitance. An optimal value of $c_l^* = 0.4 \cdot c_l$ instead of $c_l^{'} = 0.5 \cdot c_l$ for the capacitance was found empirically but a theoretical explanation is presented in Section 3.3. This value is valid for all the line lengths.

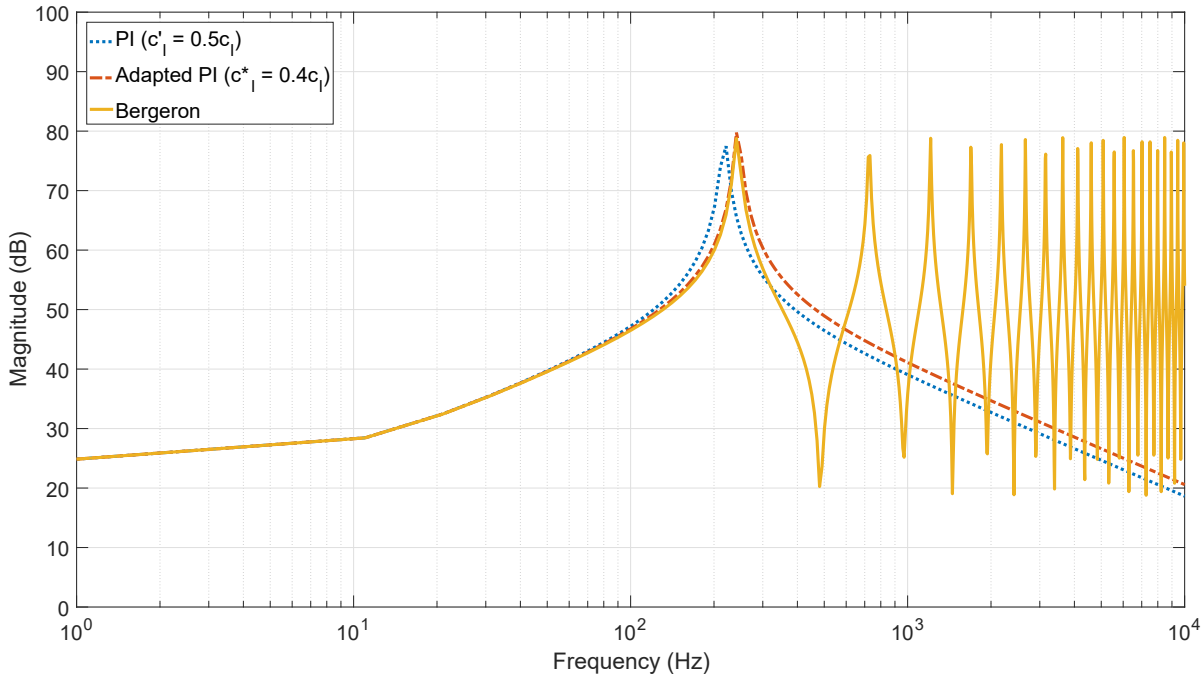

Figure 3.4: Bode's curves comparison between a π and an adapted π model of line of 300 km

As explained in Appendix B the resonance frequency is given by (3.7). Fig. 3.5 shows the resonance frequencies for different distances to fault. In this example the parameters of the transmission line are $l_l = 0.955$ mH/km and $c_l^* = 0.0049$ μF/km (typical values for a 220 kV power system [34]). For close-in faults or short lines the resonance frequency is very high. The high frequencies may be deleted by the filters of the data acquisition system. It is important to keep this fact in mind when analysing the RLC identification method presented in Section 3.5. For a distance to fault of 120 km the resonance frequency is around 600 Hz and it drops to 250 Hz for a distance to fault of 300 km. This curve will be useful to implement correctly the low-pass filter necessary to remove the high frequencies above the first resonance frequency of the faulted line simulated by a distributed parameters model.

$$f_{res} = \frac{1}{2\pi m \sqrt{c_l^* l_l}} \tag{3.7}$$

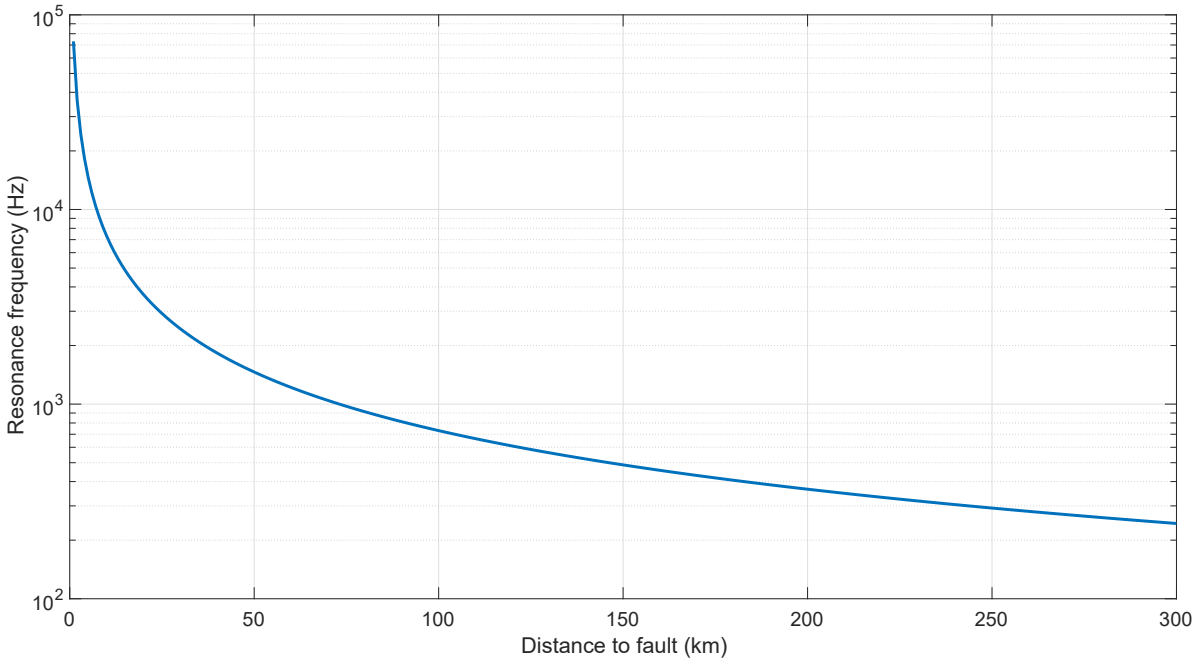

Figure 3.5: Resonance frequencies versus the distance to fault for an adapted π model of line

3.2.3 RLC T line

Fig. 3.6 shows the equivalent circuit of the RLC T model of line.

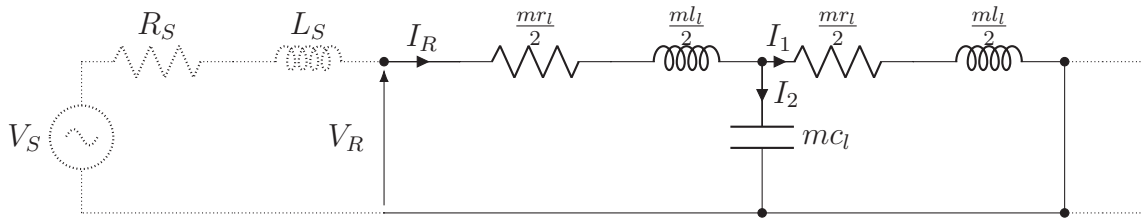

Figure 3.6: T model of a faulted line

After introducing $l'_l = 0.5 \cdot l_l$ and $r'_l = 0.5 \cdot r_l$, the KVL and KCL give the following equations:

$$\begin{cases} V_S - R_S I_R - j\omega L_S I_R - mr'_l I_R - j\omega ml'_l I_R - \dfrac{1}{j\omega mc_l} I_2 = 0 & (3.8) \\ \dfrac{1}{j\omega mc_l} I_2 - mr'_l I_1 - j\omega ml'_l I_1 = 0 & (3.9) \\ I_R = I_1 + I_2 & (3.10) \end{cases}$$

Finally, the transfer function is given by:

$$H_{RLC\ T}(j\omega) = \frac{V_R(j\omega)}{I_R(j\omega)} = \frac{(j\omega ml'_l + mr'_l)((j\omega)^2 mc_l ml'_l + j\omega mc_l mr'_l + 2)}{(j\omega)^2 mc_l ml'_l + j\omega mc_l mr'_l + 1} \tag{3.11}$$

Fig. 3.7 shows that the π model and the T model of line have a similar frequency response until the resonance frequency. After the resonance both models differ from the Bergeron model of line. The T model does not improve the fitting despite a more complex transfer function. Note that for the π and T models a correction factor of **0.4** instead of 0.5 and **0.8** instead of 1 is taken respectively for the capacitance of the line in order to fit better the Bergeron model of line. For the T model the value of 0.8 for the correction factor was also found empirically.

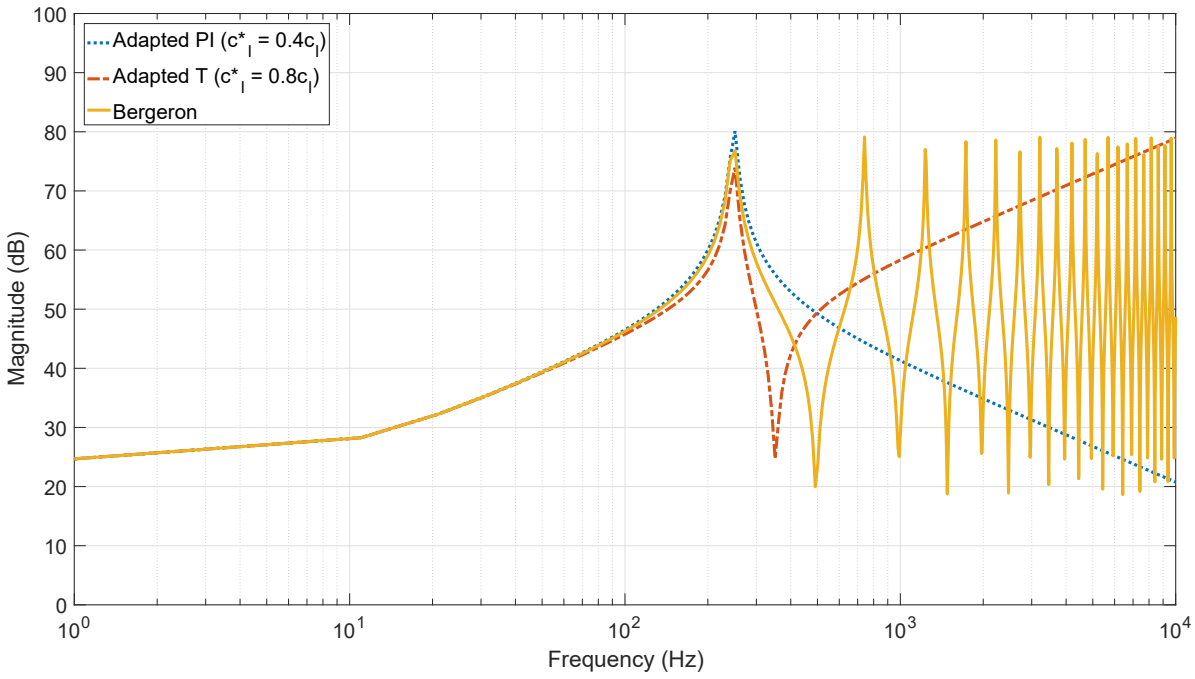

Figure 3.7: Bode's curves comparison between an adapted π and an adapted T model of line of 300 km

3.2.4 Multi-PI line

The same developments can be made for the multi-π model of line. In Section 2.4 it was shown that the multi-π model is the most accurate lumped parameters model of line for the transient analysis. However, even with only two cascaded-π sections, the transfer function of this model is very complex (3.12). Moreover, as it will be explained in Section 3.4.2 the use of a linear least-squares method implies that the model is linear in parameters. The linearisation of the multi-π model of line is not possible.

$$H_{2PI}(j\omega) = \frac{(j\omega)^3 ml'_l mr'_l mc'_l + (j\omega)^2 2ml'_l mr'_l mc'_l + (j\omega)\left((mr'_l)^2 mc'_l + 2ml'_l\right) + 2mr'_l}{(j\omega)^4 0.5(ml'_l mc'_l)^2 + (j\omega)^3 ml'_l mr'_l (mc'_l)^2 + (j\omega)^2\left(1.5ml'_l mc'_l + 0.5(mr'_l mc'_l)^2\right) + (j\omega)\left(1.5mr'_l mc'_l + ml'_l\right) + mr'_l + 1} \quad (3.12)$$

3.2.5 Models discussion

Some first conclusions can be made according to the previous results:

- the RL model is accurate only for very short lines in transient analysis. However, thanks to its very simple transfer function this model can be efficient for short lines and is therefore not rejected. Moreover, one of the objectives of this thesis is to prove that the use of a model of line more accurate than the RL model would permit to implement a faster distance element algorithm. The RL model will also implemented and its performances will be compared with a more complex model of line.

- the adapted Γ model is accurate enough for long lines in a relatively wide frequency range. This model will be implemented and deeply analysed. Remember that the Γ model represents a half branch of the π model in the fault conditions.

- the T model of line has a more complex transfer function than the Γ model while it has a similar behaviour until the resonance frequency. It is therefore not relevant to implement the T model.

- as explained before the multi-π model leads to a very complex transfer function which cannot be linearised in order to use a linear least-squares method. This model will be rejected too.

3.3 Adapted PI model of line

The transfer function of the adapted π model of line subject to a short-circuit is given by (3.13):

$$H_{RLC} = \frac{V}{I} = \frac{j\omega ml_l + mr_l}{(j\omega)^2 mc_l^* ml_l + j\omega mc_l^* mr_l + 1} \quad (3.13)$$

By defining:

$$\begin{cases} Z = j\omega ml_l + mr_l & (3.14) \\ Y = j\omega mc_l & (3.15) \end{cases}$$

it leads to:

$$H_{RLC} = \frac{Z}{1 + k_{corr} ZY} \tag{3.16}$$

The objective is to find a corrective factor k_{corr} that improves the fitting between the π model and the distributed parameters model of line until the first resonance frequency. For a classic π model of line the capacitance is split in two equal parts put at the beginning and at the end of the line. In this case the corrective factor is $k_{corr} = 0.5$. However, it appeared that the matching between the transfer function of the π model and the Bergeron model is not achieved until the resonance frequency.

A constant distributed parameters model of line is governed by the steady-state relations (3.17) and (3.18) as demonstrated in [40, page 115].

$$\begin{cases} V(x) = V_2 \cosh(\gamma x) + Z_C I_2 \sinh(\gamma x) & (3.17) \\ I(x) = \dfrac{V_2}{Z_C} \sinh(\gamma x) + I_2 \cosh(\gamma x) & (3.18) \end{cases}$$

where x is the position on the transmission line taken from the end of the line, V_2 and I_2 are respectively the voltage and the current at the end of the line. When a bolted short-circuit appears on the line it is possible to consider only the fraction of the transmission line between the relay and the fault position. In this case the beginning of the line, and thus the relay location, is localized at the position $x = m$ and the voltage V_2 at the end of the line, and thus at the fault position, drops to zero. The transfer function of the faulted line seen at the relay location becomes:

$$H = \frac{V(m)}{I(m)} = Z_C \frac{\sinh(\gamma m)}{\cosh(\gamma m)} \tag{3.19}$$

If the conductance of the line is neglected the following equation results:

$$H = \sqrt{\frac{j\omega l_l + r_l}{j\omega c_l}} \frac{1}{\coth(\gamma m)} \tag{3.20}$$

In order to compare the transfer function of the adapted π model and the distributed model the hyperbolic function is approximated by a Taylor Series Expansions [41].

$$H = \sqrt{\frac{j\omega l_l + r_l}{j\omega c_l}} \frac{1}{\frac{1}{\gamma m} + \frac{\gamma m}{3} + ...} \tag{3.21}$$

Using (3.14) and (3.15) and the fact that $\gamma m = \sqrt{ZY}$ it leads to:

$$H = \sqrt{\frac{Z/m}{Y/m}} \frac{1}{\frac{1}{\sqrt{ZY}} + \frac{\sqrt{ZY}}{3}} = \frac{Z}{1 + \frac{1}{3} ZY} \tag{3.22}$$

This development shows that in a first approximation the corrective factor to apply to

the transfer function of the π model of line is:

$$k_{corr} = \frac{1}{3} = 0.3333... \tag{3.23}$$

Of course the factor found here is coming from a first order approximation of the hyperbolic function and is thus not exactly equal to the empirical factor found which is equal to 0.4. However, it permits to explain that the use of a factor lower than 0.5 may permit to improve the equivalence between the transfer function of a lumped parameters and a distributed parameters model of line.

3.4 Line parameters determination

In this section a linear least-squares algorithm for the parameters identification of the faulted line will be presented. The developments are done for the two selected models of line: the RL model and the RLC-Γ model. It is possible to derive the temporal relations between the voltage and the current at the relay location from the transfer functions found before. When a fault occurs on the line the "*fault detection element*" of the relay protection will give a starting time as output. From this starting time several samples of voltage and current are collected. The number of samples depends on the window length used for the distance element algorithm and on the sampling rate. The objective is to construct an overdetermined linear system of equations as follows:

$$Ax = b \tag{3.24}$$

where the matrices **A** and **b** are function of the voltage and the current at the relay location. **x** is the vector of the faulted line parameters (R_l, L_l and C_l) to be identified by the least-squares method. Theoretically, only 3 samples are needed to solve a system of 3 unknowns. In practice, the data may be noisy and an error term may be present for each sample (called residuals). The method of least-squares consists in adjusting the unknowns of an overdetermined system by minimizing the sum of the squares of the residuals. Assuming that the linear parameters r_l, l_l and c_l are known, the distance to fault can be directly deduced from the identified line parameters. It will be shown that first and second order derivative functions are present in the system (3.24). However, the numerical approximation for the derivative function may be unstable because the round-off error can grow while the truncation error is reduced [42, page 182]. Moreover, the derivative terms are more sensitive to the high frequency noises and harmonic interferences and the noises may be amplified. For these reasons, the integral form of the models will be implemented. The numerical approximations used in this thesis are shown in Appendix C.

3.4.1 RL model identification method

The transfer function given by (3.1) leads to the relation (3.25) in the temporal domain:

$$V(t) = L_l \frac{dI(t)}{dt} + R_l I(t) \tag{3.25}$$

which by using the fact that $L_l = ml_l$, $R_l = mr_l$ and by integrating both sides leads to:

$$ml_l(I(t) - I(t_0)) + mr_l \int_{t_0}^{t} I(\tau)d\tau = \int_{t_0}^{t} V(\tau)d\tau \tag{3.26}$$

by renaming:

$$I(I)_{t_i} = \int_{t_0}^{t_i} I(\tau)d\tau \tag{3.27}$$

$$I(V)_{t_i} = \int_{t_0}^{t_i} V(\tau)d\tau \tag{3.28}$$

the matrix form $\mathbf{Ax} = \mathbf{b}$ gives finally:

$$\mathbf{A} = \begin{bmatrix} I_{t_1} - I_{t_0} & I(I)_{t_1} \\ I_{t_2} - I_{t_0} & I(I)_{t_2} \\ \vdots & \vdots \end{bmatrix} \tag{3.29}$$

$$\mathbf{b} = \begin{bmatrix} I(V)_{t_1} \\ I(V)_{t_2} \\ \vdots \end{bmatrix} \tag{3.30}$$

$$\mathbf{x} = \begin{bmatrix} ml_l \\ mr_l \end{bmatrix} \tag{3.31}$$

where the i^{th} row corresponds to the i^{th} sample.

3.4.2 RLC model identification method

The idea of using a π model of line for a distance protection algorithm is not new but has been already investigated a few decades earlier. In [43] written in 1979 a similar time-domain algorithm based on an RLC model of line was proposed but rapidly the impedance-based method with an RL model of line established itself in the power system protection domain. Some other algorithms based on the π model have been developed but in the frequency domain [44]. Recent works have proposed a time-domain algorithm based also on a π model of line but they present some limitations. For example the method proposed in [45] requires the measurement of the voltage and the current signal at both terminal of the transmission line. In [46] a single-end algorithm was proposed but the method implies an iterative process which is not suitable for an ultra-fast algorithm as explained above.

In this Section a solution breaking the previous limitations is proposed. The method implemented is a non-iterative time-domain algorithm based on the RLC Γ model of line and using the measurements of only one terminal of the line. The time-domain relation can be deduced from the transfer function (3.6) and gives:

$$C_l L_l \frac{d^2V(t)}{dt^2} + C_l R_l \frac{dV(t)}{dt} + V(t) = L_l \frac{dI(t)}{dt} + R_l I(t) \tag{3.32}$$

In this formulation there are 4 parameters to identify R_l, L_l, $C_l R_l$ and $C_l L_l$ but only 3 independent line parameters R_l, L_l and C_l. However, the use of a linear least-squares algorithm implies that the model is linear in parameters [47, page 2]. The linearity means that all the partial derivatives of the model represented by (3.32) with respect to each of the parameters R_l, L_l and C_l are independent of the parameters. It is obvious that the model presented above is not linear in parameters and the use of a linear least-squares method can lead to wrong results. Unfortunately, the use of a non-linear least-squares method involves an iteration process. This is not suitable for an ultra-fast algorithm because it implies that for each new sample an iteration process is necessary to update the solution. Moreover, the convergence is not always guaranteed for a non-linear least-squares method [48]. Assuming that there is no fault resistance the following transformations can be made:

$$C_l = m \cdot c'_l \tag{3.33}$$

$$L_l = m \cdot l_l = \frac{C_l}{c'_l} l_l \tag{3.34}$$

$$R_l = m \cdot r_l = \frac{C_l}{c'_l} r_l \tag{3.35}$$

The relation (3.32) becomes:

$$\frac{C_l^2}{c'_l} \left(l_l \frac{d^2V(t)}{dt^2} + r_l \frac{dV(t)}{dt} \right) + V(t) = L_l \frac{dI(t)}{dt} + R_l I(t) \tag{3.36}$$

which represents now a linear model defined by the three parameters C_l^2, L_l and R_l. If the fault resistance R_f is not equal to zero the relation (3.32) is not exactly correct because (3.35) becomes:

$$R_l = m \cdot r_l + R_f = \frac{C_l}{c'_l} r_l + R_f \tag{3.37}$$

If the fault resistance is introduced in the model it leads again to a non-linear model. The presence of a fault resistance may impact the identified parameters R_l and C_l^2/c'_l. The distance to fault must be deduced from the identified inductance L_l. In Section 3.5 the impact of a fault resistance on the identified parameters will be analysed in order to ensure that the identified inductance remains accurate enough. The relation (3.36) is the derivative form of the RLC model. As explained before it is better to limit the use of

numerical derivatives in the algorithm. As for the RL model, the integral form will be implemented. However, the relation (3.36) is integrated only once in order to limit the complexity of the least-squares system. It leads to the following relation:

$$\frac{C_l^2}{c_l'}\left[l_l\left(\frac{dV(t)}{dt}-\dot{V}(t_0)\right)+r_l\left(V(t)-V(t_0)\right)\right]+\int_{t_0}^{t}V(\tau)d\tau = L_l\left(I(t)-I(t_0)\right)+R_l\int_{t_0}^{t}I(\tau)d\tau \quad (3.38)$$

By renaming:

$$I(I)_{t_i}=\int_{t_0}^{t_i}I(\tau)d\tau \quad (3.39)$$

$$I(V)_{t_i}=\int_{t_0}^{t_i}V(\tau)d\tau \quad (3.40)$$

it finally leads to the matrix form $\mathbf{Ax}=\mathbf{b}$:

$$\mathbf{A}=\begin{bmatrix} l_l[\dot{V}_{t_1}-\dot{V}_{t_0}]+r_l[V_{t_1}-V_{t_0}] & -I_{t_1}+I_{t_0} & -I(I)_{t_1} \\ l_l[\dot{V}_{t_2}-\dot{V}_{t_0}]+r_l[V_{t_2}-V_{t_0}] & -I_{t_2}+I_{t_0} & -I(I)_{t_2} \\ \vdots & \vdots & \vdots \end{bmatrix} \quad (3.41)$$

$$\mathbf{b}=\begin{bmatrix} -I(V)_{t_1} \\ -I(V)_{t_2} \\ \vdots \end{bmatrix} \quad (3.42)$$

$$\mathbf{x}=\begin{bmatrix} m^2c_l' \\ ml_l \\ mr_l \end{bmatrix} \quad (3.43)$$

3.5 Validation of the identification methods

First of all the two parameters identification systems ((3.26) and (3.38)) developed before must be validated with a perfect simulation model of line corresponding exactly to the identification model of line. For these tests the following settings are used:

- the sampling rate of the algorithm f_{algo} is equal to 8 kHz.
- the window length of the algorithm is equal to 4 ms (32 samples).
- the starting time of the algorithm is taken 0.5 ms after the fault occurrence.
- a transmission line of 300 km is supplied by a strong source (SIR = 0.1). The line is defined by $r_l = 0.058\ \Omega$/km, $l_l = 0.955$ mH/km and $c_l = 0.0124\ \mu$F/km (only for the RLC model).

The relative error given by (3.44) permits to evaluate the accuracy of the identified distance to fault. For the relay applications another significant indicator is the error given

by (3.45) of the identified distance to fault compared to the total line length m_{total}. This information is useful to define a secured reaching distance and to avoid the over-reaching of the distance protection.

$$e_{rel} = \frac{m_{actual} - m_{identified}}{m_{actual}} \cdot 100\ (\%) \tag{3.44}$$

$$e_{tot} = \frac{m_{actual} - m_{identified}}{m_{total}} \cdot 100\ (\%) \tag{3.45}$$

3.5.1 RL method validation

Fig. 3.8 shows the electrical circuit simulated to test the RL identification algorithm. After the closing of the breaker the model seen at the relay location corresponds to a perfect RL model of line governed by (3.26).

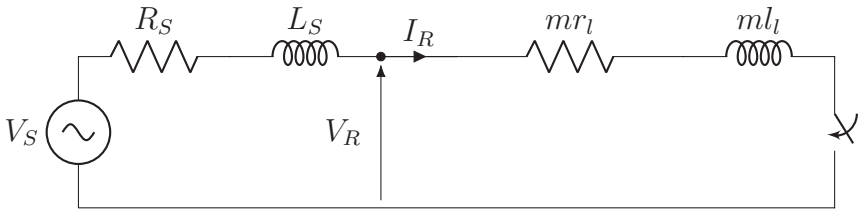

Figure 3.8: Simulation of a simple RL faulted line

Fig. 3.9 shows the voltage and the current signals at the relay location. The voltage drop and the current increase appear at t = 0 ms. The RL model of line involves only the fundamental frequency and the transient DC component. In this example a close-in fault at 30 km is shown in order to have a significant voltage drop.

The RL identification method implies the identification of two parameters of line. The distance to fault is deduced from (3.31) as follows:

$$\begin{cases} m_1 = x_1/l_l & (3.46) \\ m_2 = x_2/r_l & (3.47) \end{cases}$$

Fig. 3.10 shows the relative errors of the identified distance to fault deduced from the inductance and the resistance of the faulted line with the RL identification model. The RL transmission line simulated has a length going from 3 km to 285 km. The relative errors are very small and it can be concluded that both R and L parameters are very well identified.

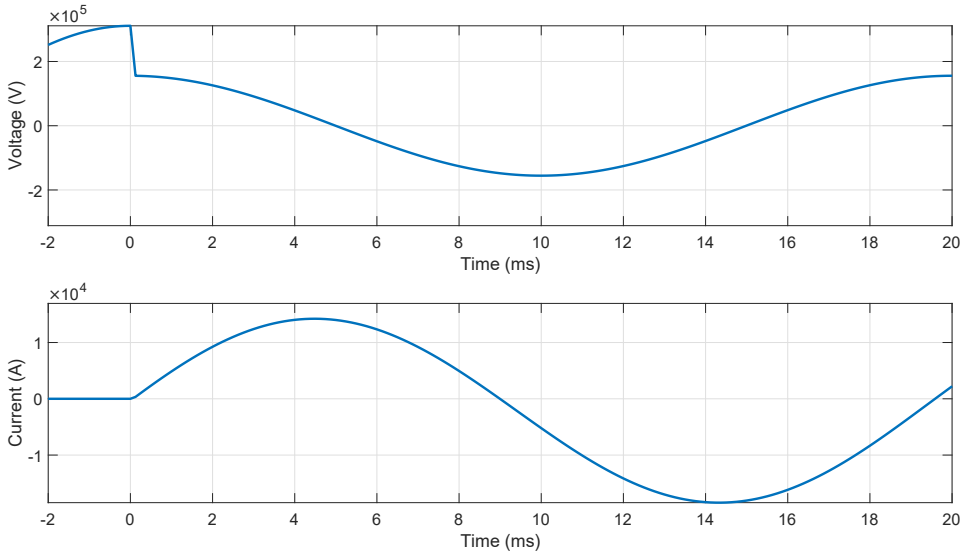

Figure 3.9: Voltage and current signals for an RL faulted line of 30 km

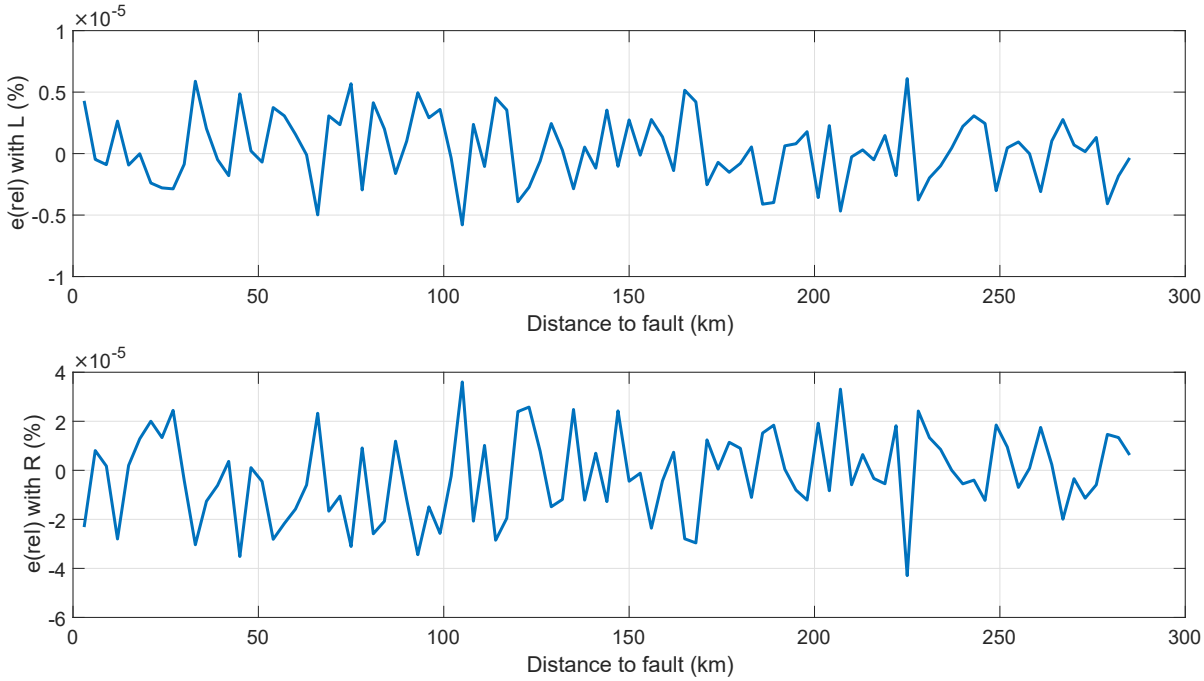

Figure 3.10: Relative errors of the distance to fault deduced from the identified inductance and resistance of an RL transmission line

3.5.2 RLC method validation

Bolted fault

Fig. 3.11 shows the electrical circuit simulated to test the RLC Γ identification algorithm. First of all a bolted fault is tested because this assumption has been made in order to

construct a linear model in parameters. The impact of a resistive fault will be discussed in the next section.

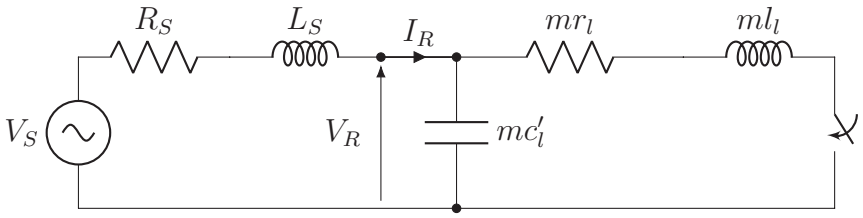

Figure 3.11: Simulation of a simple RLC Γ faulted line

Fig. 3.12 shows the voltage and the current signals at the relay location. There is a high frequency signal in addition to the fundamental frequency and the transient DC component. In this example the fault is located at 285 km.

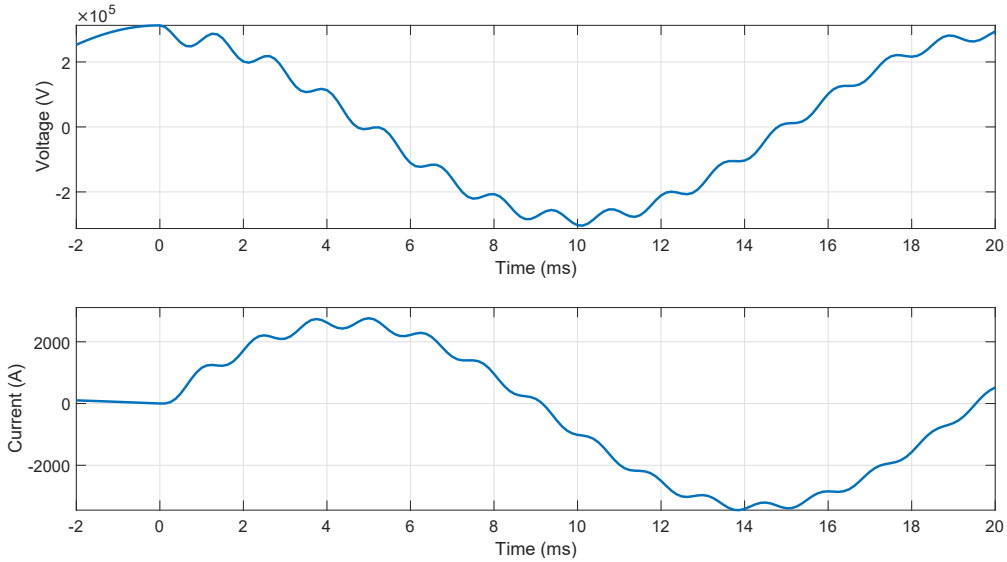

Figure 3.12: Voltage and current signals for an RLC Γ faulted line of 285 km

The RLC identification method implies the identification of three parameters of line. The distance to fault is deduced from (3.43) as follows:

$$\begin{cases} m_1 = \sqrt{x_1/c'_l} & (3.48) \\ m_2 = x_2/l_l & (3.49) \\ m_3 = x_3/r_l & (3.50) \end{cases}$$

The RLC model of line involves very high frequencies for close-in faults or short lines as shown in Fig. 3.5. Indeed, the resonance frequency may be higher than 10 kHz. With a sampling rate of only 8 kHz, an anti-aliasing filter must be used. However, the use of a low-pass filter may have an impact on the least-square algorithm. For this reason the

validation of the method is first done with a sampling rate of 1 MHz in order to accurately simulate the high frequency components and to avoid the use of a filter. As shown in Fig. 3.13 the three parameters R, L and C are well identified. However, at 1 MHz 4000 samples are used for a window of 4 ms. It is therefore necessary to test the algorithm with a lower sampling rate of 8 kHz but while keeping in mind the possible effects of the anti-aliasing filter.

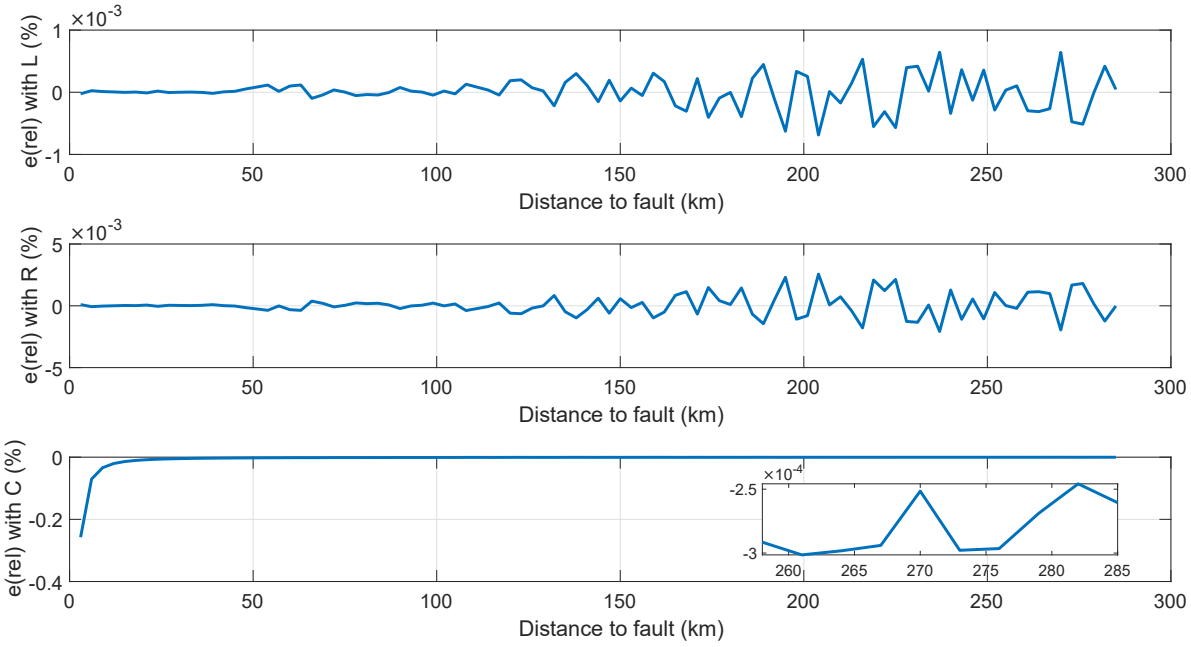

Figure 3.13: Relative errors of the distance to fault deduced from the identified inductance, resistance and capacitance of an RLC Γ transmission line with a sampling rate of 1 MHz

According to the Nyquist–Shannon theorem an anti-aliasing filter must be used before the down-sampling at 8 kHz. A deep analysis to find the best implementation of the filtering process will be done in Chapter 7. At this step the default low-pass filter given by the decimation function of Matlab Software is used [49], [50]. It is an Infinite Impulse Response (IIR) Chebyshev Type 1 low-pass filter. The order of this filter is equal to 6 and the cut-off frequency is set at 3200 Hz. The characteristics of the filter are shown in Fig. 3.15. In order to take into account the delay added by the filtering process the starting time is set at 1 ms after the fault occurrence.

The relative errors on the distance to fault deduced from the three identified parameters are shown in Fig. 3.14. The following conclusions can be highlighted:

- the errors on the identified distance to fault are greater than for the RL identification method. Indeed, for the RLC model an anti-aliasing filter is required before the down-sampling. As it will be shown next, the IIR filter has an impact on the transient behaviour of the signals. However, the magnitude of the errors remains acceptable.

- for close-in faults the identified capacitance is not correct. The high frequencies seen in the signals are very high and cannot be accurately identified with a sampling rate of 8 kHz because these high frequencies are removed by the filter. This conclusion is very important because it implies that the identified capacitance of the line cannot be used directly to identify the distance to fault in all the cases.

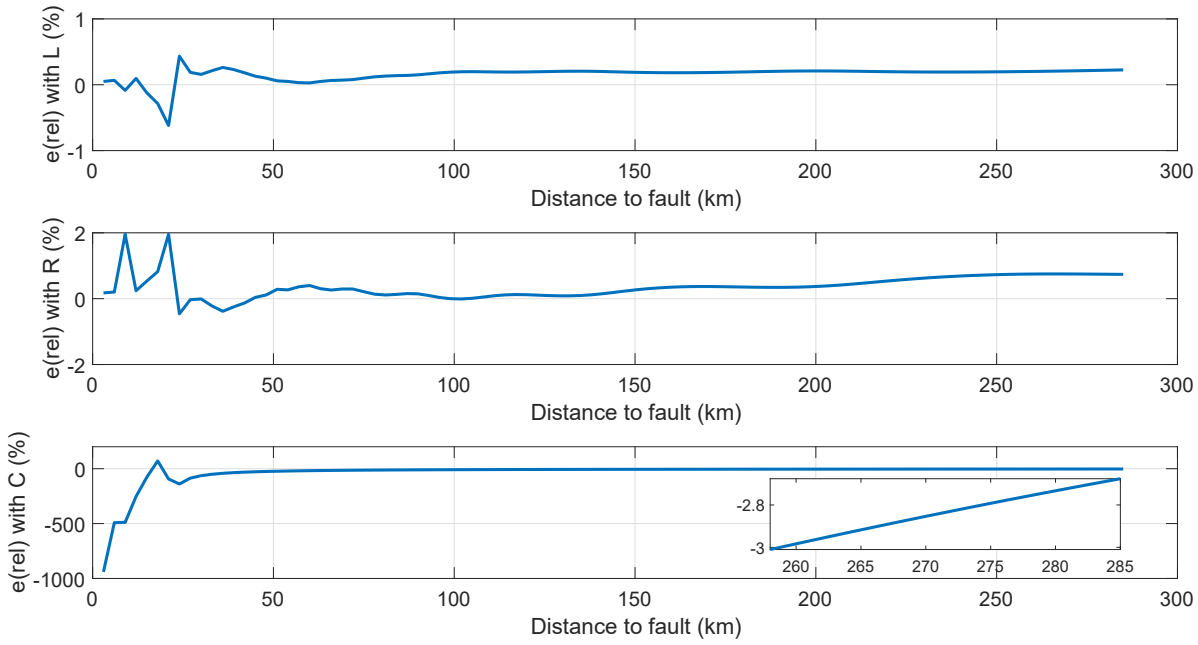

Figure 3.14: Relative errors of the distance to fault deduced from the identified inductance, resistance and capacitance of an RLC Γ transmission line with a sampling rate of 8 kHz

Some considerations must be made about the aliasing phenomenon. To avoid totally the aliasing of the signals one of the two following assumptions must be respected [51]:

- the signal is band-limited in the frequency domain.
- the anti-aliasing filter is an ideal low-pass filter without a transition zone between the pass-band and the stop-band.

However, none of these two assumptions is true for a real-world system. Indeed, the first assumption implies that the signals are not time-limited [52] and the second assumption implies that the order of the filter is infinite.

Fig. 3.15 shows the frequency and the step response of the IIR anti-aliasing filter used above. The attenuation is around 11 dB close to the Nyquist frequency as shown in the figure. The transition band is not very narrow because the order of the filter is small. However, the increase of the order will also increase the phase delay which is around 0.2 ms. The phase delay profile is very flat in the pass-band but it varies close to the cut-off frequency. The step response of the anti-aliasing filter is oscillating during the first

samples. These oscillations will perturb the voltage and the current signals during the first samples used by the least-squares method and will therefore impact the accuracy of the identified parameters.

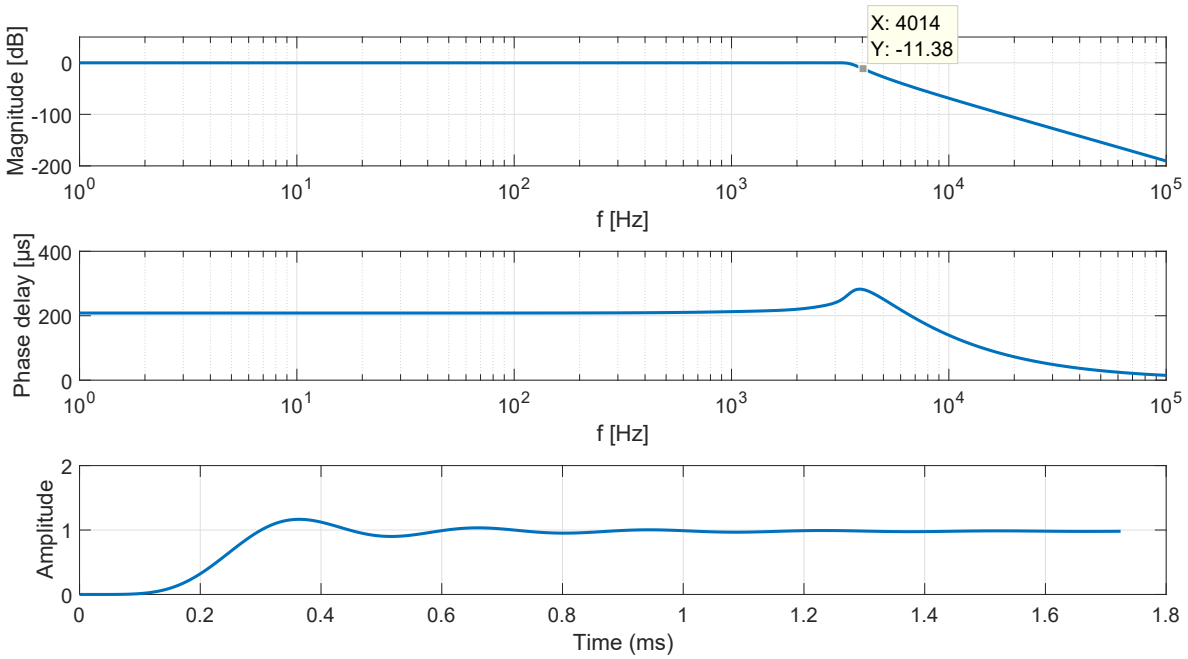

Figure 3.15: Magnitude of the frequency response (top), phase delay of the frequency response (middle) and step response (bottom) of an IIR Chebyshev Type 1 low-pass filter. The order is equal to 6 and the cut-off frequency is equal to 3200 Hz

Resistive fault

A bolted fault was assumed in order to construct a linear model of line. However, the relation (3.36) is not correct when a fault resistance is involved. It is therefore necessary to verify the impact of a fault resistance on the 3 identified parameters of the faulted line. A fault resistance of 50 Ω is put at the end of the RLC transmission line tested above. The value of the fault resistance is removed from the identified resistance in order to keep only the error due to the identification algorithm. At this step a single-end voltage source is tested. The possible impact of the fault resistance on the identified parameters is therefore only due to the linearisation of the model of line and not to the well-known remote injection impact which will be discussed later.

Fig. 3.16 shows the comparison of the results obtained with a bolted fault and a resistive fault. The distance to fault identified from the three parameters R, L and C are presented. The errors are given in percent of the total line length. The additional error due to the resistive fault is limited for the identified inductance and capacitance of the line. However, the impact on the identified resistance of the line cannot be neglected. Even after subtracting the fault resistance the error remains high. It is not an issue for

the protection relay algorithm because the distance to fault is not deduced directly from the identified resistance. However, it is important to keep in mind that the accuracy of the identified resistance is not very good.

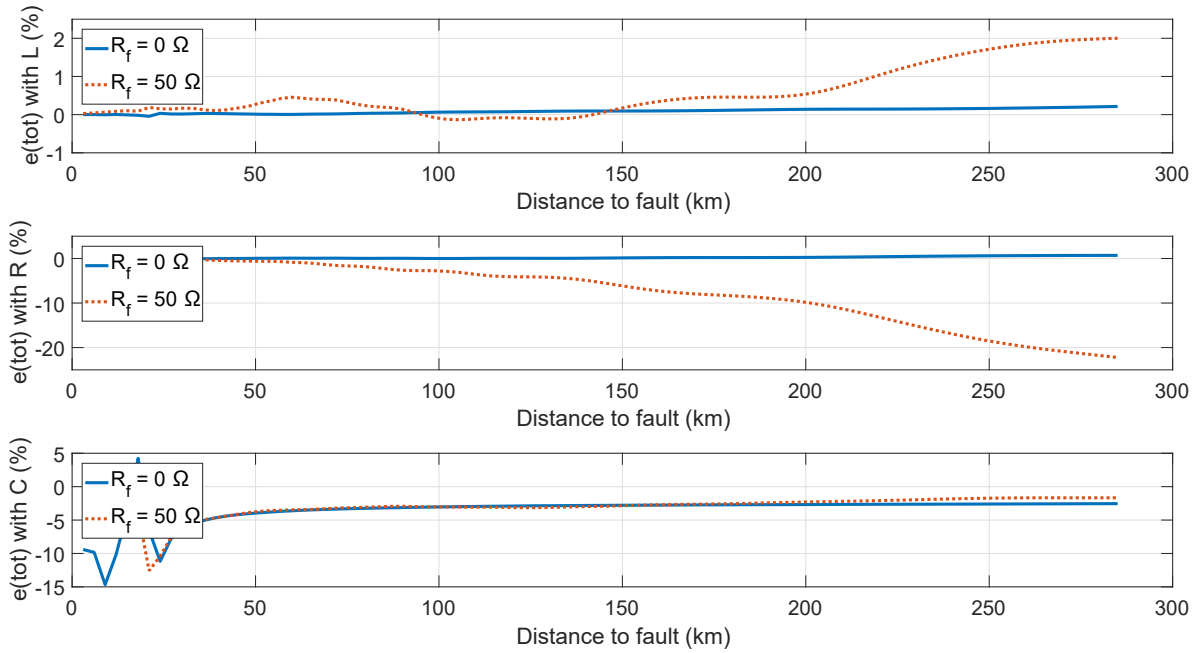

Figure 3.16: Relative errors (in % of the line length) of the distance to fault deduced from the identified inductance, resistance and capacitance of an RLC Γ transmission line. Comparison between a bolted fault and a resistive fault of 50 Ω

3.6 Source Impedance Ratio impact

In Section 2.4, it has been shown that an RLC model can fit a Bergeron model of line until the first resonance frequency. A low-pass filter is used in order to keep only this frequency band. If all frequency content of the voltage and the current is included in this frequency band, all line parameters can be accurately identified. However, the high frequencies excited by the system do not correspond to the resonance frequency but depend on the complete power system network. Indeed, it will be shown in this section that the SIR has a big impact on the frequency content of the signals. This phenomenon is also problematic for the classical impedance-based distance protection algorithms [53]. When the SIR increases the high frequencies get closer to the fundamental frequency and are therefore more difficult to filter.

Fig. 3.17 shows the signals of a faulted Γ model of line of 300 km with a fault located at the middle of the line. The voltage and the current are shown for a strong source (on the left) and a weak source (on the right). The resonance frequency at 150 km evaluated thanks to (3.7) is equal to 435.8 Hz.

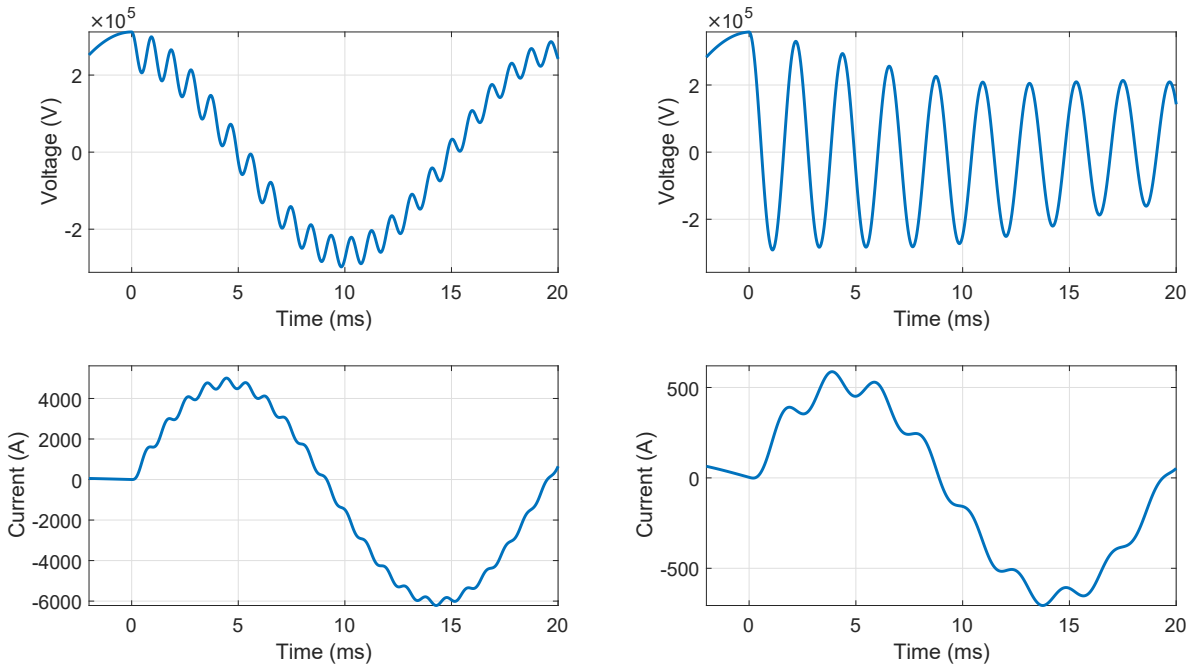

Figure 3.17: Voltage and current signals for a Γ model of line of 300 km faulted at the middle. SIR equals to 0.1 (on the left) and SIR equals to 5 (on the right)

For the strong system the fundamental frequency is dominant for both voltage and current signals. The high frequency is about 1080 Hz and is therefore very far from the resonance frequency. For a strong power network the high frequencies will be always filtered by the low-pass filter. The capacitance of the line cannot be accurately identified in this case. The RL algorithm can be used if the line is not too long but it may become unsuitable because the high frequencies are not filtered enough if the line is too long.

For the weak system the steady-state frequency is almost zero for the voltage. The high frequency is dominant and is about 457 Hz. This frequency is close to the resonance frequency. The high frequencies will not be filtered by the low-pass filter in this case. The capacitance of the line can be identified by the RLC algorithm. However, the RL algorithm is not accurate for this kind of network because it does not include the high frequency behaviour in its model.

A faulted line signal may be composed by different components: the transient DC component, the fundamental frequency component and the transient high frequencies components. As seen before in Fig. 3.17, the frequency content present in the faulted signals depends on the complete power network. The accuracy of the three identified parameters may also depend on this frequency content. Fig. 3.18 shows the impact of the line parameters variation on the transfer function of the Γ model. A reference transfer function is compared with the transfer function obtained if one of the three parameters is increased by a factor of 1.5. It appears that a variation of the inductance will impact the transfer function in a wide area from very low frequencies to the resonance frequency.

A variation of the resistance will impact mostly low frequencies. Finally, the capacitance changes the resonance frequency and the behaviour of the higher frequencies. It explains why the capacitance is not well identified when the high frequencies are filtered.

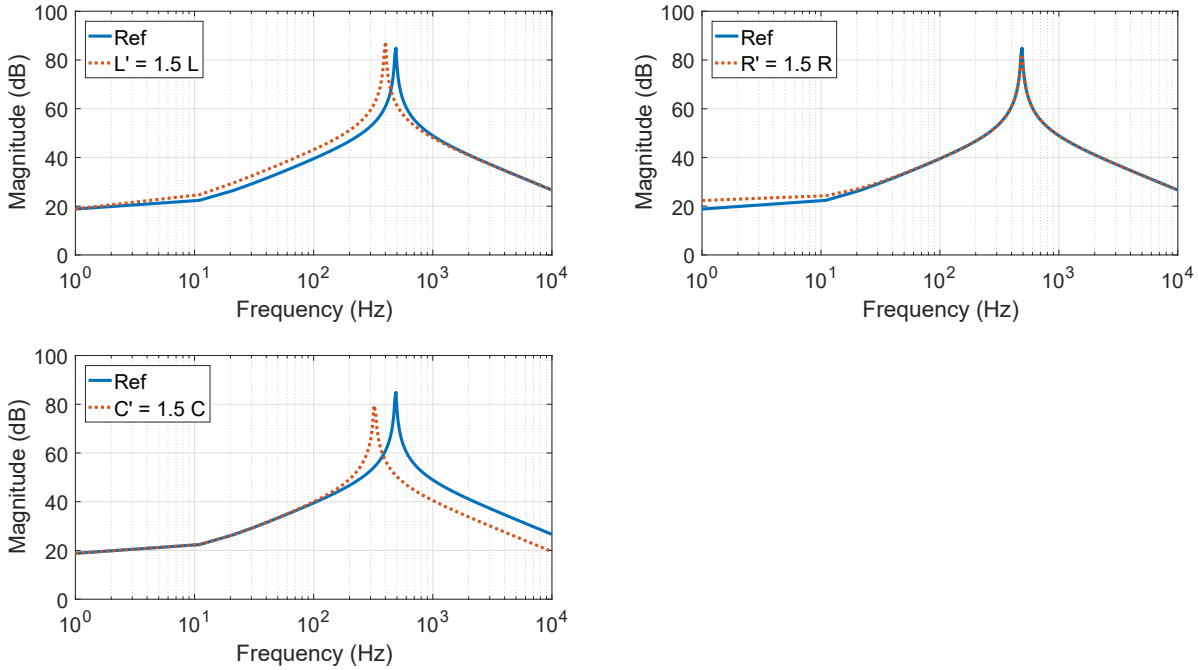

Figure 3.18: Impact of the line parameters variation on the transfer function of the Γ model of line

3.7 Distributed line model

In the previous sections the RL and the RLC identification methods have been validated for an RL and an RLC model of line respectively. In this section both methods will be tested for a distributed parameters model of line. Only the Bergeron model is tested in this section. As explained before the J. Marti model of line will be tested for a three-phase model of line because the frequency impact on the line parameters is more significant for the zero components.

Fig. 3.19 shows the voltage signal of a faulted Bergeron model of line of 150 km. On the top of the figure the signal is simulated with a sampling rate F_S of 1 MHz (corresponding to a simulation step of 1 μs). The fault occurs at 0 ms but the voltage seen at the relay location drops after about 0.5 ms due to the propagation delay of the electromagnetic travelling waves. On the bottom of the figure the same signal passes through the IIR anti-aliasing filter presented before in order to be down-sampled at 8 kHz. Moreover, it was shown in Section 3.2.2 that a low-pass filter is necessary to remove the frequency content of the signals after the resonance frequency of the adapted π model of line. The

filter implemented here is a Finite Impulse Response (FIR) Hamming low-pass filter. The order of this filter is equal to 17 and the cut-off frequency is set at 600 Hz. The cut-off frequency depends on the length of the line to protect. The cut-off frequency must be lower than the resonance frequency of the complete line. The objective is to ensure a good accuracy of the model of line used for the identification until the end of the line and therefore to avoid the over-reaching. A complete analysis of the filters implemented in this thesis will be done in Chapter 7. As the low-pass-filter generates an extra delay (about 1 ms here), the starting time of the algorithm is taken at 2 ms. This starting time must take into account the delays due to the anti-aliasing filter, the low-pass filter and the propagation phenomena of the travelling waves.

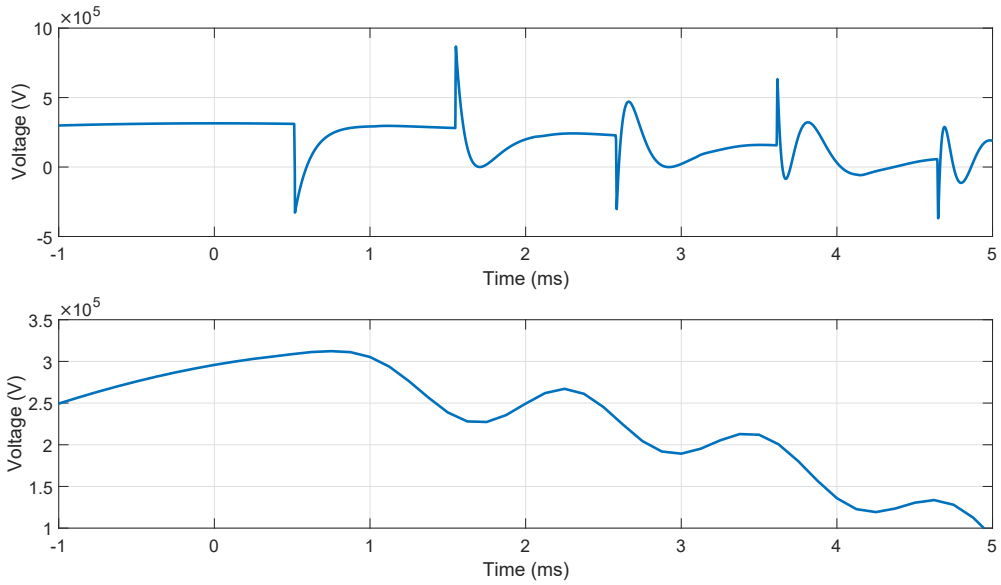

Figure 3.19: Voltage signal for a Bergeron faulted line of 150 km not filtered (above) and filtered at 600 Hz (below)

Fig. 3.20 show the errors on the identified distance to fault for a line of 100 km for a strong system (SIR equal to 0.1). Both RL and RLC identification algorithms are tested. The following conclusions can be highlighted:

- for a strong source the accuracy obtained on the identified inductance and resistance is quite similar for both RL and RLC identification methods. The errors are less than 1% of the line with the identified inductance.

- the identified capacitance with the RLC algorithm is not well identified in any tested distances to fault. For the close-in faults it was already explained that the resonance frequency was very high. However, for the remote-end faults it is due to the fact that, for a very strong system network, the high frequencies present in the signals are much higher than the resonance frequency (see Section 3.6) and are therefore also

filtered by the low-pass filter. It was shown in Section 3.6 that a good estimation of the capacitance of the line implies the presence of the high frequencies content.

- it appears that the RLC algorithm does not show any advantage compared to the RL algorithm in this case. Indeed, for a short line or a long line with a very strong system network the RL model of line is accurate enough because the high frequencies are not visible by the relay protection because of the filtering.

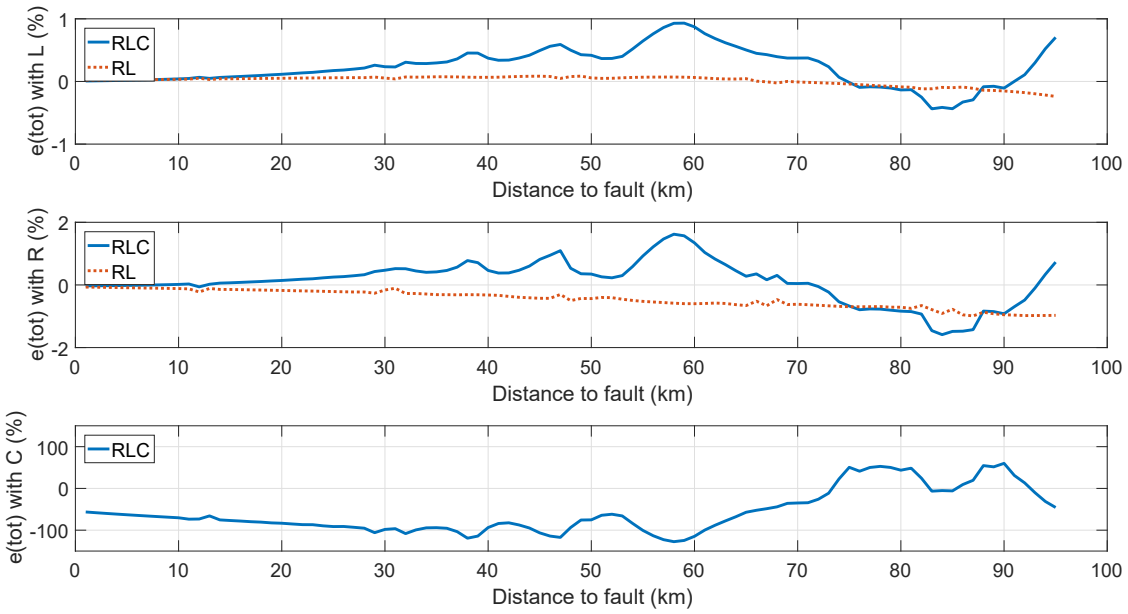

Figure 3.20: Relative errors (in % of the line) of the distance to fault for a Bergeron model of line of 100 km with the RLC and the RL identification algorithm (SIR = 0.1)

Nevertheless, the RL identification algorithm reaches its limitations if the line length increases or if the power system is too weak. Indeed, in these cases the high frequencies content cannot be neglected any more and would even be dominant. To avoid to increase the filter specifications and therefore the delay it becomes necessary to use a more accurate model of line that can take into account the high frequencies content.

Fig. 3.21 shows the results obtained with the same network but here the SIR is equal to 5. In this case it appears clearly that the RLC algorithm remains very accurate for both inductance and resistance identification. Moreover, the distance to fault identified from the capacitance of the line becomes very accurate from about 55% of the line length. In fact, for a weak power system the high frequency present in the signals is close to the resonance frequency of the Γ model. For the close-in faults, the capacitance cannot be well identified as explained before. With the RL algorithm, the errors begin to increase significantly from 65% of the line length. The errors at the end of the line are highlighted in the figures to facilitate the comparison.

Finally, Fig. 3.22 shows the results obtained for a long line of 300 km and a strong network. It appears clearly that the RL identification method is no more sufficient to identify the very long distances to fault while the RLC identification method still gives quite good results. For this last test the cut-off frequency must be decreased to 300 Hz.

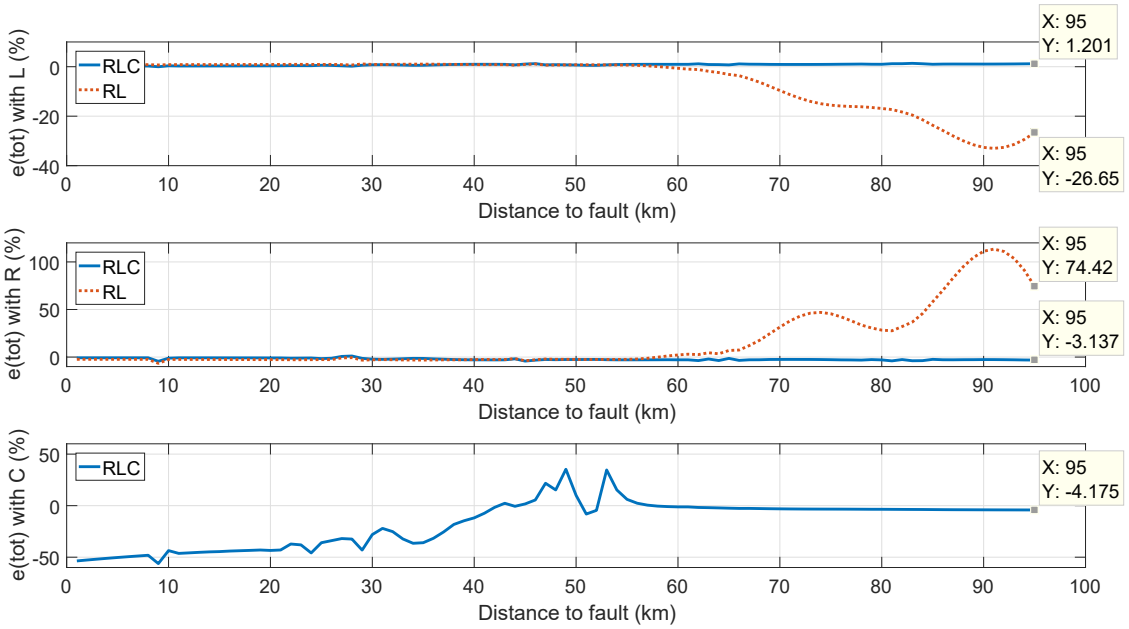

Figure 3.21: Relative errors (in % of the line) of the distance to fault for a Bergeron model of line of 100 km with the RLC and the RL identification algorithm (SIR = 5)

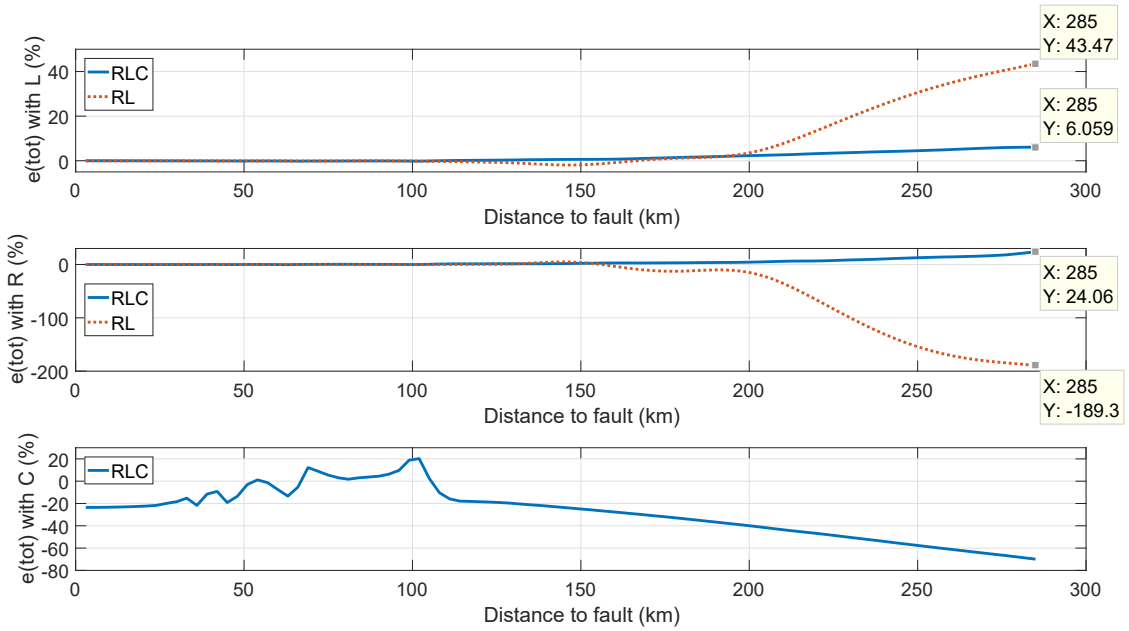

Figure 3.22: Relative errors (in % of the line) of the distance to fault for a Bergeron model of line of 300 km with the RLC and the RL identification algorithm (SIR = 0.1)

3.8 Remote injection impact

For an interconnected grid there is a voltage source at both ends of the transmission line. In this case the influence of the load-transfer on the line must be considered. The transfer of the power across the line requires a phase shift between the two voltage sources. If the transmission distances are not too high this phase shift is relatively small (10° - 15°) [34]. For a very large distance the transmission angle may reach 60°. The equivalent circuit of such a system is shown in Fig. 3.23. For more simplicity an RL model of line is considered.

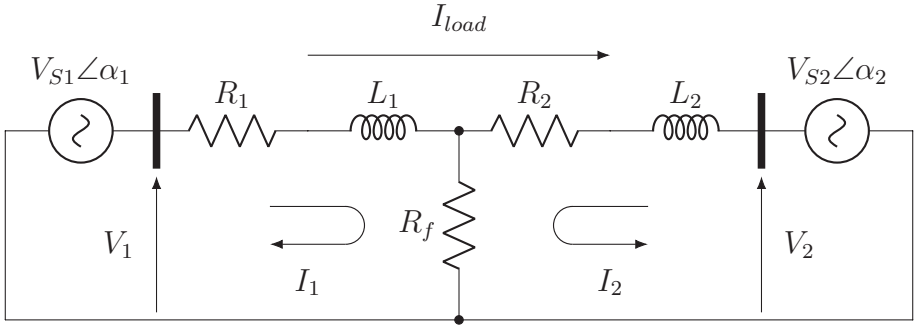

Figure 3.23: Double in-feeds RL transmission line. Impact of the remote injection

The voltage at the relay location is given by (3.51). If the fault resistance is not equal to zero, the impedance seen by the relay is therefore not only the impedance of the faulted line. The inductance seen by the relay may be under or over-estimated. It may lead to over-reaching or under-reaching depending on the load-transfer direction. The importance of the impact will depend on the value of the fault resistance R_f and on the current I_2. The current I_2 will be imposed by the fault position and the phase shift. The impact of the remote injection is greater for remote-end faults than for close-in faults because in this last case the current I_1 is more significant than the current I_2. It is therefore impossible to identify the actual faulted line impedance. In both cases the faulted line resistance seen by the relay is higher than expected. It is possible to avoid over-reaching by using a maximum resistance threshold. This phenomenon is well known for the classic relays [54].

$$\begin{aligned} V_1 &= R_1 I_1 + L_1 \frac{dI_1}{dt} + R_f(I_1 + I_2) \\ &= (R_1 + R_f) I_1 + L_1 \frac{dI_1}{dt} + R_f I_2 \end{aligned} \tag{3.51}$$

3.9 Conclusions

In this chapter a linear least-squares method has been developed to identify the parameters of the faulted transmission line. Two models were implemented for the identification

algorithm: the RL and the RLC Γ model. The Γ model was improved in order to fit better a distributed parameters model of line until the first resonance frequency. An integral form was implemented for the two models to limit the use of a derivative function which may amplify the noises present in the signals. The different methods were first validated with a perfect simulation model corresponding to the identification model. In a second step the methods were tested with a Bergeron model of line.

The RLC algorithm permitted to accurately identify the inductance of the faulted line for short and very long lines in all the tested cases (strong and weak power systems, close-in and remote faults). The maximum error was around 1% of the total line length for a line of 100 km and around 6% for a line of 300 km. The identified capacitance was not accurate for a strong power system and for close-in faults because of the filtering of the high frequencies. For this reason this parameter will not be used to estimate the distance to fault.

The RL algorithm permitted to accurately identify the inductance of the faulted line but only for a strong power system (less than 1% error of the total line length). However, the RL model does not permit to take into account the high frequencies. In the case of a weak power system the high frequencies are not sufficiently filtered and impact a lot the identification of the parameters (maximum error around 26% of the total line length). The same conclusions were made for a long line of 300 km (maximum error around 43% of the total line length). The RL algorithm would give better results for weak power systems and very long lines if the filtering of the high frequencies was improved. However, it would imply a higher filter order and thus an additional extra-delay.

In the next chapter a mathematical analysis of the least-squares method and the residuals will be performed.

Chapter 4

Least-Squares estimation method

4.1 Introduction

In Chapter 3 the transmission line parameters identification algorithms led to a multiple linear regression system $Ax = b$. The mathematical resolution was done using a linear least-squares estimation method. The linear least-squares method has three important advantages [47]:

- the method does not need any prior knowledge about the distribution of the dependent variables b (in contrary to the method of maximum likelihood).

- the least-squares estimators of the vector x are the Best Linear Unbiased Estimators (BLUE)[1].

- the linear least-squares method does not involve an iteration process contrary to the non-linear least-squares method.

In Section 4.2 the mathematical formulation of the Ordinary Least-Squares (OLS) method will be developed. It will be shown in Section 4.3 that an ill-conditioned model may lead to numerical instabilities. In Section 4.4 a Recursive Least-Squares (RLS) method will be implemented in order to improve the efficiency of the solving process. The different assumptions and a residual analysis will be done in Section 4.5 in order to define some blocking conditions if the results obtained are not reliable. Finally, the different elements implemented in this chapter will be tested with a Bergeron model of line in Section 4.6.

[1]The Gauss-Markov theorem states that if a linear regression model satisfies some particular assumptions (defined in Section 4.5.1), then the ordinary least-squares regression gives unbiased estimators that have the smallest variance of all possible linear estimators [55]

4.2 Ordinary Least-Squares

The OLS method optimizes the solution of the problem so that the sum of the squares of the residuals is minimal. If we call a_i, b_i and x_i respectively the i^{th} lines of the A, b and x matrices, m and n respectively the number of parameters to identify and the number of samples, the condition is equivalent to finding the vector x such that the function:

$$f = \sum_{i=1}^{n} \left(\sum_{j=1}^{m} a_{ij} x_j - b_i \right)^2 \tag{4.1}$$

is minimal. Equation (4.1) can be written in a matrix form. The goal is therefore to minimize the objective function $S(x)$:

$$S(x) = \|Ax - b\|_2^2 \tag{4.2}$$

The relation (4.2) is equivalent to:

$$\begin{aligned} S(x) &= (Ax - b)^T (Ax - b) \\ &= A^T x^T Ax - A^T x^T b - b^T Ax + b^T b \end{aligned} \tag{4.3}$$

$A^T x^T b$ and $b^T Ax$ are scalars and hence equal to their transpose:

$$S(x) = A^T x^T Ax - 2A^T x^T b + b^T b \tag{4.4}$$

Finally, by deriving with respect to x and equalling to 0 it leads to:

$$2A^T Ax - 2A^T b = 0 \Leftrightarrow x = (A^T A)^{-1} A^T b \tag{4.5}$$

The relation (4.5) gives the equation which is being solved when using an OLS method. If (4.5) is solved with a matrix inversion it may lead to some numerical errors if the $A^T A$ matrix is ill-conditioned as shown in the next section.

4.3 Condition number

The condition number can be seen as "how an error in the entries of A influences the results of the system $AX = B$". It can be proved that the condition number $\kappa(A)$ of a rectangular matrix A may be expressed as [56]:

$$\kappa(A) = \|A^+\| \cdot \|A\| \tag{4.6}$$

where A^+ is the Moore–Penrose inverse matrix defined by $(A^T A)^{-1} A^T$. The norm may be arbitrarily chosen. For a n-vector **v** the Euclidean **p-norm** is defined as follows [56]:

$$\|v\|_p = \left(\sum_{i=1}^{n} v_i^n\right)^{1/p} \tag{4.7}$$

The matrix norm corresponding to a given vector norm is defined by:

$$\|A\|_p = \max_{x\neq 0} \frac{\|Ax\|_p}{\|x\|_p} = \max_{\|x\|_p=1} \|Ax\|_p \tag{4.8}$$

where $\mathbf{x}$ is any vector $\in \Re^n$. A too high condition number leads to an ill-conditioned matrix, which means that the solution is very sensitive to any errors in the entries of the matrix. A too high condition number can be defined as follows [57]:

$$log(\kappa(A)) > C \tag{4.9}$$

where C is the precision of the matrix entries related to the precision of the measurements. Fig. 4.1 shows the logarithm of the condition number for different distances to fault. The least-squares algorithm is tested here with the Bergeron model of line of 100 km studied in Section 3.7. Both RL and RLC identification methods are tested.

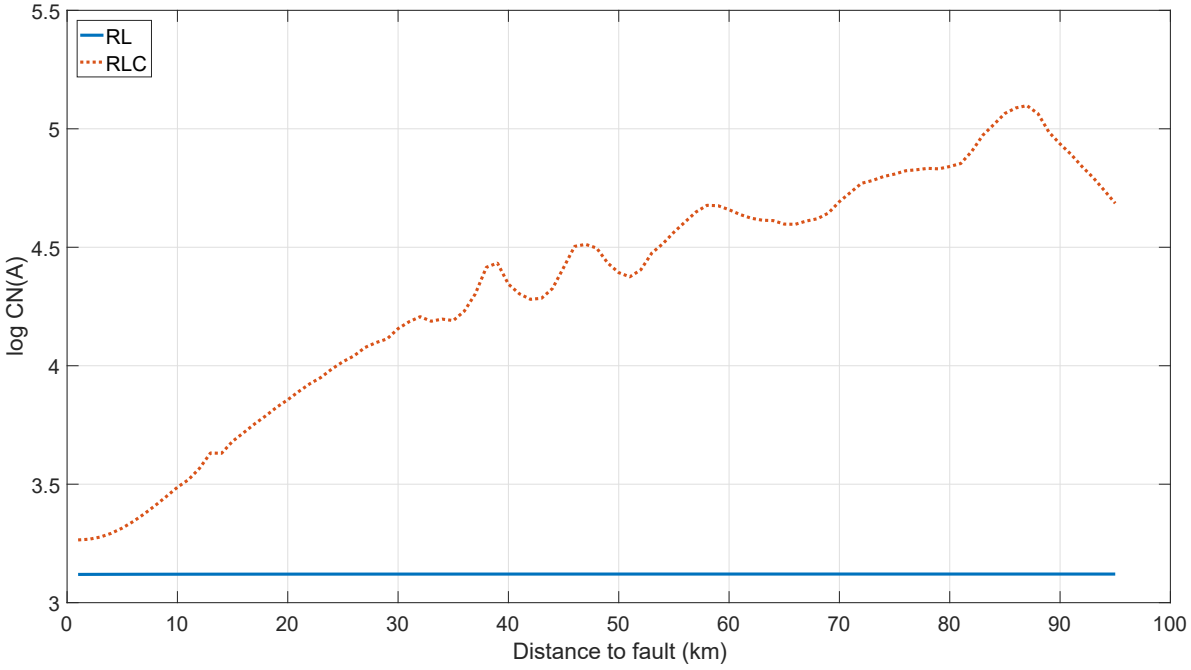

Figure 4.1: Condition number for different distances to fault of a Bergeron model of 100 km for the RL and RLC identification method

The following observations can be drawn:

- the RLC identification method involves much higher condition numbers. This can be explained by noting that in (3.36) there is a second derivative term that is involved in the matrix A. As a consequence, the different columns have different orders of

magnitude. In (3.25) however, only a first derivative is used, leading to a much better conditioned matrix.

- the condition numbers of the RL method are less fluctuating. Indeed, (3.29) involves only terms relative to the current which has a slower dynamic than the voltage. This may be explained by the high inductance and the low capacitance involved in the transmission lines.

In conclusion, the matrix A is more ill-conditioned with the RLC identification method than with RL identification method. As a consequence, the results are more sensitive to the accuracy of the entries of the matrix. It is also possible to solve the system (4.5) without the use of a matrix inversion and therefore avoid the problem of ill-conditioning presented above. It can be achieved by different methods like the Singular Value Decomposition (SVD) for example [56]. In the next section a more efficient way to solve a linear least-squares problem will be presented.

4.4 Recursive Least-Squares

4.4.1 Description

One of the main issues of the least-squares method introduced before and described in (4.5) is the inversion of the matrix $A^T A$. This inversion may lead to numerical errors if the matrix is ill-conditioned. As mentioned before it is possible to use some factorization algorithms that permit to avoid this inversion. However, in all the cases when a new sample is available, it is necessary to go all the way back to the first sample and to solve the complete least-squares system again. This solution is not suitable for a real-time application because the computational complexity increases with the number of samples.

The RLS algorithm which is a recursive implementation of the OLS method permits to find the estimators recursively. It means that each new sample is used to update the previous solution. It is not necessary to use all the complete set of data to update the estimation of the unknowns. The number of algebraic operations and required memory locations is reduced from $\mathcal{O}(m^3)$ to $\mathcal{O}(m^2)$ per cycle (where m is the number of estimators) [58]. It was demonstrated in [59] that the RLS method with an exponential forgetting factor is exponentially convergent. A complete description of the RLS algorithm can be found in [60] and is also summarized below.

The objective of the RLS algorithm is to estimate the vector x of the system $Ax = b$, respecting the least-squares criterion described in Section 4.2, but on-line, which means that each sample coming in the algorithm should update the value of the estimated x. Hence, the matrices are split in n vectors corresponding to the n samples: $A =$

$a(1-1,...,m),\ a(2-1,...,m),\ ...,\ a(n-1,...,m),\ b = b(1),\ b(2),\ ...,\ b(n)$. The m final values of x (where m is the number of parameters) should minimize the squared error:

$$\epsilon(n) = \sum_{i=1}^{n} \beta(n,i)[e(i)]^2 \tag{4.10}$$

where $\beta(n,i)$ is a forgetting factor decreasing the influence of old data, usually written:

$$\beta(n,i) = \lambda^{n-i} \tag{4.11}$$

with $(0 < \lambda < 1)$ and $e(i)$ is the error defined as:

$$e(i) = b(i) - \sum_{k=0}^{m-1} x_k(n)a(i-k) \tag{4.12}$$

i is the index counting the number of samples and k is counting the number of parameters in x. The criterion can hence be written as:

$$\epsilon(n) = \sum_{i=1}^{n} \lambda^{n-i} \left[b(i) - \sum_{k=0}^{m-1} x_k(n)a(i-k) \right]^2 \tag{4.13}$$

or, if

$$\begin{cases} a'(i-k) = \sqrt{\lambda^{n-i}}a(i-k) & (4.14) \\ b'(i) = \sqrt{\lambda^{n-i}}b(i) & (4.15) \end{cases}$$

it leads to:

$$\epsilon(n) = \sum_{i=1}^{n} [b'(i) - \sum_{k=0}^{m-1} x_k(n)a'(i-k)]^2 \tag{4.16}$$

This reformulation reveals the well-known least-squares formulation, in the quantities a'_{ik} and b'_i. The solution, as developed in (4.5), can be written as:

$$\begin{aligned} x(n) &= \left(\sum_{i=1}^{n} \lambda^{n-i} a(i)a(i)^T \right)^{-1} \sum_{i=1}^{n} \lambda^{n-i} a(i)b(i) \\ &= [\Phi(n)]^{-1}\Psi(n) \end{aligned} \tag{4.17}$$

The idea is to find a recursive way to compute $[\Phi(n)]^{-1}\Psi(n)$. The variables $\Phi(n)$ and $\Psi(n)$ should then be expressed as a function of $\Phi(n-1)$ and $\Psi(n-1)$.

$$\begin{aligned} \Phi(n) &= \sum_{i=1}^{n} \lambda^{n-i} a(i)a(i)^T \\ &= \lambda \sum_{i=1}^{n-1} \lambda^{n-1-i} a(i)a(i)^T + a(n)a(n)^T \\ &= \lambda\Phi(n-1) + a(n)a(n)^T \end{aligned} \tag{4.18}$$

$$\begin{aligned}\Psi(n) &= \sum_{i=1}^{n} \lambda^{n-i} a(i)b(i) \\ &= \lambda \sum_{i=1}^{n-1} \lambda^{n-1-i} a(i)b(i) + a(n)b(n) \\ &= \lambda\Psi(n-1) + a(n)b(n)\end{aligned} \tag{4.19}$$

The end of the development, shown in [61], finally gives:

$$x(n) = x(n-1) + k(n)\alpha(n) \tag{4.20}$$

$$k(n) = \frac{\lambda^{-1}P(n-1)a(n)}{1 + \lambda^{-1}a^T(n)P(n-1)a(n)} \tag{4.21}$$

$$\alpha(n) = b(n) - a(n)^T x(n-1) \tag{4.22}$$

$$P(n) = \lambda^{-1}P(n-1) - \lambda^{-1}k(n)a^T(n)P(n-1) \tag{4.23}$$

The complete RLS algorithm extracted from [61] may be summarized as follows:

Given data $a(1), a(2), ..., a(n)$ and $b(1), b(2), ..., b(n)$

1. Initialize $x(0) = 0$, $P(0) = \delta I$
2. For each time instant $i = 1$, ..., n, compute
    1. $\pi = a^T(i)P(i-1)$
    2. $\gamma = \lambda + \pi a(i)$
    3. $k(i) = \frac{\pi^T}{\gamma}$
    4. $\alpha(i) = b(i)$ - $x^T(i-1)a(i)$
    5. $x(i) = x(i-1) + k(i)\alpha(i)$
    6. $P' = k(i)\pi$
    7. $P(i) = \frac{1}{\lambda}(P(i-1) - P')$

4.4.2 Validation

In order to validate the RLS algorithm a comparison between the outputs given by the OLS and the RLS methods is done in this section. The tests are done again for the Bergeron model of line of 100 km. The algorithm window length is 4 ms. Both RL and RLC identification methods are compared. There are two parameters that may impact

the outputs of the RLS algorithm. The first parameter is the forgetting factor λ between 0 and 1. Generally, the best choice of the forgetting factor is a compromise between the stability and the tracking ability [62]. In [63] a method based on a variable forgetting factor is proposed in order to improve the performances of the RLS algorithm. When λ is small, the contribution of the previous samples decreases. It may be very useful for the identification of the parameters of a non-stationary model or if the first samples are not accurate enough. With finite data the forgetting factor should be set close to 1 because all samples should be taken into account. The case where λ is equal to 1 corresponds to a growing window algorithm. The second parameter is δ which depends on the initial knowledge of the covariance matrix of the outputs. Since this knowledge is poor, the initial value must be high. The recommended value for δ according to [61] is:

$$\delta > 100\sigma_a^2 \tag{4.24}$$

where σ_a^2 is the variance of the vector a. Some exact initializations of the RLS algorithm were developed and may be useful when the true parameters to identify are known [64]. In this thesis the rule (4.24) is used. The RL and the RLC methods were tested for different values of δ. Both methods lead to a very good convergence between the OLS and the RLS for a wide range of δ between [10^2 - 10^6]. Fig. 4.2 and 4.3 show the identified line parameters for the RL and the RLC identification methods. The values used for λ and δ are respectively 1 and 10^3.

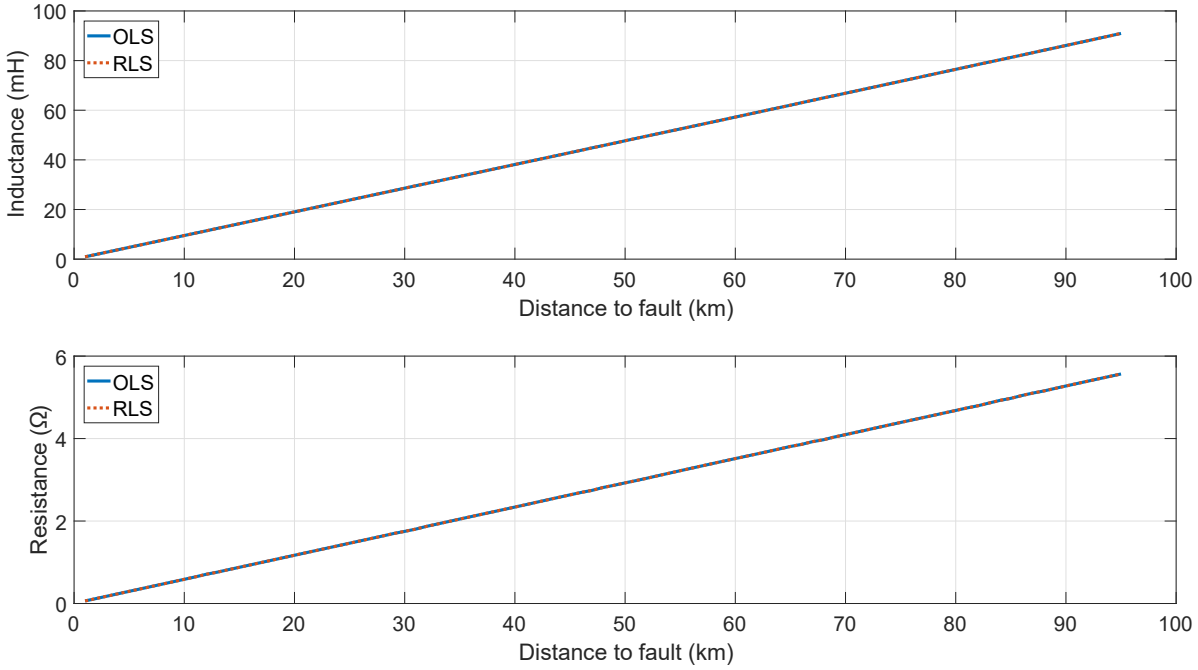

Figure 4.2: Inductance and resistance identified with the RL algorithm with an OLS and an RLS method. The RLS parameters are $\lambda = 1$ and $\delta = 10^3$

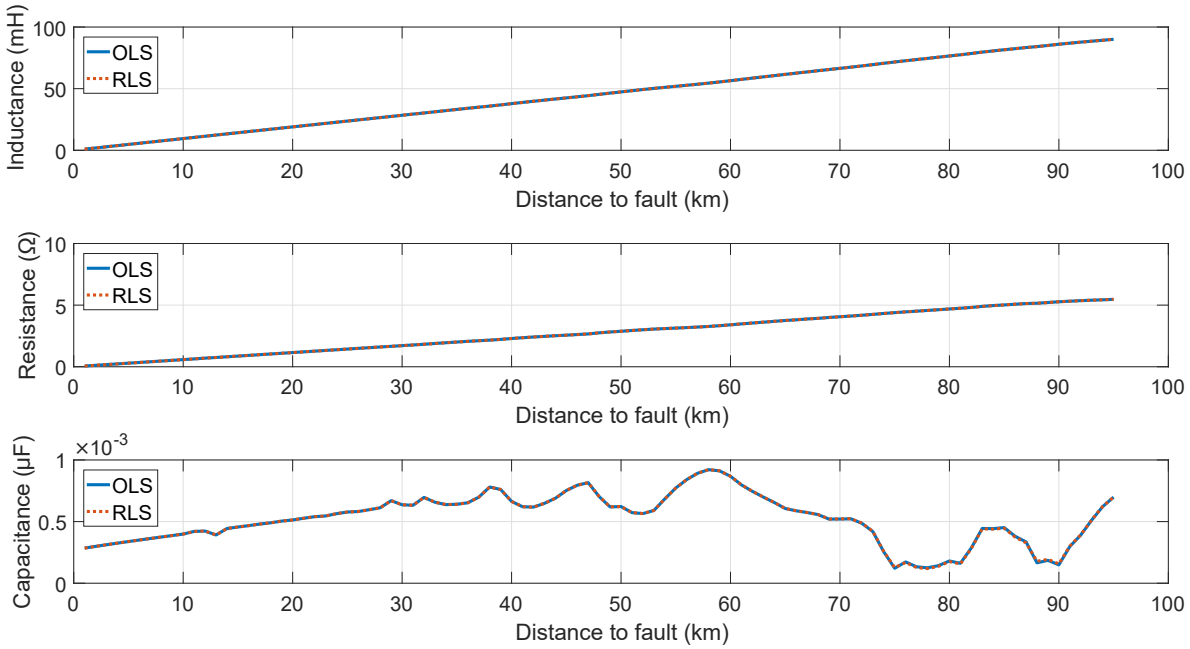

Figure 4.3: Inductance, resistance and capacitance identified with the RLC algorithm with an OLS and an RLS method. The RLS parameters are $\lambda = 1$ and $\delta = 10^3$

4.5 Analysis of Least-Squares Estimations

The distance to fault is identified using the least-squares method presented before. However, several parameters may impact the results of the algorithms. These parameters may be internal (model accuracy, SIR, remote injection, ...) or external (noises, hardware precision, ...). It is necessary to analyse the reliability of the results to improve the security of the distance protection. Some statistical indicators can be used to evaluate the reliability of the least-squares method outputs. In this section the Mean Squared Error (MSE) and the Confidence Interval (CI) will be presented.

4.5.1 OLS assumptions

As the RLS algorithm is a recursive implementation of the OLS method it is necessary to check the mathematical assumptions related to this last. Indeed, several assumptions are made when working with a least-squares method. These assumptions ensure that the solution found is BLUE. Some assumptions are related to the error terms present in the model. However, this term is never really known and the residuals are used instead. The major assumptions are according to [47], [65], [66]:

1. the multiple regression model is linear in parameters.

2. the mean of the error term is zero.

3. the variance of the error term must be constant for each observation and in particular does not depend on the value of the independent variables (homoscedasticity).

4. the observations of the error term are uncorrelated.

5. all independent variables are uncorrelated with the error term.

6. the dependent variable is a perfect linear function of other independent variables.

7. the error term is normally distributed.

4.5.2 Residual analysis

The least-squares method is used to solve the system:

$$Ax = b \tag{4.25}$$

The i^{th} row of the system (corresponding to the i^{th} sample) is:

$$\sum_{j=1}^{m} a_{ij} x_j = b_i \tag{4.26}$$

The i^{th} residual is defined as the difference between the measured output b_i and the predicted output $\hat{b}_i$. This definition gives:

$$e_i = b_i - \hat{b}_i = b_i - \sum_{j=1}^{m} a_{ij} \hat{x}_j \tag{4.27}$$

where $\hat{x}_j$ is the j^{th} identified parameter. Using the Residual Sum of Squares (RSS) defined as:

$$RSS = \sum_{i=1}^{n} e_i^2 \tag{4.28}$$

and if the OLS assumptions are respected the estimate variance is obtained as:

$$\sigma^2 = \frac{1}{n-m} \sum_{i=1}^{n} \left(b_i - \sum_{j=1}^{m} a_{ij} \hat{x}_j \right)^2 = \frac{1}{n-m} \sum_{i=1}^{n} e_i^2 = \frac{RSS}{n-m} = MSE \tag{4.29}$$

4.5.3 Standardized residuals

The residuals as defined before depend on the magnitude of the data. In order to easily compare the residuals from different models or methods, it is important to scale the residuals. There exists different normalization forms. The simplest normalised residual is the standardized residual defined as:

$$z_i = \frac{e_i}{\sqrt{MSE}} \tag{4.30}$$

A faulted RLC Γ model of line of 300 km is simulated in Fig. 4.4. The figure on the top shows the evolution of the standardized residuals of the OLS RLC algorithm. The figure on the bottom is a plot of the i^{th} residual against the $(i-1)^{th}$ residual. The following findings regarding the OLS assumptions appear:

- the mean of the residuals must be zero. This condition can be considered as respected because the mean appears to be negligible (equal to 0.0032).

- the variance of the residuals is not constant. This point will be discussed more deeply in Section 4.5.5.

- the 4^{th} assumption suggests that the residuals are uncorrelated. This assumption can be achieved when the data are randomly sampled. However, for a time-series data, this assumption is often violated because the sampling is done successively with a constant step. In this case the auto-correlation of the residuals may be observed. Some procedures have been developed to solve these issues but they are not well adapted to an on-line ultra-fast algorithm [67], [68]. The estimation of the parameters remains unbiased but the MSE and the CI are not correct [55]. The figure on the bottom may be useful to check the correlation of the residuals. In this example a possible correlation between the residuals does not appear clearly.

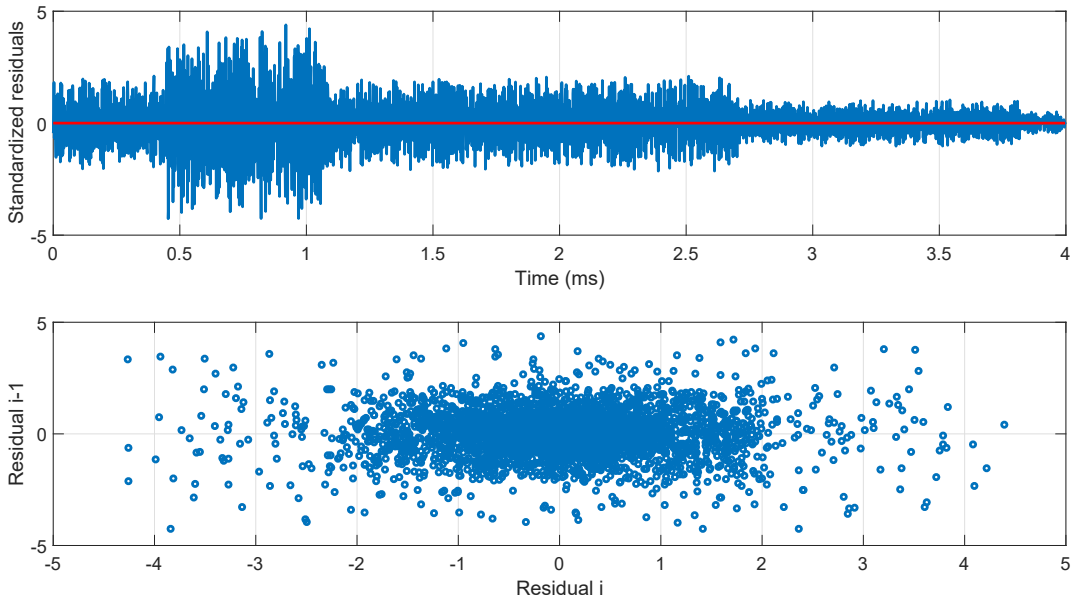

Figure 4.4: Standardized residuals evolution (above) and $(i-1)^{th}$ residual versus i^{th} residual (below)

The filters used in the algorithm may also impact the behaviour of the residuals. Indeed, the filtering process implies the previous samples to evaluate the value of the current sample. This process may perturb the independence of the residuals. Fig. 4.5 shows the two previous graphs but this time with the anti-aliasing filter implemented in Chapter 3. These figures show clearly that the filtering process has introduced a correlation in the residuals.

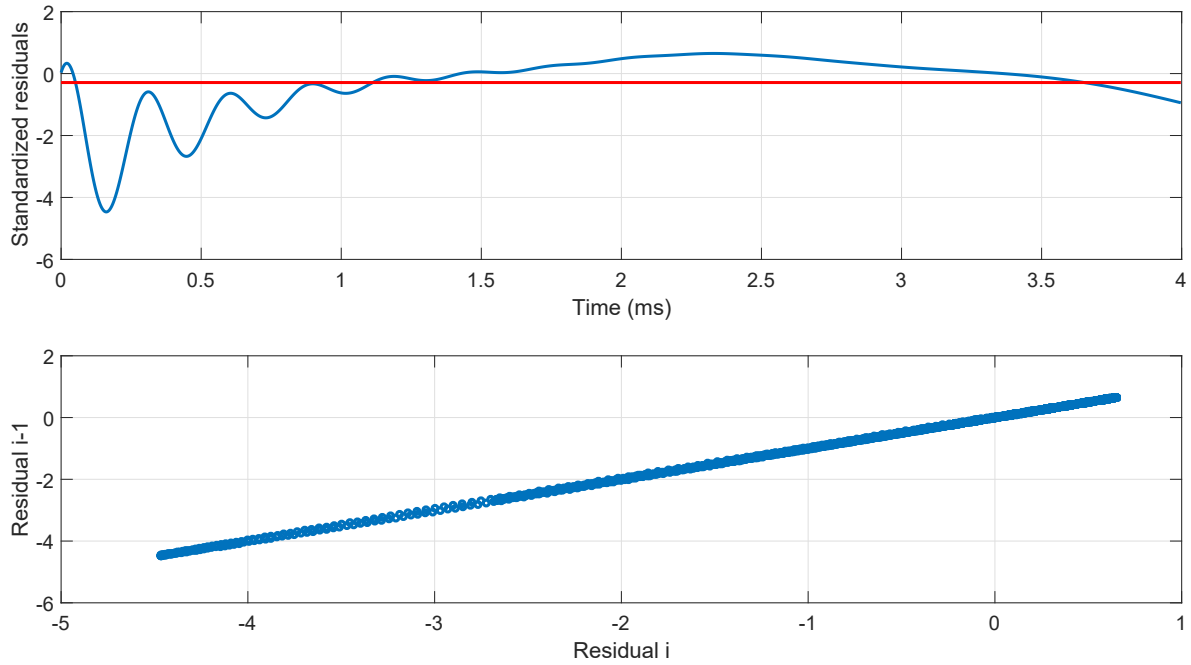

Figure 4.5: Standardized residuals evolution (above) and $(i-1)^{th}$ residual versus i^{th} residual (below). Impact of the anti-aliasing filter

4.5.4 Confidence interval

It is possible to develop a CI around the identified distance to fault thanks to the variance of the residuals if the OLS assumptions presented in Section 4.5.1 are respected. The MSE can be rewritten as:

$$\sigma^2 = \frac{1}{n-m} \|A\hat{x} - b\|^2 \tag{4.31}$$

The estimated variance associated to the j^{th} item of the x vector, is defined as [69]:

$$var(x_j) = \tau_j^2 \sigma^2 \tag{4.32}$$

where τ_j^2 is the j^{th} diagonal element of matrix $(A^T A)^{-1}$. The CI is finally given by:

$$x_j \pm SF_{CI}\sqrt{var(x_j)} \tag{4.33}$$

where SF_{CI} depends on the confidence level. The CI for the distance to fault is given by:

$$m \in \frac{x_j \pm SF_{CI}\sqrt{var(x_j)}}{l_l} \tag{4.34}$$

where $j = 1$ for the RL identification and $j = 2$ for the RLC identification.

4.5.5 Robust variance

The CI described above is constructed under the assumptions presented in Section 4.5.1. Even if the homoscedasticity is not verified (no constant variance) the OLS method gives unbiased estimators. However, the identification is not BLUE because the variance of the residuals is not the smallest [70]. It is possible to construct an Heteroscedasticity-Consistent (HC) standard error based on the Huber-White's approach [70], [71]. The covariance matrix of the regression coefficients is then given by:

$$cov(X) = (A^T A)^{-1} A^T \Phi A (A^T A)^{-1} \tag{4.35}$$

where Φ is the covariance matrix of the residuals. If the assumption of homoscedasticity and the assumption of uncorrelated errors are respected, Φ is equal to $\sigma^2 I$ which leads to (4.32). In the case of HC several estimators have been proposed for Φ [72]:

$$\Phi = diag\left[e_i^2\right] \qquad \text{HC0} \tag{4.36}$$

$$\Phi = \frac{n}{n-m} diag\left[e_i^2\right] \qquad \text{HC1} \tag{4.37}$$

$$\Phi = diag\left[\frac{e_i^2}{1-h_{ii}}\right] \qquad \text{HC2} \tag{4.38}$$

$$\Phi = diag\left[\frac{e_i^2}{(1-h_{ii})^2}\right] \qquad \text{HC3} \tag{4.39}$$

where h_{ii} is the leverage value given by:

$$h_{ii} = diag\left(A(A^T A)^{-1} A^T\right) \tag{4.40}$$

4.6 Bergeron overhead transmission line

In this last section the residuals analysis is applied on a Bergeron model in order to define some criteria permitting to test the reliability of the results given by the least-squares method. Only the RLC identification algorithm is presented here. The same conclusions can be done for the RL identification algorithm. The anti-aliasing filter and the low-pass FIR filter are used.

The classical use of the CI is the calculation of an interval in which the value of the identified parameters is reliable with a certain level of confidence. However, as mentioned before, the statistical indicators may be biased for time-series data because the sampling is not done randomly but successively. The different observations are in this case represented by the different times of the algorithm window. In this thesis an alternative use of the CI is proposed.

The objective is to add a security margin on the identified distance to fault in order to avoid a possible over-reaching. However, instead of adding a constant margin it is proposed to add a margin which is related to the residuals of the least-squares estimation. If the residuals are low, which suggests a good identification, the margin must be low too. If the residuals are high the margin must be high too. The margin added to the identified parameter x_j will be $SF_{CI}\sqrt{var(x_j)}$ which represents the classical formulation of the CI.

In Fig. 4.6 the security margins (related to the CIs as explained above) evaluated with different forms of the covariance matrix Φ are compared with the relative errors on the distance to fault evaluated with the identified inductance of the line. It appears that they have a similar shape. A difference can be seen only between 80 and 90 km where the homoscedasticity form is lower than the others. This last form, which is also the simplest, leads to a better fitting between the security margins and the errors of the identification. The other forms over-estimate more the errors done on the distances to fault between 80 and 90% of the line. In this thesis the homoscedasticity form will be implemented.

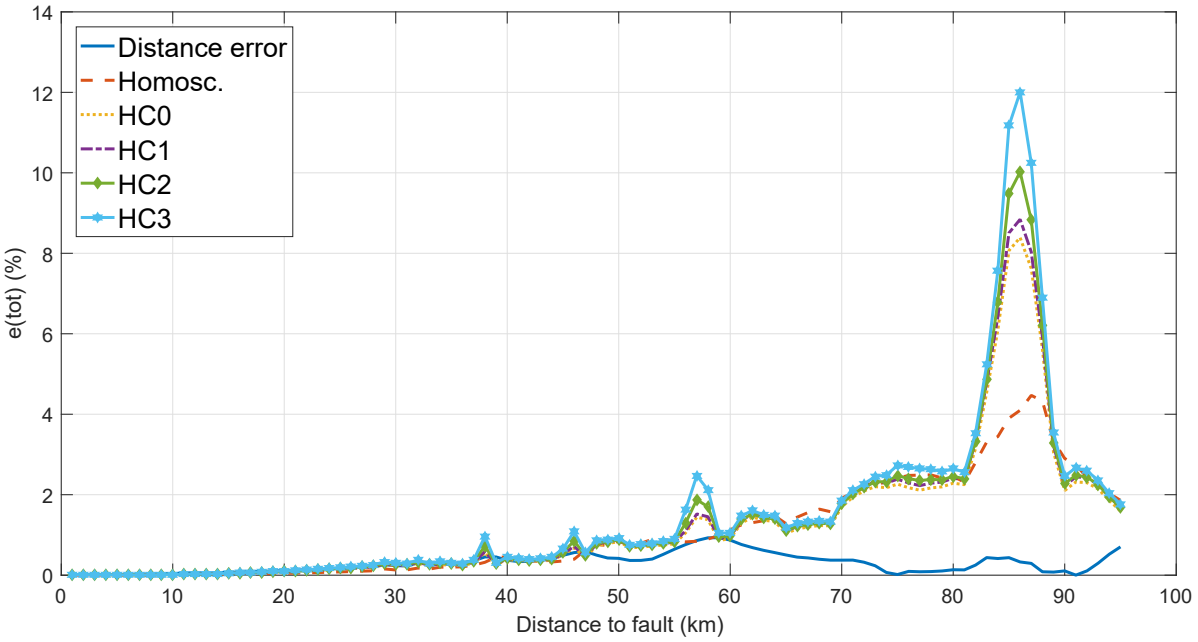

Figure 4.6: Comparison of the errors on the distance to fault and the different forms of the security margin ($SF_{CI} = 10$)

4.7 Conclusions

In this chapter the mathematical aspects of the OLS method and the related assumptions have been presented. The optimisation of the computational loads was done by the use of an RLS algorithm. This algorithm permits also to avoid some numerical problems linked to the matrix inversion. The RLS algorithm was validated for the RL and the RLC identification methods by comparing the results given by the OLS and the RLS. The optimal values for the forgetting factor λ and the initialisation factor δ were defined.

The analysis of the residuals permitted to highlight two important issues. The first one is the fact that the residuals of a time-series model may be correlated. The second finding is the non-constant variance of the residuals. These two issues may lead to a biased MSE and CI evaluation. For these reasons the use of the MSE and the CI cannot be based directly on statistical tables to define some security margins.

Chapter 5

Generalization to three-phase line

5.1 Introduction

In Chapter 3 a single-phase transmission line was assumed. This was useful to help to understand the physical phenomena occurring and the methods implemented to solve the problem. Each phase has a phase resistance R_l and inductance L_l as well as a capacitance C_l with respect to the ground to take into account the leakage current flowing towards the ground. All those parameters were already incorporated in the previous models. However, the single-phase model does not take into account the influence of the other phases belonging to the same transmission line. Indeed, each phase has also a mutual resistance R_m[1], inductance L_m and capacitance C_m with respect to the two other phases. Fig. 5.1 summarizes all the components that need to be modelled when studying the behaviour of a three-phase line. In Section 5.2 the matrices characterising a three-phase electrical circuit will be established. In Section 5.3 the Fortescue and the Clarke transformations will be applied in order to decouple the three-phase lines into three standalone lines for a frequency and a time domain respectively.

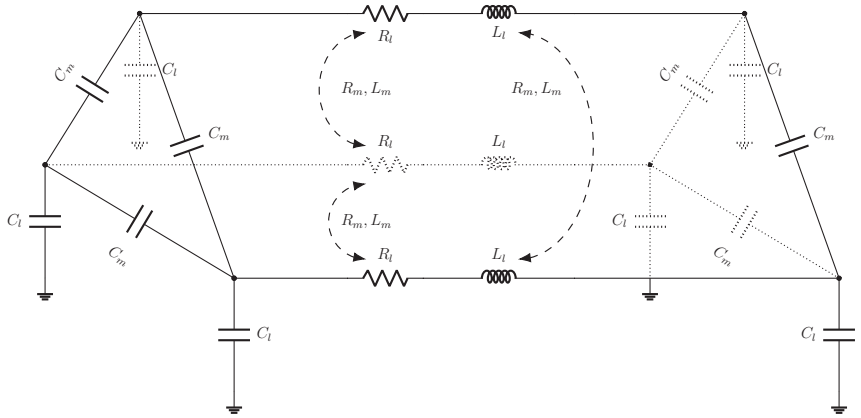

Figure 5.1: Representation of the π equivalent circuit of a three-phase transmission line

[1]due to the presence of the earth-return path

The main issue of the generalization to the three-phase case is that the three phases are not decoupled any more: each phase needs to take into account the influence of the two other phases for their respective voltage and current. The goal of this chapter is to present a method to decouple the phases into an equivalent line model where all the three phases may be studied as standard standalone line.

5.2 System matrices definition

This section will help defining the R_T, L_T, C_T and Z_T matrices which are used to represent a general three-phase transmission line. The assumptions that may be used to simplify the problem are [6]:

- the lines are fully transposed[2].
- the three phases are supposed equivalent to one another.
- the aerial space and the earth are homogeneous.
- the spacing between conductors is significantly larger that their radius (avoid proximity effects).

As a result, the parameters of the three different phases may be assumed to be the same. The previous assumptions permit also to assume that the ground wire potential is continuously zero. It is possible to reduce the resistance, the inductance and the capacitance matrices [24]. Using the indices **u** for the ungrounded conductors and **g** for the ground wire, it leads to the matrix system (5.1).

$$-\begin{bmatrix} dV_u/dx \\ dV_g/dx \end{bmatrix} = \begin{bmatrix} Z'_{uu} & Z'_{ug} \\ Z'_{gu} & Z'_{gg} \end{bmatrix} \begin{bmatrix} I_u \\ I_g \end{bmatrix} \tag{5.1}$$

where Z' represent a per length impedance matrix. Since V_g and dV_g/dx are zero the system (5.1) can be reduced by eliminating I_g. It finality leads to:

$$-\left[dV_u/dx\right] = \left[Z'_{reduced}\right]\left[I_u\right] \tag{5.2}$$

where:

$$[Z'_{reduced}] = [Z'_{uu}] - \left[Z'_{ug}\right]\left[Z'_{gg}\right]^{-1}\left[Z'_{gu}\right] \tag{5.3}$$

The same reduction is made for the capacitance matrix. All the line parameters matrices used in this thesis are related to the reduced matrices.

[2]as the self and the mutual parameters of a three-phase line depend on the configuration of the three-phase system (distance of the conductors to the ground, distance between the different pairs of conductors, etc.), the line is never truly balanced. It is therefore necessary to make a cyclic permutation of the three phases

5.2.1 Impedance matrix

As the conductances are usually neglected for a transmission line, the R_T and L_T matrices are straightforward:

$$R_T = \begin{bmatrix} R_l & R_m & R_m \\ R_m & R_l & R_m \\ R_m & R_m & R_l \end{bmatrix} \tag{5.4}$$

$$L_T = \begin{bmatrix} L_l & L_m & L_m \\ L_m & L_l & L_m \\ L_m & L_m & L_l \end{bmatrix} \tag{5.5}$$

It leads to:

$$V_T = (R_T + j\omega L_T)\, I_T = Z_T I_T \tag{5.6}$$

5.2.2 Capacitance matrix

The influence of the ground-to-line capacitances complicates the computation of the C_T matrix. Fig. 5.2 is a close-up version of the transmission line presented in Fig. 5.1. The currents i_{gj}, i_j and i_{jk} are respectively the ground current of the phase j, the line current of the phase j and the current flowing from the phase j to the phase k through the mutual capacitance.

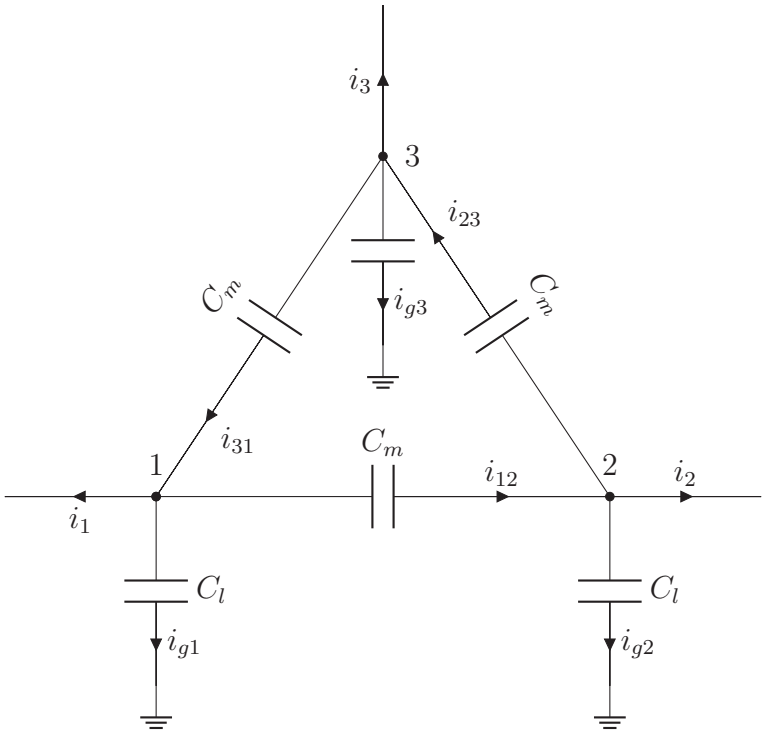

Figure 5.2: Capacitance coupling for a three-phase π model of line

The capacitance is defined by the relations (5.7) and (5.8):

$$i_{jk} = C_m \frac{dV_{jk}}{dt} \qquad \forall j,k = 1,2,3,\ j \neq k \tag{5.7}$$

$$i_{gj} = C_l \frac{dV_j}{dt} \qquad \forall j = 1,2,3 \tag{5.8}$$

By applying the KCL to the node 1 it leads to:

$$i_1 + i_{g1} + i_{12} - i_{31} = 0 \tag{5.9}$$

Using (5.7) and (5.8) it leads to:

$$i_1 = -C_l \frac{dV_1}{dt} + C_m \frac{d(V_2 - V_1)}{dt} + C_m \frac{d(V_3 - V_1)}{dt} \tag{5.10}$$

By applying the same development to the nodes 2 and 3, it finally leads to:

$$I_T = C_T \frac{dV_T}{dt} \tag{5.11}$$

where:

$$C_T = \begin{bmatrix} -C_l - 2C_m & C_m & C_m \\ C_m & -C_l - 2C_m & C_m \\ C_m & C_m & -C_l - 2C_m \end{bmatrix} \tag{5.12}$$

5.3 Symmetrical components

5.3.1 Fortescue transformation

The Fortescue transformation decouples the a, b and c phases into homopolar, direct and reverse phases. If F is a transformation matrix, then a three-phase system $A_T = [A_a\ A_b\ A_c]$ is linked to the three symmetrical components $A_F = [A_0\ A_d\ A_i]$ by the following relation:

$$A_T = F A_F \tag{5.13}$$

The Kirchoff's law extended to the three-phases system gives the matrix equation:

$$V_T = Z_T I_T \tag{5.14}$$

By using (5.13) it gives:

$$F V_F = Z_T F I_F \Leftrightarrow V_F = (F^{-1} Z_T F) I_F \tag{5.15}$$

where $(F^{-1}Z_TF)$ is the equivalent Fortescue impedance matrix renamed Z_F. It finally leads to:

$$V_F = Z_F I_F \tag{5.16}$$

If the transformation matrices are defined as:

$$F = \begin{bmatrix} 1 & 1 & 1 \\ 1 & \alpha^2 & \alpha \\ 1 & \alpha & \alpha^2 \end{bmatrix} \tag{5.17}$$

$$F^{-1} = \frac{1}{3}\begin{bmatrix} 1 & 1 & 1 \\ 1 & \alpha & \alpha^2 \\ 1 & \alpha^2 & \alpha \end{bmatrix} \tag{5.18}$$

where:

$$\alpha = e^{\frac{j2\pi}{3}} \tag{5.19}$$

it can be proved that Z_F is diagonal if the assumptions presented in Section 5.2 are respected [6]:

$$Z_F = \begin{bmatrix} Z_0 & 0 & 0 \\ 0 & Z_d & 0 \\ 0 & 0 & Z_i \end{bmatrix} \tag{5.20}$$

However, the Fortescue transformation involves the use of a complex number matrix and is therefore more suitable for a phasor domain than for a time domain.

5.3.2 Clarke transformation

The working principle of the Clarke transformation is the same as the Fortescue transformation: a transformation matrix T is used to transpose the regular a, b and c phases in 3 other phases which may be decoupled in order to solve the problem. However, the matrix T is real and can be easily applied to the instantaneous values of voltage and current signals. The transformation matrix is defined as:

$$T = \begin{bmatrix} 1 & 0 & 1 \\ -\frac{1}{2} & \frac{\sqrt{3}}{2} & 1 \\ -\frac{1}{2} & -\frac{\sqrt{3}}{2} & 1 \end{bmatrix} \tag{5.21}$$

$$T^{-1} = \begin{bmatrix} \frac{2}{3} & -\frac{1}{3} & -\frac{1}{3} \\ 0 & \frac{1}{\sqrt{3}} & -\frac{1}{\sqrt{3}} \\ \frac{1}{3} & \frac{1}{3} & \frac{1}{3} \end{bmatrix} \tag{5.22}$$

The equivalent Clarke parameters matrices are:

$$R_C = T^{-1} R_T T = \begin{bmatrix} R_l - R_m & 0 & 0 \\ 0 & R_l - R_m & 0 \\ 0 & 0 & R_l + 2R_m \end{bmatrix} = \begin{bmatrix} R_\alpha & 0 & 0 \\ 0 & R_\beta & 0 \\ 0 & 0 & R_0 \end{bmatrix} \tag{5.23}$$

$$L_C = T^{-1} L_T T = \begin{bmatrix} L_l - L_m & 0 & 0 \\ 0 & L_l - L_m & 0 \\ 0 & 0 & L_l + 2L_m \end{bmatrix} = \begin{bmatrix} L_\alpha & 0 & 0 \\ 0 & L_\beta & 0 \\ 0 & 0 & L_0 \end{bmatrix} \tag{5.24}$$

$$C_C = T^{-1} C_T T = \begin{bmatrix} C_l + 3C_m & 0 & 0 \\ 0 & C_l + 3C_m & 0 \\ 0 & 0 & C_l \end{bmatrix} = \begin{bmatrix} C_\alpha & 0 & 0 \\ 0 & C_\beta & 0 \\ 0 & 0 & C_0 \end{bmatrix} \tag{5.25}$$

It is possible to prove that the α, β and 0 sequence parameters of the line are equal to the positive (direct), negative (reverse) and zero (homopolar) sequence parameters respectively. The three-phase π model of a transmission line is governed by the following symmetrical components relations:

$$V_C = R_C I_C + L_C \frac{dI_C}{dt} \tag{5.26}$$

and

$$I_C = C_C \frac{dV_C}{dt} \tag{5.27}$$

where $V_C = [V_\alpha \; V_\beta \; V_0]$ and $I_C = [I_\alpha \; I_\beta \; I_0]$.

5.4 Conclusions

The relations (5.23), (5.24) and (5.25) prove that the Clarke transformation is suited to decouple the three-phase lines into three standalone lines (see Fig. 5.3) if the assumptions presented in Section 5.2 are met.

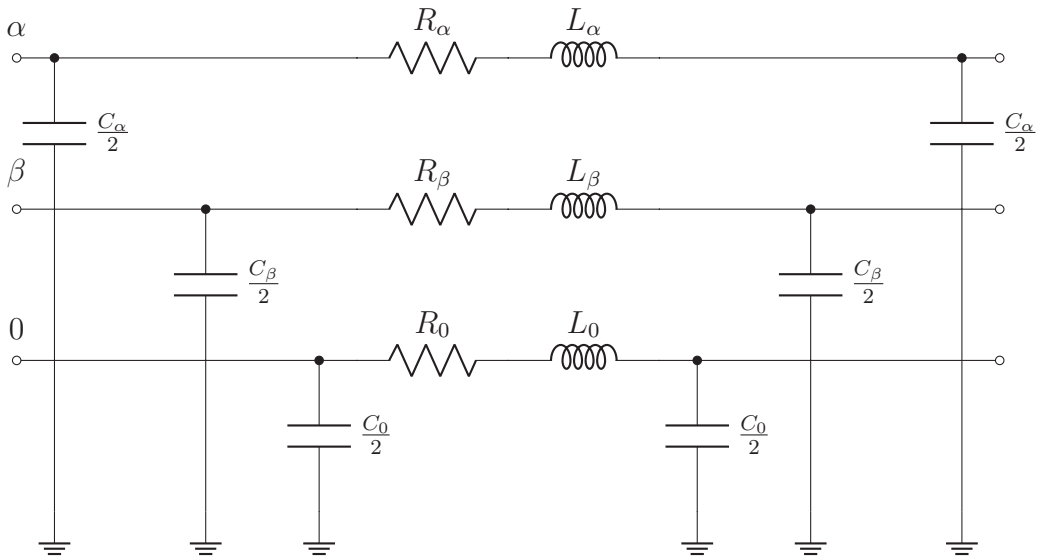

Figure 5.3: Equivalent three-phase decoupled π transmission line in Clarke components

Chapter 6

Three-phase fault study

6.1 Introduction

In Chapter 3 a parameters identification algorithm was presented for a single-phase model of line. Chapter 5 permitted to construct a decoupled three-phase system for a π model thanks to the Clarke transformation. For an actual three-phase transmission line system, there are several possible fault types (phase-to-ground, phase-to-phase, phase-to-phase-to-ground, three-phase). As explained in [73], when such a fault occurs in a three-phase system, the equivalent circuit can be represented by a series or parallel association of the α, β and 0 sequence circuits. Consider a three-phase Γ faulted line as represented in Fig. 6.1.

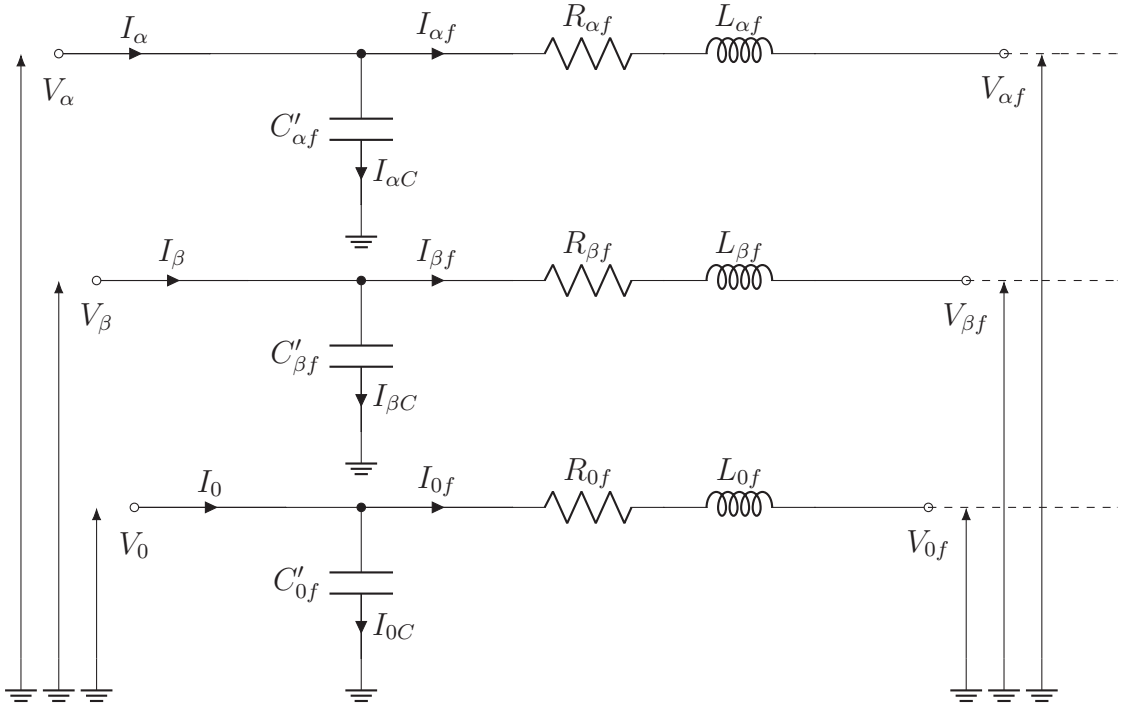

Figure 6.1: Representation of the Γ equivalent circuit of a three-phase line

The line is defined in modal domain by (6.1) and (6.2).

$$\begin{pmatrix} V_\alpha \\ V_\beta \\ V_0 \end{pmatrix} = \begin{pmatrix} V_{\alpha f} \\ V_{\beta f} \\ V_{0f} \end{pmatrix} + \begin{pmatrix} R_{\alpha f} & 0 & 0 \\ 0 & R_{\beta f} & 0 \\ 0 & 0 & R_{0f} \end{pmatrix} \begin{pmatrix} I_{\alpha f} \\ I_{\beta f} \\ I_{0f} \end{pmatrix} + \begin{pmatrix} L_{\alpha f} & 0 & 0 \\ 0 & L_{\beta f} & 0 \\ 0 & 0 & L_{0f} \end{pmatrix} \begin{pmatrix} dI_{\alpha f}/dt \\ dI_{\beta f}/dt \\ dI_{0f}/dt \end{pmatrix} \tag{6.1}$$

$$\begin{pmatrix} I_\alpha \\ I_\beta \\ I_0 \end{pmatrix} = \begin{pmatrix} I_{\alpha f} \\ I_{\beta f} \\ I_{0f} \end{pmatrix} + \begin{pmatrix} C'_{\alpha f} & 0 & 0 \\ 0 & C'_{\beta f} & 0 \\ 0 & 0 & C'_{0f} \end{pmatrix} \begin{pmatrix} dV_\alpha/dt \\ dV_\beta/dt \\ dV_0/dt \end{pmatrix} \tag{6.2}$$

where the links between the phase and the Clarke components are given by (6.3) and (6.4):

$$\begin{cases} V_a &= V_\alpha + V_0 \\ V_b &= -\frac{1}{2}V_\alpha + \frac{\sqrt{3}}{2}V_\beta + V_0 \\ V_c &= -\frac{1}{2}V_\alpha - \frac{\sqrt{3}}{2}V_\beta + V_0 \end{cases} \tag{6.3}$$

$$\begin{cases} I_a &= I_\alpha + I_0 \\ I_b &= -\frac{1}{2}I_\alpha + \frac{\sqrt{3}}{2}I_\beta + I_0 \\ I_c &= -\frac{1}{2}I_\alpha - \frac{\sqrt{3}}{2}I_\beta + I_0 \end{cases} \tag{6.4}$$

In Section 6.2 and 6.3 the RL and the RLC identification algorithms will be adapted for a phase-to-phase and a phase-to-ground fault respectively. The results will be summarised in Sections 6.4. The resulting equations will be tested with a three-phase Bergeron model of line in Section 6.5 and 6.6. It is also necessary to verify if the algorithms implemented in this project are accurate also for a frequency-dependent parameters transmission line model. This test will be done in Section 6.7 for a three-phase J. Marti model of line. Finally, the case of a double-circuits will be discussed in Section 6.8.

6.2 Phase-to-phase fault

The first fault type studied is the phase-to-phase fault. Consider a phase-to-phase fault between the phases **b** and **c**. At the fault location the following relations are verified:

$$\begin{cases} V_{bf} &= V_{cf} \\ I_{bf} &= -I_{cf} \\ I_{af} &= 0 \end{cases} \tag{6.5}$$

It is important to point out that the relations given by (6.5) are only exact if assuming a bolted fault (avoid the remote-ends injection effects) and if the load flow currents can be neglected compared to the short-circuit currents. It follows from the previous relations:

$$\begin{cases} V_{\beta f} &= 0 \\ I_{\alpha f} &= 0 \\ I_{0f} &= 0 \end{cases} \tag{6.6}$$

The relations of (6.6) give in the temporal domain (6.7) for an RL model and (6.8) for an RLC model of line.

$$V_\beta(t) = R_{\beta f} I_\beta(t) + L_{\beta f} \frac{dI_\beta(t)}{dt} \tag{6.7}$$

$$\frac{C_{\beta f}^2}{c'_\beta} \left(l_\beta \frac{d^2 V_\beta(t)}{dt^2} + r_\beta \frac{dV_\beta(t)}{dt} \right) + V_\beta(t) = R_{\beta f} I_\beta(t) + L_{\beta f} \frac{dI_\beta(t)}{dt} \tag{6.8}$$

where $R_{\beta f}$, $L_{\beta f}$ and $C_{\beta f}$ are the β faulted line resistance, inductance and capacitance respectively. As the relations (6.3) and (6.4) are true for the voltage and the current at any point of the line, it leads to $V_\beta = V_b - V_c$ and $I_\beta = I_b - I_c$. The β sequence parameters of the faulted line are therefore given by the difference between the voltage and the difference between the current involved in the fault. The same conclusions can be made for the other phase-to-phase faults.

6.3 Phase-to-ground fault

Consider now a phase-to-ground fault between the phase **a** and the ground. In this case the faulted voltage at the fault location is equal to zero for a bolted short-circuit. At the fault location the system (6.3) gives (6.9) which can be represented by the equivalent circuit shown in Fig. 6.2.

$$V_{\alpha f} + V_{0f} = 0 \tag{6.9}$$

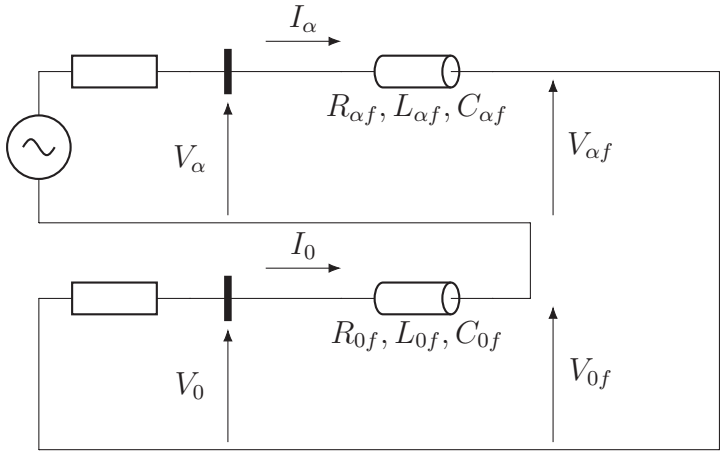

Figure 6.2: Equivalent circuit for a phase-to-ground fault

6.3.1 RL line model

In the case of an RL model of line the relation (6.9) leads to:

$$V_\alpha(t) - R_{\alpha f} I_\alpha(t) - L_{\alpha f}\frac{dI_\alpha(t)}{dt} + V_0(t) - R_{0f} I_0(t) - L_{0f}\frac{dI_0(t)}{dt} = 0 \tag{6.10}$$

By using:

$$\begin{cases} V_\alpha + V_0 = V_a & (6.11) \\ I_\alpha + I_0 = I_a & (6.12) \end{cases}$$

it results to:

$$\begin{aligned} V_a(t) &= R_{\alpha f} I_\alpha(t) + R_{0f} I_0(t) + L_{\alpha f}\frac{dI_\alpha(t)}{dt} + L_{0f}\frac{dI_0(t)}{dt} \\ &= R_{\alpha f} I_a(t) + L_{\alpha f}\frac{dI_a(t)}{dt} + (R_{0f} - R_{\alpha f}) I_0(t) + (L_{0f} - L_{\alpha f})\frac{dI_0(t)}{dt} \\ &= R_{\alpha f}(I_a(t) + k_R I_0(t)) + L_{\alpha f}\left(\frac{dI_a(t)}{dt} + k_L \frac{dI_0(t)}{dt}\right) \end{aligned} \tag{6.13}$$

where:

$$\begin{cases} k_R = \dfrac{r_0 - r_\alpha}{r_\alpha} & (6.14) \\ k_L = \dfrac{l_0 - l_\alpha}{l_\alpha} & (6.15) \end{cases}$$

are known as the compensation factors already implemented in classical protections. By renaming:

$$I_a(t) + k_R I_0(t) = I_{a1}(t) \tag{6.16}$$

$$I_a(t) + k_L I_0(t) = I_{a2}(t) \tag{6.17}$$

it finally leads to:

$$V_a(t) = R_{\alpha f} I_{a1}(t) + L_{\alpha f}\frac{dI_{a2}(t)}{dt} \tag{6.18}$$

The α sequence parameters of the faulted line are therefore given by the faulted voltage and the compensated current (depending on the faulted current and the zero sequence current).

6.3.2 RLC line model

The RLC model of line is governed by the temporal relation (3.36). By applying this relation to both α and 0 circuit and using (6.9), it results to:

$$\begin{aligned} &\frac{C_{\alpha f}^2}{c'_\alpha}\left(l_\alpha \frac{d^2 V_\alpha(t)}{dt^2} + r_\alpha \frac{dV_\alpha(t)}{dt}\right) + V_\alpha(t) + \frac{C_{0f}^2}{c'_0}\left(l_0 \frac{d^2 V_0(t)}{dt^2} + r_0 \frac{dV_0(t)}{dt}\right) + V_0(t) \\ &\qquad = R_{\alpha f} I_\alpha(t) + L_{\alpha f}\frac{dI_\alpha(t)}{dt} + R_{0f} I_0(t) + L_{0f}\frac{dI_0(t)}{dt} \end{aligned} \tag{6.19}$$

Using (6.11) and (6.12), it leads to:

$$\frac{C_{\alpha f}^2}{c'_\alpha}\left[l_\alpha\left(\frac{d^2V_a(t)}{dt^2}+k_{CL}\frac{d^2V_0(t)}{dt^2}\right)+r_\alpha\left(\frac{dV_a(t)}{dt}+k_{CR}\frac{dV_0(t)}{dt}\right)\right]+V_a(t)$$
$$=L_{\alpha f}\left[\frac{dI_a(t)}{dt}+k_L\frac{dI_0(t)}{dt}\right]+R_{\alpha f}\left[I_a(t)+k_RI_0(t)\right] \quad (6.20)$$

where:

$$\begin{cases} k_{CR}=\dfrac{c'_0r_0-c'_\alpha r_\alpha}{c'_\alpha r_\alpha} & (6.21)\\ k_{CL}=\dfrac{c'_0l_0-c'_\alpha l_\alpha}{c'_\alpha l_\alpha} & (6.22)\end{cases}$$

are two new compensation factors. By renaming:

$$I_a(t)+k_RI_0(t)=I_{a1}(t) \quad (6.23)$$
$$I_a(t)+k_LI_0(t)=I_{a2}(t) \quad (6.24)$$
$$V_a(t)+k_{CR}V_0(t)=V_{a1}(t) \quad (6.25)$$
$$V_a(t)+k_{CL}V_0(t)=V_{a2}(t) \quad (6.26)$$

it finally leads to:

$$\frac{C_{\alpha f}^2}{c'_\alpha}\left(l_\alpha\frac{d^2V_{a2}(t)}{dt^2}+r_\alpha\frac{dV_{a1}(t)}{dt}\right)+V_a(t)=R_{\alpha f}I_{a1}(t)+L_{\alpha f}\frac{dI_{a2}(t)}{dt} \quad (6.27)$$

6.4 Summary for all types of fault

The previous calculations may be applied to all the fault types. Table 6.1 summarizes the results. This table gives the input voltages and currents. In all the cases the output parameters identified are the α line parameters.

Fault type		**Input voltage**	**Input current**
phase(j)-to-ground	RL	V_j	I_j, I_0
	RLC	V_j, V_0	I_j, I_0
phase(j)-to-phase(k)		V_j - V_k	I_j - I_k
phase(j)-to-phase(k)-to-ground		V_j - V_k	I_j - I_k
three-phase		$V_j - V_k, \forall j \neq k$	$I_j - I_k, \forall j \neq k$

Table 6.1: Input voltages and currents for the different types of fault

6.5 Numerical results

In this section the validation of the identification algorithms extended to a three-phase model of line will be done. To achieve this goal the same base case presented in Section 3.7 will be tested but this time with a three-phase model of line. It is a Bergeron model of 100 km. The window algorithm is 4 ms and both RL and RLC identification methods are tested. A strong source impedance with an SIR equal to 0.1 is implemented. The distances to fault are deduced from the identified α sequence parameters of the line. The transmission line parameters are: $r_\alpha = 0.058\ \Omega$/km, $r_0 = 0.22\ \Omega$/km, $l_\alpha = 0.955$ mH/km, $l_0 = 3.151$ mH/km, $c_\alpha = 0.0124\ \mu$F/km and $c_0 = 0.0078\ \mu$F/km.

Fig. 6.3 shows the results obtained for a phase-to-phase fault. The range of the errors is the same than the one obtained for the single-phase line in Fig. 3.20. The three-phase algorithm is therefore well implemented for a phase-to-phase fault. The phase-to-phase-to-ground fault and the three-phase fault involve exactly the same equation (see Table 6.1) and will give the same results. In this example the RL identification method gives better results than the RLC method as for the single-phase line. However, it is important to recall that the RL method becomes inaccurate when the SIR or the line length increases.

Fig. 6.4 shows the results obtained for a phase-to-ground fault. The maximum errors on the identified inductance and resistance remain acceptable. However, the errors of the RLC method are higher than for the phase-to-phase fault while the RL method leads to the same accuracy. This phenomenon is studied in the next section.

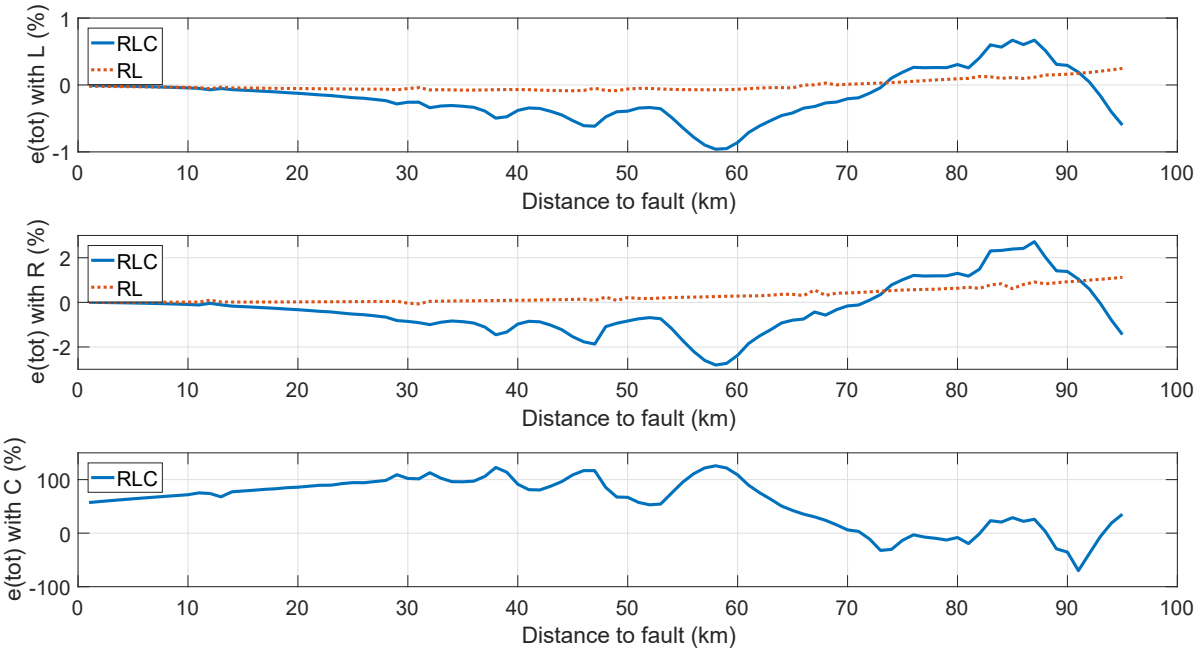

Figure 6.3: Relative errors (in % of the line) of the distance to fault for a three-phase Bergeron model of 100 km with the RLC and the RL algorithm. Phase-to-phase fault

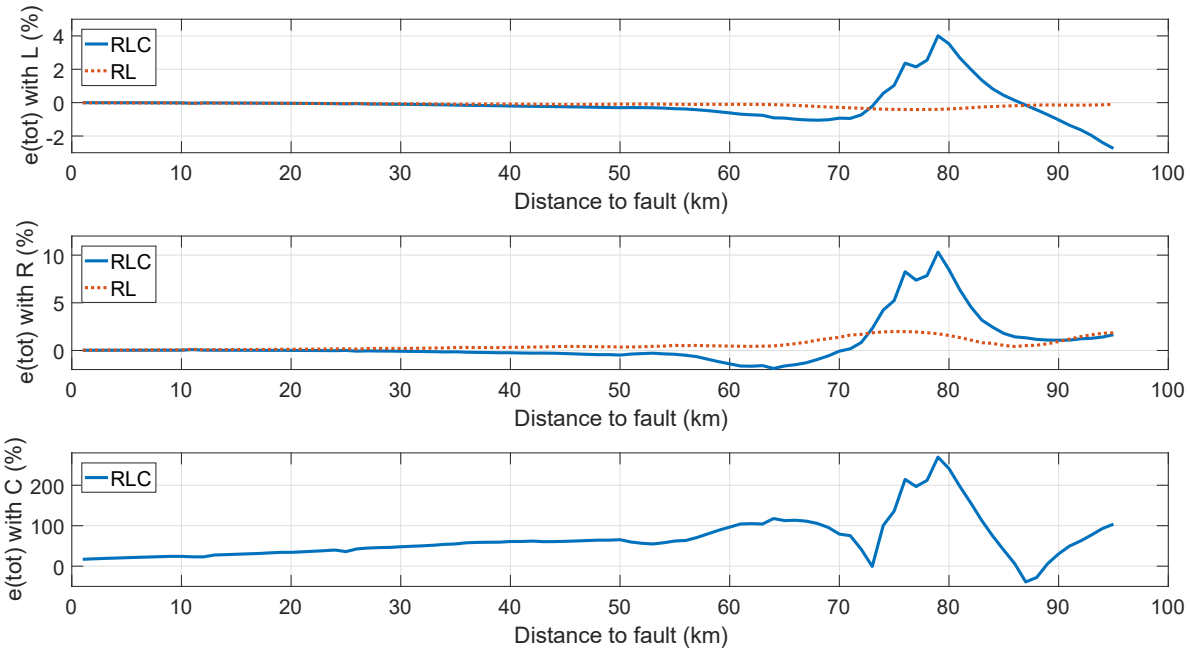

Figure 6.4: Relative errors (in % of the line) of the distance to fault for a three-phase Bergeron model of 100 km with the RLC and the RL algorithm. Phase-to-ground fault

6.6 Phase-to-ground fault discussion

In the case of a phase-to-ground fault, the equivalent circuit is composed by two Γ models of line (the α and the 0 sequence circuit). In Appendix A the transfer function of a phase-to-ground fault is calculated. It corresponds to the α sequence parameters identified by the algorithm. It is shown that this equivalent transfer function is a second order function constructed from a series of two second order transfer functions. This construction seems to be very sensitive to a parameter variation as shown below.

Fig. 6.5 shows the comparison of the Bode's curves for a single-phase and a three-phase Γ model of line in the case of a phase-to-ground fault. It appears that the transfer function of the three-phase line is very sensitive to a parameter variation. The figure on the top left shows that there is a perfect fitting of the transfer functions if the parameters of the line are perfectly known. In the three other figures the line parameters are taken at 90% of the value used in the simulation. In these cases the error done on the line parameters leads to a mismatch of the three-phase transfer function around the resonance frequency. There is always a small variation between a real-world line represented by a distributed model and a lumped Γ model because this last is an approximative (simplified) representation of the true model of line. Moreover, the line parameters are never known with a perfect accuracy. If there is a difference between the parameters of the line used in the algorithm and the true parameters, the transfer function of the model used for the algorithm and for the transfer function of the model simulated may differ significantly. If the frequency content

of the signal includes only frequencies higher than the resonance frequency it will have no impact thanks to the filter. However, if the frequency content includes lower harmonics (close to the perturbed zone of the transfer function) the accuracy will decrease.

In the case tested in the previous section, the high frequencies are normally far from the resonance frequency because a very strong source was used. However, the filtering process is not perfect and a small amount of the high frequencies still remains in the signals and will impact the results because of the phenomenon presented here.

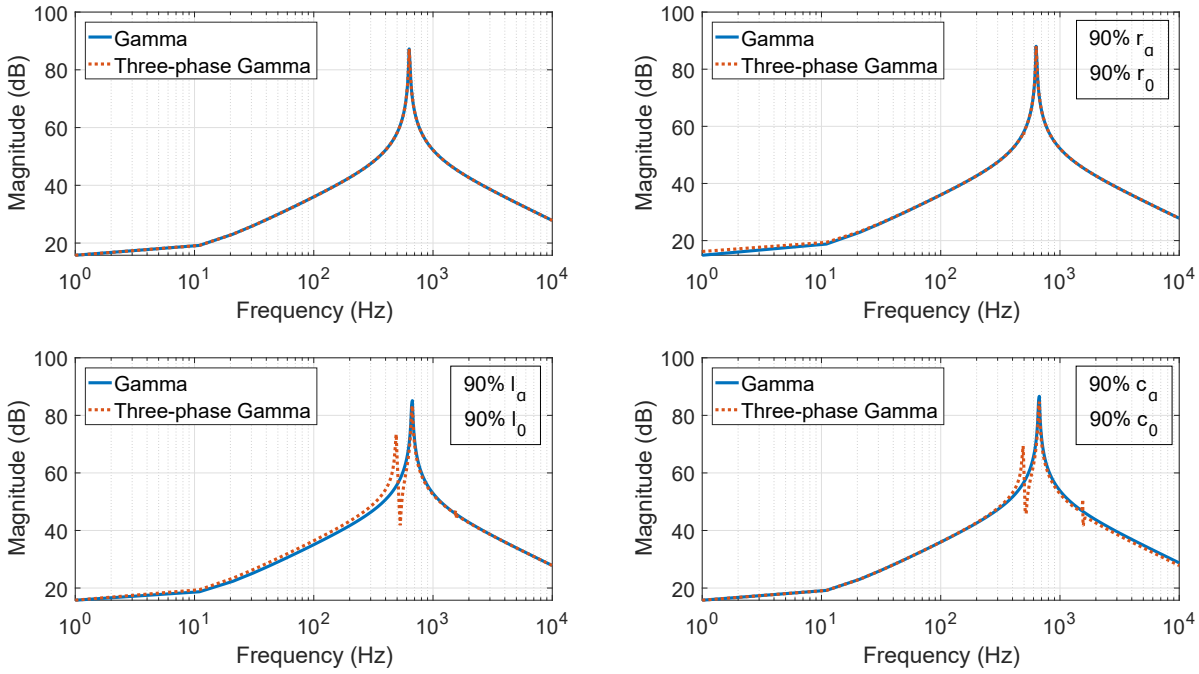

Figure 6.5: Parameters variation impact on Bode's curves of a single-phase and a three-phase Γ model of line of 100 km

6.7 J. Marti model of line

The reference model of line chosen to represent a real-world transmission line model was the Bergeron model. This model is represented by constant distributed parameters. However, as mentioned in Chapter 2, the J. Marti model is more accurate. Indeed, this model takes into account the frequency dependence of the distributed parameters. The objective is to prove that the use of the Bergeron model of line instead of the J. Marti leads to the same results for a frequency range limited to the first resonance frequency. Indeed, Fig. 2.11 showed that the transfer functions of the two models are quite similar until the first resonance frequency. The 0 sequence parameters show strongest frequency dependence. Therefore, only the phase-to-ground fault is tested here. Fig. 6.6 shows the results given by both RL and RLC algorithms for a J. Marti line of 100 km for and

phase-to-ground fault. By comparing with the results obtained for the Bergeron model in Fig. 6.4 it appears that they are in the same range. As a conclusion, the validation of the identification method implemented in this thesis can be done with the Bergeron model.

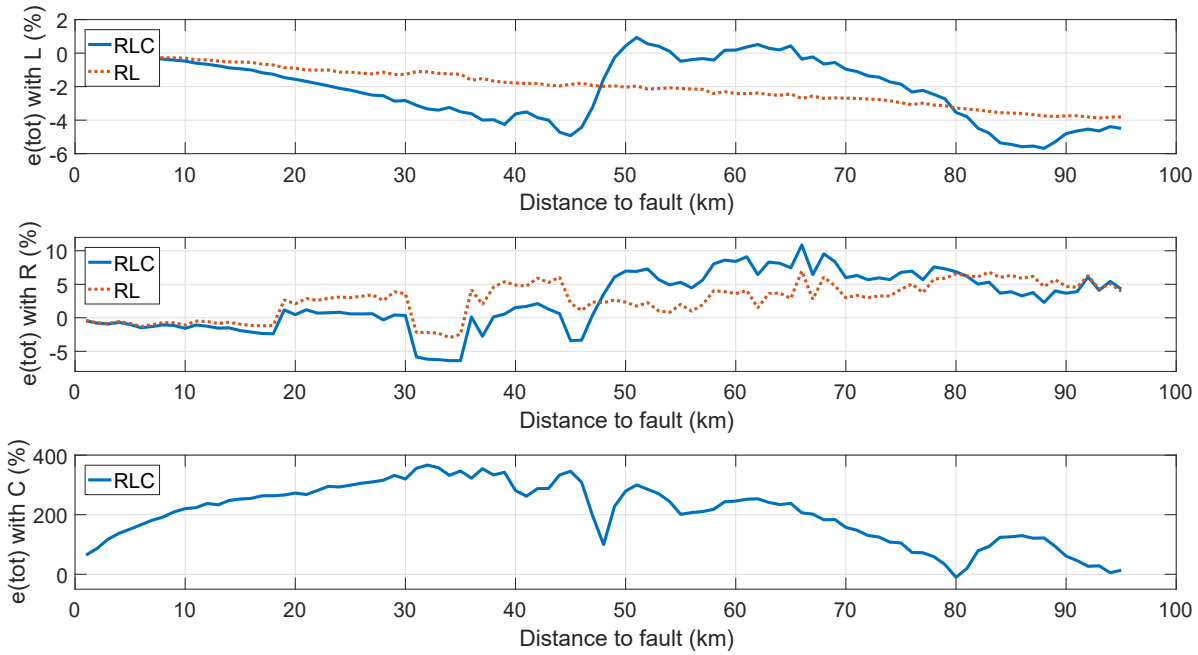

Figure 6.6: Relative errors (in % of the line) of the distance to fault for a three-phase Marti model of 100 km with the RLC and the RL algorithm. Phase-to-ground fault

6.8 Parallel lines

When the transmission lines are on the same tower or paralleled along the same right way, the mutual coupling between the lines may have an impact on the identified distance to fault. It is necessary to study this impact in order to avoid an unwanted tripping. Assuming that the lines are equivalent and fully transposed, the α and the β sequence mutual coupling can usually be neglected [11]. However, the mutual coupling of the zero sequence must be taken into account. As the zero sequence is involved only for a phase-to-ground fault, the other types of fault are not impacted by the presence of the parallel lines. Fig. 6.7 shows the zero sequence circuit of two parallel lines connected to the same buses S and R. In this example, it is assumed that the fault occurs on the protected line denoted by the number I. The two lines are split in two according to the fault position. The complete development will be done for a three-phase RL model of line and then extended to a three-phase RLC Γ model of line. The impact of the parallel line denoted by II on the protected line I during a fault depends on the 0 sequence current I_0^{II} flowing through the line II. It is therefore necessary to simulate a closed circuit with a voltage source at both ends in order to permit this current flow.

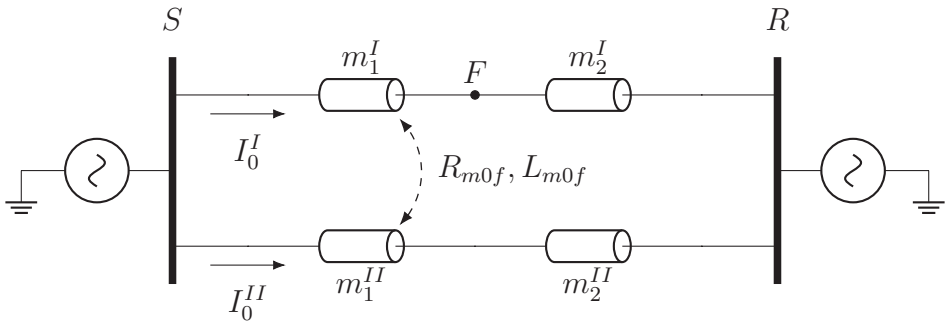

Figure 6.7: Zero sequence mutually coupled line

It was demonstrated that a phase-to-ground fault is governed by (6.9). The α and the 0 sequence voltage at the fault location are given by:

$$\begin{cases} V_{\alpha f}(t) = V_\alpha(t) - R_{\alpha f} I_\alpha^I(t) - L_{\alpha f} \dfrac{dI_\alpha^I(t)}{dt} & (6.28) \\ V_{0f}(t) = V_0(t) - R_{0f} I_0^I(t) - L_{0f} \dfrac{dI_0^I(t)}{dt} - R_{m0f} I_0^{II}(t) - L_{m0f} \dfrac{dI_0^{II}(t)}{dt} & (6.29) \end{cases}$$

Using (6.11), (6.12) and the compensation factors, it finally leads to:

$$V_a(t) = R_{\alpha f} \left(I_a^I(t) + k_R I_0^I(t) + k_{RM} I_0^{II}(t) \right) + L_{\alpha f} \left(\frac{dI_a^I(t)}{dt} + k_L \frac{dI_0^I(t)}{dt} + k_{LM} \frac{dI_0^{II}(t)}{dt} \right) \quad (6.30)$$

where:

$$\begin{cases} k_{RM} = \dfrac{r_{m0}}{r_\alpha} & (6.31) \\ k_{LM} = \dfrac{l_{m0}}{l_\alpha} & (6.32) \end{cases}$$

.

are two new compensation factors that take into account the mutual coupling between the two parallel lines. It appears that it is necessary to know the zero sequence current flowing through the second line in order to compensate correctly the mutual coupling effect. This information is available only if the two lines are connected to the same bus in the substation. If the parallel lines are not connected to the same bus the compensation is no more possible and a greater security margin must be used for the setting zone of the distance element.

The same development is done for the RLC Γ model of line. The demonstration is based on Fig. 6.8 that shows the zero sequence of two parallel lines represented by a Γ model. The right part of the line I located after the fault is not represented because it

can be neglected in the case of a bolted fault. Note that the second line is represented by a complete π model because it is not faulted. It is assumed that the two lines are connected to the same buses at both ends.

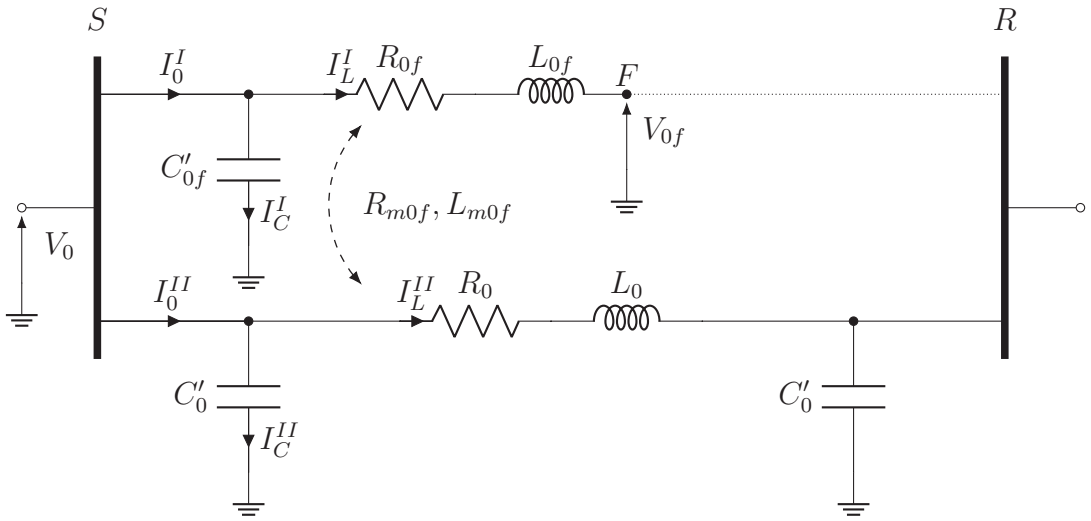

Figure 6.8: Zero sequence mutually coupled line for a Γ model

The 0 sequence voltage at the fault location is given in Laplace domain by:

$$V_{0f} = V_0 - (R_{0f} + sL_{0f}) \cdot I_L^I - (R_{m0f} + sL_{m0f}) \cdot I_L^{II} \tag{6.33}$$

Using the following relations:

$$\begin{cases} I_0^I = I_L^I + I_C^I & (6.34) \\ I_0^{II} = I_L^{II} + I_C^{II} & (6.35) \\ I_C^I = sC'_{0f}V_0 & (6.36) \\ I_C^{II} = sC'_0V_0 & (6.37) \end{cases}$$

it leads in the temporal domain to:

$$\begin{aligned} V_{0f}(t) = V_0(t) + C'_{0f}L_{0f}\frac{d^2V_0(t)}{dt^2} + C'_{0f}R_{0f}\frac{dV_0(t)}{dt} - L_{0f}\frac{dI_0^I(t)}{dt} - R_{0f}I_0^I(t) \\ - L_{m0f}\frac{dI_0^{II}(t)}{dt} - R_{m0f}I_0^{II}(t) + L_{m0f}C'_0\frac{d^2V_0(t)}{dt^2} + R_{m0f}C'_0\frac{dV_0(t)}{dt} \end{aligned} \tag{6.38}$$

The second line II is not faulted, the capacitance C'_0 is therefore proportional to the full line length L^{II}. As the second line may have a different length than the protected line it is preferable not to include this parameter in the algorithm. The following approximation is assumed:

$$C'_0 = c'_0 \cdot L^{II} \simeq C'_{0f} = c'_0 \cdot m \tag{6.39}$$

where m is the distance to fault. This simplification is exact only when the distance to fault is equal to the total length of the second line. The faulted capacitance is therefore not well identified. By combining the α and the 0 sequence, it finally leads to the following result:

$$\frac{C_{\alpha f}^2}{c'_\alpha}\left[l_\alpha\left(\frac{d^2V_a(t)}{dt^2}+k_{CLM}\frac{d^2V_0(t)}{dt^2}\right)+r_\alpha\left(\frac{dV_a(t)}{dt}+k_{CRM}\frac{dV_0(t)}{dt}\right)\right]+V_a(t)$$
$$=L_{\alpha f}\left[\frac{dI_a^I(t)}{dt}+k_L\frac{dI_0^I(t)}{dt}+k_{LM}\frac{dI_0^{II}(t)}{dt}\right]+R_{\alpha f}\left[I_a^I(t)+k_RI_0^I(t)+k_{RM}I_0^{II}(t)\right] \quad (6.40)$$

where:

$$\begin{cases} k_{CLM}=\dfrac{c'_0l_0-c'_\alpha l_\alpha+c'_0l_{m0}}{c'_\alpha l_\alpha} & (6.41)\\ k_{CRM}=\dfrac{c'_0r_0-c'_\alpha r_\alpha+c'_0r_{m0}}{c'_\alpha r_\alpha} & (6.42)\end{cases}$$

This subject is quite broad because a lot of different configurations are possible [74], [75]. If the two parallel transmission lines are connected to the same bus at the relay location it is possible to compensate the mutual coupling effects using the relation (6.40). Moreover, for the truly parallel transmission lines (paralleled along the complete line length), the approximation (6.39) is not necessary. It the two lines are not parallel along the complete line length the approximation (6.39) may be used. Finally, if the lines are not connected to the same bus, the compensation of the mutual coupling effects is not possible and a higher security margin would be used. In this Chapter, the configuration shown in Fig. 6.7 is implemented in order to test the algorithm. The results for these three cases are shown in Fig. 6.9. In this test the zero sequence mutual impedance is taken at two third of the zero sequence self impedance as suggested in [76]. A power system with two parallel Bergeron transmission lines of 100 km for a phase-to-ground fault is implemented. The distance to fault is evaluated thanks the identified inductance with the RLC algorithm. As expected, the errors are higher if the mutual coupling is not taken into account by the identification algorithm. However, the results are almost identical if the approximation (6.39) is used or not. It can be explained by the fact that this approximation is related to the capacitance of the line which is not used to deduce the distance to fault. This result is important because it implies that the implemented method is also accurate if the transmission lines are not truly parallel along the complete length of the protected line.

6.9 Conclusions

In this chapter the RL and the RLC identification methods have been implemented and validated for all kind of faults. It has been achieved by assuming a perfect bolted fault. It

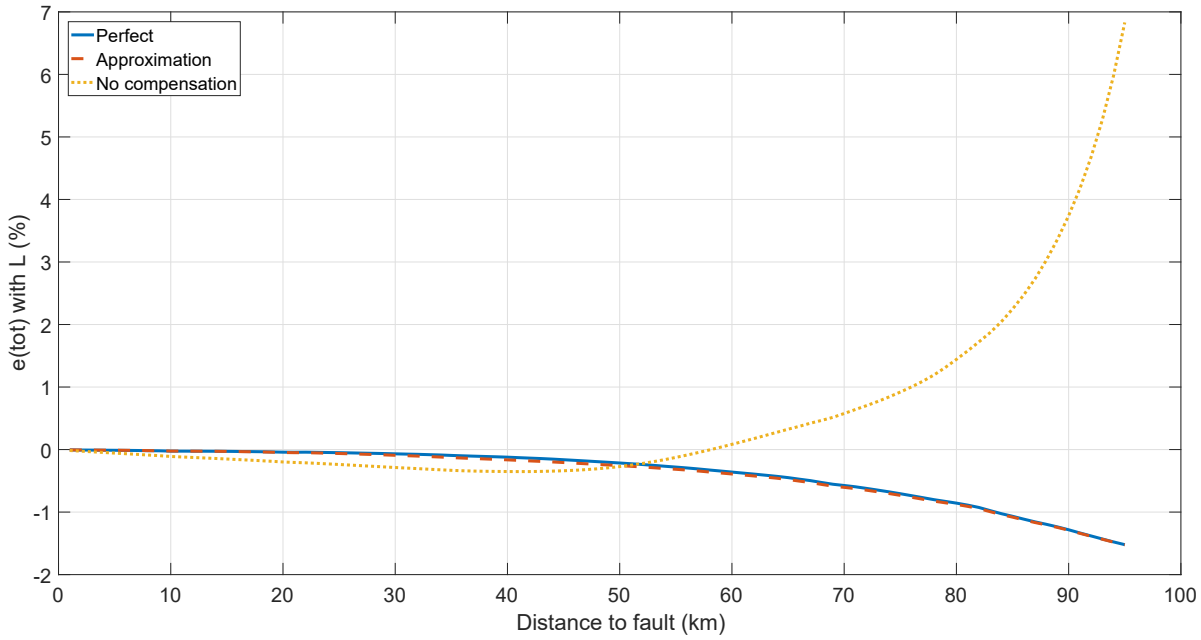

Figure 6.9: Relative errors (in % of the line) of the distance to fault evaluated thanks to the inductance for a phase-to-ground fault. The system is composed by two Bergeron parallel lines of 100 km. Comparison between the case of truly parallel lines (without the approximation (6.39)), the case with the use of the approximation (6.39) and the case without mutual compensation

is important to keep in mind that the accuracy of the distance to fault identification will decrease when the fault resistance increases. A blocking condition based on a maximum resistance threshold will be implemented in order to avoid the over-reaching.

It was shown that the phase-to-ground fault is more sensitive to an approximative knowledge of the parameters of the transmission line. The transfer function of the Γ model is less stable around the resonance frequency for this type of fault. The identification of the distance to fault may be less accurate than for the other types of fault if the frequency content of the signals is not zero around the resonance frequency.

It was also shown that the use of a constant distributed parameters model of line is accurate enough to represent a real-world transmission line (represented by a J. Marti model in this work) if the frequency range is limited to the first resonance frequency of the line. This frequency range depends on the length of the transmission line. Using Fig. 3.5, it is possible to define the cut-off frequency of the low-pass filter.

Finally, the RL and the RLC algorithm were adapted to take into account the mutual coupling effects of a parallel transmission line.

Chapter 8

Development of blocking conditions

8.1 Introduction

In the previous chapters an RLS estimation algorithm of the parameters of a faulted transmission line was implemented. The method was based on both RL and RLC models of line and was extended to a three-phase model for the different fault types. Moreover, a complete data acquisition system was implemented and tested. Compared to the impedance-based method, the time-domain algorithm proposed here, involves shorter algorithm windows. The decrease of the algorithm window may lead to a lower accuracy. It is thus important to develop some blocking criteria in order to avoid over-reaching. These blocking conditions will increase the security but will also decrease the dependability. When a fault is missed by the ultra-fast protection algorithm the regular protections can take over with a higher tripping time for some critical cases.

First, Section 8.2 defines the different test cases. It is important to make sure that the blocking conditions are efficient in all the cases. Secondly, the different security criteria will be presented and tested. Four different criteria will be implemented in this chapter: the convergence of the estimated parameters by the RLS method in Section 8.3; the use of a CI to add a security margin on the identified distance to fault in Section 8.4; a resistance threshold is defined to manage the impact of the remote injections in Section 8.5 and finally Section 8.6 shows how the Normalized Mean Squared Error (NMSE) can be used to avoid the over-reacting in some particular cases.

8.2 Test cases definition

The RLS identification methods based on the RL and the RLC model of line will be tested in this chapter. The forgetting factor λ and the initialisation factor δ used for the RLS algorithm are set to 1 and 10^3 respectively as suggested in Chapter 4. The complete data acquisition process presented in Chapter 7 will be used. It involves the CT and the VT,

the analog anti-aliasing filter, the CIC decimation filter and the FIR low-pass filter. The starting time of the algorithm is set to 2 ms after the true fault inception in order to take into account the delays of the data acquisition process and the electromagnetic travelling waves propagation.

The reference case is a three-phase Bergeron model of line of 100 km. The phase-to-ground fault and the phase-to-phase fault will be tested. The transmission line is fed by two voltage sources at both ends. The phase shift between the two sources is equal to 10° to permit an initial power flow in the transmission line. This phase shift is also necessary to study the remote injection impact when the resistance of the fault is not zero. The fault inception angle is 90°. Finally, a strong source and a weak source will be tested with an SIR equal to 0.1 and 5 respectively. The complete power system network is shown in Fig. 8.1.

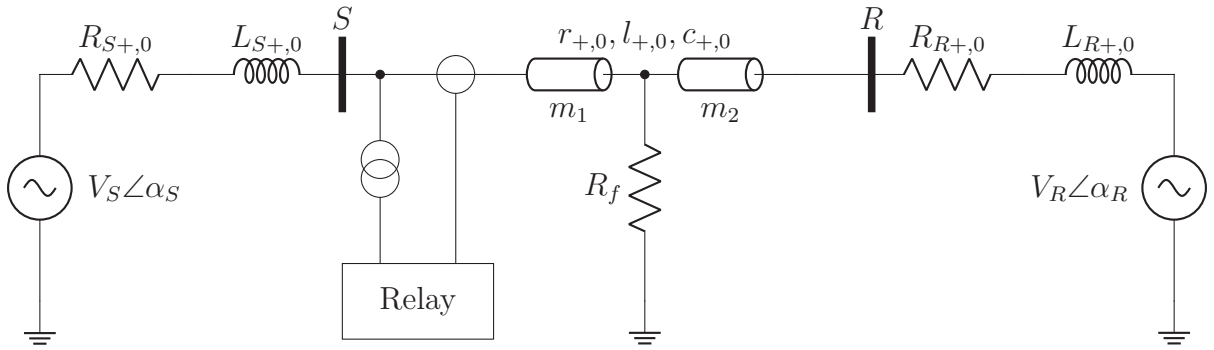

Figure 8.1: Double in-feeds Bergeron transmission line of 100 km

8.3 Convergence criteria

As the RLS algorithm continuously re-computes the evaluated distance to fault the identification could run on-line and could be stopped when a convergence criterion is met. Fig. 8.2 shows the evolution of the identified distance to fault based on the inductance as a function of the window length for the reference case faulted at the end of the line. The shape of the curve shows a fast convergence of the algorithm. In this section a convergence criterion of the algorithm will be defined. Moreover, the initialisation of the different parameters of the RLS method will be defined too.

A minimum window length W_{min} is imposed to increase the robustness of the algorithm. The convergence criterion implemented is defined as follows: the difference between two successive identified distances to fault $m_{i+1} - m_i$ is evaluated. If N_S successive differences are below a threshold d_{thres} the convergence is assumed (8.1).

$$|m_{i+1} - m_i| < d_{thres} \quad \forall i \in \{1, ..., N_S\} \tag{8.1}$$

This criterion is applied only on the inductance in order to avoid to decrease the performances of the algorithm. The values for the convergence parameters W_{min}, N_S and d_{thres} are shown in Table 8.1. These values can be optimized empirically by testing a large database of tests. The RLS method implies also some initialisation parameters. The parameters λ and δ have been already discussed in Chapter 4. It is also necessary to define a first estimation of the parameters to identify. As no a priori information about these parameters is available, it seems more efficient to initialise them at the middle line length $L/2$. The last parameter to identify K coming from the inclusion of the transformer model is initialised at 1. The values for the initialisation parameters are also shown in Table 8.1.

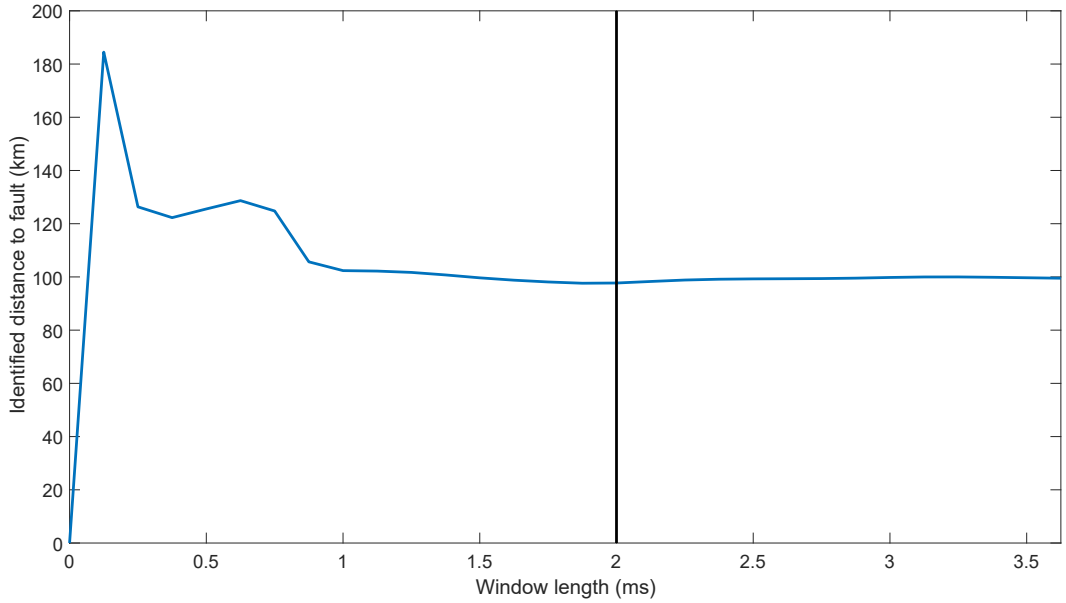

Figure 8.2: Evolution of the identified distance to fault as a function of the window length. Phase-to-ground fault at the end of a Bergeron transmission line of 100 km

Initialisation parameters						**Convergence parameters**		
$\boldsymbol{\lambda}$	$\boldsymbol{\delta}$	$\mathbf{x_1(t_0)}$	$\mathbf{x_2(t_0)}$	$\mathbf{x_3(t_0)}$	$\mathbf{x_4(t_0)}$	$\mathbf{W_{min}}$	$\mathbf{N_S}$	$\mathbf{d_{thres}}$
1	10^3	$c^*_\alpha \cdot (L/2)^2$	$l_\alpha \cdot L/2$	$r_\alpha \cdot L/2$	1	2 ms	4	1 km

Table 8.1: RLS parameters

8.4 Confidence interval

As explained in Section 4.5.4 it is possible to add a security margin on the identified parameters based on residuals. This security margin is related to the evaluation of a

CI. The CI depends only on the matrices involved in the identification algorithm. The parameter SF_{CI} (depending on the confidence level) is the only external parameter to fix. Firstly, the discussions will be made for the RLC identification algorithm. The conclusions for the RL identification algorithm will be presented at the end of the section. Fig. 8.3 shows that the distance to fault is under-estimated for the reference case (on the top). This under-estimation will lead to over-reaching. By adding the CI on the identified distance to fault, it gives a secured distance to fault which is always higher or equal to the actual distance to fault (on the bottom). In this example the value of SF_{CI} is 15. Generally, the value of the parameter SF_{CI} is given by a statistical tables. For example the Student's t-distribution table gives $SF_{CI} = 3.674$ for a confidence level of 99.95% and $n-m$ degrees of freedom [83]. However, as explained in Chapter 4, the CI may be biased and is used in an alternative way (add a security margin related to residuals and therefore to the estimation errors). It is therefore necessary to take a greater security margin by taking a greater value of SF_{CI}. The objective of this section is to define a value of SF_{CI} by testing the different cases presented before.

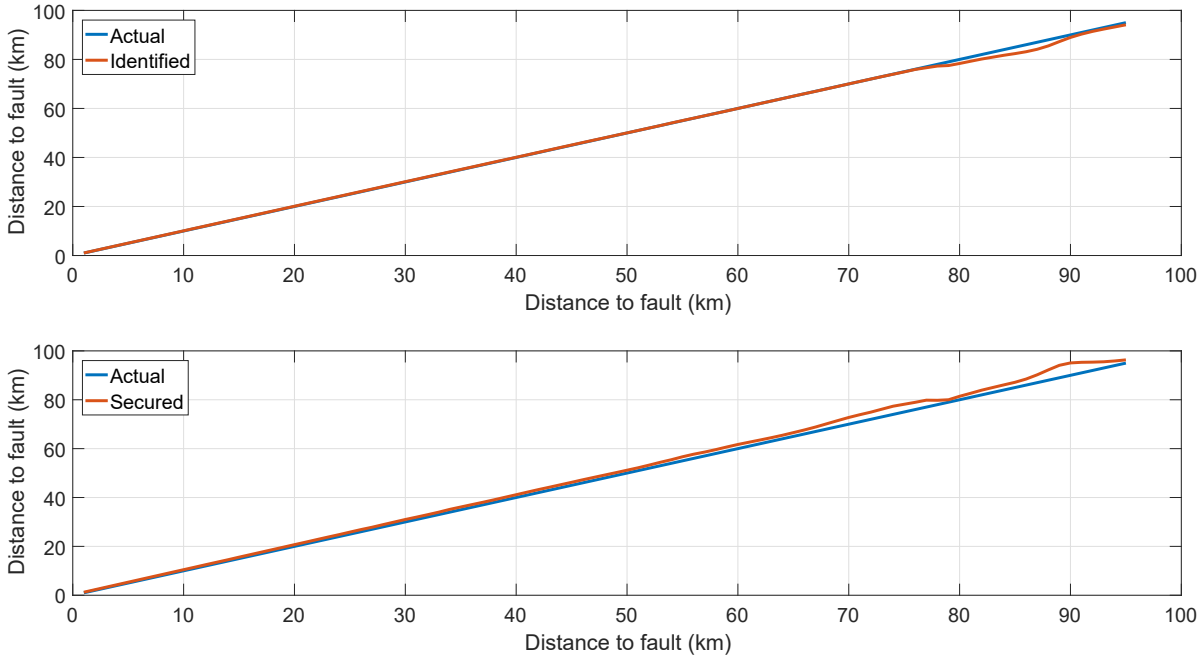

Figure 8.3: Actual distance to fault versus identified distance to fault (above) or secured distance to fault (below)

Another possibility would be to add a security margin based on the residuals indicator MSE. However, the MSE depends a lot on the magnitude of the signals. For example the MSE's obtained for a fault with an inception angle of 90° and 0° can show a ratio of several dozens. Define $m_{secured}$ as the secured identified distance to fault thanks to the CI and $m_{setting}$ as the protected zone by the ultra-fast distance algorithm. Indeed, the protected zone also called zone 1 for the conventional relays is limited at a fraction of the

total line length due to some uncertainties. It permits to avoid over-reaching even if some errors remain possible. A usual value for the zone 1 is 80% of the total line length [84]. Fig. 8.4 shows the results obtained for the three-phase Bergeron model of 100 km with a phase-to-phase fault. The figure on the left side shows the actual distances to fault versus the secured identified distances to fault. 4 areas are delimited by $m_{setting}$:

- the area 1 corresponds to the faults correctly identified as inside the zone 1: $m_{actual} \leq m_{setting}$ and $m_{secured} \leq m_{setting}$.
- the area 2 corresponds to the faults correctly identified as outside the zone 1: $m_{actual} \geq m_{setting}$ and $m_{secured} \geq m_{setting}$.
- the area 3 corresponds to the faults wrongly identified as outside the zone 1. These faults are missed: $m_{actual} \leq m_{setting}$ but $m_{secured} \geq m_{setting}$.
- the area 4 corresponds to the faults wrongly identified as inside the zone 1. It corresponds to an over-reaching (according to $m_{setting}$): $m_{actual} \geq m_{setting}$ but $m_{secured} \leq m_{setting}$.

The number of faults present in the area 3 must be minimized. The area 4 must be absolutely avoided because it would lead to an unwanted tripping. The figure on the right shows the algorithm times. The performances are very good because almost all the faults are tripped in 2 ms which corresponds to the minimum window. The maximum algorithm window was set at 10 ms.

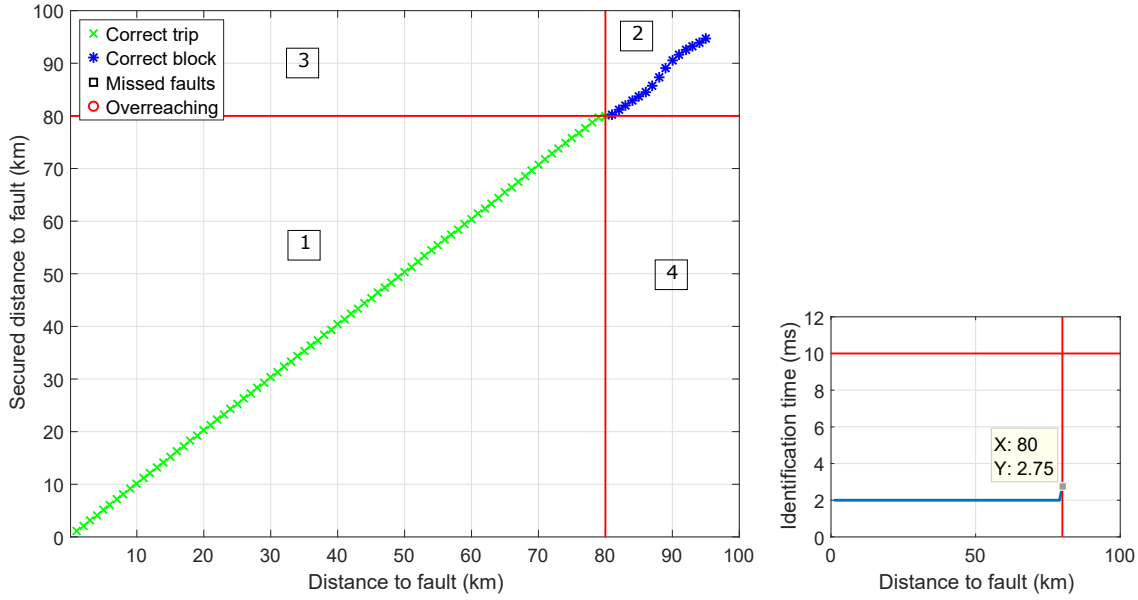

Figure 8.4: Distances to fault versus secured distances to fault (left) and identification times (right) for $SF_{CI} = 4$

The results for the different tests are presented in Appendix E. The phase-to-phase and the phase-to-ground faults for a strong and a weak source are tested. Both RL and RLC identification method are compared. The following findings appear:

- the value for the parameter SF_{CI} is chosen in order to avoid the over-reaching and to reduce the number of missed faults. For the RLC model SF_{CI} is equal to 6 and it is equal to 2 for the RL model. It is due to the fact that for the tested cases the distance to fault is under-estimated in the most of the cases for the RLC method while it is over-estimated in the most of the cases for the RL method.

- with the RLC method there is no missed faults for the tested cases. However, there is a small over-reaching for the phase-to-ground faults. Indeed, the faults until 82% of the line are tripped instead of 80%. The value of SF_{CI} necessary to avoid these over-reaching is very high and will decrease the time performances of the algorithm. As the over-reaching is very limited it seems more judicious to maintain the algorithm performances.

- with the RL method there is no over-reaching for the tested cases. However, there are some missed faults from 74% of the line length.

- finally, the tripping times of both methods are compared. For a strong network all the faults are tripped in maximum 3 ms with the RLC method and 4 ms with the RL method. For a weak network all the fault are tripped in maximum 4 ms with the RLC method. With the RL method the tripping times become greater than 5 ms from 54% of the line length.

8.5 Resistance threshold

The identified resistance of the faulted line is not used directly to estimate the distance to fault because the fault itself may have a not negligible resistance. Compared to the phasor-based methods the accuracy of the identified resistance may be lower for the fast distance algorithm implemented in this thesis. Firstly, the linearisation of the RLC model of line was made by assuming a bolted fault. It was shown in Section 3.5.2 that the identified resistance of the line is less accurate for a resistive fault. Secondly, it was also shown that a bad knowledge of the time constant of the transformers impacted the accuracy of the identified resistance of the line. For all these reasons, the distance to fault is deduced from the identified inductance. However, the remote injection presented in Section 3.8 will impact the value of the inductance of the line in the case of a resistive fault. It may lead to an under-reaching or an over-reaching depending on the power flow direction. It is a well known phenomenon and a lot of methods have been proposed and implemented in order to solve or to limit this impact [85]–[88]. This phenomenon is therefore not

directly linked to the new distance algorithm implemented in this thesis. A simple rule is implemented in this thesis in order to limit the possible over-reaching. Of course, this point could be improved based on all the available literature on this specific subject. The idea is to define an upper and a lower limit for the identified resistance R_{ident}:

$$-10\%\ R_{line} \leq R_{ident} \leq R_{thres} + R_{setting} \tag{8.2}$$

where R_{thres} is the maximum fault resistance accepted. This value is a setting depending on several parameters like the line length and the phase shift between the sources at both ends of the line. In this thesis a maximum fault resistance of 10 Ω and 5 Ω is considered for a phase-to-ground and a phase-to-phase fault respectively. $R_{setting}$ is the resistance of the transmission line at the end of the protected zone. The upper limit permit to avoid the over-reaching due to the remote end impact. The lower limit defined here as -10% of the line resistance is useful for the very small distances to fault. Indeed, when the fault is located very close to the relay, the line parameters identified could be negative due to the possible inaccuracies of the algorithm or the metering. A small negative resistance should be tolerated. The lower limit of the inductance will be discussed later because it implies the directional element of the protection. The case presented in Fig. 8.4 is now tested with a fault resistance of 5 Ω between the faulted phases. The results are shown in Fig. 8.5 where it appears that there are some over-reaching until 89% of the line length while the secured zone is set at 80%. In this case the resistance limits defined above are not used. Not that the power flow direction was chosen to lead to over-reaching and not to under-reaching.

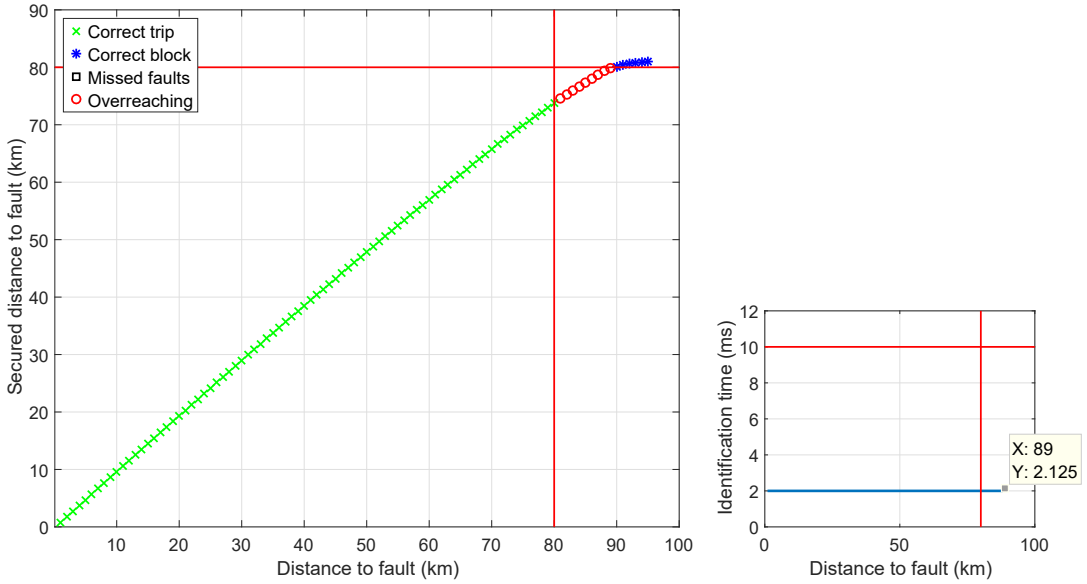

Figure 8.5: Distances to fault versus secured distances to fault (left) and identification times (right). Fault resistance of 5 Ω without any resistance threshold

Fig. 8.6 shows the tripping times obtained with the resistance limits (8.2) for three different values of R_{thres}. The choice of this parameter implies a compromise between the security (over-reaching) and the dependability (under-reaching) of the protection.

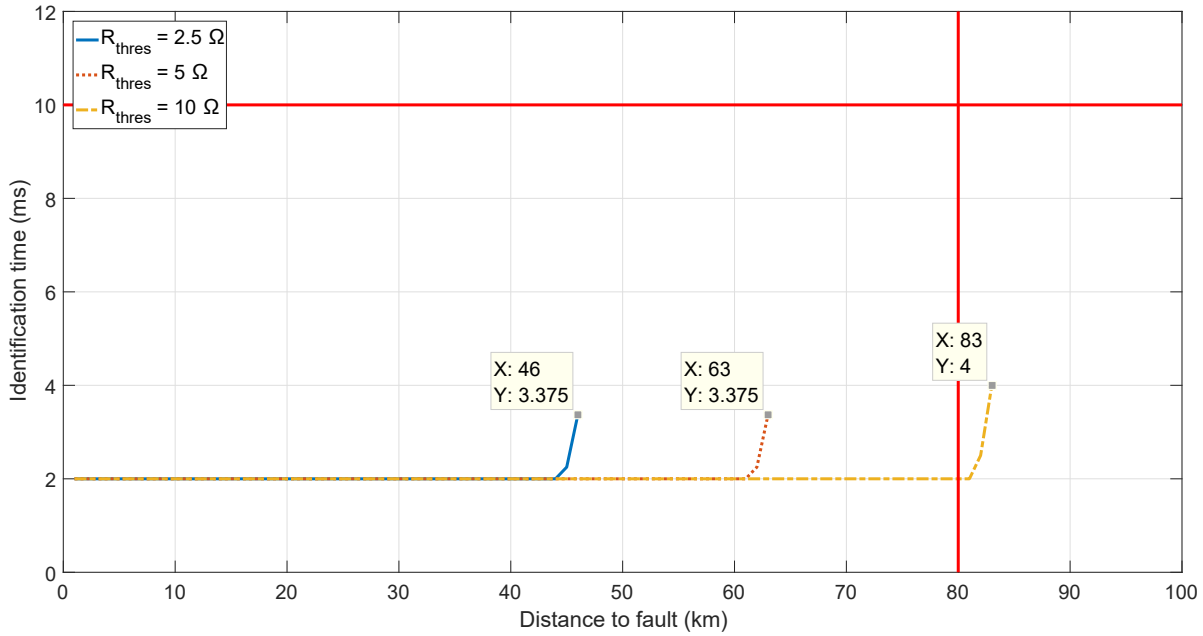

Figure 8.6: Distances to fault versus identification times. Fault resistance of 5 Ω and a resistance threshold of 2.5 Ω , 5 Ω and 10 Ω

8.6 Normalized Mean Squared Error

In Section 3.6 it was shown that the SIR had an impact on the high frequencies present in the signals of the faulted line. For a very strong voltage source the high frequencies were very far from the resonance frequency and therefore well filtered. It led to a bad capacitance identification but the inductance was correctly identified. For a very weak source the high frequency was close to the resonance and participated to a good identification of all the parameters of the line.

Fig. 8.7 shows a power transmission network with a transmission line connected before and after the protected line BC. The lengths of the transmission lines are 100 km, 100 km and 200 km for AB, BC and CD respectively. The objective of this test is to highlight the impact of the presence of some unwanted high frequencies remaining in the signals during the fault. The resonance frequency of a transmission line of 100 km is equal to about 730 Hz. As the cut-off frequency of the FIR low-pass filter is set at 600 Hz it permits to filter the frequencies higher than the resonance. However, if the fault is located in the next transmission line CD the relay will see a very long faulted line with a resonance frequency going from 730 Hz to 243 Hz at the end of the next line. In this case the filtering process

will not be sufficient if the high frequencies present in the signals are lower than 600 Hz. For the weak sources the high frequencies tend to be closer to the resonance frequency and therefore lower than 600 Hz for a long line.

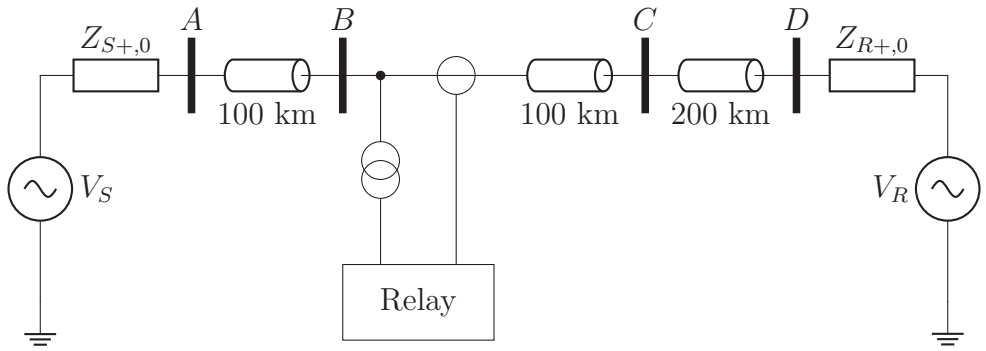

Figure 8.7: Network power system

Fig. 8.8 shows the distances to fault for a phase-to-phase fault located at different positions (from the protected line BC to the end of the next line CD). The actual, the identified and the secured distance to fault are represented for a strong source with an SIR of 0.1 (above) and a weak source with an SIR of 5 (below).

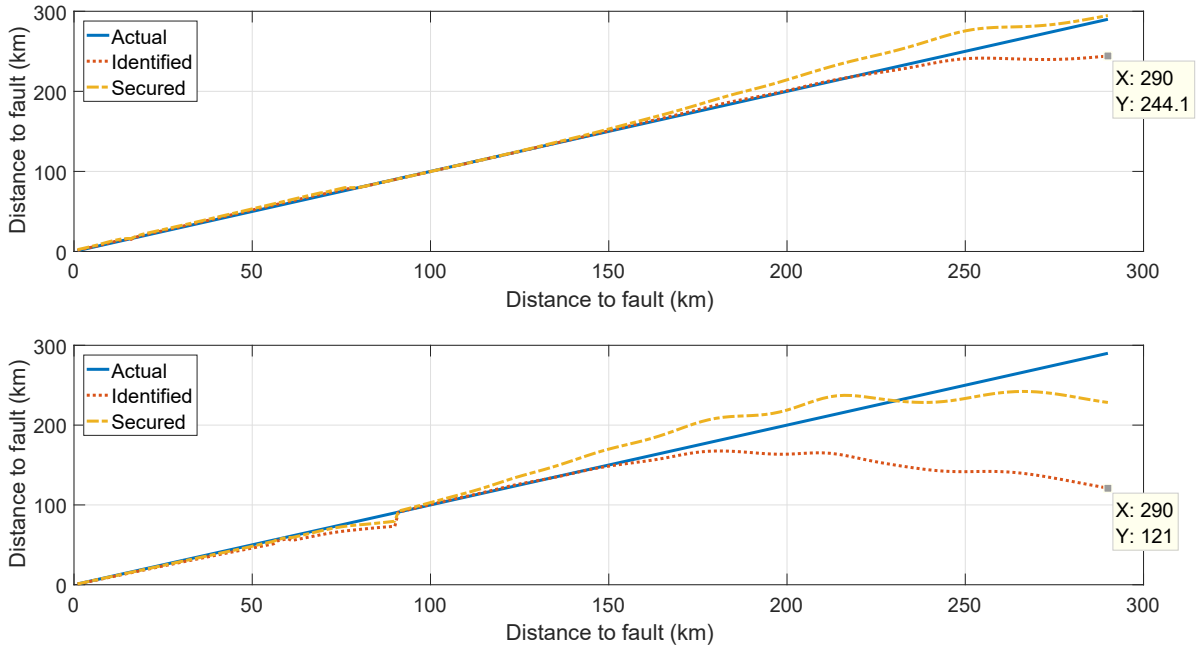

Figure 8.8: Actual, identified and secured distance to fault for an SIR equal to 0.1 (above) and an SIR equal to 5 (below)

For the strong system the identification becomes less accurate at the end of the next line. The identified distance to fault is 244.1 km instead of 290 km. However, the CI permits to obtain a secured distance to fault higher than the actual one. For a weak

system it appears that the distances to fault are under-estimated a lot from 200 km. The under-estimation is such that the secured distances to fault are lower than the actual distances. It is possible to imagine that in some configurations the distance to fault identified is such that it may lead to an over-reaching.

It is necessary to introduce a new criteria to avoid the possible over-reaching for a fault located very far from the relay. This criteria can be flexible because the possible over-reaching close to the end of the protected line is already controlled by the use of a secured distance to fault based on the CI. The solution of increasing the security factor of the CI is not efficient because it will decrease the dependability. It was mentioned before that the MSE was not suitable due to the difficulty to define a maximum threshold because it depended a lot on the signals involved. However, here the objective is to define a simple criterion that permits to block the algorithm if the identification is supposed unreliable. The threshold can be therefore more flexible. Nevertheless, a normalized MSE will be used to limit the dependence to the magnitude of the data involved. The NMSE used is defined as follows:

$$NMSE = \frac{MSE}{b_{max} - b_{min}} \tag{8.3}$$

where b is the vector of measured output of the least-squares system $Ax = b$. It corresponds to a normalization by the range of the data. In order to define a threshold for the NMSE the results of four different cases are presented in Fig. 8.9. They correspond to a phase-to-ground fault for a strong and a weak voltage source. Moreover, two different fault inception angles are tested. On the top of the figure the NMSE is plotted for the different distance to faults. On the bottom the identification errors of the distance to fault are plotted for the different distance to faults. The following findings appear:

- from a global point of view, the NMSE and the errors are increasing with the distance to fault. It is therefore possible to use the NMSE to limit the maximum error to acceptable values.

- the NMSE are very low when the errors are not too big and become very large for the very bad identifications. The maximum NMSE for a fault close to the end of the protected line (at 102 km) is 0.013 and it is close to 1 for the very distant faults. This difference of range is useful to define a threshold with a certain flexibility.

- the maximum admissible error on the distance to fault estimation is set to 20% of the protected line length. It corresponds to 166 km and 210 km for the tests with a fault inception angle of 90°. It leads to a maximum value for the NMSE of 0.225. The threshold defined at this step is equal to 0.2. Of course, this value may be adapted when testing the final algorithm with a complete database of tests.

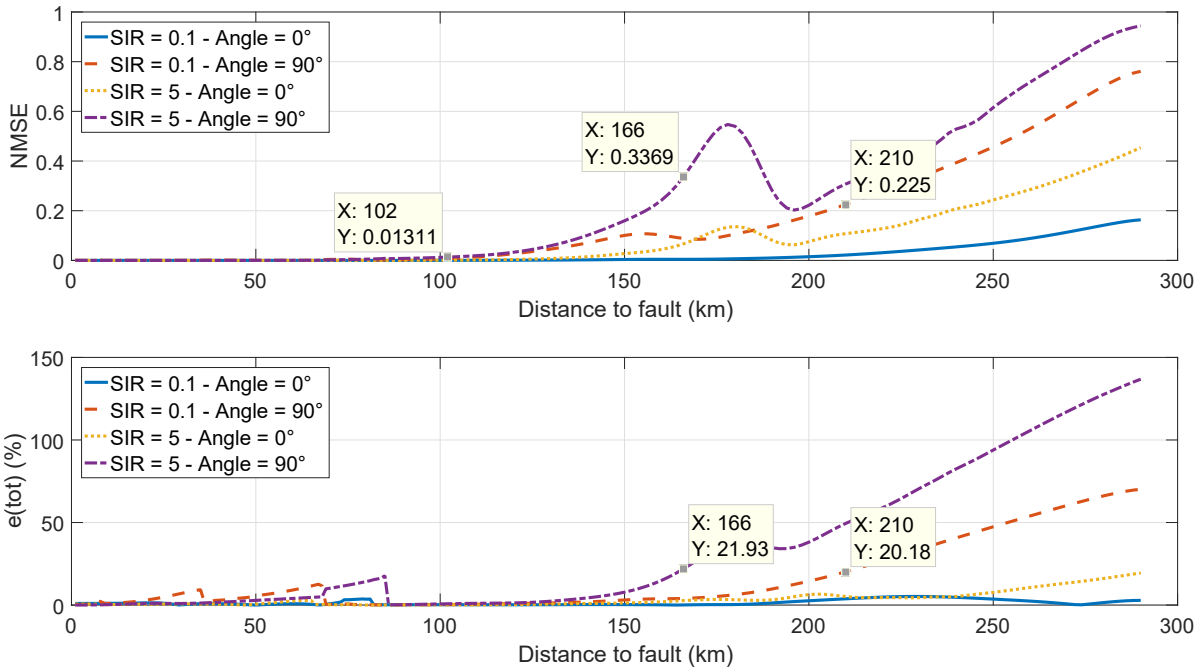

Figure 8.9: Distances to fault versus NMSE (above) and distances to fault versus distance identification errors in percent of the line length (below)

8.7 Conclusions

Fig. 8.10 summarizes all the blocking conditions implemented in order to avoid an over-reaching: the convergence of the identified distance to fault is required; a security margin based on the CI is added on the distance to fault in order to be more secure close to the end of the zone 1; a maximum permissible identified resistance is implemented in order to control the remote injection impact; finally an NMSE threshold is used to block very bad identifications that may occur for some very distant faults.

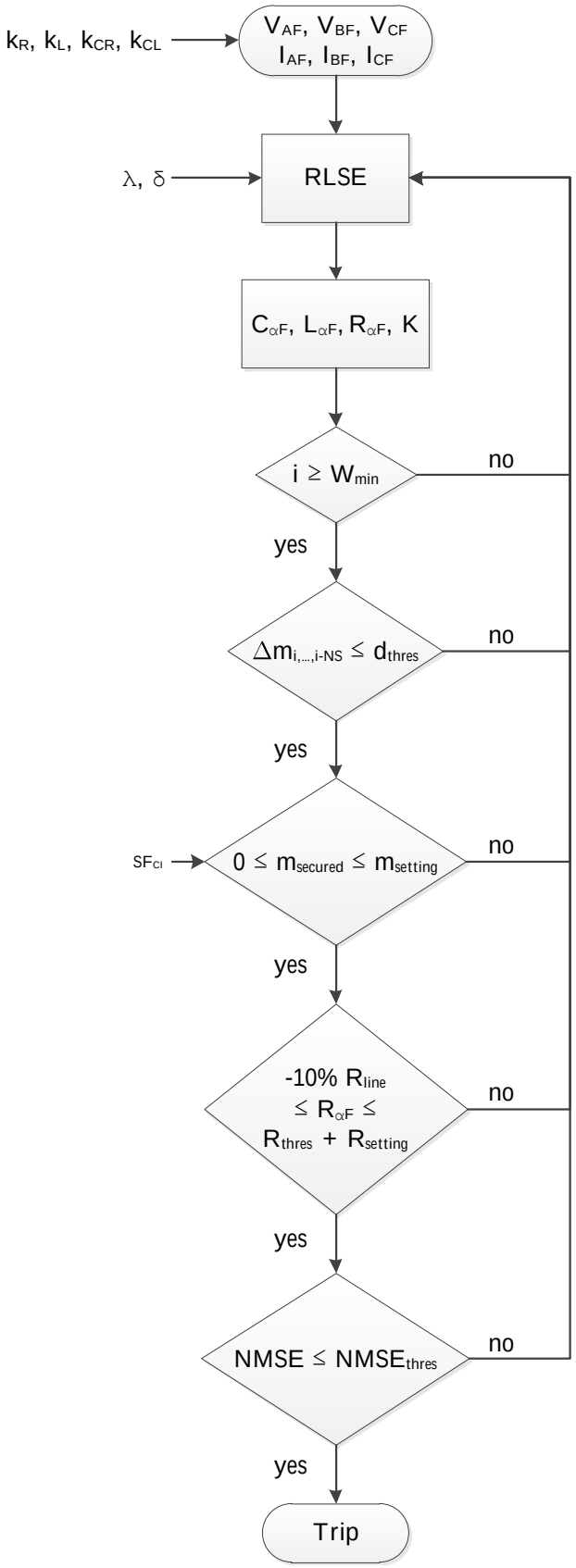

Figure 8.10: Complete blocking conditions process description

Chapter 9

Directional element algorithm

9.1 Introduction

The security is a fundamental aspect of the protection of a power transmission network. The previous chapters focused on the over-reaching. However, it is also necessary to avoid an unwanted tripping when the fault is located behind the relay. It is the role of the directional element. Its objective is to give accurately the direction of the fault (forward or reverse). In classical relays the fault direction is determined thanks to the phase shift between a polarizing quantity (usually the faulted phase voltage) and an operate quantity (usually the faulted phase current). The operating signal can be directly the angle between the two quantities [11] or the so-called torque signal [89], [90] detailed later. The direction may be also determined from the sign of the faulted impedance [34]. For the ultra-speed protection these methods cannot be applied directly because they are based on the phasors. However, the logic behind these methods can be exploited because it corresponds in time domain to a change of sign in the relation between the voltage and the current (and therefore to a negative distance to fault identified). For a fault not too close to the relay location the directional element would not be essential because the direction can be deduced from the sign of the identified parameters of the faulted line. However, for a close-in fault the voltage may be so low that a secure decision between a forward or a reverse fault is not possible. The existing fast directional algorithms are based on the incremental quantities. These methods will be implemented and tested in this chapter. The objective is to define the limitations of the existing methods and to propose some improvements. In Section 9.2 the concept of the incremental quantities will be first introduced. The main used directional algorithm based on these incremental quantities will be studied in Section 9.3. This method is based on the sign of a torque operating signal constructed with the incremental voltage and replica current at the relay location. Finally, the performances of the different methods proposed will be tested for different cases in Section 9.4.

9.2 Incremental quantities

The concept of the incremental quantities is based on two well-know principles of electricity: the first one is the Thévenin's theorem which holds that any linear electrical network can be reduced to an equivalent single voltage source and an equivalent single impedance. The second one is the superposition principle which holds that for a linear system the responses caused by several sources is the sum of the responses caused by each sources individually. It implies that a faulted network can be considered as the superposition of a pre-fault network and a pure fault network as shown in Fig. 9.1.

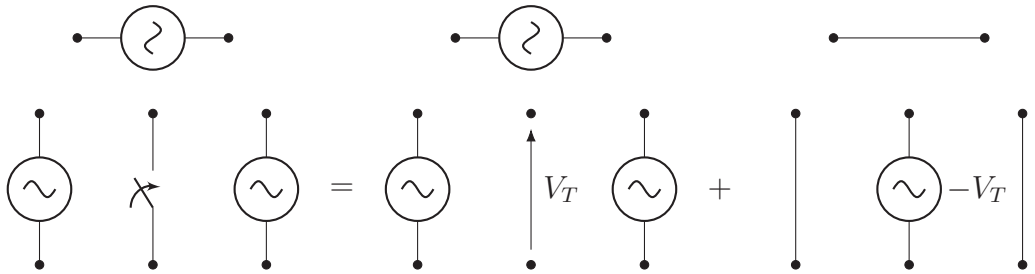

Figure 9.1: Illustration of the superposition principle of electrical circuit

The faulted network is the standard network studied in the previous chapters. The voltage and the current are governed by the voltage source, the loads and the fault. The pre-fault network is in steady-state and their signals correspond to the load components of the voltage and the current. The voltage V_T corresponds to the voltage at the fault location before this last. The fault network corresponds to a network governed only by an equivalent source of voltage $-V_T$ at the fault location. The physical voltage sources appear short-circuited. The fault network has the advantage that it does not depend on the load but only on the network parameters. The fault network can be therefore obtained by the difference between the faulted network and the pre-fault network. Their signals correspond to the so-called incremental quantities. For a voltage and a current signal the incremental quantities are represented by the following relations:

$$\begin{cases} \Delta V(t) &= V(t) - V_p(t) \\ \Delta I(t) &= I(t) - I_p(t) \end{cases} \tag{9.1}$$

where:

$$\begin{cases} V_p(t) &= V(t-T) \\ I_p(t) &= I(t-T) \end{cases} \tag{9.2}$$

The parameter T is the fundamental period of the signals. Theoretically, the pre-fault

conditions may be chosen a few cycles before but it is not recommended because of the possible frequency deviation.

9.3 Torque signal method

9.3.1 Forward fault

The first method studied was presented in [13], [91]. This method is based on the incremental quantities presented before. It is also assumed that the voltage sources and the transmission lines can be represented by a simple RL model as shown in Fig. 9.2 for a faulted network.

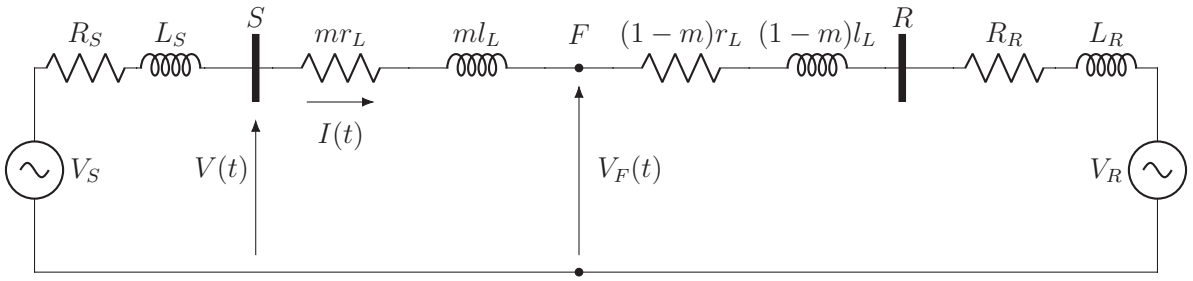

Figure 9.2: Double in-feeds RL transmission line faulted at F

Fig. 9.3 shows the corresponding fault network using the delta quantities. The transmission line is split in two parts: before and after the fault location F. The voltage step at F is the leading source of this network. The relay located at the bus S gives the incremental quantities $\Delta V(t)$ and $\Delta I(t)$.

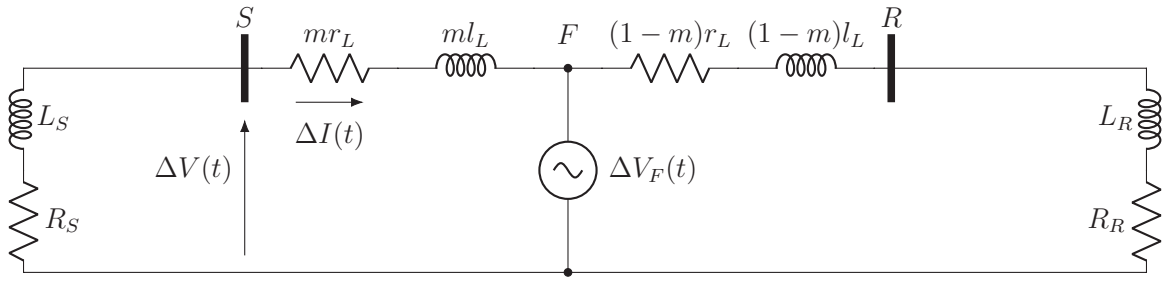

Figure 9.3: Incremental quantities of a faulted transmission line for a forward fault

The incremental voltage and current are linked by the following relation:

$$\Delta V(t) = -\left(R_S \Delta I(t) + L_S \frac{d}{dt} \Delta I(t)\right) \tag{9.3}$$

Dividing the right-hand side by the magnitude of the source impedance at the fundamental frequency, it leads to:

$$\Delta V(t) = -\left|Z_S\right| \left(\frac{R_S}{|Z_S|} \Delta I(t) + \frac{L_S}{|Z_S|} \frac{d}{dt} \Delta I(t) \right) \tag{9.4}$$

At this step the term of incremental replica current is introduced and is defined as follows:

$$\Delta I_Z(t) = D_0 \Delta I(t) + D_1 \frac{d}{dt} \Delta I(t) \tag{9.5}$$

where:

$$\begin{cases} D_0 = \dfrac{R_S}{|Z_S|} & (9.6) \\ D_1 = \dfrac{L_S}{|Z_S|} & (9.7) \end{cases}$$

It finally leads to:

$$\Delta V(t) = -\left|Z_S\right| \Delta I_Z(t) \tag{9.8}$$

Note that an equivalent method was also proposed in [15] but the concept of replica impedance was used instead of the incremental replica current. The replica impedance may be defined as follows:

$$Z_Z = -\left(R_S + L_S \frac{d}{dt} \right) \tag{9.9}$$

The relation (9.8) shows that the incremental voltage and replica current are linked by the opposite of the source impedance. The forward fault is therefore defined by the elements behind the relay location. The source impedance before and after the protected line must include the impedance of all the elements before and after this line (previous and next transmission lines, voltage sources, capacitor banks, transformers, ...). In practice, the parameter used to represent the source impedance is the SIR. However, the SIR is not always very well know and moreover this last changes with the topology of the transmission network. It is suggested in [92] to calculate the SIR under normal conditions and under N-1 conditions (considering a single outage of any system element like a generator, a transmission line, a transformer, etc.) to chose the parameters of the protection for the critical cases. It is possible to determine the resistance R_S and the inductance L_S of the equivalent source from the parameters of the protected line and the SIR. The SIR can be expressed as follows:

$$SIR = \frac{|Z_S|}{|Z_L|} = \frac{\sqrt{R_S^2 + (\omega L_S)^2}}{\sqrt{R_L^2 + (\omega L_L)^2}} = \frac{\sqrt{R_S^2 + (\omega \tau_S R_S)^2}}{\sqrt{R_L^2 + (\omega \tau_L R_L)^2}} = \frac{R_S}{R_L} \frac{\sqrt{1 + (\omega \tau_S)^2}}{\sqrt{1 + (\omega \tau_L)^2}} \tag{9.10}$$

where the parameters τ_S and τ_L are the time constants of the source and the line respec-

tively. They are defined by the relations (9.11) and (9.12).

$$\begin{cases} \tau_S = L_S/R_S & (9.11) \\ \tau_L = L_L/R_L & (9.12) \end{cases}$$

If it is assumed that the time constants of the equivalent source and the line are not too different, it leads to the following approximations:

$$\begin{cases} R_S \approx SIR \cdot R_L & (9.13) \\ L_S \approx SIR \cdot L_L & (9.14) \end{cases}$$

These results permit to define the parameters D_0 and D_1 directly from the line parameters as follows:

$$\begin{cases} D_0 = \dfrac{R_S}{|Z_S|} \approx \dfrac{R_L}{|Z_L|} & (9.15) \\ D_1 = \dfrac{L_S}{|Z_S|} \approx \dfrac{L_L}{|Z_L|} & (9.16) \end{cases}$$

9.3.2 Reverse fault

The case of a reverse fault is represented by the equivalent fault network in Fig. 9.4.

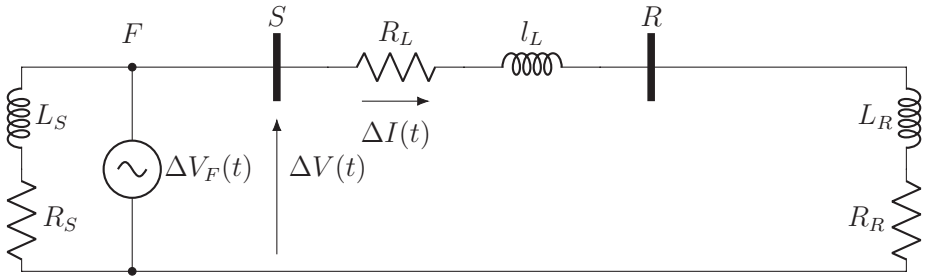

Figure 9.4: Incremental quantities of a faulted transmission line for a reverse fault

The incremental voltage and current are linked by the following relation:

$$\begin{aligned} \Delta V(t) &= (R_L + R_R)\,\Delta I(t) + (L_L + L_R)\,\frac{d}{dt}\Delta I(t) \\ &= |Z_L + Z_R| \left(\frac{R_L + R_R}{|Z_L + Z_R|}\Delta I(t) + \frac{L_L + L_R}{|Z_L + Z_R|}\frac{d}{dt}\Delta I(t) \right) \\ &= |Z_L + Z_R| \left(\frac{R_L(1+SIR)}{|Z_L(1+SIR)|}\Delta I(t) + \frac{L_L(1+SIR)}{|Z_L(1+SIR)|}\frac{d}{dt}\Delta I(t) \right) \\ &= |Z_L + Z_R| \left(D_0 \Delta I(t) + D_1 \frac{d}{dt}\Delta I(t) \right) \\ &= |Z_L + Z_R|\,\Delta I_Z(t) \end{aligned} \tag{9.17}$$

It appears that the reverse fault is defined by the element in front of the relay location (protected line and remote-end voltage source). The final form of the previous relation is exact only if $\tau_L = \tau_R = \tau_S$. This assumption already mentioned before is important for the implementation of the method. First, it permitted to define the parameters D_0 and D_1 needed for the replica current directly from the transmission line parameters. Secondly, it permitted to construct a single replica current without a prior knowledge of the fault direction. Indeed, without this assumption the replica current for a forward and a reverse fault depends on the parameters of the equivalent source before and after the protected line respectively. Fortunately, it has been already proved in [91] that the impact of this assumption is not critical for the performances of the algorithm.

9.3.3 Torque operating signal

In the previous section the relation between the incremental voltage and the incremental replica current was shown for a forward and a reverse fault. The directional algorithm proposed in [13] used a torque operating signal defined by (9.18).

$$s_{OP}(t) = \Delta V(t) \cdot \Delta I_Z(t) \tag{9.18}$$

Using the relations (9.8) and (9.17) it is possible to determine the analytical value of the torque signal for an ideal case (RL model and uniform time constant). It leads to (9.19) and (9.20) for a forward and a reverse fault respectively.

$$s_{OP}(t) = -\left|Z_S\right| \cdot \left(\Delta I_Z(t)\right)^2 \qquad \text{forward fault} \tag{9.19}$$

$$s_{OP}(t) = \left|Z_L + Z_R\right| \cdot \left(\Delta I_Z(t)\right)^2 \qquad \text{reverse fault} \tag{9.20}$$

This results is very important because it shows that the torque operating signal is always negative for a forward fault and always positive for a reverse fault. Theoretically, a simple comparison of the torque signal with zero would permit to determine the fault direction. However, the security may be improved by comparing the torque operating signal with two adaptive thresholds $s_{FWD}(t)$ and $s_{REV}(t)$ deduced from (9.19) and (9.20). The adaptive thresholds are given by (9.21) and (9.22).

$$s_{FWD}(t) = -Z_{FWD} \cdot \left(\Delta I_Z(t)\right)^2 \tag{9.21}$$

$$s_{REV}(t) = Z_{REV} \cdot \left(\Delta I_Z(t)\right)^2 \tag{9.22}$$

where the relay settings Z_{FWD} and Z_{REV} are set at (9.23) and (9.24) respectively.

$$Z_{FWD} = 0.3 \cdot \left|Z_{S(MIN)}\right| \tag{9.23}$$

$$Z_{REV} = 0.3 \cdot |Z_L| \tag{9.24}$$

The value of 0.3 is a dependability factor chosen in [93] to take into account the non-homogeneity between the line and the source impedances (different time constants). With these values of Z_{FWD} and Z_{REV} the operating signal s_{OP} will be always higher or lower than the thresholds for a perfect case. The objective is mainly to take into account the possible variations or noises in the signal not due to the fault itself. Moreover, the security may be increased again by averaging the torque signals. s_{OP}, s_{FWD} and s_{REV} will be integrated first before being compared. A minimum threshold level Δ_{MIN} is finally used. The complete algorithm is summarized in Fig. 9.5.

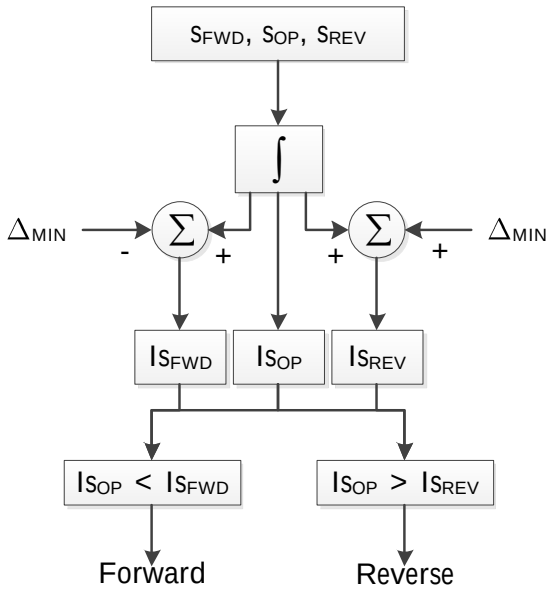

Figure 9.5: Torque operating signal algorithm

The algorithm is first applied on an ideal case in order to highlight the first conclusions. The power system network considered here is composed by only RL models for the transmission lines and the voltage sources. Fig. 9.6 and 9.7 show the signals for a line of 300 km faulted at 150 km of the relay location in forward and reverse direction respectively. The time constant is uniform in the complete network. On the top of the figures are represented the incremental voltage and replica current. As expected these two signals have an opposite polarity for a forward fault and the same polarity for a reverse fault. Moreover, the respect of these polarities may be easily visualised in the figures on the bottom left representing the torque operating signal $s_{OP}(t)$. Indeed, $s_{OP}(t)$ is strictly positive or negative at each time for the forward or reverse fault respectively. As mentioned before the operating signal exceeds directly the adaptive thresholds for an

ideal case. Finally, the figures at the bottom right shows the integrated torque signals. The fault detection time is mainly impacted by the value of the threshold Δ_{MIN}.

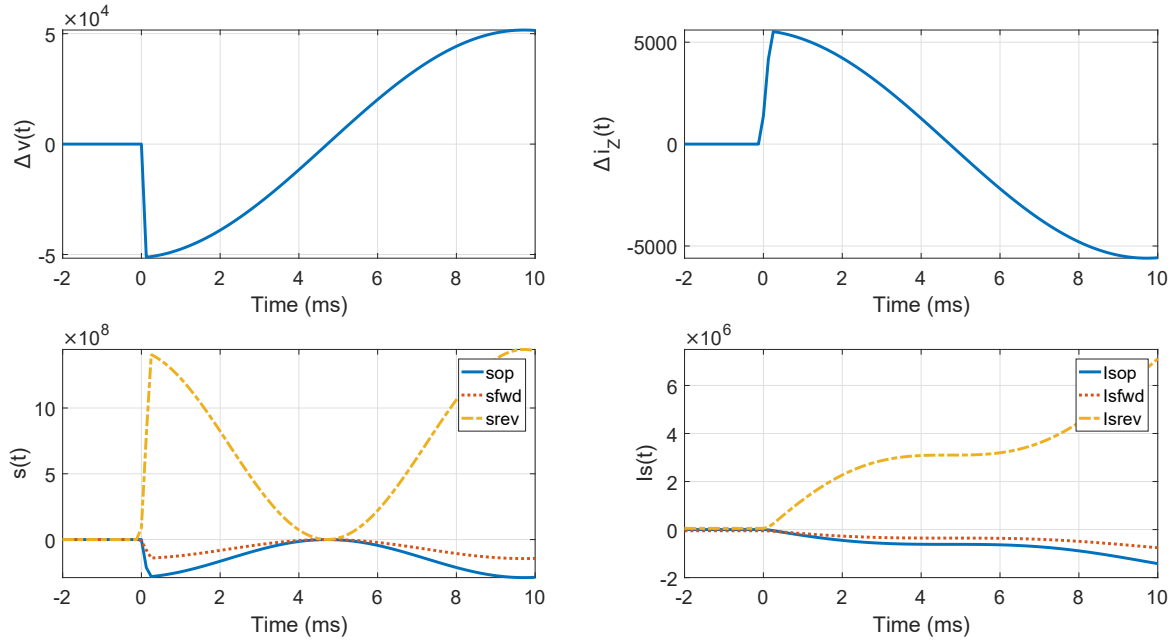

Figure 9.6: RL model of line of 300 km faulted at the middle in forward direction. $\tau_L = \tau_S = \tau_R = 16$ ms; SIR $= 0.1$; $\alpha = 90°$

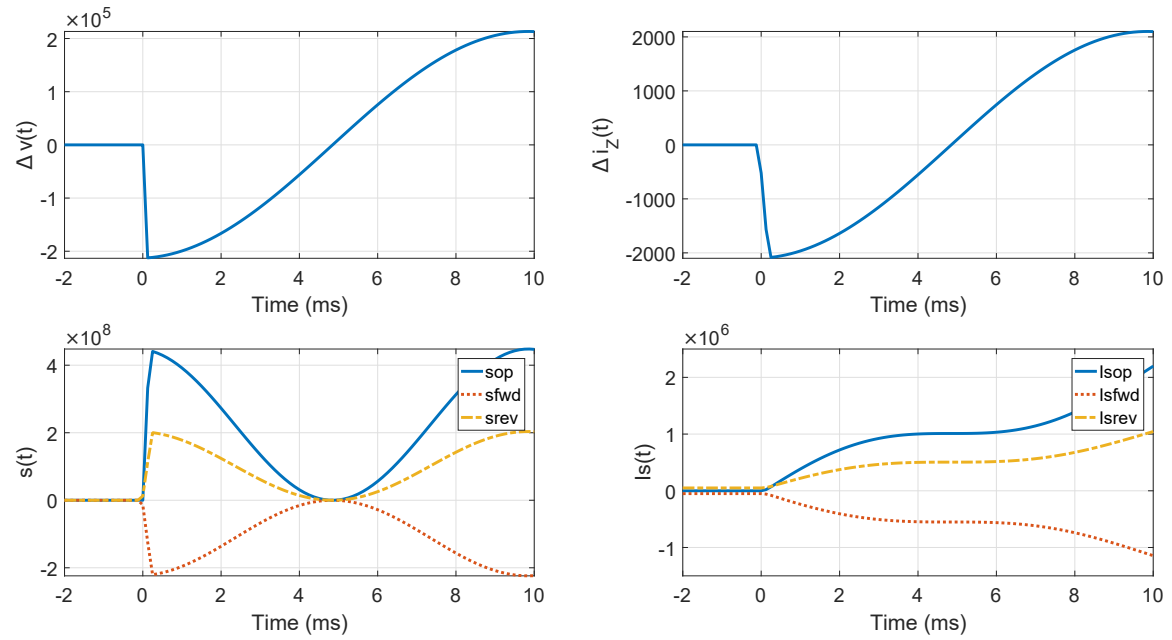

Figure 9.7: RL model of line of 300 km faulted at the middle in reverse direction. $\tau_L = \tau_S = \tau_R = 16$ ms; SIR $= 0.1$; $\alpha = 90°$

In Fig. 9.8 the tripping times of the directional algorithm are shown for forward faults (above) and reverse faults (below). The objective is to determine the impact of some

parameters on the performances of this method. The time constant of the transmission line τ_L is equal to 16 ms for all the tested cases. The first case may be used as reference because it corresponds to the most suitable scenario. Indeed, the time constant is homogeneous; the network is strong leading to a huge torque signal (linked to the short-circuit power) and the fault inception angle is equal to 90° leading to a maximum incremental voltage at the start of the fault. The following observations can be made:

- as mentioned before the difference between the time constants of the transmission line and the impedance of the sources has a limited impact on the speed of the algorithm. In this example τ_S is equal to 10 ms (fourth case).
- the SIR has a decreasing impact with the distance to fault. Indeed, for a close-in fault the short-circuit power is mainly limited by the impedance of the voltage sources. However, the increase of the tripping times remains still limited (around 1 ms in the worse case).
- for a fault inception angle of 0° the increase of the tripping time may reach 1.75 ms in the worse case. Of course the tripping times may decrease by changing the value of the constant threshold Δ_{MIN}. However, it would affect the security of the algorithm. The optimal value of Δ_{MIN} will be defined in Section 9.4 while testing the algorithm on a complete set of tests.

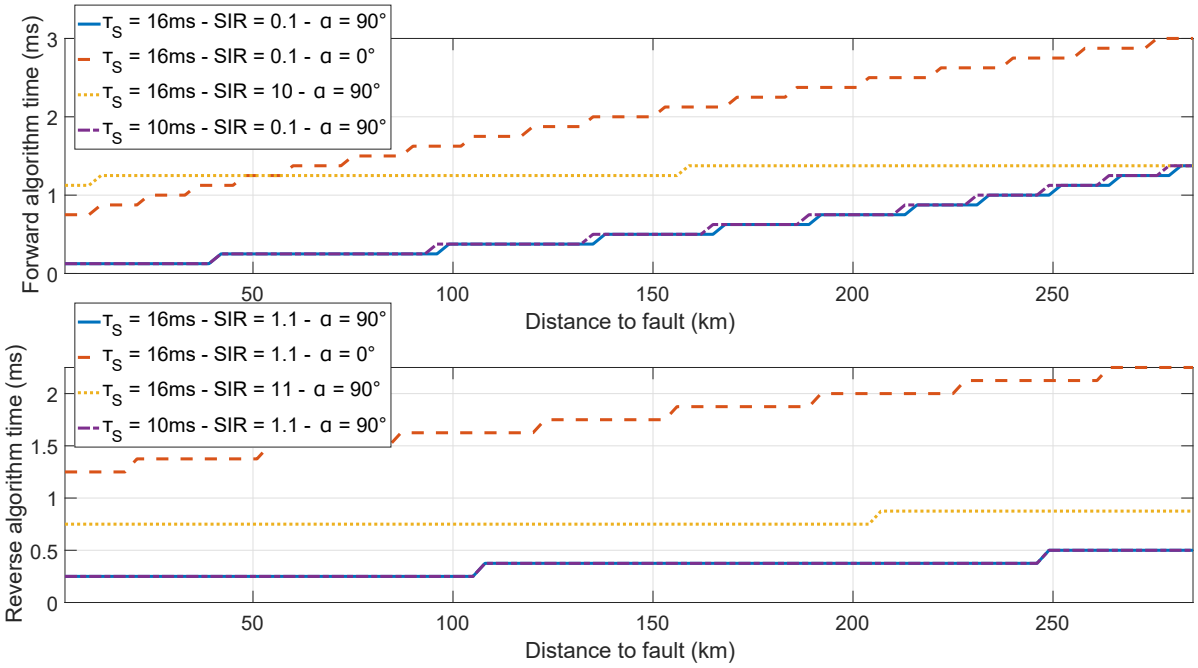

Figure 9.8: Directional algorithm tripping time for forward faults (above) and reverse faults (below)

9.3.4 Three-phase extension

In this section the directional algorithm will be extended to a three-phase system. The results obtained in Chapter 6 will be used and combined with the developments done in this chapter. The first case studied is the forward phase(A)-to-ground fault as represented in Fig. 9.9 with its equivalent fault network.

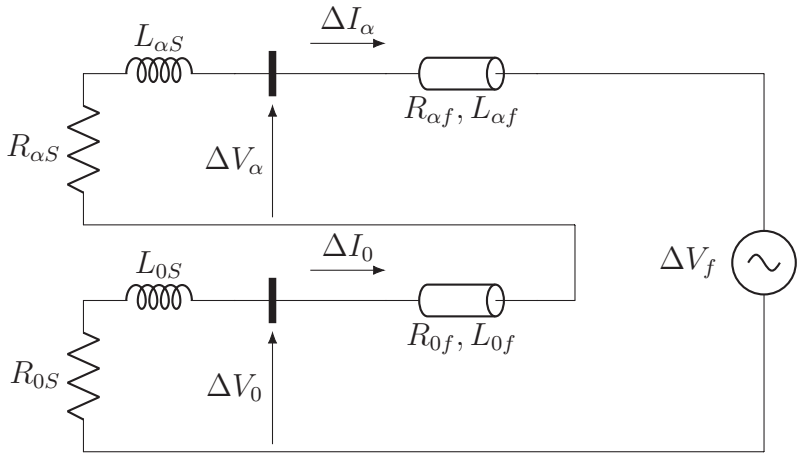

Figure 9.9: Equivalent circuit for a forward phase-to-ground fault in incremental quantities

The circuit shown above leads to the following relations:

$$\begin{cases} \Delta V_\alpha(t) = -\left(R_{\alpha S}\Delta I_\alpha(t) + L_{\alpha S}\dfrac{d}{dt}\Delta I_\alpha(t)\right) & (9.25) \\ \Delta V_0(t) = -\left(R_{0S}\Delta I_0(t) + L_{0S}\dfrac{d}{dt}\Delta I_0(t)\right) & (9.26) \end{cases}$$

The Clarke transform showed that $V_a(t) = V_\alpha(t) + V_0(t)$. As this relation is valid in a general way, the same relation is valid for the incremental voltage. It leads to:

$$\Delta V_a(t) = -\left(R_{\alpha S}\Delta I_\alpha(t) + L_{\alpha S}\frac{d}{dt}\Delta I_\alpha(t)\right) - \left(R_{0S}\Delta I_0(t) + L_{0S}\frac{d}{dt}\Delta I_0(t)\right) \quad (9.27)$$

Making the current $I_a(t)$ appear and dividing the right-hand side by the positive magnitude (equivalent to the α component) of the source impedance it leads to:

$$\begin{aligned} \Delta V_a(t) = -|Z_{\alpha S}| \Bigg[& \left(\frac{R_{\alpha S}}{|Z_{\alpha S}|}\Delta I_a(t) + \frac{L_{\alpha S}}{|Z_{\alpha S}|}\frac{d}{dt}\Delta I_a(t)\right) \\ & - \left(\frac{R_{\alpha S}}{|Z_{\alpha S}|}\Delta I_0(t) + \frac{L_{\alpha S}}{|Z_{\alpha S}|}\frac{d}{dt}\Delta I_0(t)\right) \\ & + \left(\frac{|Z_{0S}|}{|Z_{\alpha S}|}\frac{R_{0S}}{|Z_{0S}|}\Delta I_0(t) + \frac{|Z_{0S}|}{|Z_{\alpha S}|}\frac{L_{0S}}{|Z_{0S}|}\frac{d}{dt}\Delta I_0(t)\right)\Bigg] \end{aligned} \quad (9.28)$$

In order to replace the source parameters by the transmission line parameters the complete system is assumed to be homogeneous. It means that the following relations are respected:

$$\begin{cases} \tau_{\alpha S} = \tau_{\alpha R} = \tau_{\alpha L} & (9.29) \\ \tau_{0S} = \tau_{0R} = \tau_{0L} & (9.30) \\ \dfrac{|Z_{0S}|}{|Z_{\alpha S}|} = \dfrac{|Z_{0R}|}{|Z_{\alpha R}|} = \dfrac{|Z_{0L}|}{|Z_{\alpha L}|} & (9.31) \end{cases}$$

The impact of this assumption deeply studied in [93] may lead to dependability issues. The dependability factors of 0.3 used for Z_{FWD} and Z_{REV} in the adaptive thresholds were chosen to take into account the possible errors when these assumptions are not respected. The replica currents are finally introduced in (9.28) leading to:

$$\Delta V_a(t) = -\left|Z_{\alpha S}\right| \left(\Delta I_{aZ}(t) - \Delta I_{0Z}(t)\right) \tag{9.32}$$

where:

$$\begin{cases} \Delta I_{aZ}(t) = D_{0\alpha}\Delta I_a(t) + D_{1\alpha}\dfrac{d}{dt}\Delta I_a(t) & (9.33) \\ \Delta I_{0Z}(t) = D_{0\alpha}\Delta I_0(t) + D_{1\alpha}\dfrac{d}{dt}\Delta I_0(t) - \dfrac{|Z_{0L}|}{|Z_{\alpha L}|}\left(D_{00}\Delta I_0(t) + D_{10}\dfrac{d}{dt}\Delta I_0(t)\right) & (9.34) \end{cases}$$

and

$$\begin{cases} D_{0\alpha} = R_{\alpha L}/\left|Z_{\alpha L}\right| & (9.35) \\ D_{1\alpha} = L_{\alpha L}/\left|Z_{\alpha L}\right| & (9.36) \\ D_{00} = R_{0L}/\left|Z_{0L}\right| & (9.37) \\ D_{10} = L_{0L}/\left|Z_{0L}\right| & (9.38) \end{cases}$$

The same relations can be written for the other phase-to-ground faults. Moreover, for a reverse fault as for a single-phase system the incremental voltage and replica current are linked by the impedance seen in front of the relay. It leads to:

$$\Delta V_a(t) = \left|Z_{\alpha L} + Z_{\alpha R}\right| \left(\Delta I_{aZ}(t) - \Delta I_{0Z}(t)\right) \tag{9.39}$$

For a phase-to-phase fault the single-phase relations may be used directly if the β sequence components are used for the voltage and the current. The β sequence components correspond to the difference between the phases involved in the fault. Table 9.1 summarizes the input incremental voltages and replica currents needed for the different types of fault.

Loop	Voltage	Current
L(i)-G	ΔV_i	$\Delta I_{iZ} - \Delta I_{0Z}$
L(i)-L(j)	$\Delta V_i - \Delta V_j$	$\Delta I_{iZ} - \Delta I_{jZ}$

Table 9.1: Input voltages and currents for the different types of fault

9.4 Performances evaluation

In this section the directional algorithm will be tested with a three-phase Bergeron transmission line model. As shown in Fig. 9.10 the network is composed by a transmission line of 100 km behind and in front of the relay location in order to test the faults in both directions. The faults will be mainly very close to the relay location because, as mentioned before, the distance element algorithm is able to accurately determine the fault direction itself thanks the sign of the identified inductance. Moreover, a fault directly at the relay location will be tested in both directions (0^+ and 0^-).

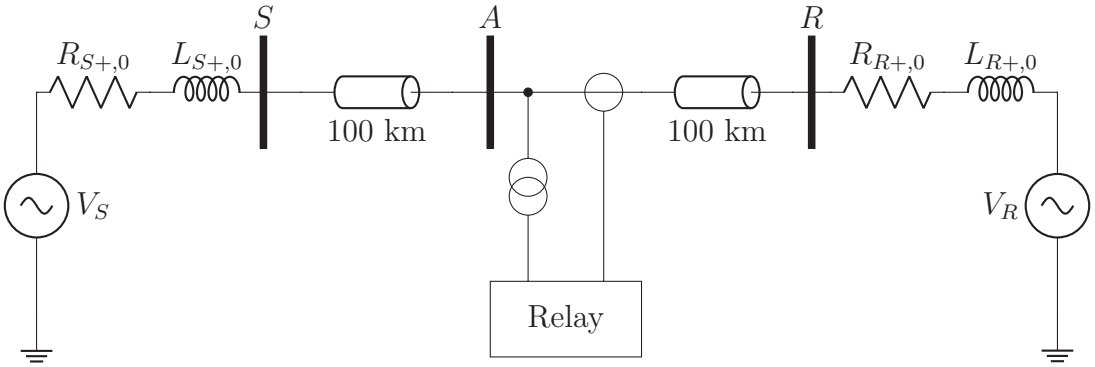

Figure 9.10: Network power system with a protected line of 100 km and a line behind the relay location of 100 km

For the first case a perfectly homogeneous system is assumed (see (9.29), (9.30) and (9.31)). A phase-to-phase fault is tested with an SIR of 1.1 behind the relay (it takes into account the voltage source impedance and the transmission line of 100 km). First of all, the distance element algorithm is tested for this configuration in order to highlight some observations. The results are shown in Fig. 9.11. The focus is made around -5 km and 5 km only. In this figure two graphs are represented. For the first one, only a strictly positive distance to fault is permitted. For the second, a negative value of -10 km (-10% of the line length) is tolerated. In this example two different possible issues can be highlighted:

- as expected, the distance element algorithm may identify a wrong fault direction for very close-in faults. The faults located at -900 m, -700 m and 0^- m have been

identified as forward faults. The voltage signal is so close to zero that all the possible sources of error (numerical approximations of derivatives and integrals, filters, ...) may impact the reliability of the identification. For the faults located further from the relay, the distance element algorithm was accurate.

- the distance element algorithm may be delayed for close-in faults. Indeed, during the identification process the parameters may oscillate between negative and positive values. In this example the tripping times for the faults at 700 m and 900 m are delayed if only positive values are tolerated. It is therefore possible to improve the performances of the algorithm by setting a small threshold for negative distance to fault and to confirm the fault direction with the directional element.

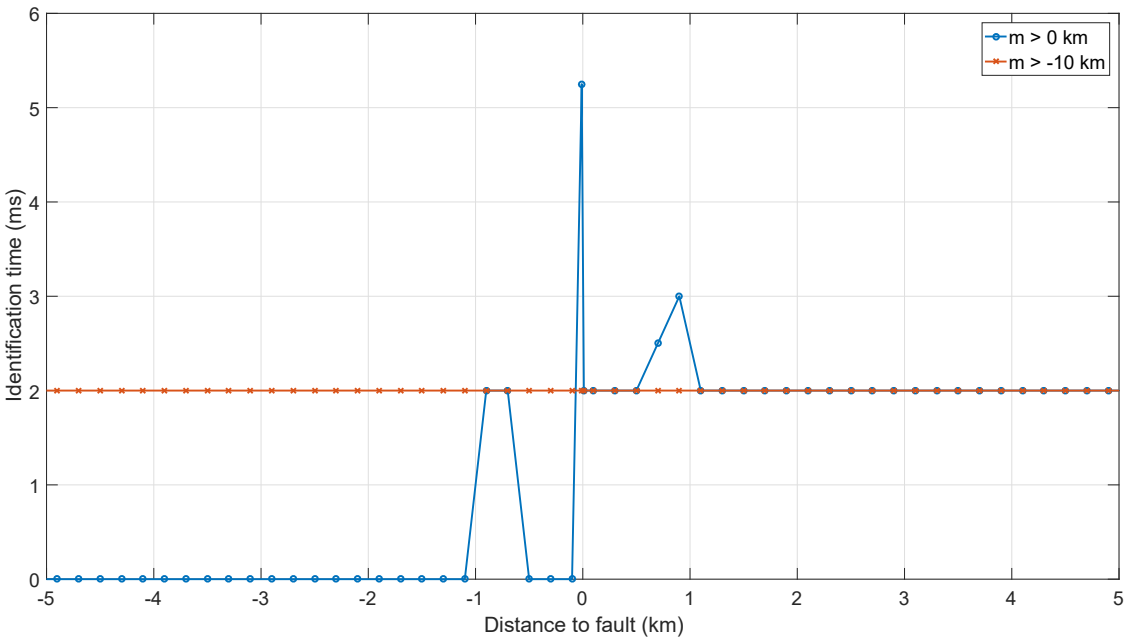

Figure 9.11: Distance element algorithm times for very close-in faults with strictly positive distances and negative distances tolerated until -10 km

Fig. 9.12 shows the algorithm times for the forward and the reverse tests. The fault direction was correctly determined for all the tested fault locations in both directions. The identification of the direction was very fast (maximum 0.375 ms after the start of the algorithm). Of course the speed of the algorithm depends on the value of the threshold Δ_{MIN} which was set at $5 \times 10^5\ V^2/\Omega$. In Fig. 9.13 and 9.14 the different signals used in this algorithm are shown for a fault located at 500 m and - 500 m from the relay respectively. The incremental voltage and replica current are shown on the top of the figures. These signals have an opposite polarity for the forward fault and the same polarity for the reverse fault. The torque signals and the integrated torque signals are shown on the bottom of the figures. The high frequencies present in the signals have a very small magnitude

and do not impair the polarity of the torque signal. It is important to observe that the actual fault time is set at 0 ms. However, due to the filtering process the incremental quantities begin to increase after about 1 ms. Moreover, as the exact starting time is not known because this information must be given by the fault detection element which is not implemented in this thesis, a constant starting time of 2 ms was chosen as for all the previous chapters. The torque signals increase only after 2 ms.

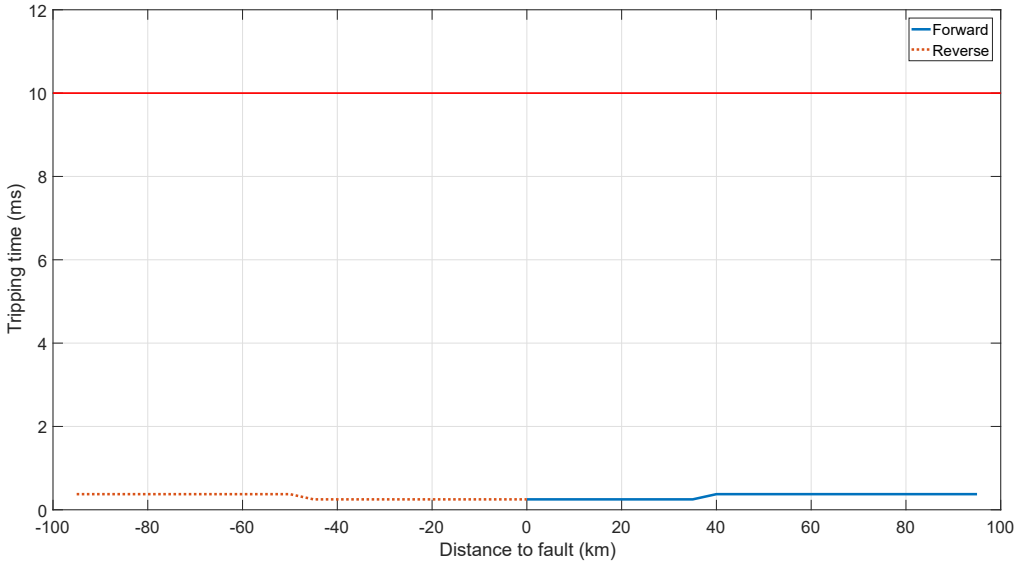

Figure 9.12: Forward and reverse algorithm times for phase-to-phase faults. Homogeneous system with $\tau = 16.46$ ms; SIR = 1.1

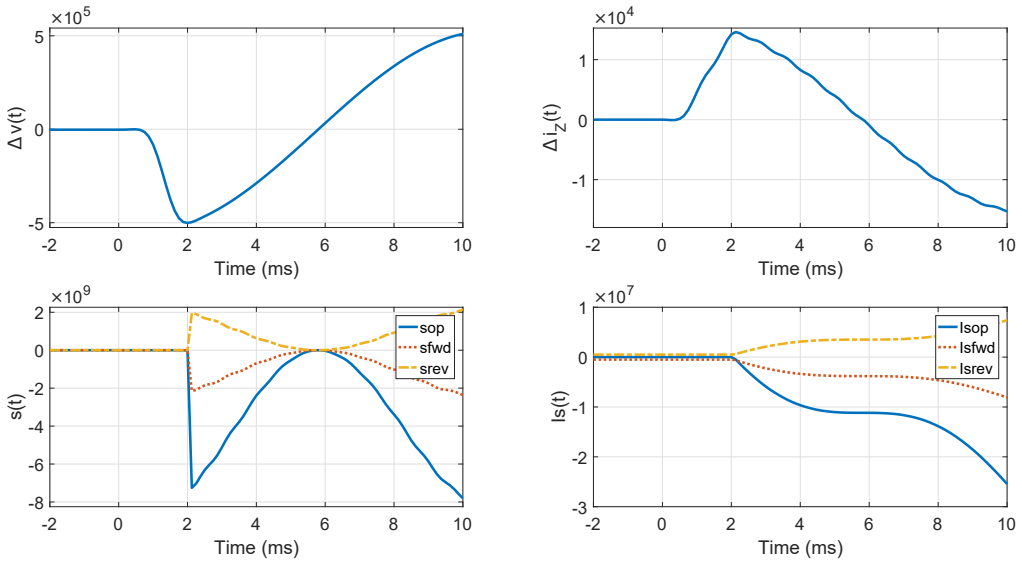

Figure 9.13: Incremental voltage (top right) and replica current (top left). Torque signals (bottom left) and integrated torque signals (bottom right). Homogeneous system; SIR = 0.1. $\Delta_{MIN} = 5 \times 10^5$. Forward fault at 500 m

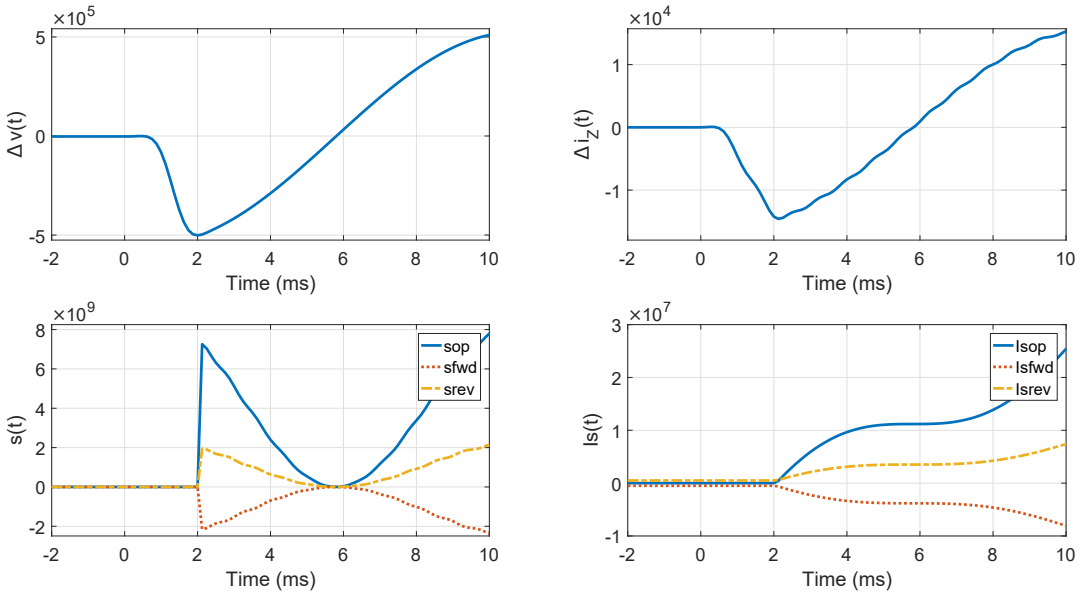

Figure 9.14: Incremental voltage (top right) and replica current (top left). Torque signals (bottom left) and integrated torque signals (bottom right). Homogeneous system; SIR = 0.1. $\Delta_{MIN} = 5 \times 10^5$. Reverse fault at -500 m

In Appendix F the results for all the tested cases are available. Phase-to-phase and phase-to-ground faults are tested. The transmission lines and the voltage source are not homogeneous. Strong and weak systems are tested with a fault inception angle of 90° and 0°. For a strong system the performances are very good even if the system is not homogeneous. The maximum algorithm times were 0.375 ms and 1.625 for a fault inception angle of 90° and 0° respectively. However, the method is not working well for a weak system as shown in Fig. 9.15. It appears that the algorithm has given the wrong fault direction for the faults far from the relay location. Moreover, no direction was identified for forward close-in faults. Fig. 9.16 and 9.17 show the signals for a fault occurring in forward direction a 500 m and 50 km respectively. The high frequencies are clearly visible in the incremental quantities signals. The directional element algorithm implemented in this chapter is based on a simple RL model of line which does not take into account these frequencies. It explains why the polarities are not well respected. It would be possible to improve the method by using an RLC model of line as for the distance element. However, it would imply a sufficient knowledge of the positive and negative capacitance of the network behind and in front of the relay. For the close-in fault, it appears that the integrated torque signal grows in the right direction but it never reaches the threshold. Unfortunately, the decrease of the threshold seems not to be a secure solution because as seen for the fault at 50 km it would lead to the wrong direction. Another solution would consist to decrease the starting time. Indeed, during the first ms the signals have the right polarity even with the presence of the high frequencies. However, this finding would depend on the period of the high frequencies involved and it would be not very

secure. Moreover, it is important that the integration of the torque signals does not begin before the actual starting time of the fault because it would delay or impair the torque signals if there are some disturbances in the pre-fault signals. With the actual state of the directional element algorithm it is not possible to determine accurately the fault direction for the close-in faults if the power system network is too weak.

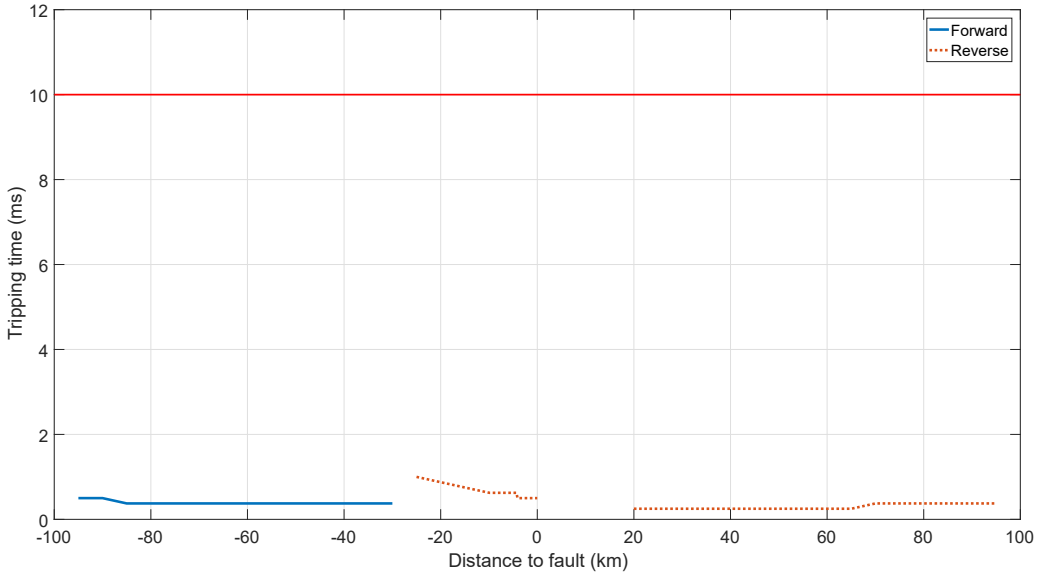

Figure 9.15: Forward and reverse algorithm times for phase-to-phase faults. $\tau_L^+ = 16.46$ ms; $\tau_L^0 = 14.32$ ms; $\tau_S^+ = 23.05$ ms; $\tau_S^0 = 12.03$ ms; $SIR^+ = 4.47$; $SIR^0 = 2.12$; $\alpha = 90°$

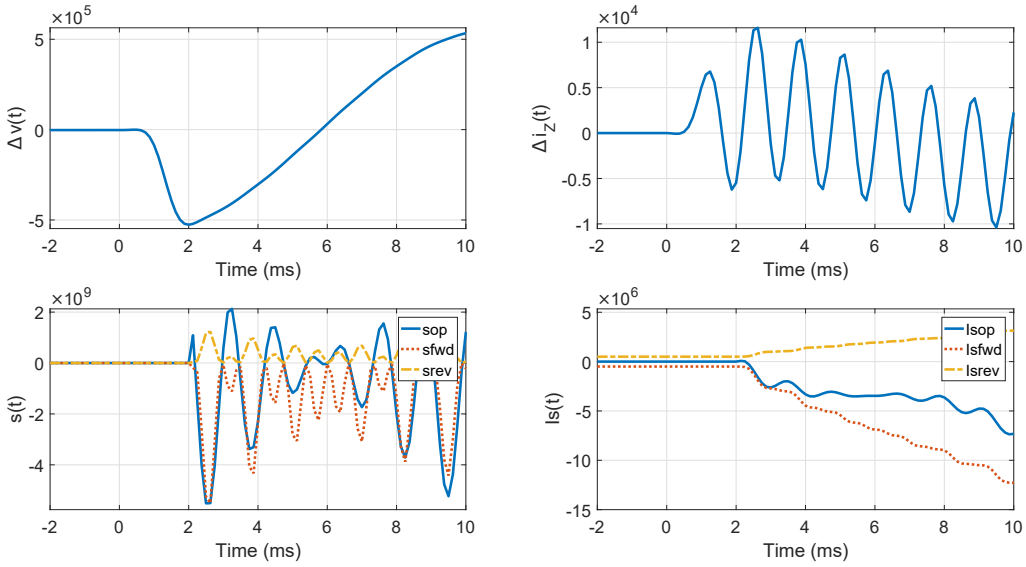

Figure 9.16: Incremental voltage (top right) and replica current (top left). Torque signals (bottom left) and integrated torque signals (bottom right). Weak inhomogeneous system. Forward fault at 500 m

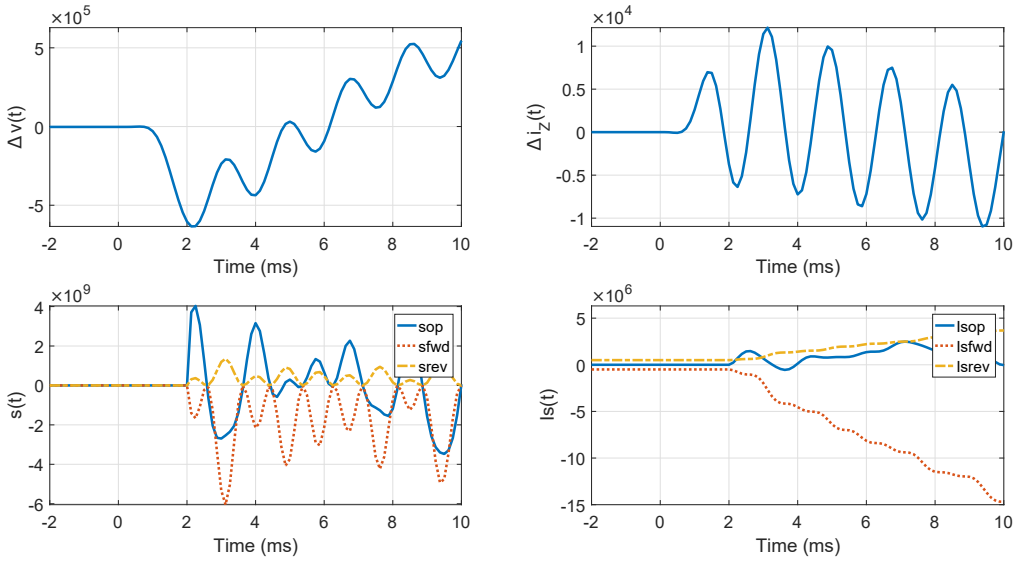

Figure 9.17: Incremental voltage (top right) and replica current (top left). Torque signals (bottom left) and integrated torque signals (bottom right). Weak inhomogeneous system. Forward fault at 50 km

9.5 Conclusions

In this chapter the fast directional element algorithm developed in [13] was presented and tested. This time-domain method was based on the incremental quantities involved during a fault. The algorithm consisted of a comparison between a torque signal and two adaptive thresholds. The first assumption of this method was that the complete power system network (transmission lines and voltage sources) may be represented by a simple RL model. For a strong power system the performances of this method were very satisfying (fast and secure). However, this assumption showed its limitation because the performances analysis proved that it was not possible to determine accurately the fault direction if the power system network is too weak. Of course, it should be interesting to test more cases in order to determine a maximum permissible SIR for different transmission line length. For the faults located further from the relay location the distance element algorithm permitted to determine accurately the fault direction even for a very weak system. A possible solution to improve the directional algorithm would be to use a more accurate model to represent the network. However, it is important to keep in mind that currently a sufficient knowledge of the capacitance of the complete power system behind and in front of the relay is seldom available by the protection designers because these parameters were not necessary for the classical protections.

Chapter 11

Complete distance protection performances

11.1 Introduction

In this chapter the performances of the complete distance protection algorithm implemented in the previous chapters are analysed. The tests will be performed on a model which is as close as possible to a real-world power system. The complete data acquisition process presented in Chapter 7 will be simulated. The transmission line used is a three-phase Bergeron model of 100 km. The power system is not homogeneous (different SIR for positive and zero sequence components) and the transmission line is supplied with a 400 kV voltage source at both ends. The different test cases are based on the standard [101]. It implies the testing of four different fault inception angles: 0°, 30°, 60° and 90°. Four different values of SIR must be also tested. For a long line it corresponds to the values: 0.2, 0.5, 5 and 10. This standard gives also the pre-fault exporting and importing load which is set at 1200 A. It implies that the phase shifts between the two voltage sources are: 15°, 20°, 30° and 35° for the different SIR respectively. As explained in Section 3.8, the power flow direction impacts the value of the inductance seen at the relay location in the case of resistive faults. Both power flow directions are tested in this chapter. Finally, the different types of fault must be tested (phase-to-ground, phase-to-phase, phase-to-phase-to-ground and three-phase). The fault resistance is equal to 5 Ω and 10 Ω between two phases and between a phase and the ground respectively. The complete block schemes of the distance element, the directional element and the loop selection element are shown in Fig. 8.10, 9.5 and 10.8 respectively. All the simulations and algorithms parameters are available in Appendix H.

11.2 Performances analysis

As the directional element implemented in Chapter 9 is not reliable enough for high values of SIR, the reversal faults are not tested more in this section. The tests for forward faults are based on the power system shown in Fig. 11.1.

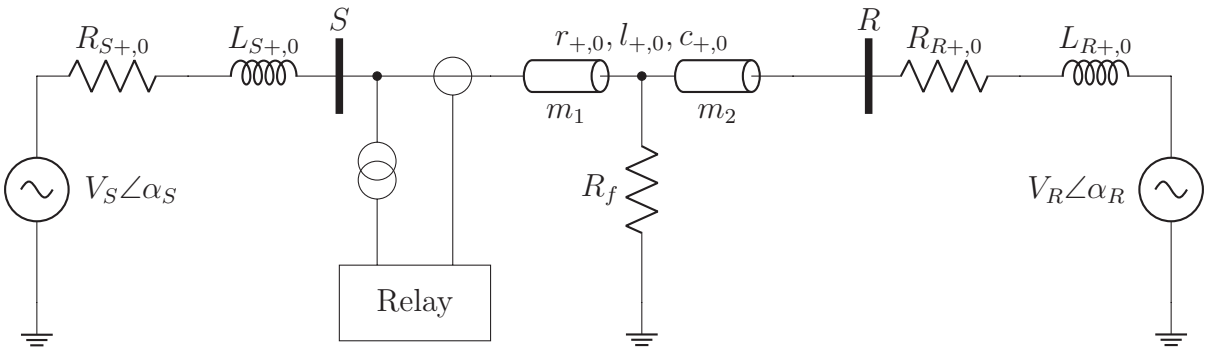

Figure 11.1: Double in-feeds Bergeron transmission line of 100 km

The first case tested is a phase(A)-to-ground fault without fault resistance (bolted fault). The results are presented in the SIR diagrams shown in Fig. 11.2 and 11.3. The SIR diagrams show the tripping times of the distance protection algorithm for different values of the SIR at different fault locations. The tripping times are defined as the times from the start of the algorithm (2 ms after the fault inception to take into account the delays of the filters and the propagation phenomena of the travelling waves) to the trip output. A maximum tripping time of 10 ms is used even if the target is 4 ms because the back-up impedance-based relay would not operate before 10 ms. It is therefore more efficient to try to detect a fault within 10 ms than to stop the ultra-fast algorithm after 4 ms. As different fault inception angles are tested for each fault, the tripping times may be different for each of them. The maximum tripping times represent the worse scenario in term of dependability and speed. The minimum tripping times are also important in order to verify that there is no over-reaching. The complete results are available in Appendix I. The dependability, the security and the speed are the three criteria used to analyse the performances of the algorithm. The faults are correctly identified until 79.2% of the line length for a setting set at 80%. The dependability achieved is very good even for a very weak power system. The most distant fault identified is located at 81.6% of the line length. The security can be easily ensured in this case. Finally, the faults are tripped in 4 ms until 56% and 74.4% of the line length in the worse case and in the best case respectively.

Fig. 11.4 shows the maximum tripping times if a simple RL model of line is used for the distance element algorithm. It appears clearly that the performances are less good. For a weak power system the dependability and the speed of the algorithm are

very limited. This example justifies the use of a more accurate transmission line model to improve the performances of the ultra-fast distance protection.

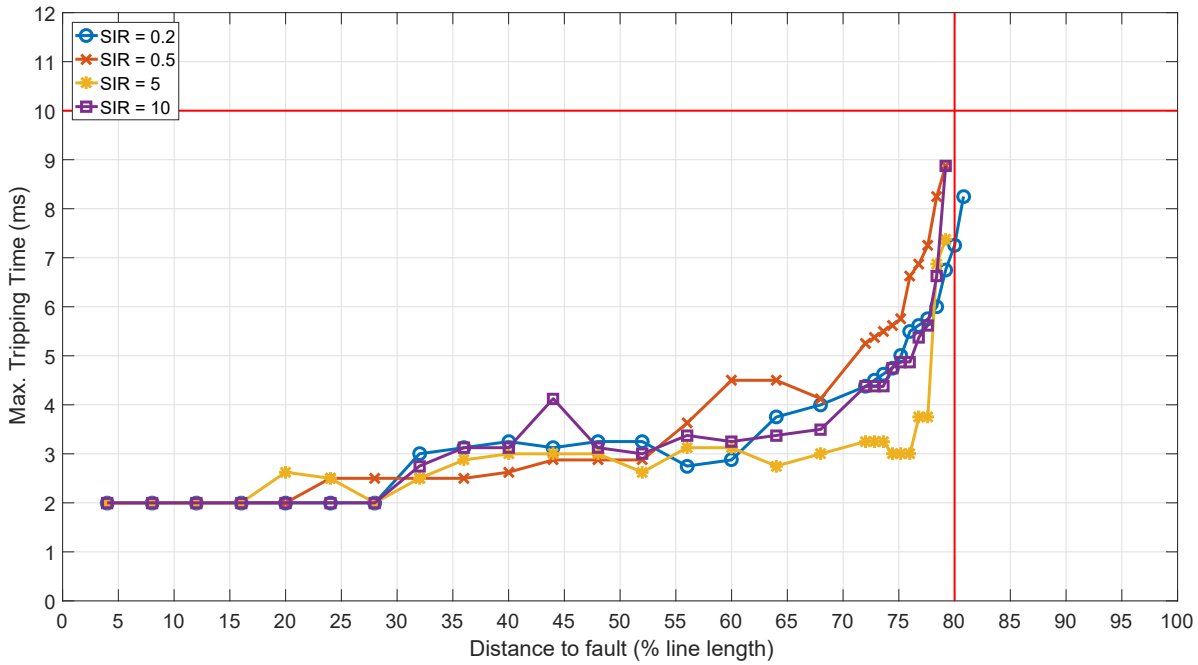

Figure 11.2: SIR diagram for the phase-to-ground fault with no fault resistance (maximum tripping times with RLC distance algorithm)

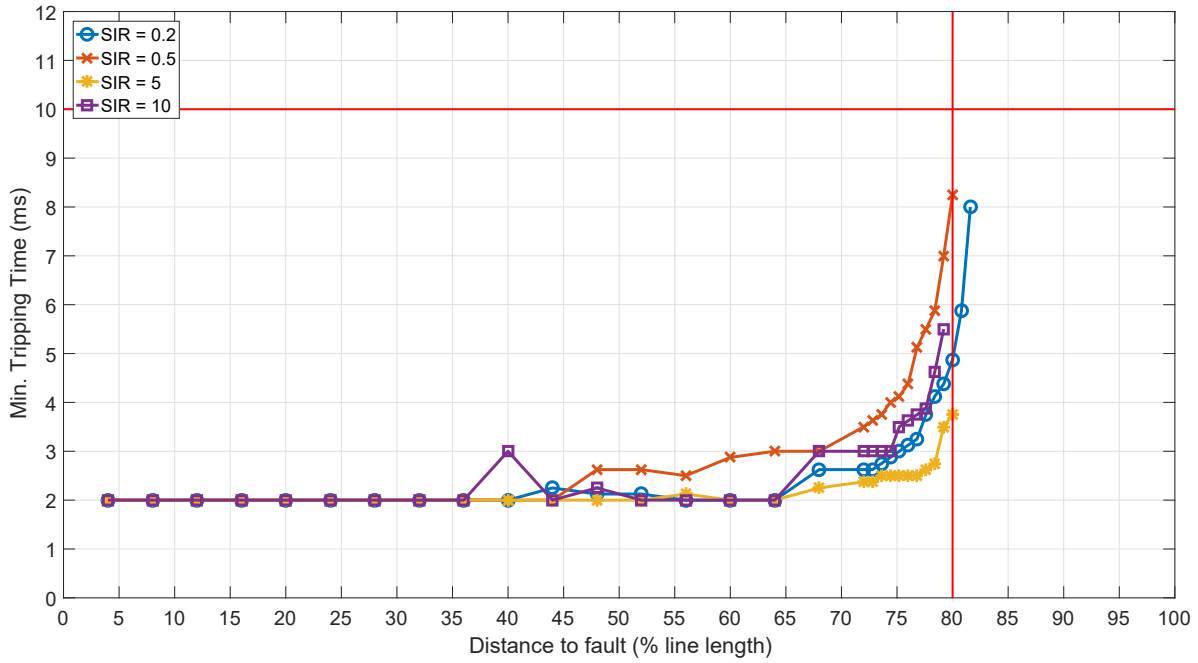

Figure 11.3: SIR diagram for the phase-to-ground fault with no fault resistance (minimum tripping times with RLC distance algorithm)

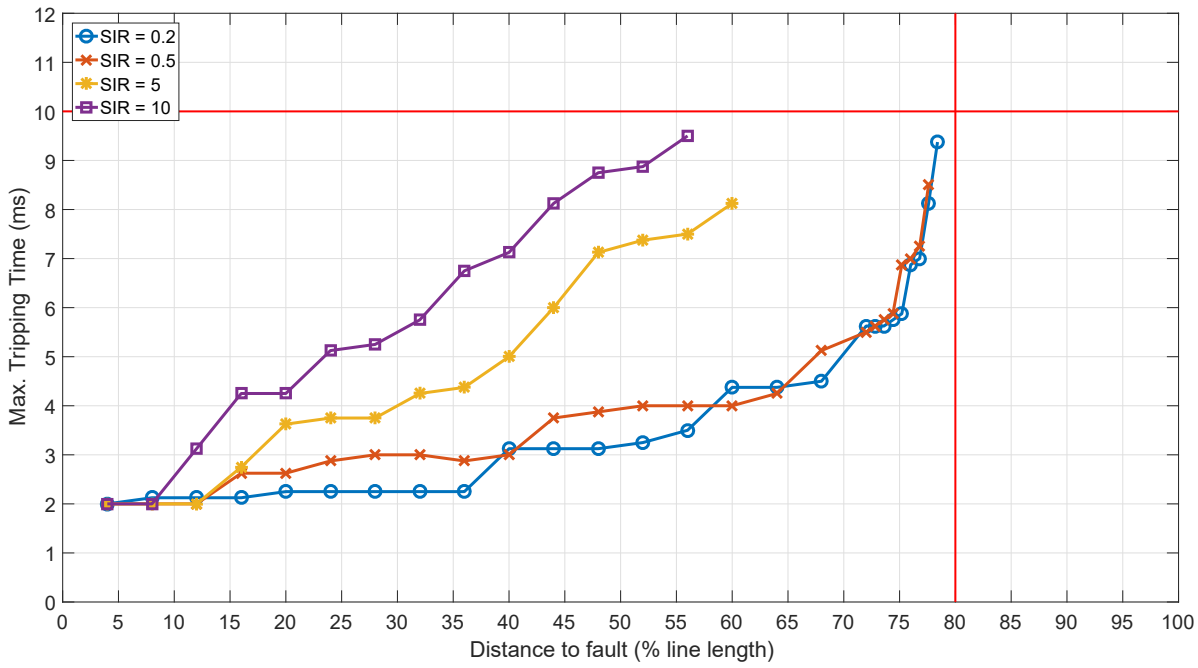

Figure 11.4: SIR diagram for the phase-to-ground fault with no fault resistance (maximum tripping times). Distance element algorithm based on the RL model of line

Fig. 11.5 shows the maximum tripping times for a phase-to-ground fault with a fault resistance of 10 Ω in the case of an importing power flow. The fact that the dependability is limited was expected because a threshold is used to limit the maximum value of the identified resistance. As explained in Section 8.5, it permits to avoid the over-reaching due to the remote injection impact. More important is the fact that the tripping times are quite high for the close-in faults for a weak power system. A deep analysis of the complete process has highlighted that it is due to the convergence criterion of the identified inductance. Fig. 11.6 shows the results for the same case if the convergence criterion is relaxed. In this last test the parameter d_{thres} representing the maximum variation of the identified distance to fault between two successive samples is set at 5 km instead of 1 km. It appears that the tripping times are improved for the close-in faults. However, this solution may impact the security of the method. A better implementation suggested is the use of an adaptive threshold. The convergence may be relaxed when the identified distance to fault is small in order to increase the speed of the algorithm and is kept at the normal level for the faults close to the setting. The solution implemented is as follows: if the identified distance to fault is higher than the half line length the convergence criterion is not relaxed; else the parameter d_{thres} is increased after each ms until a maximum value of 5 km.

The results for the phase-to-phase faults are presented in Appendix I. The same conclusions can be made for this type of fault. For the bolted faults, they are correctly identified until the setting (80% of the line length). The most distant fault identified is

located at 80.8% of the line length (very limited over-reaching). Finally, the faults are tripped in 4 ms until 68% and 77.6% of the line length in the worse case and in the best case respectively.

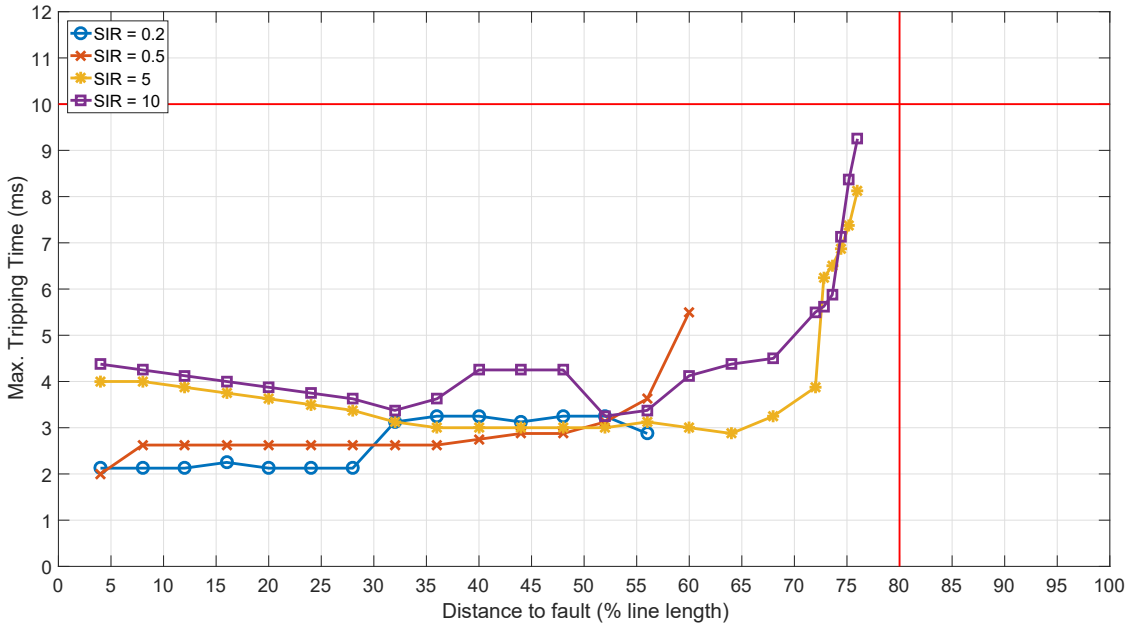

Figure 11.5: SIR diagram for the phase-to-ground fault with a fault resistance and an importing power flow (maximum tripping times with RLC distance algorithm)

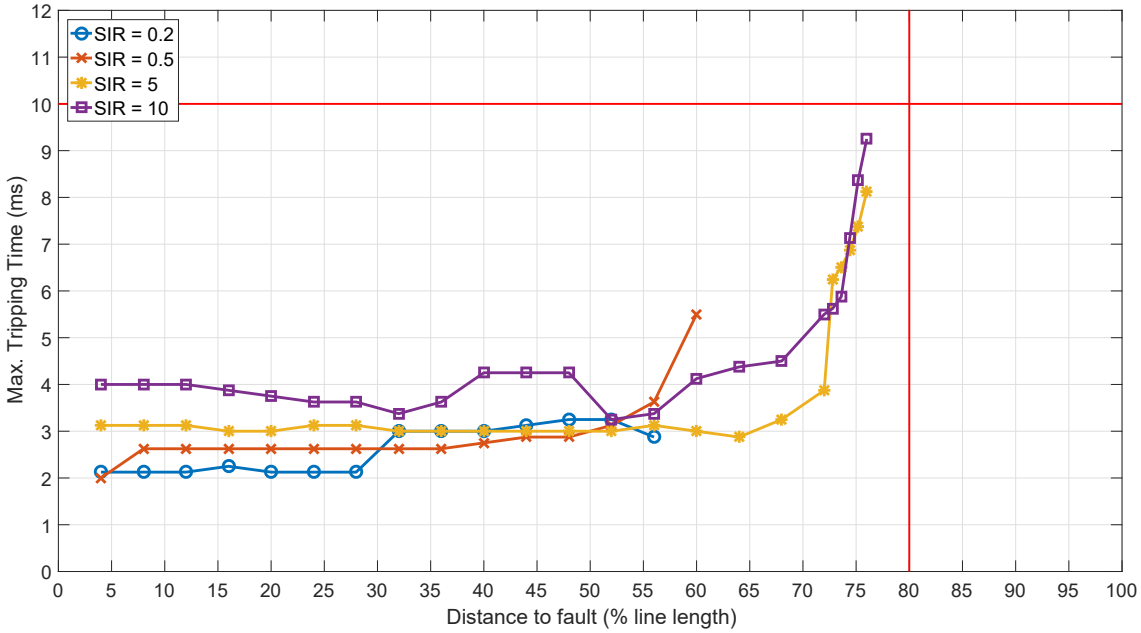

Figure 11.6: SIR diagram for the phase-to-ground fault with a fault resistance and an importing power flow (maximum tripping times with RLC distance algorithm). Relaxed convergence criteria

The phase-to-phase-to-ground faults are the most difficult to deal with in term of loop selection. The delta quantities involved are less different and it is therefore more difficult to define some general criteria to differentiate them from the other types of fault. Among all the tested cases in this chapter for this type of fault (1920 in total considering the different fault positions, fault inception angles, SIR, fault resistances and power flow directions) only 2 led to a wrong loop selection. It is for 2 bolted close-in faults at 4 km for an SIR of 0.2 and 0.5. as shown in Fig. 11.7. Note that this figure indicates only which loop is selected during the complete window algorithm of 10 ms but it does not indicate the fault inception angle involved and the instant of the detection. The analysis of the process may show that the phase(C)-to-ground fault has been identified at 2 ms while the correct loop BC-G was not already detected by the loop selection algorithm. It may lead to a single-phase tripping instead of a three-phase tripping. This scenario is not acceptable from the security point of view even if the occurrence is quite limited. A solution suggested in [15] is to include also the voltage incremental quantities in the loop selection tests. For the selection of a phase-to-ground fault the additional rule is as follows: the incremental voltage of the faulted loop is much higher than the incremental phase-to-phase voltage of the healthy loops (e.g. $\Delta V_A > K_V \Delta V_{BC}$ for a phase(A)-to-ground fault). The threshold K_V must be selected such that the security is improved while the speed is not decreased. For the tests performed in this chapter it permitted to solve this issue.

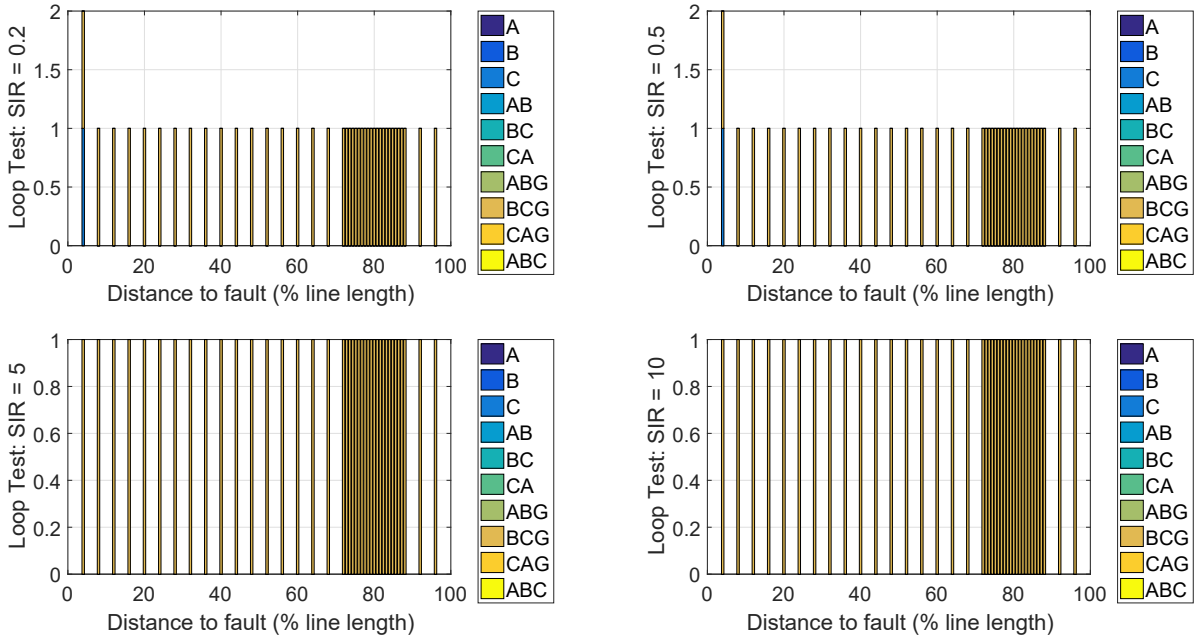

Figure 11.7: Loop selection algorithm for the phase-to-phase-to-ground bolted faults

Fig. 11.8 shows the results for the phase-to-phase-to-ground resistive faults in the case of an importing power flow. It appears that the maximum tripping times are very high

for the weak systems. This time it is not due to a problem of convergence but to the loop selection algorithm. Depending on the fault inception angle the criteria based on a comparison of the rectified values of the incremental quantities may take several ms to be met. This phenomenon represents a limitation of the performances of a method based on the incremental quantities.

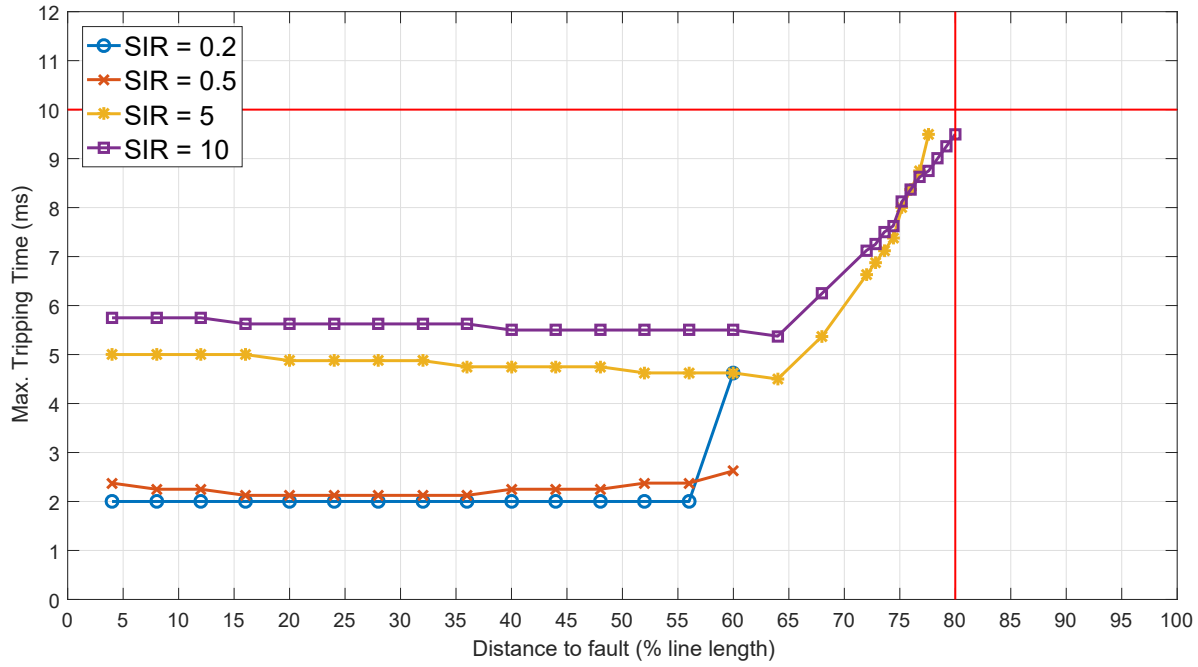

Figure 11.8: SIR diagram for the phase-to-phase-to-ground fault with a fault resistance and an exporting power flow (maximum tripping times with RLC distance algorithm)

Finally, the performances for the three-phase faults are as follows: for the bolted faults, they are correctly identified until the setting (80% of the line length). The most distant fault identified is located at 80.8% of the line length (very limited over-reaching). The faults are tripped in 4 ms until 64% and 68% of the line length in the worse case and in the best case respectively.

11.3 Conclusions

In this last chapter the complete distance protection proposed in this PhD was tested (excepted the directional element which is not sufficient for some extreme cases). The objective was to simulate a database of tests as close as possible to a real-world transmission power system. It implied the use of an accurate model of line and the simulation of the complete data acquisition process developed by Siemens AG. The set of tests was quite big (6400 cases) because the impact of the following parameters were tested: fault position, type of fault, SIR, fault inception angle, fault resistance and power flow direction.

First of all, the results permitted to justify the use of a Γ model of line instead of a simple RL model. The dependability, the security and the speed of the algorithms were improved by the use of a more accurate model of line.

In a second time, the tests performed in this chapter permitted to highlight some limitations of the algorithms. The speed of the distance element algorithm was improved for the close-in faults and weak sources by the use of relaxed criteria of the convergence of the distance to fault. Moreover, the accuracy of the loop selection element was also improved by the use of the incremental voltage in the decision process.

Finally, it can be concluded that the methods proposed in this thesis led to very good results. Indeed, the maximum over-reaching was less than 5% after the setting zone even for resistive faults. For bolted faults the dependability obtained permitted to trip the faults until 79.2% of the line length. This is a huge improvement compared to the current ultra-fast method developed by SEL (see Table 1.1). Moreover, the faults were tripped in 4 ms until around 60% of the line length. However, it appeared that the loop selection element, which is based on the incremental quantities, may be sometimes too slow (5 ms to 6 ms) for resistive faults and very weak power systems with a fault inception angle of 0°.

Chapter 12

Conclusions and future work

12.1 Conclusions

The relay protections of the transmission lines play a fundamental role in the electrical power systems. They permit to ensure the security and the reliability of the electricity transmission from the generators to the final consumers. The objective of a relay protection is to provide a corrective action as quickly as possible when an abnormal condition of the power system is detected. The quickness of the response would permit to limit the stress on the equipments of the power systems and the consumers, to ensure the security of the people, to improve the power quality and to maintain the stability of the power systems. The protective relaying systems have evolved a lot since their first implementation in the 1900's. However, the electrical power systems are in constant evolution and the reliability of the protective relaying systems becomes more and more challenging. The three main characteristics of the relay protections which are security, dependability and speed must be continuously improved to achieve these objectives. The major relay protections implemented nowadays are based on frequency-domain methods. These methods are intrinsically limited in speed by the phasor estimation of the voltage and current signals. More recent methods based on incremental quantities permitted to break this limitation by working directly in time-domain. Despite the speed of these methods, the dependability is usually limited in order to ensure the security. The main ultra-fast algorithms implemented are based on a simple RL model of line. This assumption is valid only for short lines or strong power systems (low SIR).

In this PhD thesis, it was proposed to develop a time-domain ultra-fast non-pilot distance protection based on a Γ model of line in order to improve the security, the dependability and the speed for long lines (until 100 km) and weak power system (SIR until 10). This protection included a loop selection element, a directional element and a distance element. The distance element algorithm developed in this thesis permitted to achieve the target tripping time of 4 ms until around 60% of the line length in the worse case. The

dependability of the protection was improved compared to the current ultra-fast distance protections implemented. The faults were tripped until 79.2% of the line length for a setting zone of 80%. This improvement was done while respecting the security because the maximum over-reaching was less than 5% after the setting zone. Another objective was to take into account the effects and the limitations of an existing hardware developed by Siemens AG. In this context, the complete data acquisition system was simulated. It permitted to highlight the important impact of the current and the voltage transformer on the performances of the distance element algorithm. The directional element algorithm studied in this work showed very good performances in term of speed but the reliability was not sufficient in the case of very weak power systems. The loop selection element algorithm permitted to identify accurately the faulted phases. However, in some extreme cases (resistive fault and very weak power system), the tripping times were higher than 4 ms even for close-in faults.

Chapter 2 presented different models of transmission lines and their frequency behaviour. The reference model chosen in this thesis to represent a real-world transmission line was the constant distributed parameters Bergeron model because it was accurate enough until the first resonance frequency (which is the limit frequency range of the Γ model implemented in this work) even if it did not take into account the frequency dependence of the parameters. The objective was to define the range of frequencies in which the other models fitted the reference model.

Chapter 3 presented the distance element algorithm developed in this thesis. The algorithm was based on the identification of the parameters of the faulted line using a linear Least-Squares estimation method. This method was developed only for the RL and the RLC Γ model of line because it was not possible to obtain a linear model in parameters for more complex models. Moreover, the Γ model was also improved in order to fit better the Bergeron model until the first resonance frequency. The tests performed on a Bergeron model showed that only the Γ-based algorithm was accurate enough for very long lines or weak power systems.

Chapter 4 showed the mathematical concepts related to the Least-Squares estimation method and some issues due to a possible ill-conditioning. A recursive implementation of the Least-Squares method was proposed to improve the performances of the method in term of computational loads. This chapter was useful to analyse the accuracy of the results obtained and to define some security margins based on the MSE and the CI. However, it appeared that these indicators may be biased for a time-series model and therefore the statistical tables, used usually for cross-sectional data[1], may not be relevant.

Chapters 5 and 6 permitted to extend the distance element algorithms to a three-phase power system with the use of the Clarke transform. The different types of fault

[1]cross-sectional data are observations that come from different individuals or groups at a single point in time

were treated. It led to the introduction of new compensation factors of the zero sequence voltage for the Γ model during a phase-to-ground fault. Moreover, a solution was proposed to deal with the parallel transmission lines.

In Chapter 7, the complete data acquisition process based on the existing hardware was simulated. It permitted to highlight the impact of the CT and the VT on a time-domain algorithm. The high-pass behaviour of the transformers led to a wrong distance to fault evaluation. A solution was proposed to solve this issue by including the CT and VT model in the equations of the distance element algorithms. It led to the introduction of a new parameter to identify. This parameter was linked to the value of the voltage and the current of the first sample at the primary side of the transformers.

Chapter 8 presented the different security criteria implemented for the distance element algorithms in order to avoid a possible over-reaching. The use of criteria based on the residuals analysis permitted to improved the security while optimising the dependability of the methods.

The distance element was completed by a directional element and a loop selection element. The algorithms proposed for the two elements were both based on existing methods using the incremental quantities. Chapter 9 showed that the directional element algorithm proposed had some limitations not yet resolved. Indeed, the directional element algorithm was based on a simple RL model which was not accurate enough for very weak power systems. The directional element algorithm must be improved as explained in the next section. The loop selection element algorithm presented in Chapter 10 gave very good results except for the specific cases mentioned above.

Finally, Chapter 11 presented the performances of the complete distance protection for a big database of tests (6400 tested cases). The limitations of the directional element was already mentioned. For the other elements of the distance protection the performances obtained were satisfying in term of security, dependability and speed.

The major contributions of this PhD thesis were related to the time-domain distance element algorithm:

- implementation of a Γ model of transmission line for an ultra-high-speed distance protection in the time-domain thanks to a Linear Recursive Least-Squares Estimation method.

- improvement of the frequency behaviour of the Γ model of line until the first resonance frequency of a distributed parameters model of line.

- the use of the integral form of the equations representing the model of a line in order to limit the impact of a noisy signal.

- inclusion of a simple model of the voltage and the current transformers in the transmission line model.

- the use of a residual analysis to ensure the security of the method and to improve its dependability.

12.2 Future work

The future work can be splitted in two parts: the first one is related to the possible improvements of the algorithm developed in this thesis; the second one is related to more specific cases not tested yet.

In Chapter 2 the transfer functions of a Bergeron and a J. Marti model of line were compared. It was concluded that both models had a similar frequency behaviour until the first resonance frequency. However, it would be interesting to evaluate the impact on the parameters of the line of the type of ground, the earthing method used, the type of conductors, etc.

In Chapter 4 it was shown that the statistical indicators of a Least-Squares estimation may be biased for a time-series model. It would be necessary to study this problematic deeper in order to develop a more suited method to evaluate the accuracy of the results and therefore to improve the security of the method.

The directional element algorithm based on the incremental quantities with a simple RL model showed its limitations. The development of a more efficient method is necessary because it does not permit to protect accurately the very weak power systems, which is one of the main advantages of the distance element developed in this thesis.

The loop selection algorithm developed in Chapter 10 showed very good performances. However, in some cases (weak power system and resistive fault) the speed of the method is not sufficient. This problem occurred for a fault inception angle of 0°. This specific case could be improved.

The complete distance protection could be tested with data coming from an actual transmission line in order to be validated. These tests would permit to verify the impact of some possible noises on the data. If these data are not available it would be necessary to accurately simulate the different possible sources of noise. However, the possible errors or noises can be of different forms: limited or bad knowledge of transmission line parameters or CT and VT time constants; the transmission line may not be totally balanced; a frequency deviation may be possible on the steady-state signals (used for the calculation of incremental quantities); an electromagnetic noise of the environment is also possible; finally the quantification process of the ADC and the calculation limits of the hardware may affect the accuracy of the algorithms. A pertinent analysis of noisy data would therefore require a good knowledge of the type and the magnitude of these different sources of noise and then a statistical evaluation of their impact on the performances of the protection would be performed.

In this thesis it was considered that the loop involved during a fault was the same

during the complete algorithm window. However, the case of an evolving fault is also possible. The short-circuit occurring on a particular phase may be propagated to another phase. A single-phase fault may turn into a three-phase fault. It would be necessary to define a logical implementation to treat this type of fault.

It was showed in Chapter 7 that the CT and the VT may have a big impact on the performances of the distance element algorithm. These elements impacted only the low frequencies of the transient content. Fortunately, a simple model was possible to be assumed and it was included in the model of the algorithm. However, the use of a CCVT may complicate much more the problem. The transient behaviour of a CCVT may also impact a lot the distance element algorithm. Different implementation of a CCVT model were proposed in the literature and its impact on a distance protection was deeply studied [102]–[106]. However, it appeared that the model was, at first sight, too complex to be include in the distance element algorithm. Moreover, the model depended on several parameters which may vary a lot depending on the specific CCVT used. A first possible solution would be to propose a simplified model of CCVT (first order) that is enough to simulate its behaviour.

Finally, some compensation devices may be present in the transmission line and it would be necessary to study their impact on the distance protection implemented in this thesis. These devices may be shunt reactors [107], shunt capacitors [108] or series-capacitors and series-reactors [109].

Appendix A

Bode's curves calculation

In this appendix it is explained how the Bode's curves are constructed for a single-phase and a three-phase model of line. As the distance element algorithm is based on the transfer function of a Γ model of line, it will be the reference transfer function for all the cases. This transfer function represents the parameters identified by the distance element algorithm. A frequency scan is applied from 1 Hz to 10 kHz and the steady-state voltages and currents at the relay location are extracted.

A.1 Single-phase model

For a single-phase model of line the transfer function is directly given by the ratio of the voltage and the current at the relay location:

$$H(j\omega) = \frac{V(j\omega)}{I(j\omega)} = \frac{j\omega L + R}{(j\omega)^2 CL + j\omega CR + 1} \tag{A.1}$$

A.2 Three-phase model for a phase-to-phase fault

For a three-phase model of line with a phase-to-phase fault the transfer function is given by the ratio between the β sequence of the voltage and the current at the relay location. It represents the β parameters of the line and is given by the following expression:

$$H(j\omega) = \frac{V_\beta(j\omega)}{I_\beta(j\omega)} = \frac{j\omega L_\beta + R_\beta}{(j\omega)^2 C_\beta L_\beta + j\omega C_\beta R_\beta + 1} \tag{A.2}$$

A.3 Three-phase model for a phase-to-ground fault

The phase-to-ground transfer function is more difficult to define because it involves two Clarke sequences as seen in the expression given by (6.19). In the frequency domain this

equation can be written as:

$$\begin{aligned}(j\omega)^2 C_\alpha L_\alpha V_\alpha(j\omega) + j\omega C_\alpha R_\alpha V_\alpha(j\omega) + V_\alpha(j\omega) \\ + (j\omega)^2 C_0 L_0 V_0(j\omega) + j\omega C_0 R_0 V_0(j\omega) + V_0(j\omega) \\ = j\omega L_\alpha I_\alpha(j\omega) + R_\alpha I_\alpha(j\omega) + j\omega L_0 I_0(j\omega) + R_0 I_0(j\omega)\end{aligned} \quad (A.3)$$

It can be rewritten as follows:

$$\begin{aligned}\left((j\omega)^2 C_\alpha L_\alpha + j\omega C_\alpha R_\alpha + 1\right) V_\alpha(j\omega) + \left((j\omega)^2 C_0 L_0 + j\omega C_0 R_0 + 1\right) V_0(j\omega) \\ = \left(j\omega L_\alpha + R_\alpha\right) I_\alpha(j\omega) + \left(j\omega L_0 + R_0\right) I_0(j\omega)\end{aligned} \quad (A.4)$$

By defining:

$$N_0 = j\omega L_0 + R_0 \quad (A.5)$$

$$D_0 = (j\omega)^2 C_0 L_0 + j\omega C_0 R_0 + 1 \quad (A.6)$$

$$D_\alpha = (j\omega)^2 C_\alpha L_\alpha + j\omega C_\alpha R_\alpha + 1 \quad (A.7)$$

It finally leads to:

$$\begin{aligned}H(j\omega) = \frac{j\omega L_\alpha + R_\alpha}{(j\omega)^2 C_\alpha L_\alpha + j\omega C_\alpha R_\alpha + 1} \\ = \frac{V_\alpha(j\omega)}{I_\alpha(j\omega)} + \frac{1}{D_\alpha I_\alpha(j\omega)} \left(D_0 V_0(j\omega) - N_0 I_0(j\omega)\right)\end{aligned} \quad (A.8)$$

Appendix B

Resonance frequency

The transfer function of the RLC Γ model of line is given by (B.1).

$$H_{RLC}(j\omega) = \frac{j\omega m l_l + m r_l}{(j\omega)^2 m c_l^* m l_l + j\omega m c_l^* m r_l + 1} \tag{B.1}$$

where c_l^* is the adapted capacitance. The resonance frequency corresponds to the minimum module of the denominator of the transfer function. This module is given by:

$$|\underline{D}| = \sqrt{(1 - \omega^2 m c_l^* m l_l)^2 + (\omega m c_l^* m r_l)^2} \tag{B.2}$$

$|\underline{D}|$ is minimum when the derivative of the function f inside the root is equal to zero.

$$f = 1 + \omega^4 (m c_l^* m l_l)^2 - 2\omega^2 m c_l^* m l_l + \omega^2 (m c_l^* m r_l)^2 \tag{B.3}$$

$$\frac{df}{d\omega} = 4\omega^3 (m c_l^* m l_l)^2 - 4\omega m c_l^* m l_l + 2\omega (m c_l^* m r_l)^2 = 0 \tag{B.4}$$

This function has three roots:

$$\omega_1 = 0 \tag{B.5}$$

$$\omega_{2,3} = \pm \sqrt{\frac{1}{m^2 c_l^* l_l} - \frac{1}{2}\left(\frac{r_l}{l_l}\right)^2} \tag{B.6}$$

The zero and negative roots can be eliminated. Moreover, the term $0.5 \cdot (r_l/l_l)^2$ is negligible compared to the term $1/(c_l^* l_l)$. Finally, the resonance frequency is given by:

$$f_{res} = \frac{1}{2\pi m \sqrt{c_l^* l_l}} \tag{B.7}$$

Appendix C

Numerical approximation

In this appendix the numerical approximations used for the derivative and the integration functions are presented.

C.1 Differentiation

For the derivative functions the Three-Point Midpoint formula are used (Fig. C.1). The first and the second derivative functions are given by (C.1) and (C.2) respectively.

$$f'(x_0) = \frac{1}{2h}\left[f(x_0 + h) - f(x_0 - h)\right] \tag{C.1}$$

$$f''(x_0) = \frac{1}{h^2}\left[f(x_0 - h) - 2f(x_0) + f(x_0 + h)\right] \tag{C.2}$$

It is necessary to reduce the value of the step h in order to reduce the truncation error. However, this reduction will also increase the round-off error. In this sense the numerical differentiations are unstable [42].

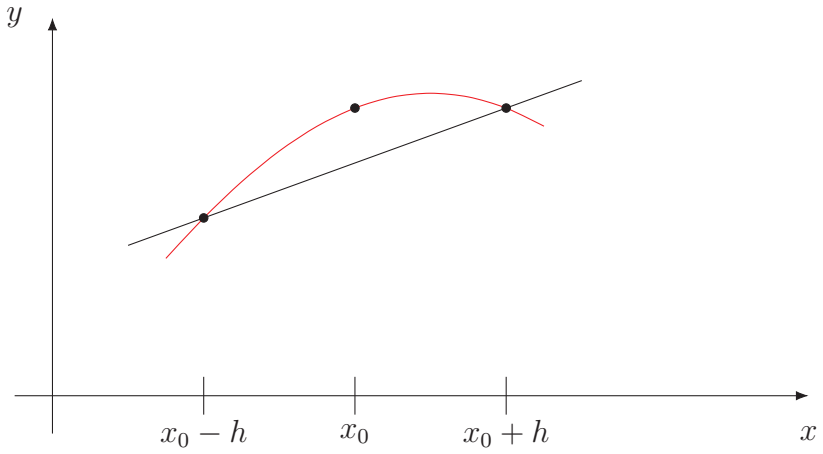

Figure C.1: Three-Point Midpoint derivative approximation

C.2 Integration

For the integration functions the trapezoidal rule given by (C.3) is used. The numerical integration method is always stable in the sense discussed above. Fig. C.2 illustrates the method.

$$\int_a^b f(x)dx = \frac{b-a}{2}\left[f(x_0) + f(x_1)\right] \tag{C.3}$$

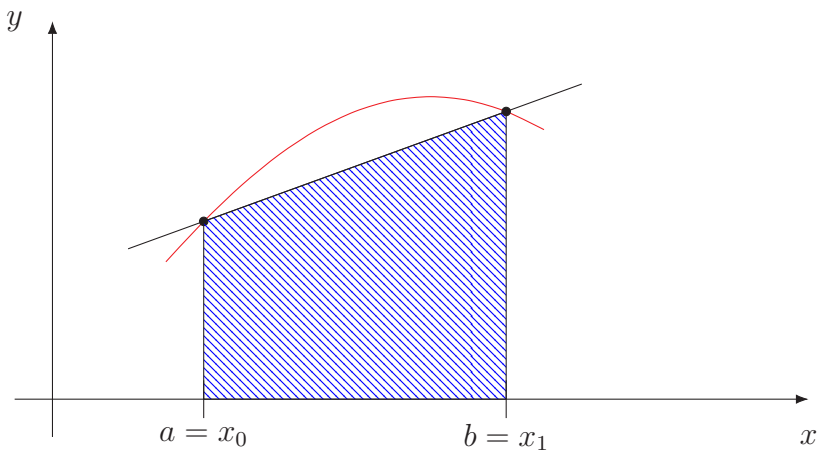

Figure C.2: Trapezoidal rule for integration approximation

Appendix D

Distance element algorithm with voltage and current transformers

D.1 Transformers model

The corrective transfer function applied on both voltage and current signals is given by (D.1).

$$H_K = \frac{s\tau_K}{1 + s\tau_K} \tag{D.1}$$

It implies that in the time-domain the input and the output signals are linked by the relations (D.2) and (D.3).

$$\begin{cases} \dfrac{dV^P(t)}{dt} = \dfrac{dV(t)}{dt} + \dfrac{1}{\tau_K} V(t) & \text{(D.2)} \\ \dfrac{dI^P(t)}{dt} = \dfrac{dI(t)}{dt} + \dfrac{1}{\tau_K} I(t) & \text{(D.3)} \end{cases}$$

where V^P and I^P are the input voltage and current which are not available by the relay protection because they are related to the primary side of the transformers. V and I are the output voltage and current which are measured by the relay protection. The following relations obtained by integrating both sides will be also useful for the next developments:

$$\begin{cases} V^P(t) - V^P(t_0) = V(t) - V(t_0) + \dfrac{1}{\tau_K} \displaystyle\int_{t_0}^{t} V(t)dt & \text{(D.4)} \\ I^P(t) - I^P(t_0) = I(t) - I(t_0) + \dfrac{1}{\tau_K} \displaystyle\int_{t_0}^{t} I(t)dt & \text{(D.5)} \end{cases}$$

D.2 Single-phase model

The line models are valid only for the primary side of the transformer. By applying (D.2), (D.3), (D.4) and (D.5) to the RL model of line given by (3.25), it leads to:

$$V(t) - V(t_0) + \frac{1}{\tau_K}\int_{t_0}^{t} V(t)dt + V^P(t_0) \\ = R\left(I(t) - I(t_0) + \frac{1}{\tau_K}\int_{t_0}^{t} I(t)dt + I^P(t_0)\right) + L\left(\frac{dI(t)}{dt} + \frac{1}{\tau_K}I(t)\right) \quad \text{(D.6)}$$

Two terms related to the primary sides remains: $V^P(t_0)$ and $I^P(t_0)$. These terms are the primary voltage and current at the starting time of the algorithm. As mentioned before the primary side signals are not available by the protection. One solution is to consider that the term $V^P(t_0) - RI^P(t_0)$ is a constant unknown to be identified by the least-squares method. When using the RLS method it is more optimal to begin with an initial state close to the correct solution. Assuming:

$$V^P(t_0) - RI^P(t_0) \sim V(t_0) \cdot K \quad \text{(D.7)}$$

where K is the new parameter to identify, it leads for the integral form of the RL model of line:

$$\int_{t_0}^{t} V(t)dt - V(t_0)\cdot(t-t_0) + \frac{1}{\tau_K}\iint_{t_0}^{t} V(t)dt \\ = R\left(\int_{t_0}^{t} I(t)dt - I(t_0)\cdot(t-t_0) + \frac{1}{\tau_K}\iint_{t_0}^{t} I(t)dt\right) \\ + L\left(I(t) - I(t_0) + \frac{1}{\tau_K}\int_{t_0}^{t} I(t)dt\right) - K\left(V(t_0)\cdot(t-t_0)\right) \quad \text{(D.8)}$$

Similarly the integral form of the RLC model of line gives (D.9) by applying the same developments to the relation (3.36).

$$\frac{C^2}{c_l'}\left(l_l\left[\frac{dV(t)}{dt} - \dot{V}(t_0) + \frac{1}{\tau_K}\left(V(t) - V(t_0)\right)\right]\right. \\ \left. + r_l\left[V(t) - V(t_0) + \frac{1}{\tau_K}\left(\int_{t_0}^{t} V(t)dt\right)\right]\right) \\ + \int_{t_0}^{t} V(t)dt - V(t_0)\cdot(t-t_0) + \frac{1}{\tau_K}\left(\iint_{t_0}^{t} V(t)dt\right) + K\left(V(t_0)\cdot(t-t_0)\right) \\ = R\left(\int_{t_0}^{t} I(t)dt - I(t_0)\cdot(t-t_0) + \frac{1}{\tau_K}\left(\iint_{t_0}^{t} I(t)dt\right)\right) \\ + L\left(I(t) - I(t_0) + \frac{1}{\tau_K}\left(\int_{t_0}^{t} I(t)dt\right)\right) \quad \text{(D.9)}$$

D.3 Three-phase model

For the phase-to-phase and the three-phase faults the relations (D.8) and (D.9) remain valid if considering the β sequence voltage, current and line parameters. For the phase-

to-ground faults the previous relations become (D.10) for the RL model and (D.11) for the RLC model of line.

$$\begin{aligned}\int_{t_0}^{t} V_a(t)dt - V_a(t_0)\cdot(t-t_0) + \frac{1}{\tau_K}\iint_{t_0}^{t} V_a(t)dt \\ = R_{\alpha f}\left(\int_{t_0}^{t} I_{a1}(t)dt - I_{a1}(t_0)\cdot(t-t_0) + \frac{1}{\tau_K}\iint_{t_0}^{t} I_{a1}(t)dt\right) \\ + L_{\alpha f}\left(I_{a2}(t) - I_{a2}(t_0) + \frac{1}{\tau_K}\int_{t_0}^{t} I_{a2}(t)dt\right) - K\left(V_a(t_0)\cdot(t-t_0)\right)\end{aligned} \tag{D.10}$$

$$\begin{aligned}&\frac{C_{\alpha f}^2}{c'_\alpha}\left(l_\alpha\left[\frac{dV_{a2}(t)}{dt} - \dot{V}_{a2}(t_0) + \frac{1}{\tau_K}\left(V_{a2}(t) - V_{a2}(t_0)\right)\right]\right. \\ &\qquad\left. + r_\alpha\left[V_{a1}(t) - V_{a1}(t_0) + \frac{1}{\tau_K}\left(\int_{t_0}^{t} V_{a1}(t)dt\right)\right]\right) \\ &+ \int_{t_0}^{t} V_a(t)dt - V_a(t_0)\cdot(t-t_0) + \frac{1}{\tau_K}\left(\iint_{t_0}^{t} V_a(t)dt\right) + K\left(V_a(t_0)\cdot(t-t_0)\right) \\ &\quad = R_{\alpha f}\left(\int_{t_0}^{t} I_{a1}(t)dt - I_{a1}(t_0)\cdot(t-t_0) + \frac{1}{\tau_K}\left(\iint_{t_0}^{t} I_{a1}(t)dt\right)\right) \\ &\qquad + L_{\alpha f}\left(I_{a2}(t) - I_{a2}(t_0) + \frac{1}{\tau_K}\left(\int_{t_0}^{t} I_{a2}(t)dt\right)\right)\end{aligned} \tag{D.11}$$

where:

$$\begin{cases} I_{a1}(t) = I_a(t) + k_R I_0(t) & \text{(D.12)} \\ I_{a2}(t) = I_a(t) + k_L I_0(t) & \text{(D.13)} \\ V_{a1}(t) = V_a(t) + k_{CR} V_0(t) & \text{(D.14)} \\ V_{a2}(t) = V_a(t) + k_{CL} V_0(t) & \text{(D.15)} \end{cases}$$

Appendix E

Confidence interval tests

E.1 Phase-to-phase faults

E.1.1 Strong network

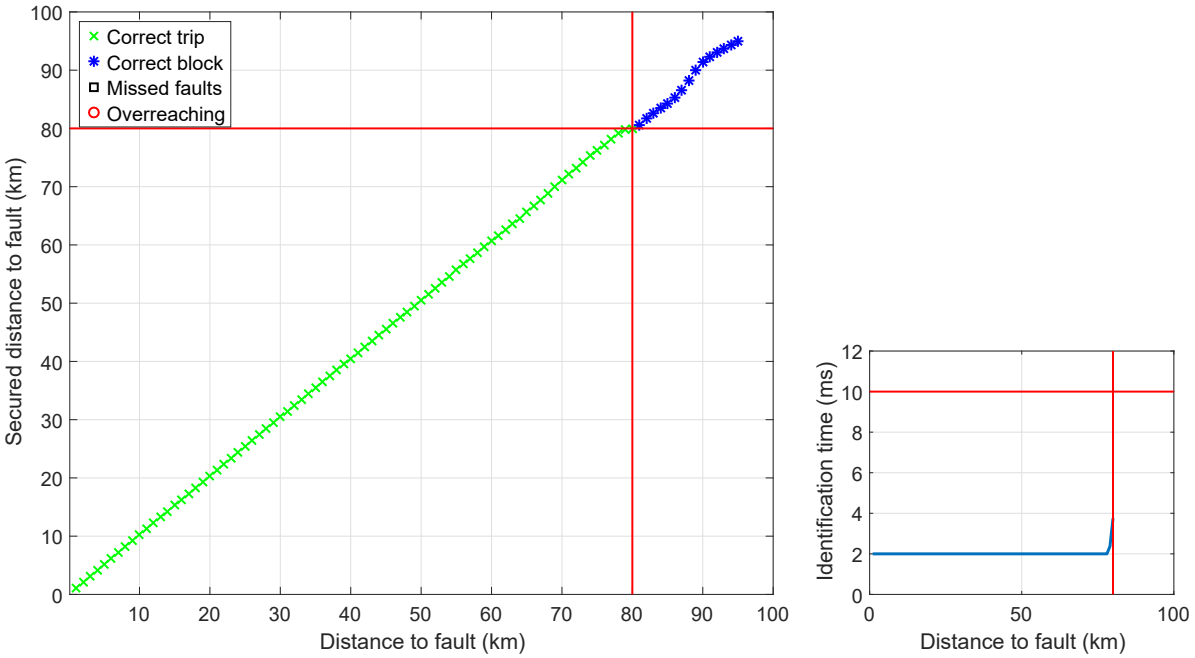

Figure E.1: Distance to fault versus secured distance to fault (left) and identification time (right). RLC algorithm with $SF_{CI} = 6$

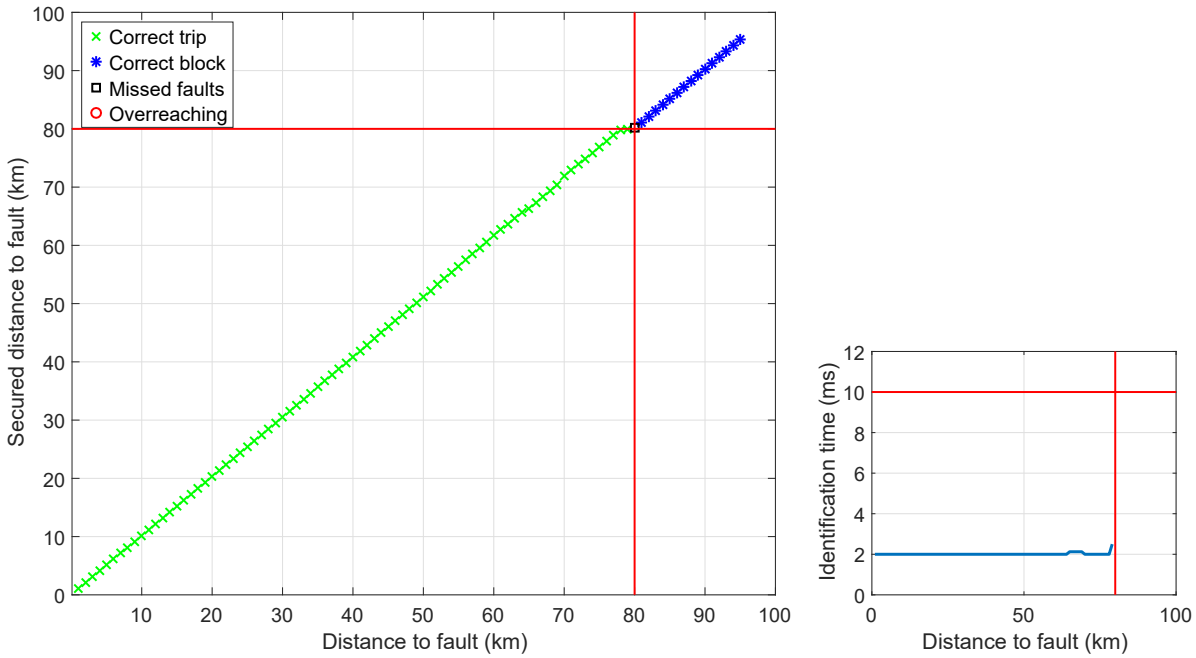

Figure E.2: Distance to fault versus secured distance to fault (left) and identification time (right). RL algorithm with $SF_{CI} = 2$

E.1.2 Weak network

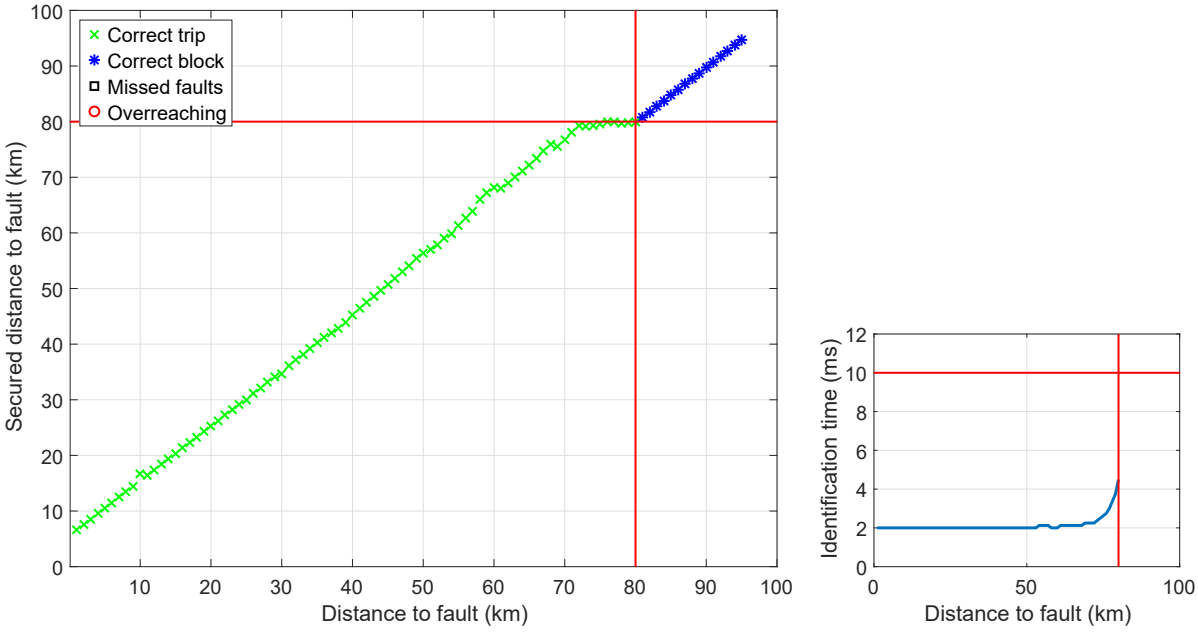

Figure E.3: Distance to fault versus secured distance to fault (left) and identification time (right). RLC algorithm with $SF_{CI} = 6$

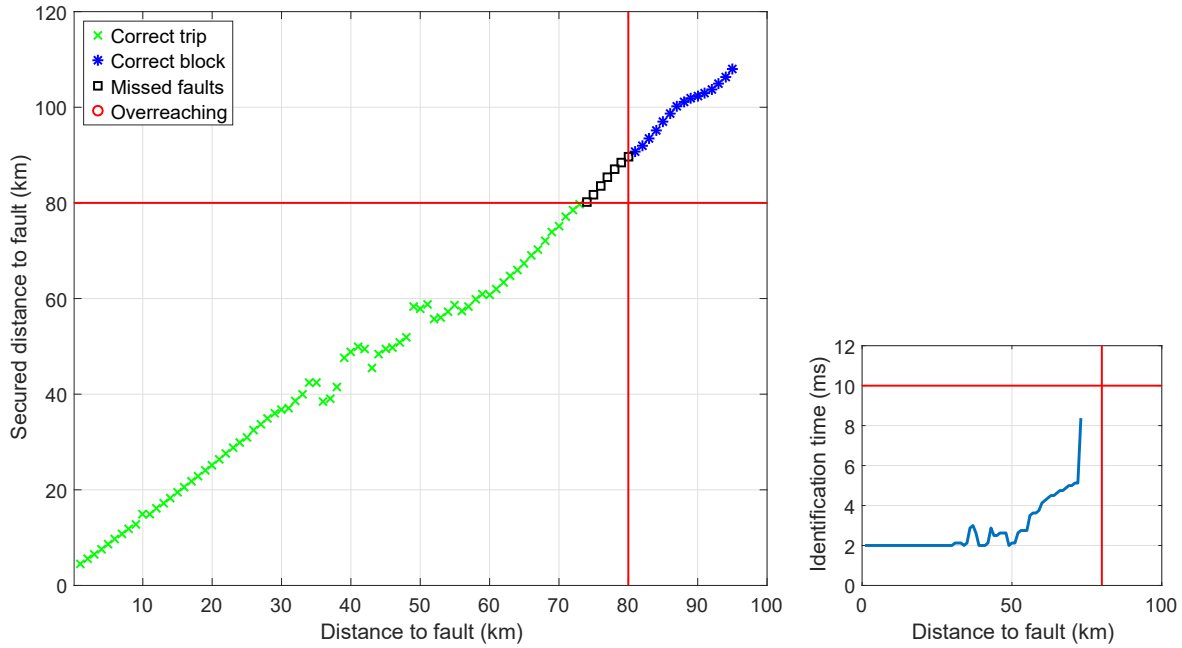

Figure E.4: Distance to fault versus secured distance to fault (left) and identification time (right). RL algorithm with $SF_{CI} = 2$

E.2 Phase-to-ground faults

E.2.1 Strong network

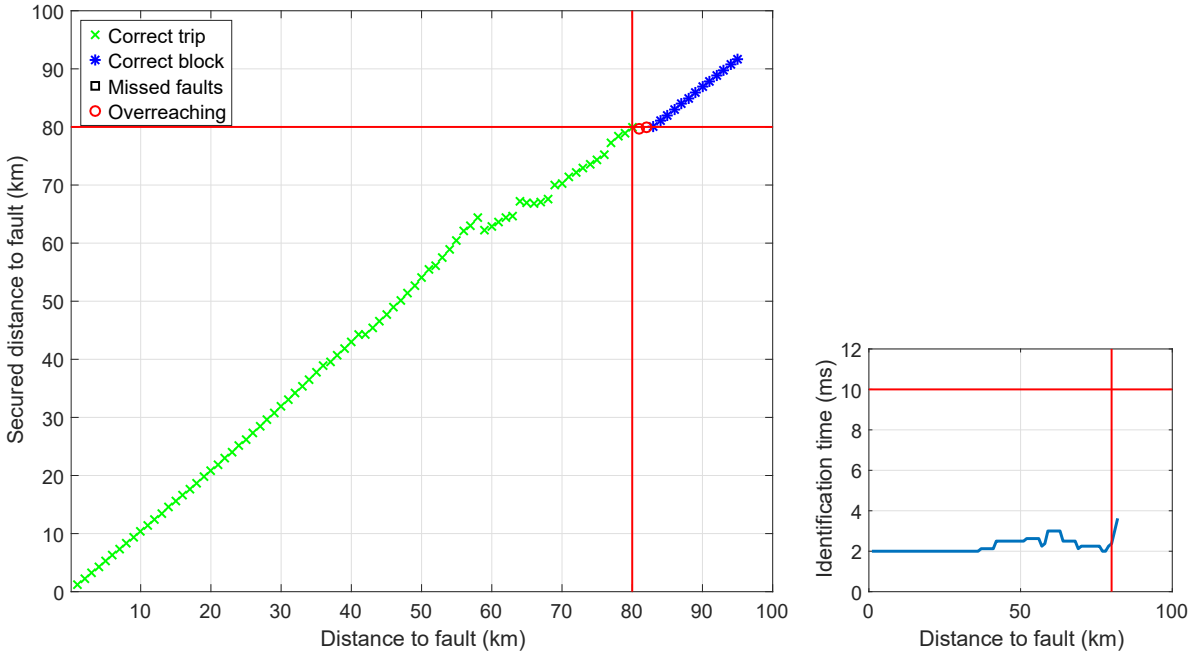

Figure E.5: Distance to fault versus secured distance to fault (left) and identification time (right). RLC algorithm with $SF_{CI} = 6$

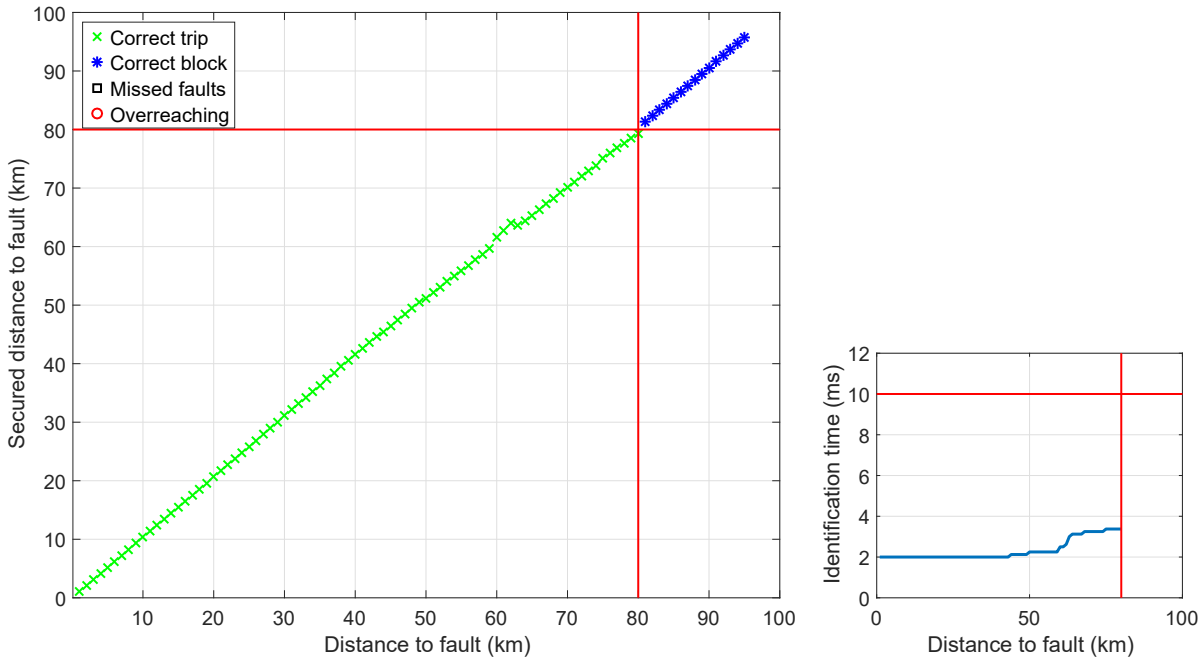

Figure E.6: Distance to fault versus secured distance to fault (left) and identification time (right). RL algorithm with $SF_{CI} = 2$

E.2.2 Weak network

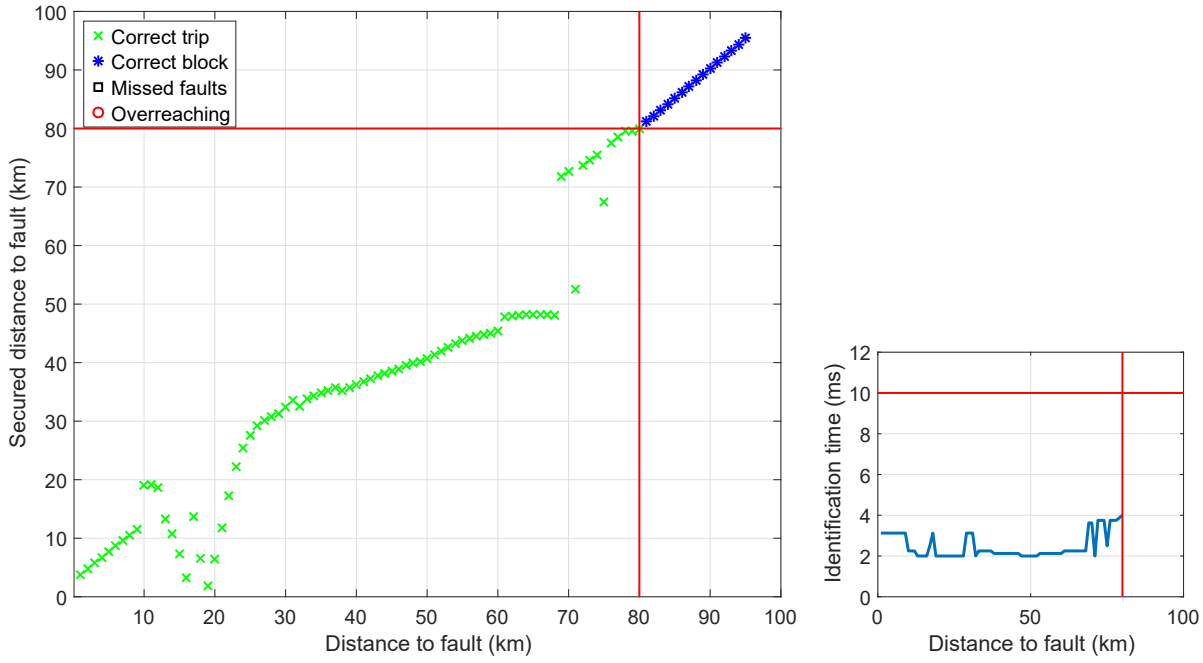

Figure E.7: Distance to fault versus secured distance to fault (left) and identification time (right). RLC algorithm with $SF_{CI} = 6$

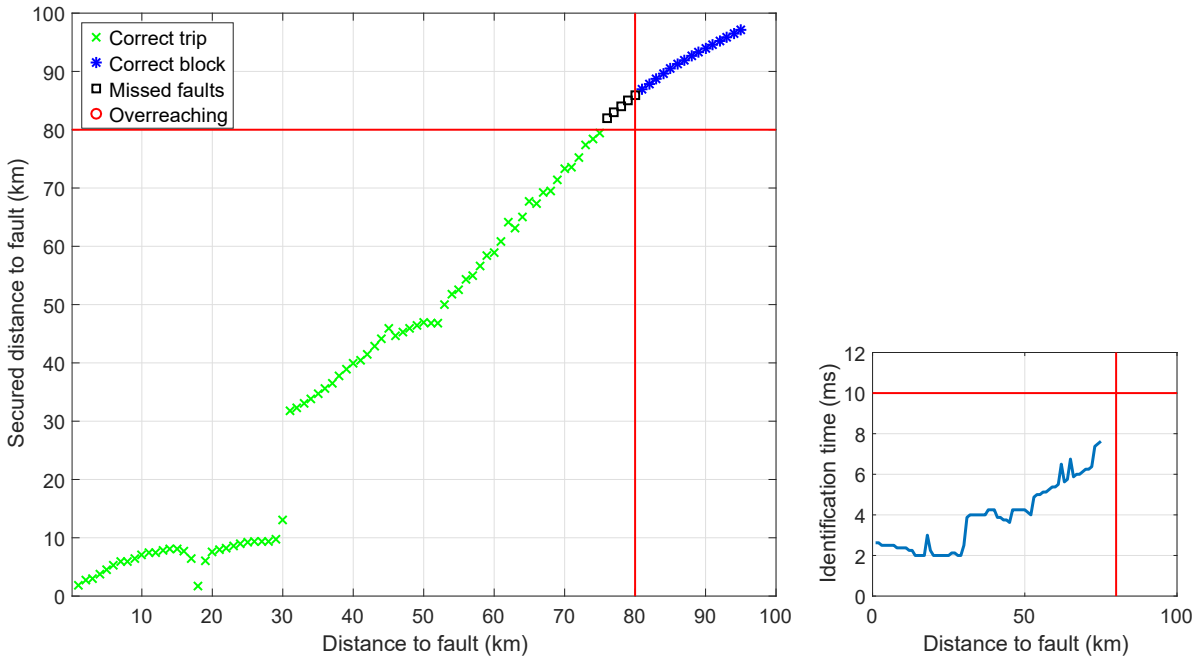

Figure E.8: Distance to fault versus secured distance to fault (left) and identification time (right). RL algorithm with $SF_{CI} = 2$

Appendix F

Directional element tests

F.1 Phase-to-phase

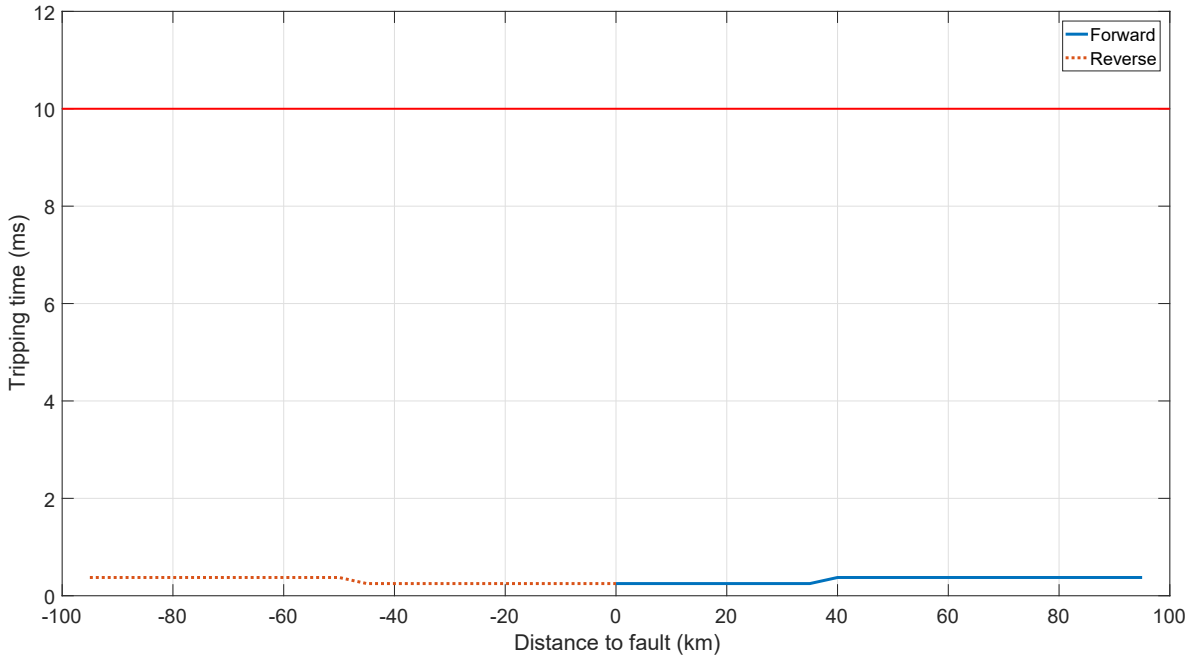

Figure F.1: Forward and reverse algorithm time. $\tau_L^+ = 16.46$ ms; $\tau_L^0 = 14.32$ ms; $\tau_S^+ = 24.69$ ms; $\tau_S^0 = 12.89$ ms; $SIR^+ = 1.15$; $SIR^0 = 1.09$; $\alpha = 90°$

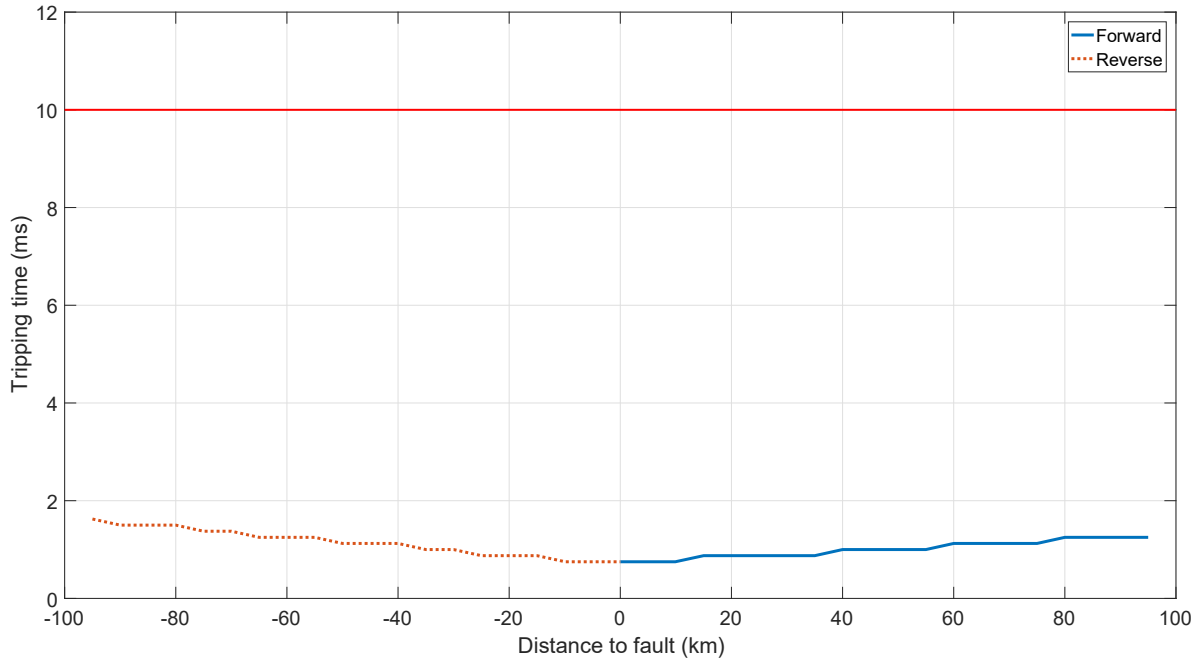

Figure F.2: Forward and reverse algorithm time. $\tau_L^+ = 16.46$ ms; $\tau_L^0 = 14.32$ ms; $\tau_S^+ = 24.69$ ms; $\tau_S^0 = 12.89$ ms; $SIR^+ = 1.15$; $SIR^0 = 1.09$; $\alpha = 0°$

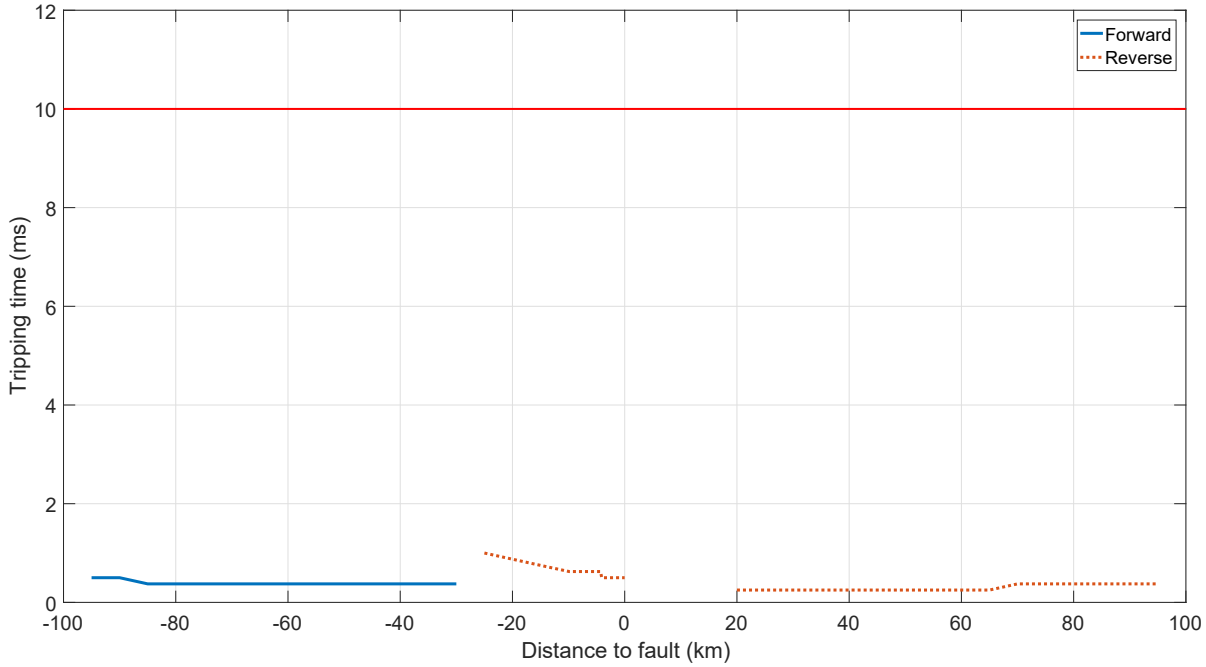

Figure F.3: Forward and reverse algorithm time. $\tau_L^+ = 16.46$ ms; $\tau_L^0 = 14.32$ ms; $\tau_S^+ = 23.05$ ms; $\tau_S^0 = 12.03$ ms; $SIR^+ = 4.47$; $SIR^0 = 2.12$; $\alpha = 90°$

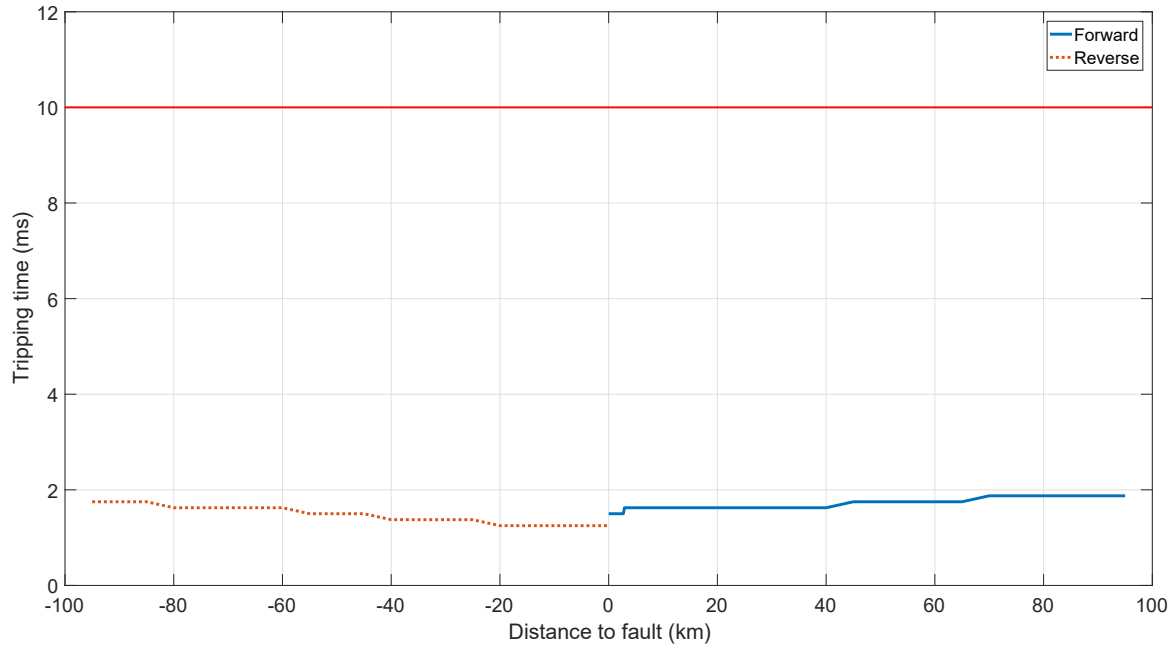

Figure F.4: Forward and reverse algorithm time. $\tau_L^+ = 16.46$ ms; $\tau_L^0 = 14.32$ ms; $\tau_S^+ = 23.05$ ms; $\tau_S^0 = 12.03$ ms; $SIR^+ = 4.47$; $SIR^0 = 2.12$; $\alpha = 0°$

F.2 Phase-to-ground

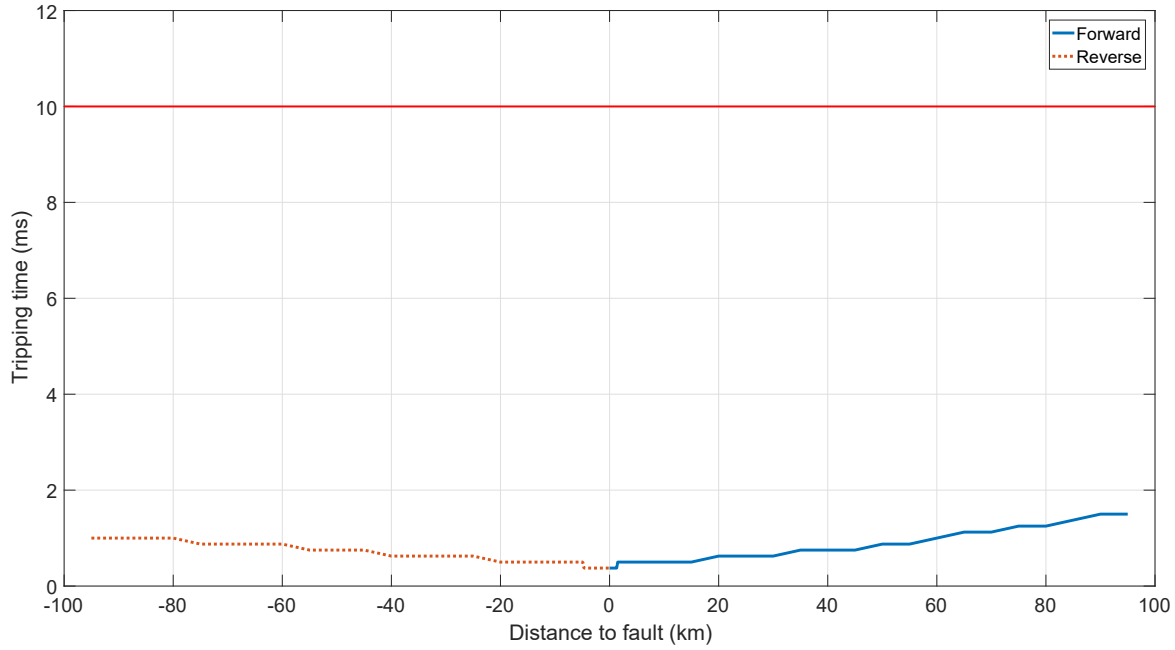

Figure F.5: Forward and reverse algorithm time. $\tau_L^+ = 16.46$ ms; $\tau_L^0 = 14.32$ ms; $\tau_S^+ = 24.69$ ms; $\tau_S^0 = 12.89$ ms; $SIR^+ = 1.15$; $SIR^0 = 1.09$; $\alpha = 90°$

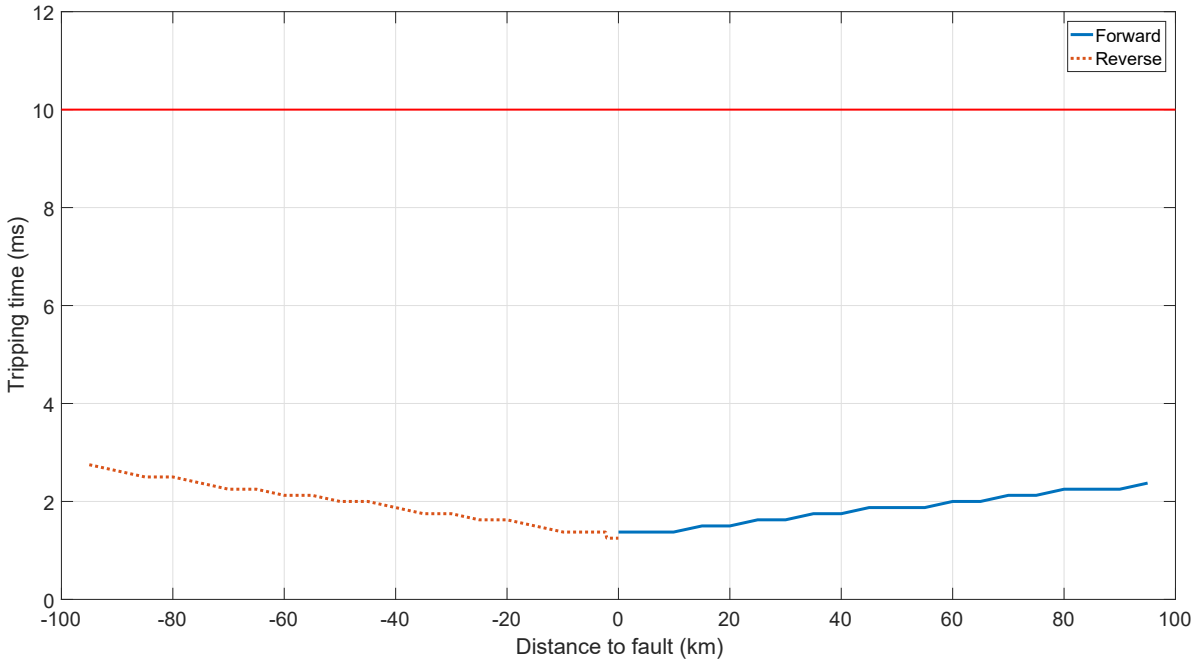

Figure F.6: Forward and reverse algorithm time. $\tau_L^+ = 16.46$ ms; $\tau_L^0 = 14.32$ ms; $\tau_S^+ = 24.69$ ms; $\tau_S^0 = 12.89$ ms; $SIR^+ = 1.15$; $SIR^0 = 1.09$; $\alpha = 0°$

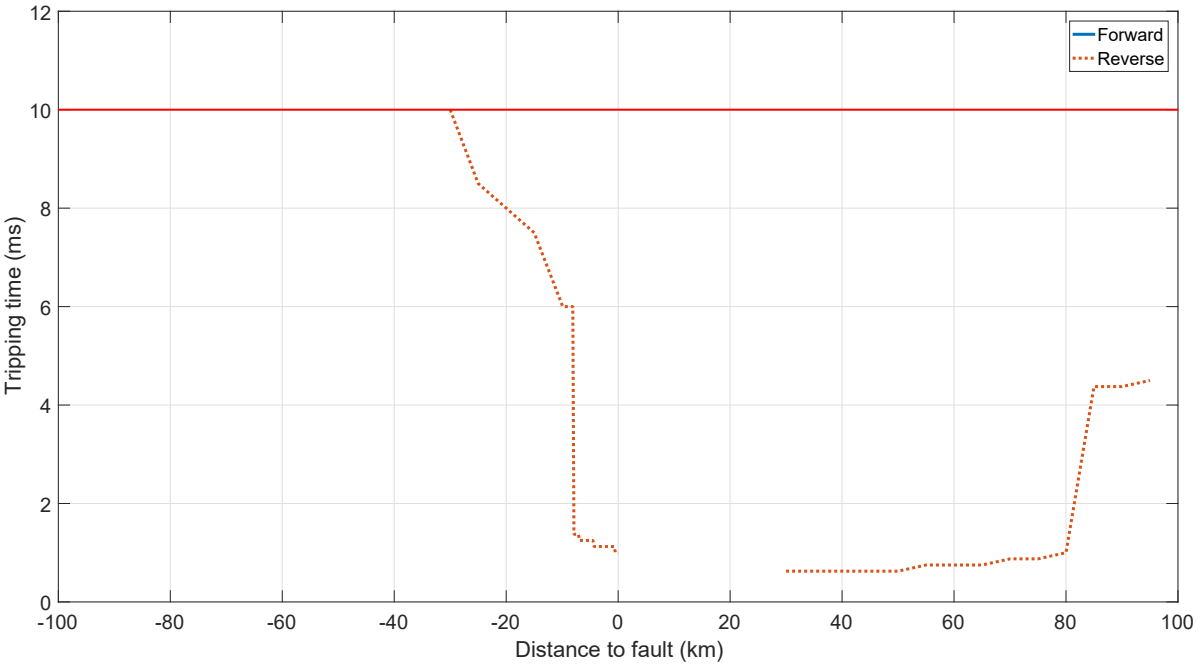

Figure F.7: Forward and reverse algorithm time. $\tau_L^+ = 16.46$ ms; $\tau_L^0 = 14.32$ ms; $\tau_S^+ = 23.05$ ms; $\tau_S^0 = 12.03$ ms; $SIR^+ = 4.47$; $SIR^0 = 2.12$; $\alpha = 90°$

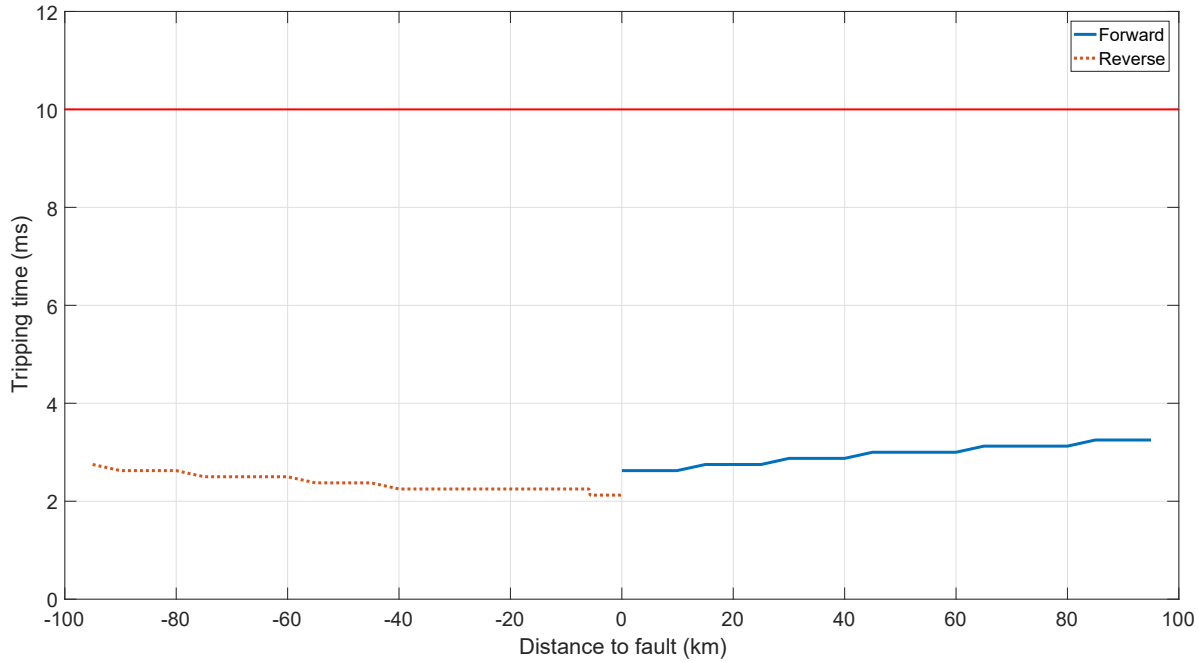

Figure F.8: Forward and reverse algorithm time. $\tau_L^+ = 16.46$ ms; $\tau_L^0 = 14.32$ ms; $\tau_S^+ = 23.05$ ms; $\tau_S^0 = 12.03$ ms; $SIR^+ = 4.47$; $SIR^0 = 2.12$; $\alpha = 0°$

Appendix G

Loop selection tests

G.1 Phase-to-ground

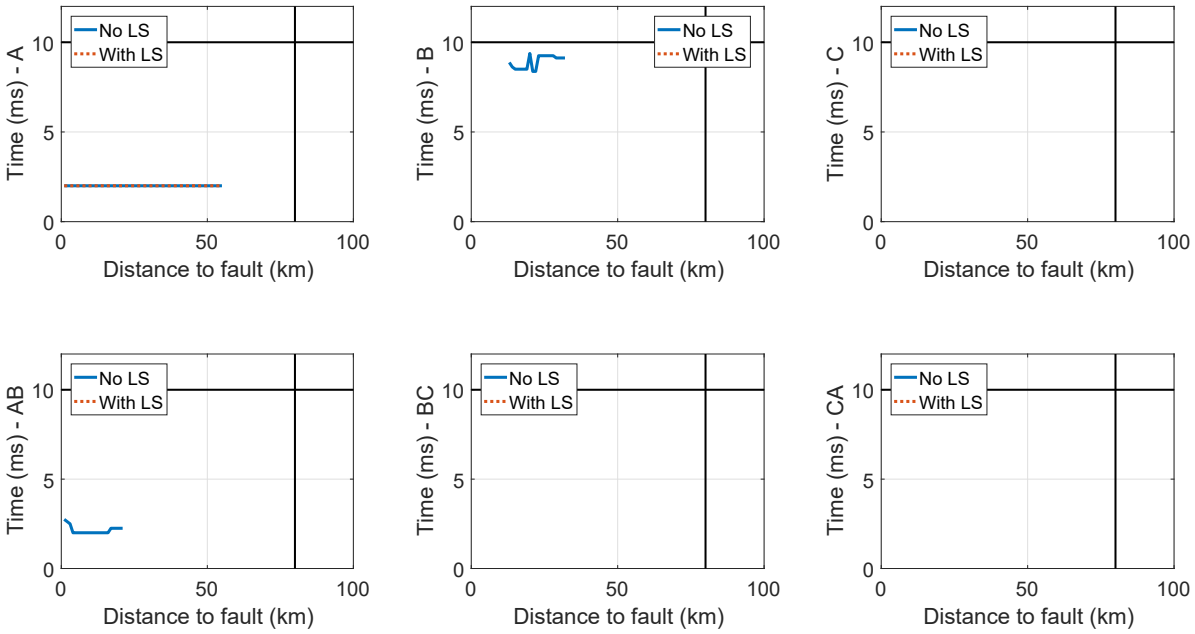

Figure G.1: Phase(A)-to-ground fault: SIR = 0.1; $\alpha = 0°$; R_F(A-G) = 10 Ω

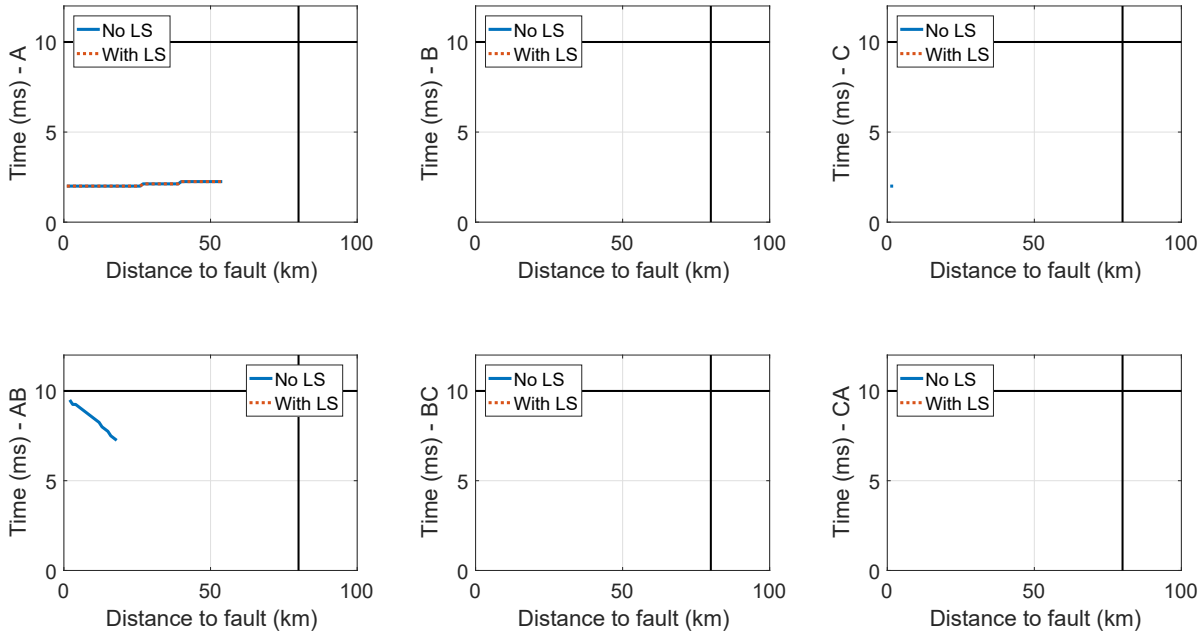

Figure G.2: Phase(A)-to-ground fault: SIR = 0.1; $\alpha = 90°$; R_F(A-G) = 10 Ω

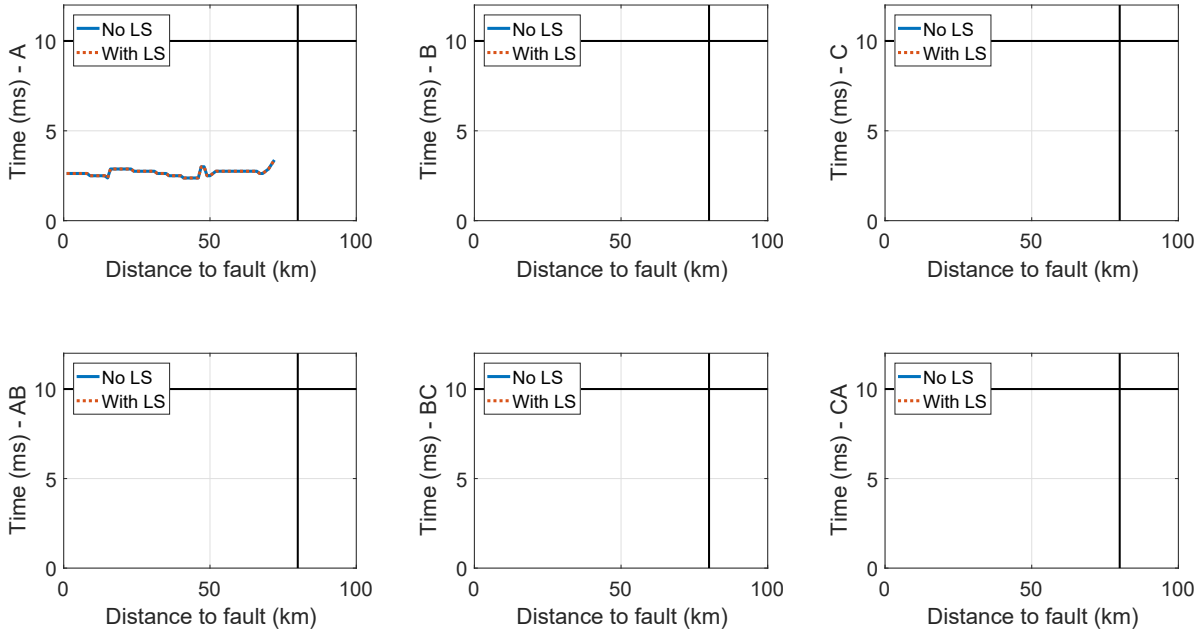

Figure G.3: Phase(A)-to-ground fault: SIR = 5; $\alpha = 0°$; R_F(A-G) = 10 Ω

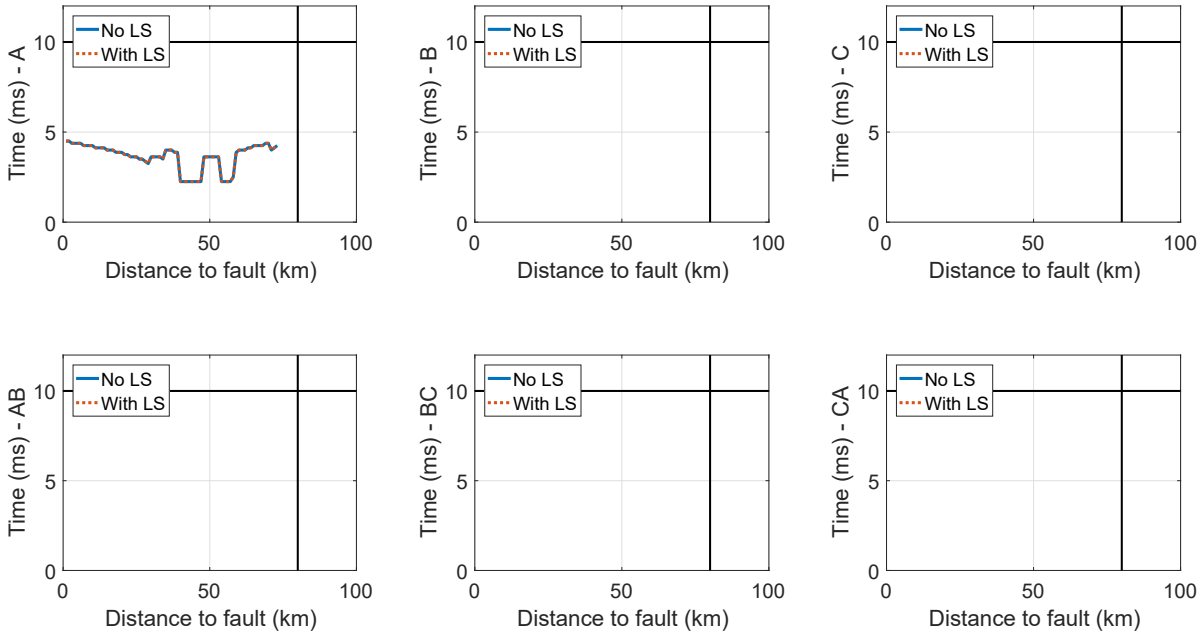

Figure G.4: Phase(A)-to-ground fault: SIR = 5; $\alpha = 90°$; R_F(A-G) = 10 Ω

G.2 Phase-to-phase

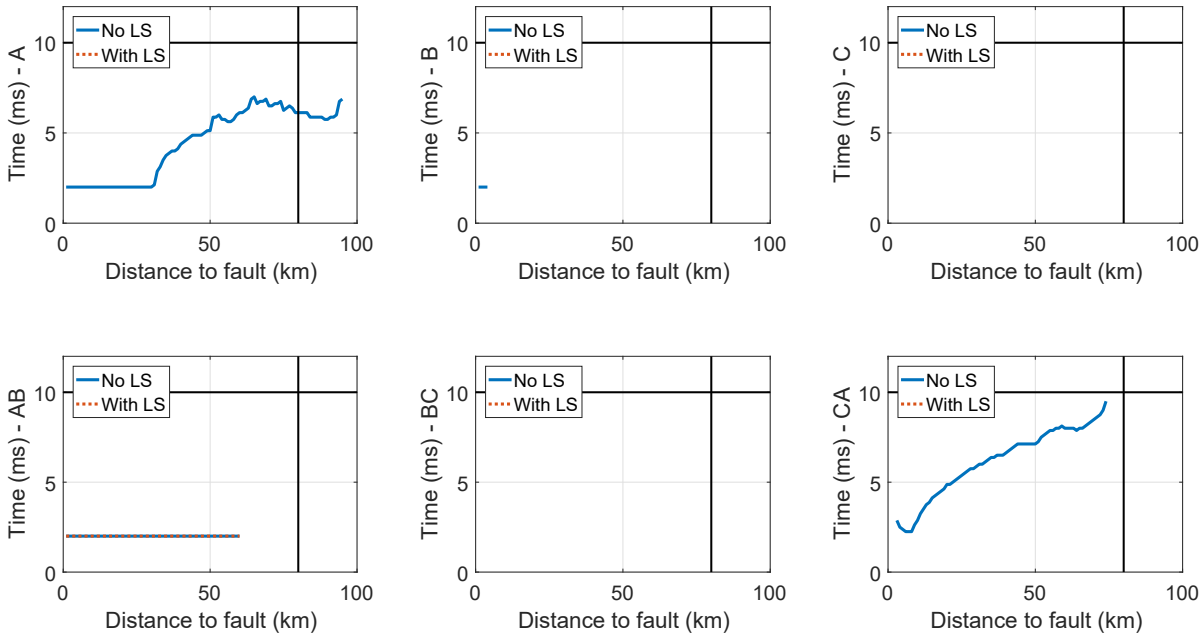

Figure G.5: Phase(A)-to-phase(B) fault: SIR = 0.1; $\alpha = 0°$; R_F(A-B) = 5 Ω

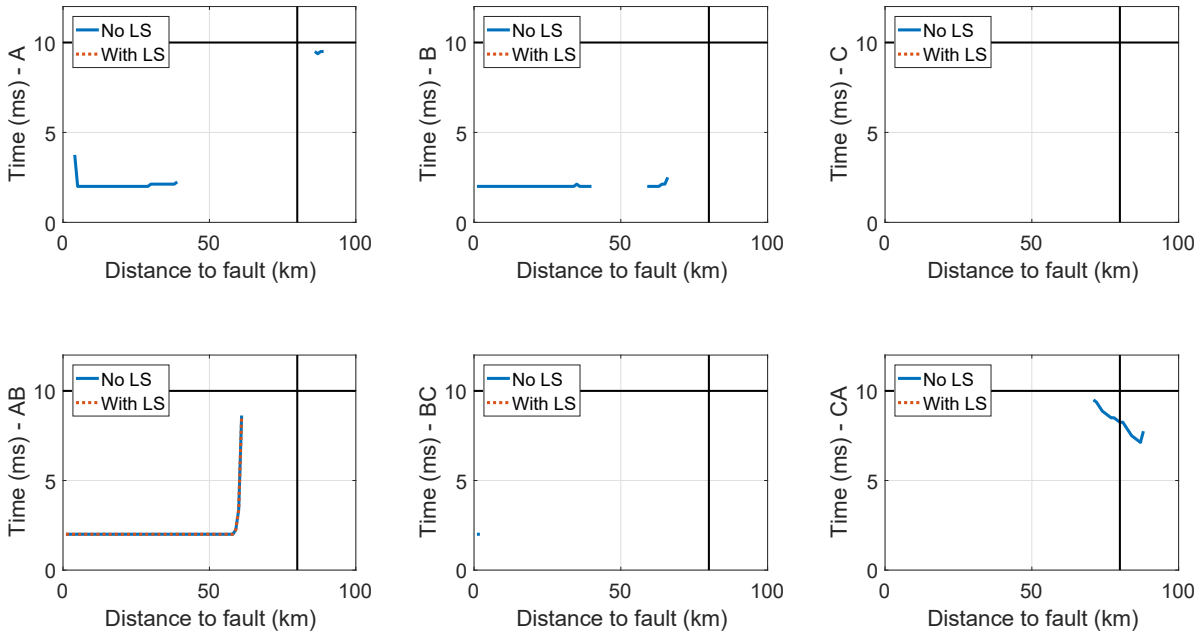

Figure G.6: Phase(A)-to-phase(B) fault: SIR = 0.1; $\alpha = 90°$; R_F(A-B) = 5 Ω

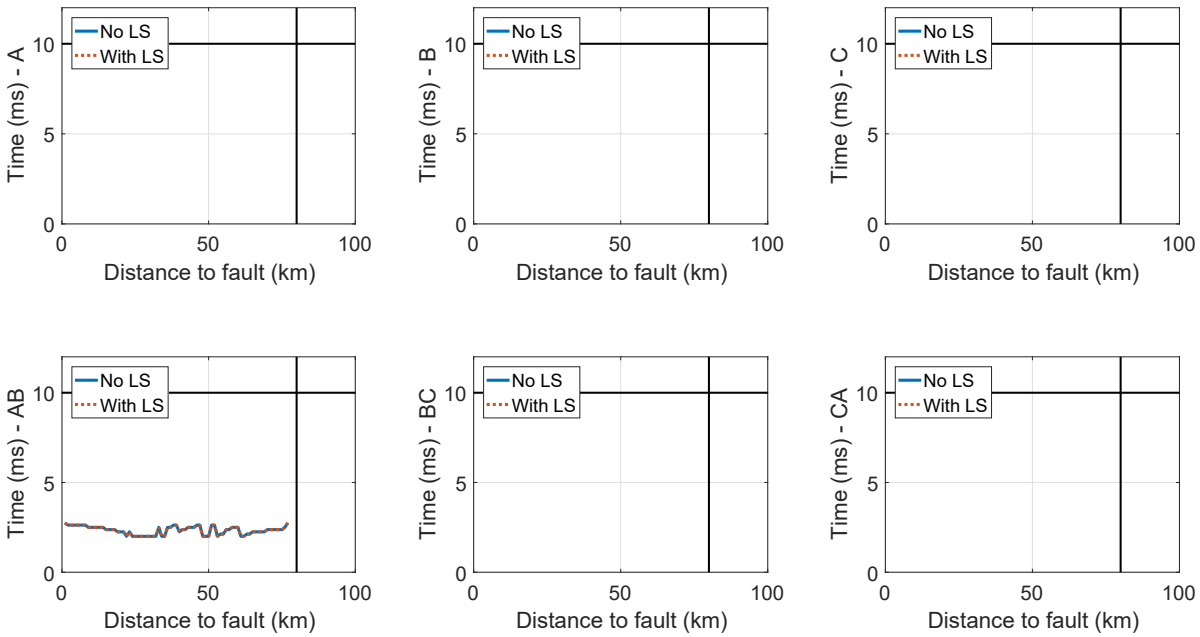

Figure G.7: Phase(A)-to-phase(B) fault: SIR = 5; $\alpha = 0°$; R_F(A-B) = 5 Ω

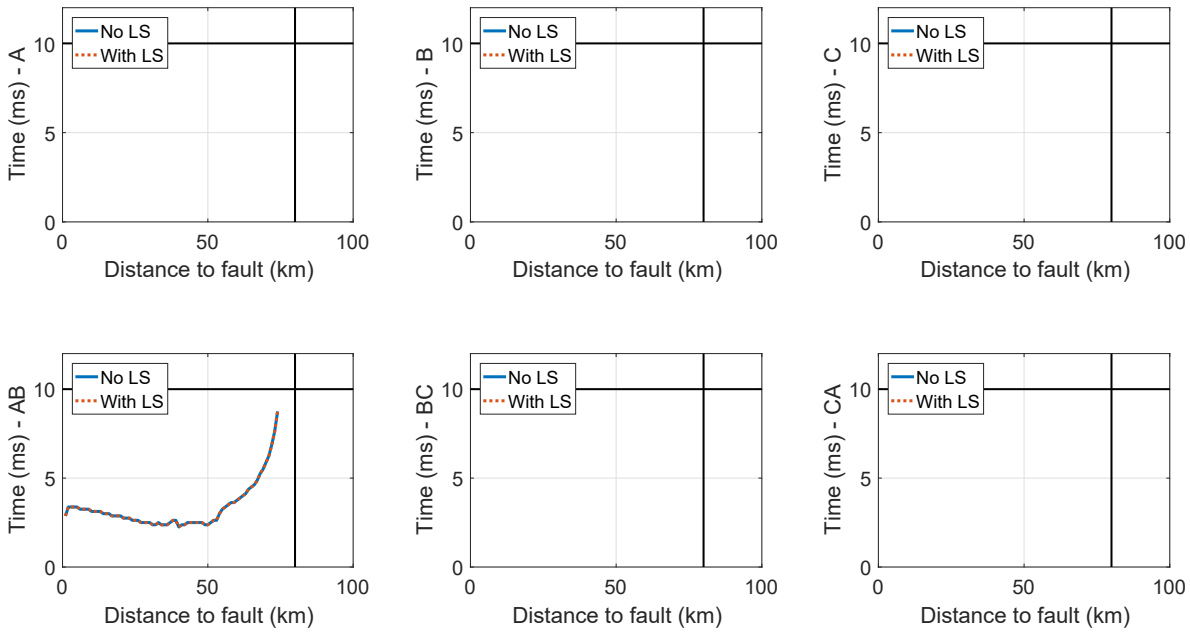

Figure G.8: Phase(A)-to-phase(B) fault: SIR = 5; $\alpha = 90°$; R_F(A-B) = 5 Ω

G.3 Phase-to-phase-to-ground

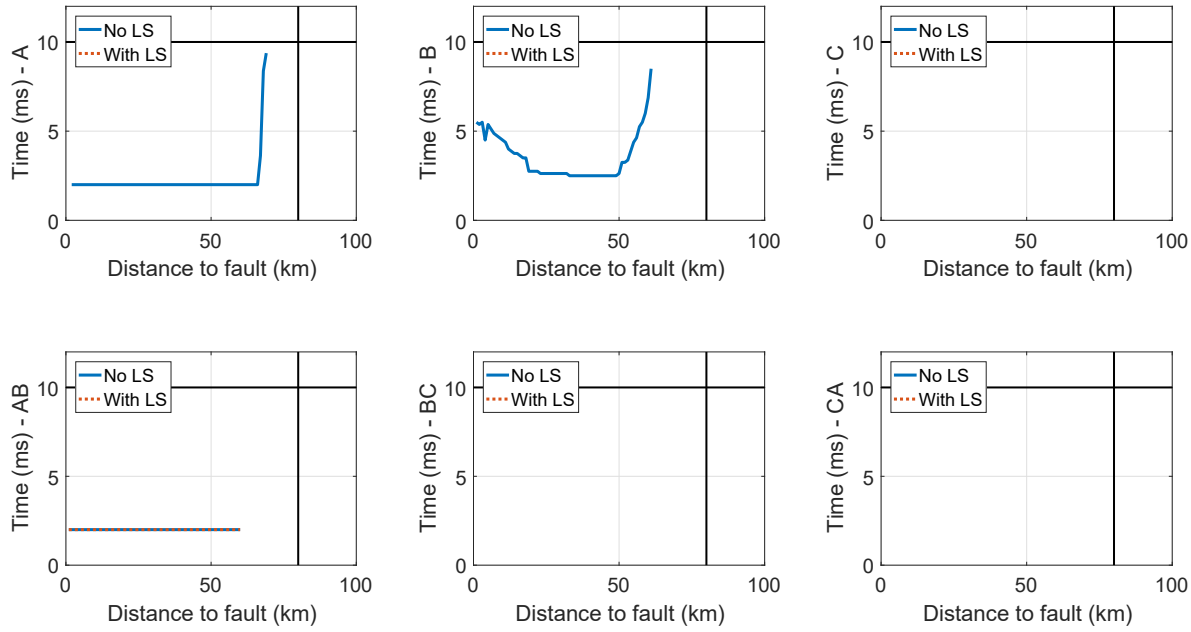

Figure G.9: Phase(A)-to-phase(B)-to-ground fault: SIR = 0.1; $\alpha = 0°$; R_F(A-G) = 10 Ω; R_F(A-B) = 5 Ω

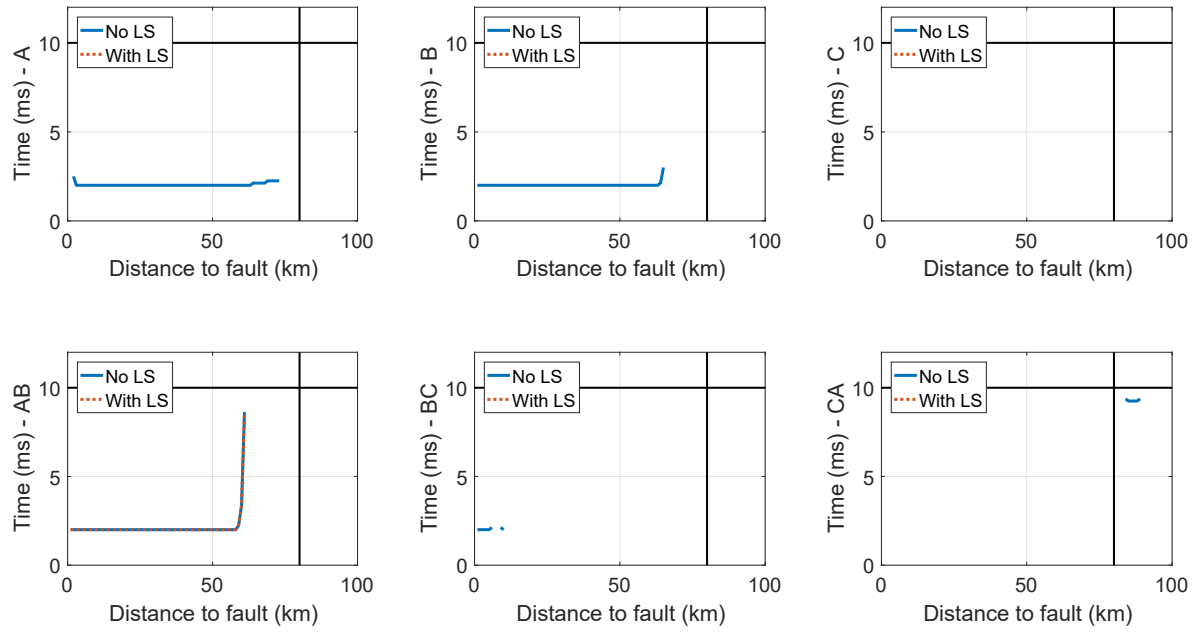

Figure G.10: Phase(A)-to-phase(B)-to-ground fault: SIR = 0.1; $\alpha = 90°$; R_F(A-G) = 10 Ω; R_F(A-B) = 5 Ω

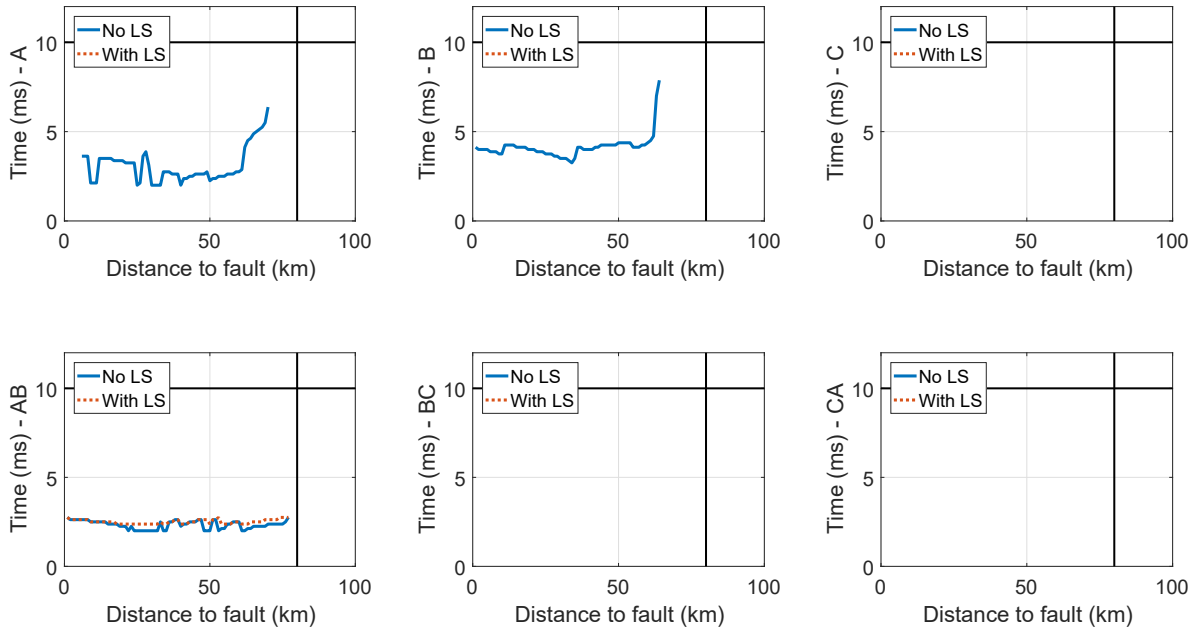

Figure G.11: Phase(A)-to-phase(B)-to-ground fault: SIR = 5; $\alpha = 0°$; R_F(A-G) = 10 Ω; R_F(A-B) = 5 Ω

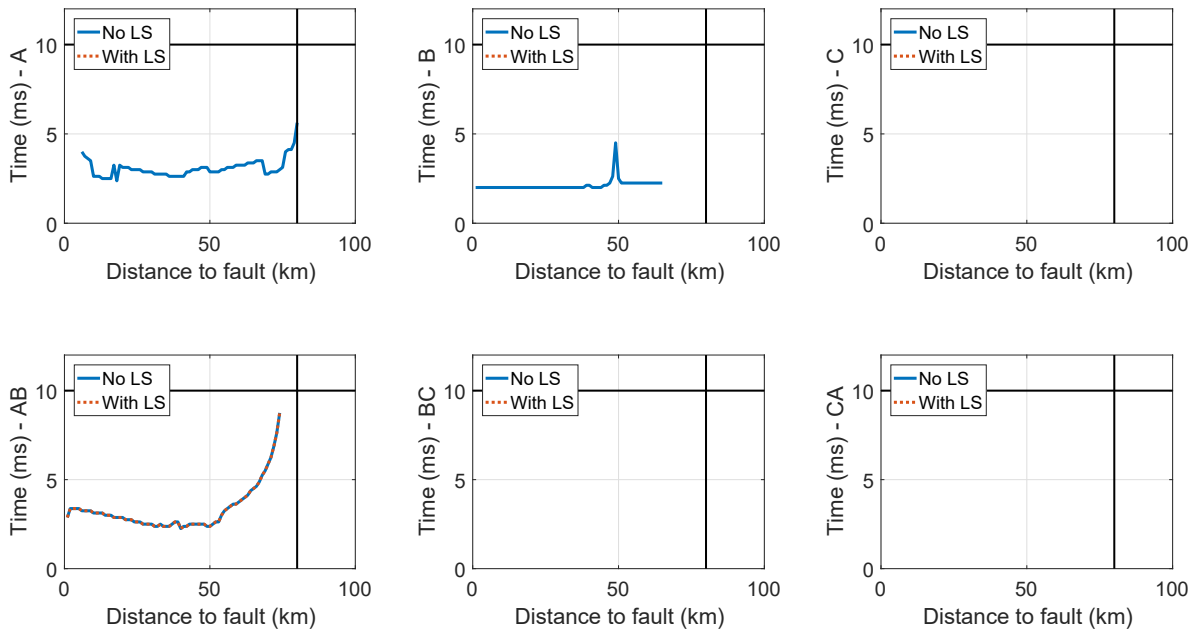

Figure G.12: Phase(A)-to-phase(B)-to-ground fault: SIR = 5; $\alpha = 90°$; R_F(A-G) = 10 Ω; R_F(A-B) = 5 Ω

Appendix I

Complete distance protection testing: results

I.1 Phase-to-ground faults

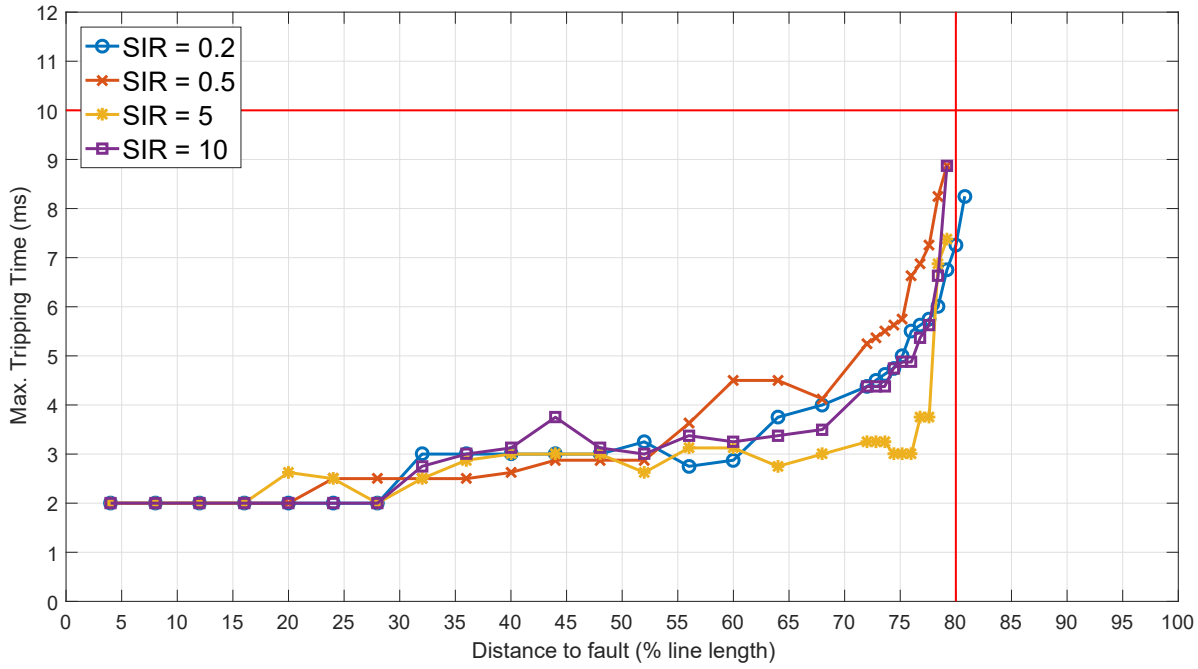

Figure I.1: SIR diagram for the phase-to-ground fault with no fault resistance (maximum tripping times)

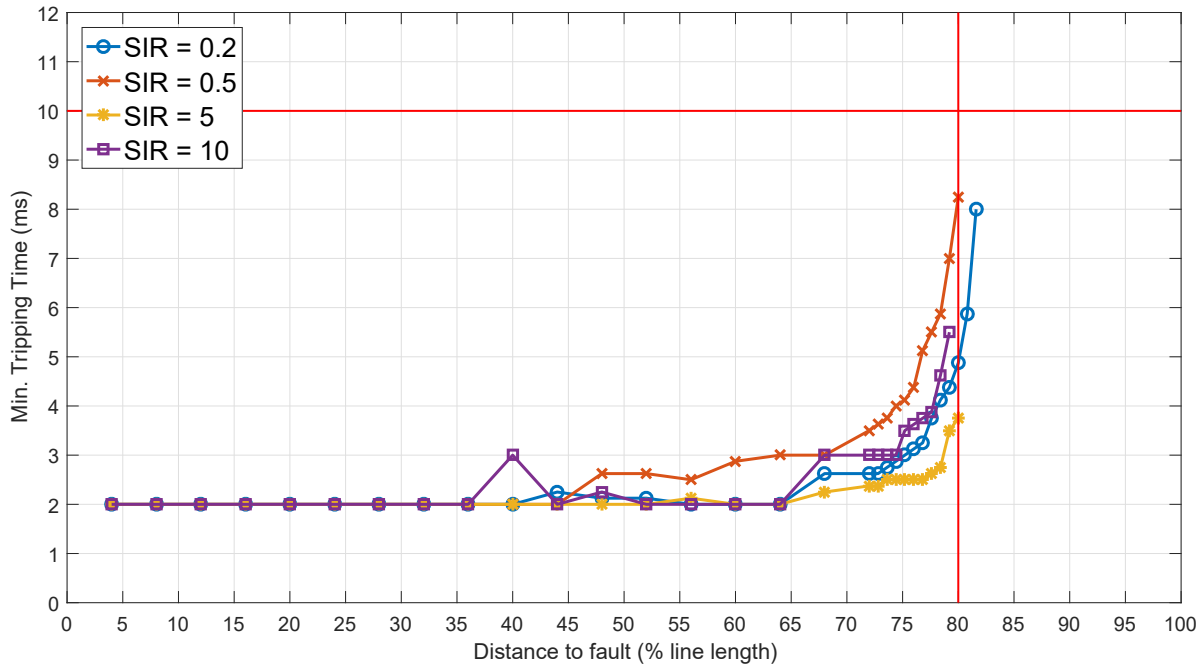

Figure I.2: SIR diagram for the phase-to-ground fault with no fault resistance (minimum tripping times)

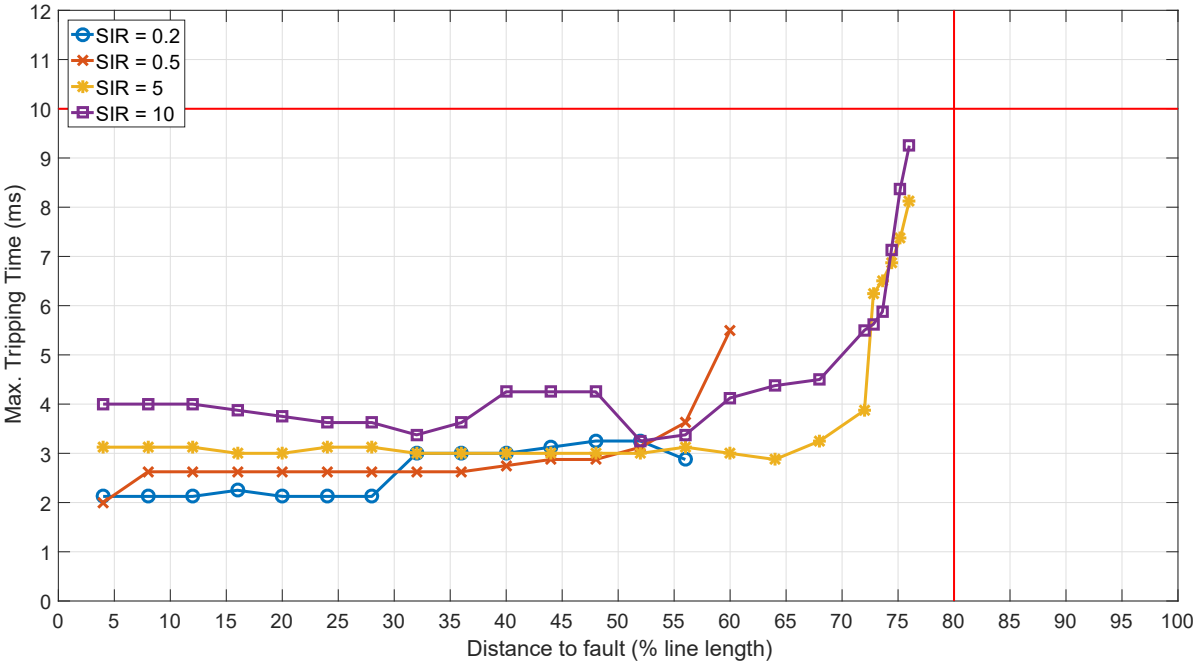

Figure I.3: SIR diagram for the phase-to-ground fault with a fault resistance and an importing power flow (maximum tripping times)

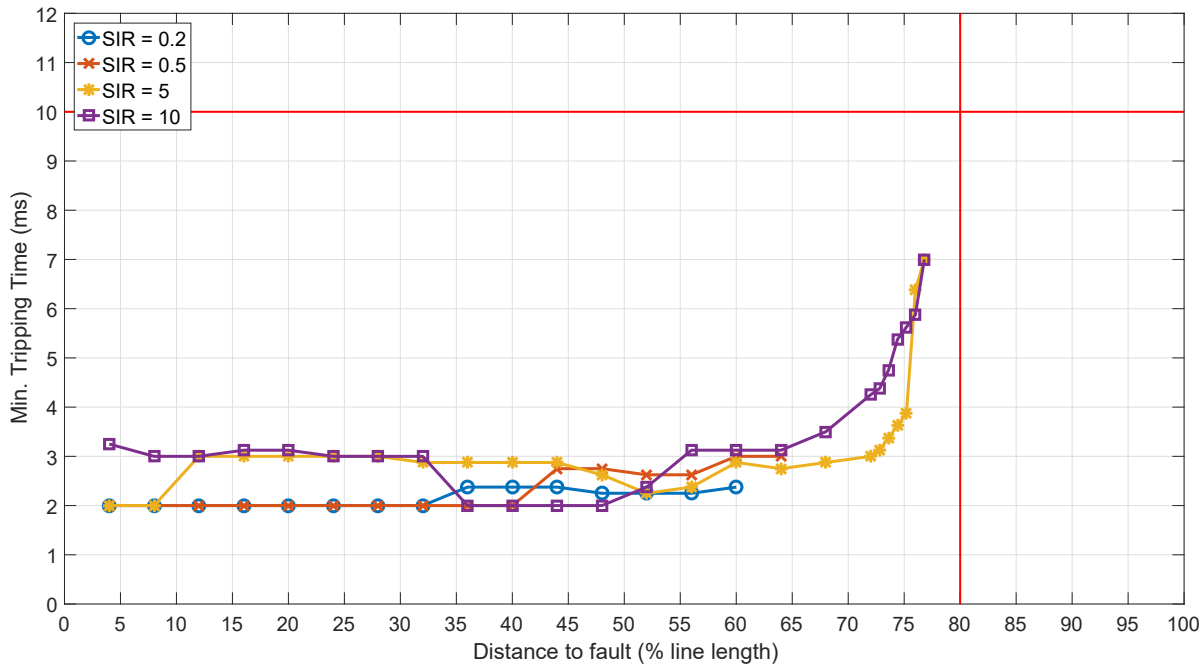

Figure I.4: SIR diagram for the phase-to-ground fault with a fault resistance and an importing power flow (minimum tripping times)

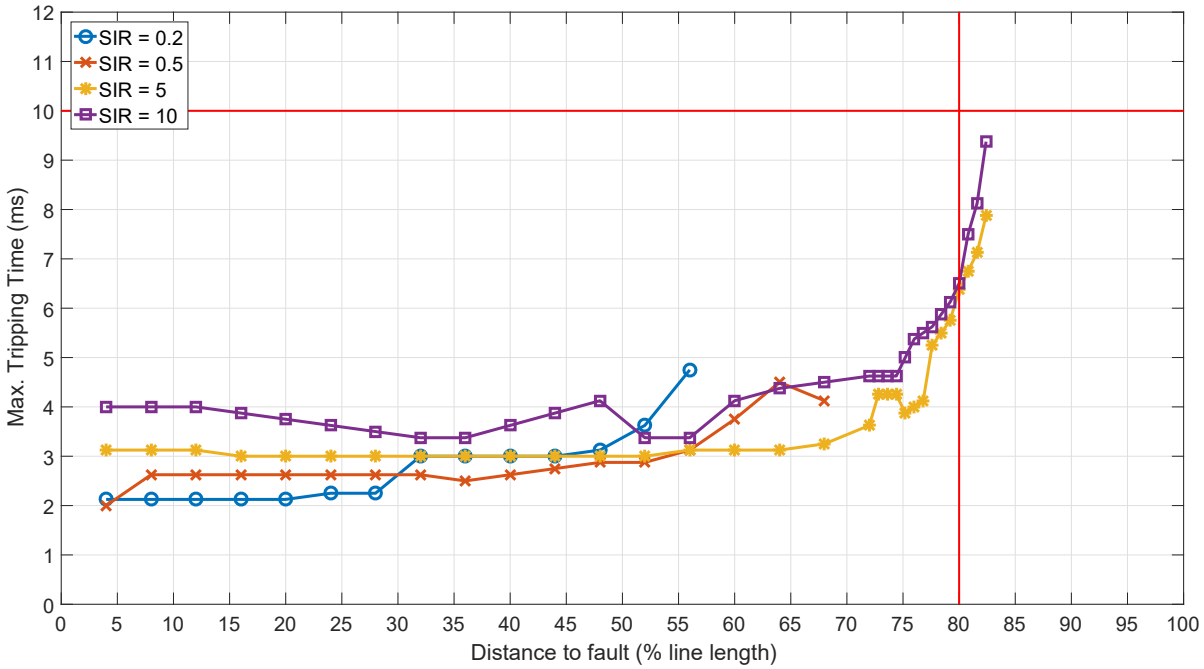

Figure I.5: SIR diagram for the phase-to-ground fault with a fault resistance and an exporting power flow (maximum tripping times)

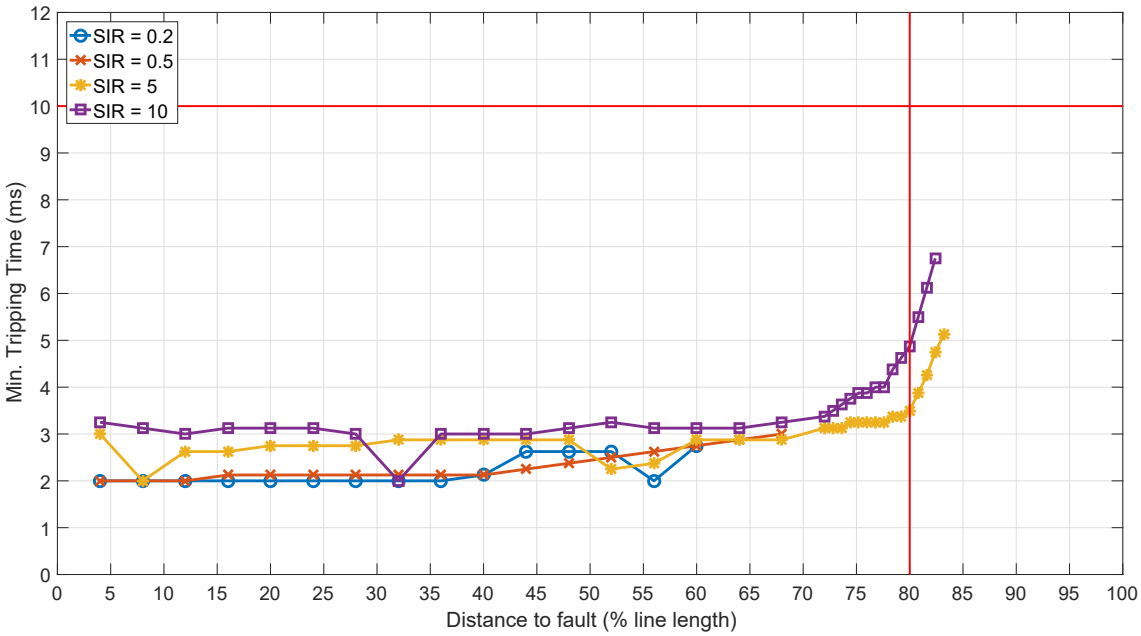

Figure I.6: SIR diagram for the phase-to-ground fault with a fault resistance and an exporting power flow (minimum tripping times)

I.2 Phase-to-phase faults

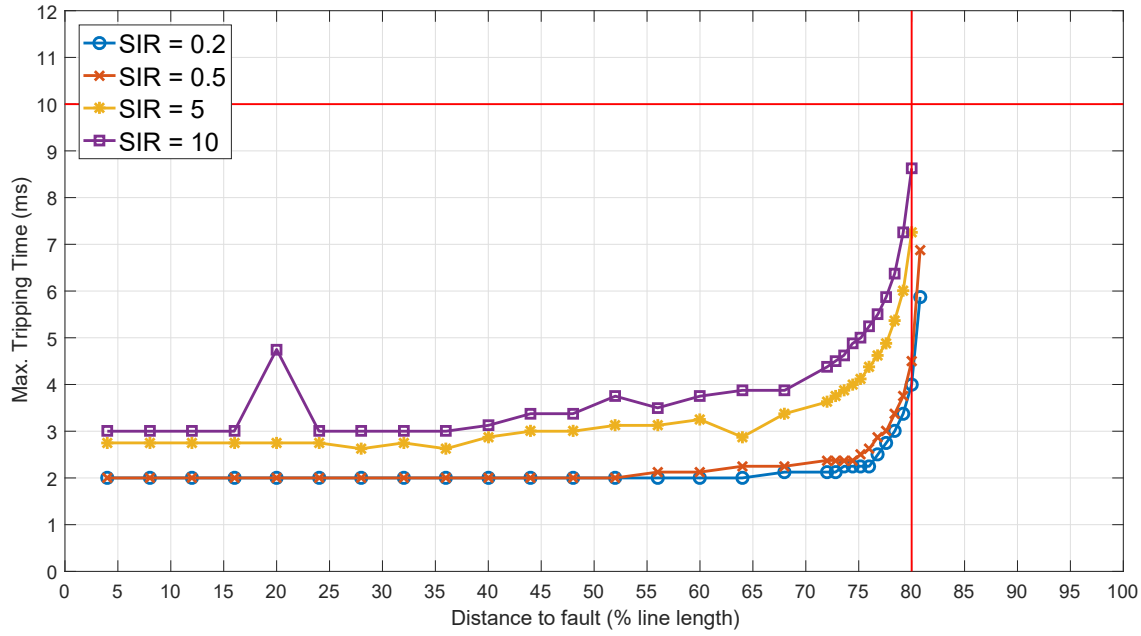

Figure I.7: SIR diagram for the phase-to-phase fault with no fault resistance (maximum tripping times)

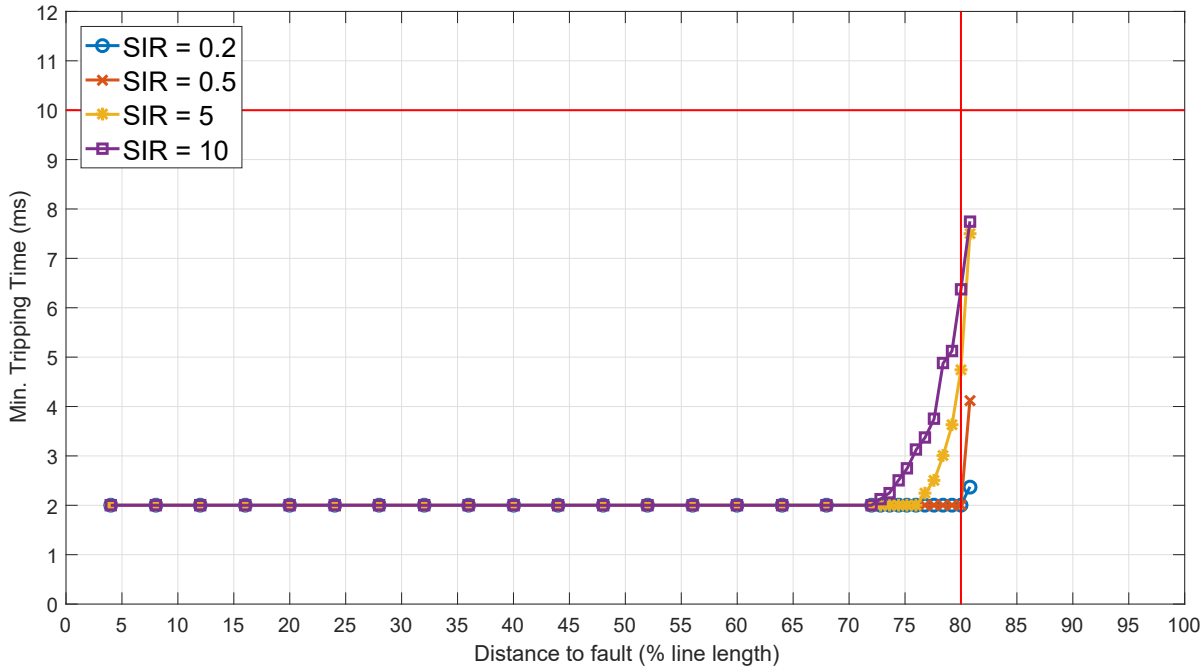

Figure I.8: SIR diagram for the phase-to-phase fault with no fault resistance (minimum tripping times)

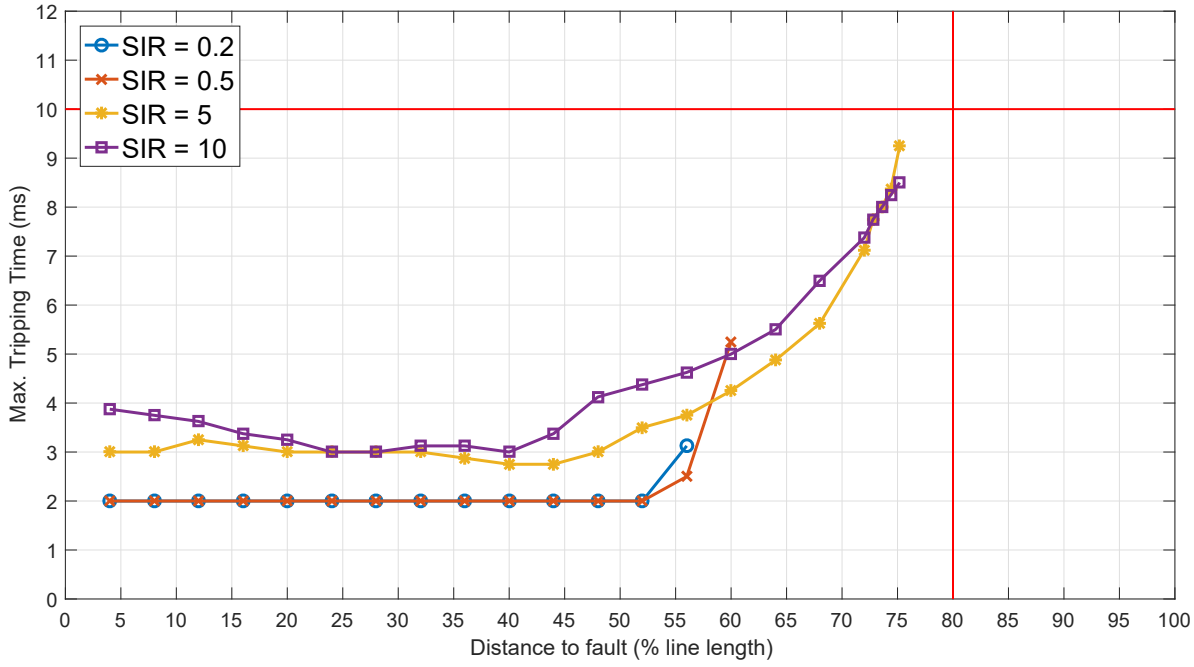

Figure I.9: SIR diagram for the phase-to-phase fault with a fault resistance and an importing power flow (maximum tripping times)

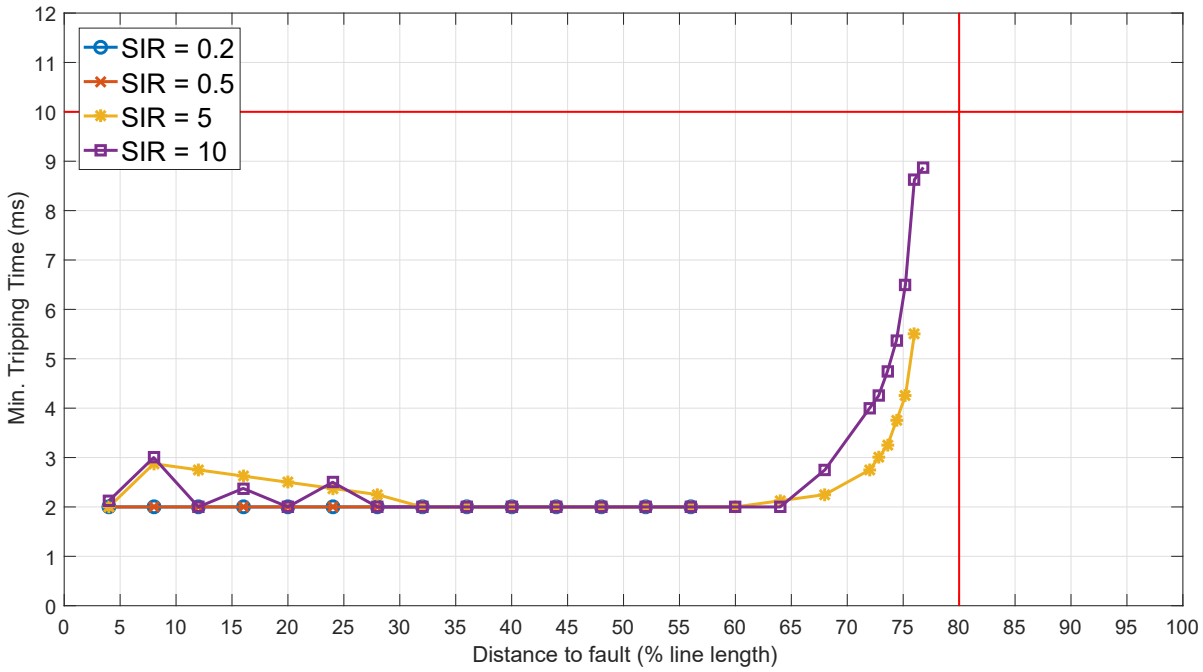

Figure I.10: SIR diagram for the phase-to-phase fault with a fault resistance and an importing power flow (minimum tripping times)

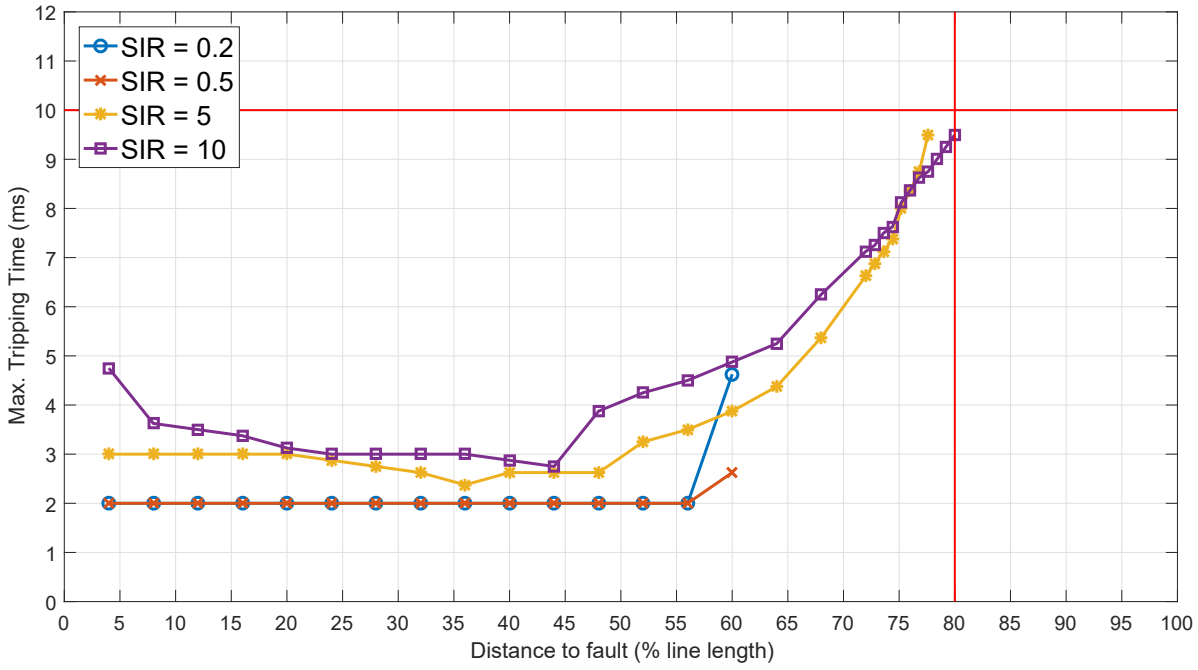

Figure I.11: SIR diagram for the phase-to-phase fault with a fault resistance and an exporting power flow (maximum tripping times)

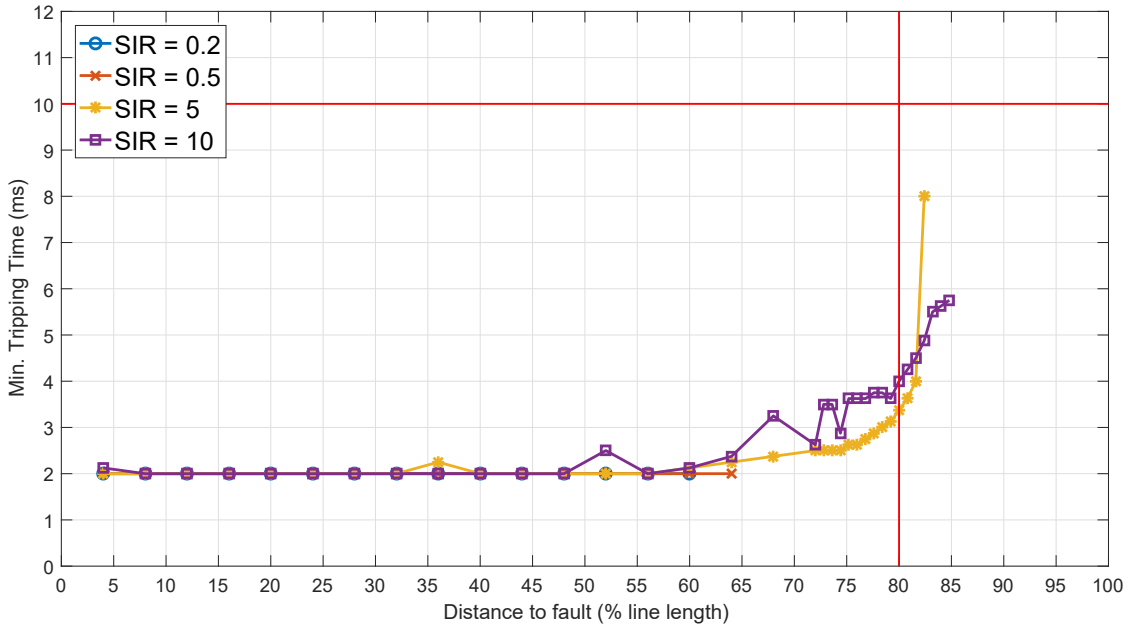

Figure I.12: SIR diagram for the phase-to-phase fault with a fault resistance and an exporting power flow (minimum tripping times)

I.3 Phase-to-phase-to-ground faults

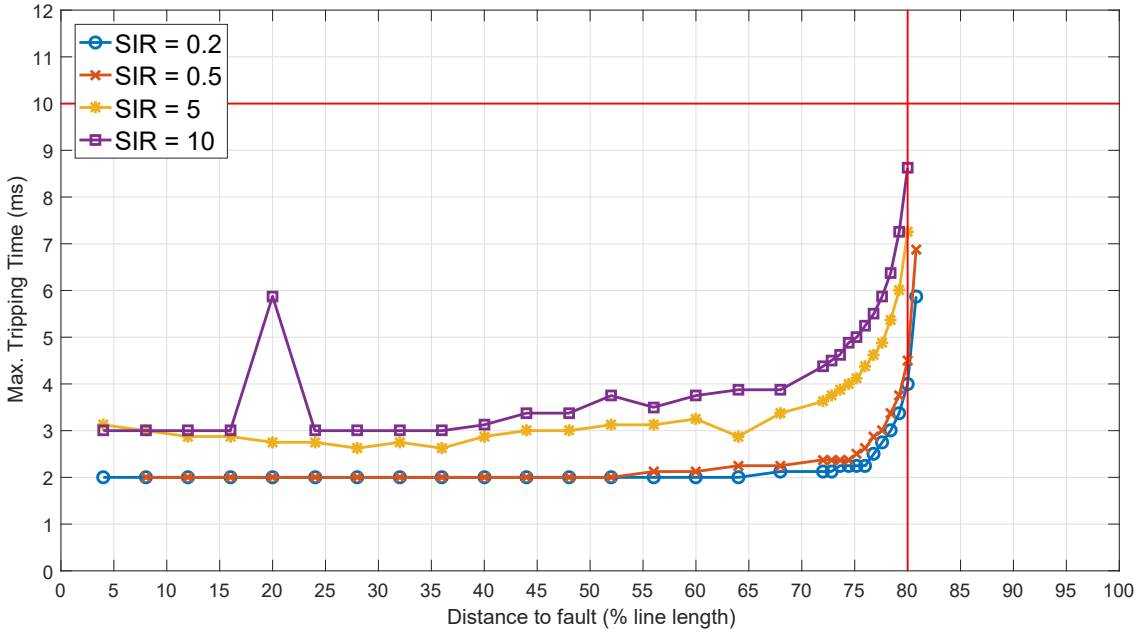

Figure I.13: SIR diagram for the phase-to-phase-to-ground fault with no fault resistance (maximum tripping times)

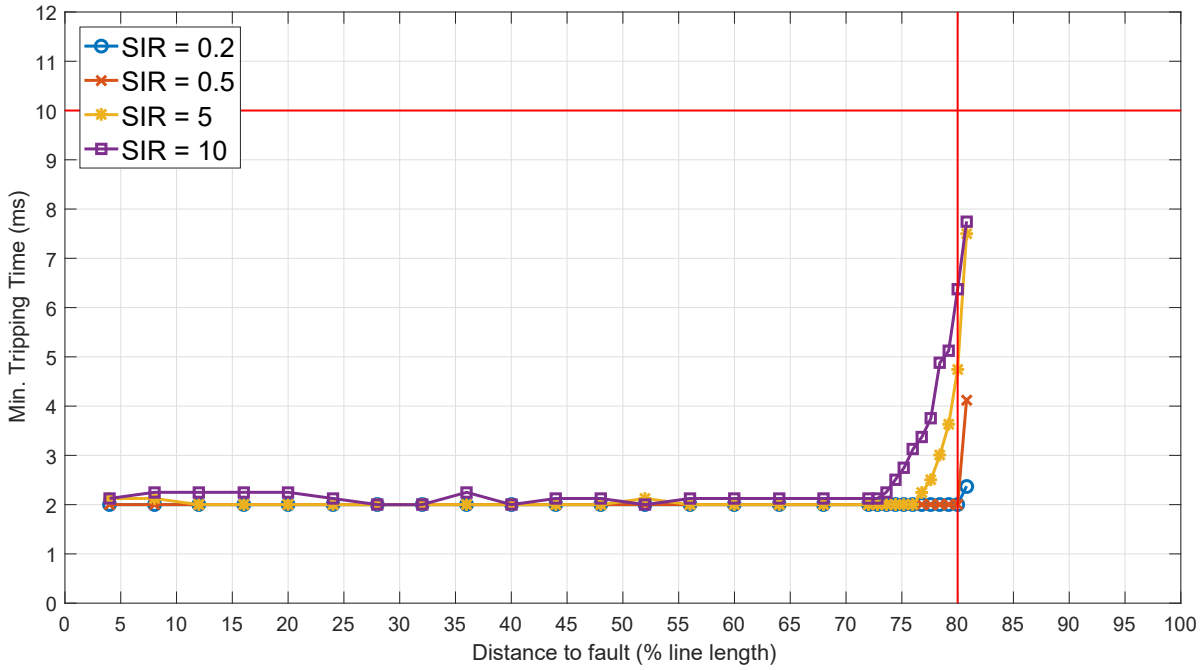

Figure I.14: SIR diagram for the phase-to-phase-to-ground fault with no fault resistance (minimum tripping times)

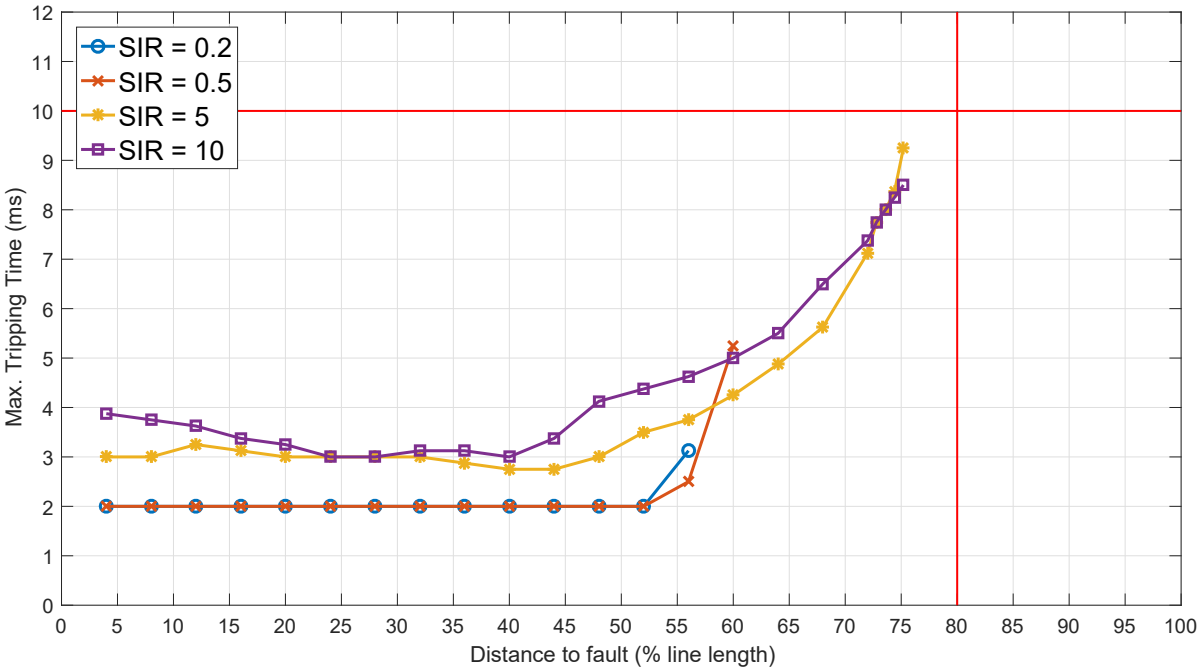

Figure I.15: SIR diagram for the phase-to-phase-to-ground fault with a fault resistance and an importing power flow (maximum tripping times)

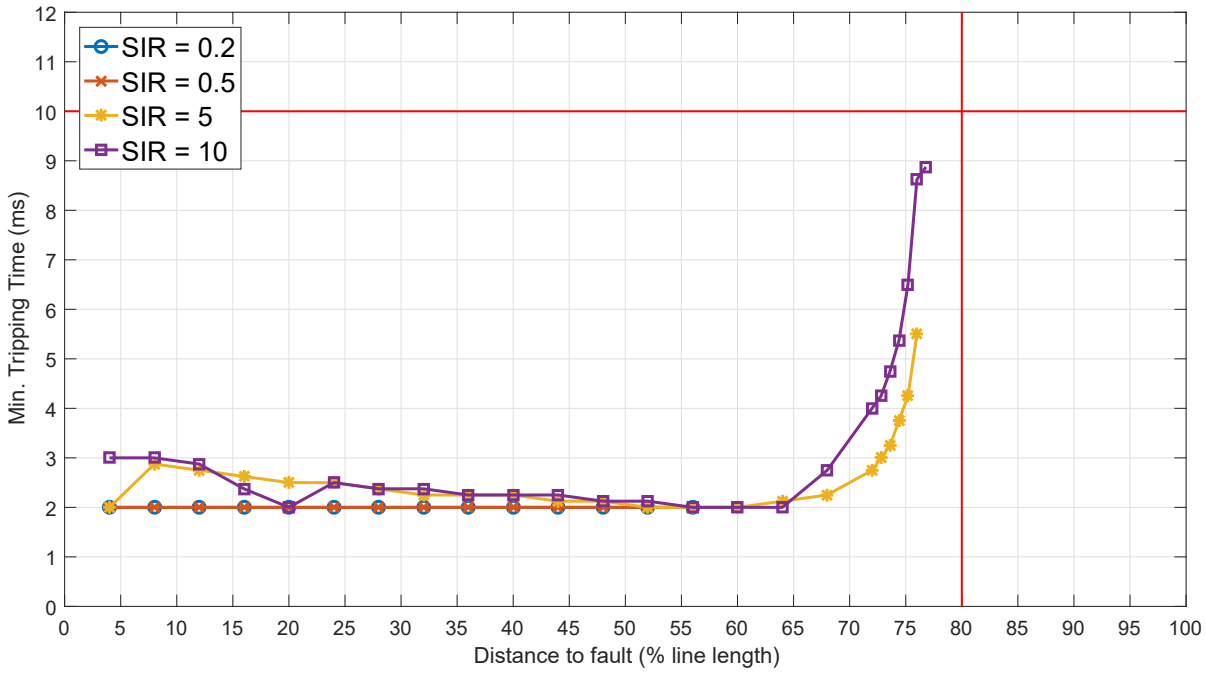

Figure I.16: SIR diagram for the phase-to-phase-to-ground fault with a fault resistance and an importing power flow (minimum tripping times)

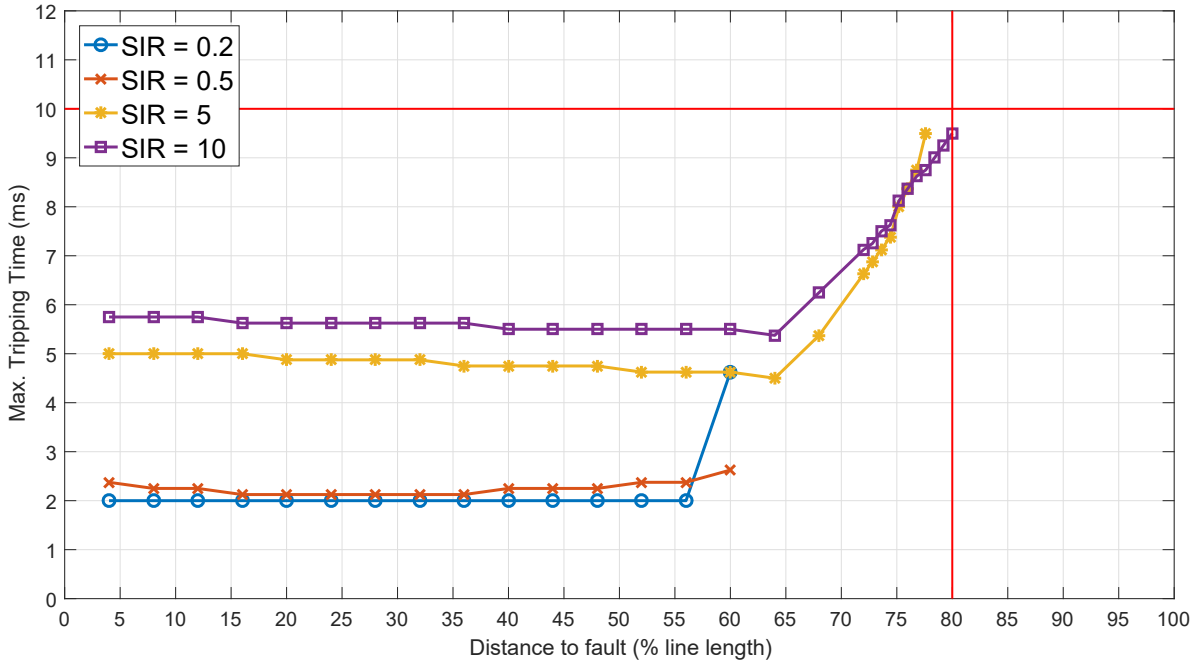

Figure I.17: SIR diagram for the phase-to-phase-to-ground fault with a fault resistance and an exporting power flow (maximum tripping times)

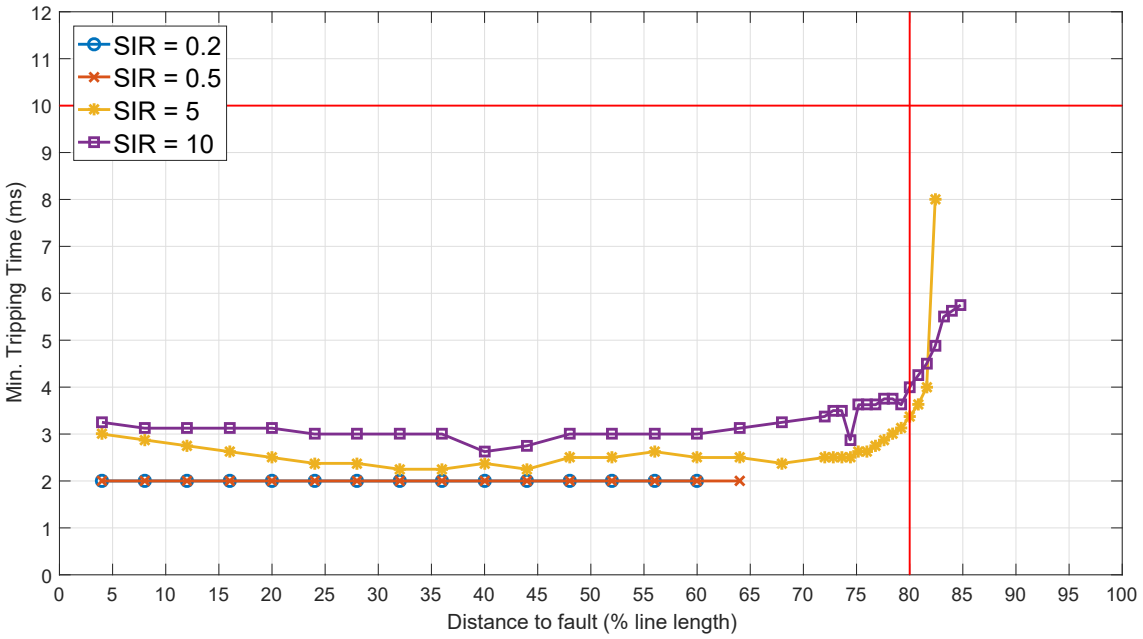

Figure I.18: SIR diagram for the phase-to-phase-to-ground fault with a fault resistance and an exporting power flow (minimum tripping times)

I.4 Three-phase faults

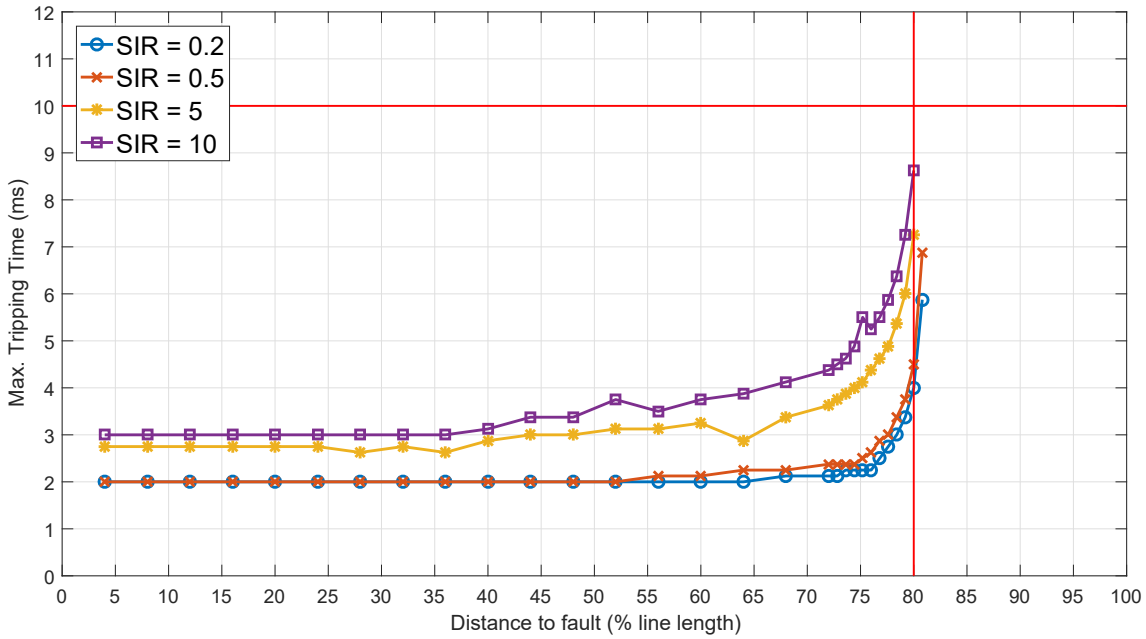

Figure I.19: SIR diagram for the three-phase fault with no fault resistance (maximum tripping times)

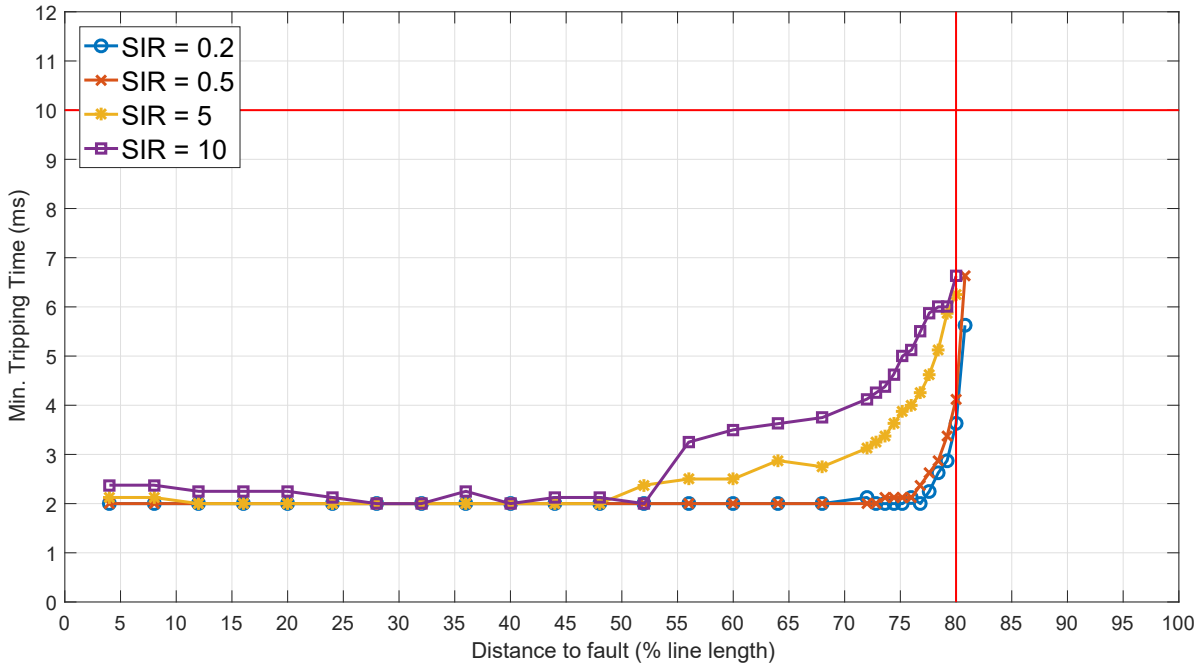

Figure I.20: SIR diagram for the three-phase fault with no fault resistance (minimum tripping times)

Bibliography

[1] Eurostat. (2020). "Electricity production, consumption and market overview," [Online]. Available: https://ec.europa.eu/eurostat/statistics-explained/index.php/Electricity_production,_consumption_and_market_overview#Household_electricity_consumption.

[2] A. Apostolov and B. Vandiver, "Requirements and methods for reducing fault clearing times in Smart Grids," in *2016 69th Annual Conference for Protective Relay Engineers (CPRE)*, IEEE, Apr. 2016, pp. 1–9.

[3] M. A. Uqaili, A. A. Sahito, I. A. Halepoto, Z. A. Memon, and S. B. Dars, "Impact of distributed generation on network short circuit level," in *2014 4th International Conference on Wireless Communications, Vehicular Technology, Information Theory and Aerospace & Electronic Systems (VITAE)*, IEEE, May 2014, pp. 1–5.

[4] V. P. Mahadanaarachchi and R. Ramakuma, "Impact of distributed generation on distance protection performance - A review," in *2008 IEEE Power and Energy Society General Meeting - Conversion and Delivery of Electrical Energy in the 21st Century*, IEEE, Jul. 2008, pp. 1–7.

[5] IEC. (1995). "Fault clearing time," [Online]. Available: http://www.electropedia.org/iev/iev.nsf/display?openform&ievref=448-13-15.

[6] N. D. Tleis, *Power Systems Modelling and Fault Analysis*. Elsevier, 2008.

[7] IEC. (2016). "Power quality," [Online]. Available: http://www.electropedia.org/iev/iev.nsf/display?openform&ievref=614-01-01.

[8] R. Abboud and D. Dolezilek, "Time-Domain Technology – Benefits to Protection, Control, and Monitoring of Power Systems," in *International Conference and Exhibition – Relay Protection and Automation for Electric Power Systems*, 2017.

[9] Circuit Globe. (2020). "Power System Stability," [Online]. Available: https://circuitglobe.com/power-system-stability.html.

[10] Entso-e, "Determining generator fault clearing time for the synchronous zone of Continental Europe," European Network of Transmission System Operators for Electricity, Tech. Rep. 1, 2017, pp. 1–15.

[11] S. H. Horowitz and A. G. Phadke, *Power System Relaying*. Chichester, UK: John Wiley & Sons, Ltd, Apr. 2008, pp. 1–331.

[12] A. Abdelmoumene and H. Bentarzi, "A review on protective relays' developments and trends," *Journal of Energy in Southern Africa*, vol. 25, no. 2, pp. 91–95, Jun. 2017.

[13] E. O. Schweitzer, B. Kasztenny, A. Guzman, V. Skendzic, and M. V. Mynam, "Speed of line protection - can we break free of phasor limitations?" In *2015 68th Annual Conference for Protective Relay Engineers*, IEEE, Mar. 2015, pp. 448–461.

[14] M. Chamia and S. Liberman, "Ultra High Speed Relay for EHV/UHV Transmission Lines – Development, Design and Application," *IEEE Transactions on Power Apparatus and Systems*, vol. PAS-97, no. 6, pp. 2104–2116, 1978.

[15] C. Dzienis, M. Kereit, J. Blumschein, and M. Claus, "An Experimental Analysis of High-Speed-Distance Protection," in *2010 Modern Electric Power Systems*, Wroclaw: IEEE, 2010, pp. 1–8.

[16] ENTSO-E. (2020). "ENTSO-E Transmission System Map," [Online]. Available: `https://www.entsoe.eu/data/map/`.

[17] Elia. (2019). "Map of the electricity transmission system 2019," [Online]. Available: `https://www.elia.be/en/infrastructure-and-projects/our-infrastructure`.

[18] J. Blumschein, C. Dzienis, and M. Kereit, "Directional Comparison based on High-Speed-Distance Protection using Delta Quantities," Siemens AG, Berlin, Tech. Rep., 2012, pp. 1–7.

[19] C. Dzienis, M. Kereit, and J. Blumschein, "Analysis of High-Speed-Distance protection," in *2011 International Conference on Advanced Power System Automation and Protection*, vol. 2, IEEE, Oct. 2011, pp. 1330–1336.

[20] A. Ametani, N. Nagaoka, T. Noda, and T. Matsuura, "A simple and efficient method for including frequency-dependent effects in transmission line transient analysis," *International Journal of Electrical Power & Energy Systems*, vol. 19, no. 4, pp. 255–261, May 1997.

[21] E. Costa, S. Kurokawa, J. Pissolato, and A. Prado, "Efficient procedure to evaluate electromagnetic transients on three-phase transmission lines," *IET Generation, Transmission & Distribution*, vol. 4, no. 9, p. 1069, 2010.

[22] P. T. Caballero, E. C. Marques Costa, and S. Kurokawa, "Fitting the frequency-dependent parameters in the Bergeron line model," *Electric Power Systems Research*, vol. 117, pp. 14–20, Dec. 2014.

[23] G. Benmouyal, N. Fischer, and B. Smyth, "Performance comparison between Mho elements and incremental quantity-based distance elements," in *2017 70th Annual Conference for Protective Relay Engineers (CPRE)*, IEEE, Apr. 2017, pp. 1–19.

[24] W. Meyer, "Overhead transmission lines," in *EMTP theory book*, Bonneville Power Administration, Ed., Bonneville Power Administration, 1981, ch. 4, pp. 4–72.

[25] L. van der Sluis, *Transients in Power Systems*. Chichester, UK: John Wiley & Sons, Ltd, Jun. 2001.

[26] E. W. Weisstein. (2020). "d'Alembert's Solution," [Online]. Available: `http://mathworld.wolfram.com/dAlembertsSolution.html`.

[27] A. T. Johns and S. K. Salman, *Digital Protection for Power Systems*. The Institution of Engineering and Technology, Michael Faraday House, Six Hills Way, Stevenage SG1 2AY, UK: IET, Jan. 1995.

[28] L. d. A. de Freitas, "Time-Domain Impedance-Based Fault Location for HVDC Transmission Lines," Ph.D. dissertation, Faculdade de Engenharia da Universidade do Porto, 2013, p. 141.

[29] Ou Junzhang and Zhang Zhonghui, "The research of fault location of transmission line based on Bergeron model," in *2010 3rd International Conference on Advanced Computer Theory and Engineering(ICACTE)*, vol. 5, Chengdu: IEEE, Aug. 2010, pp. V5–300–V5–304.

[30] J. Marti, "Accurate Modelling of Frequency-Dependent Transmission Lines in Electromagnetic Transient Simulations," *IEEE Transactions on Power Apparatus and Systems*, vol. PAS-101, no. 1, pp. 147–157, Jan. 1982.

[31] A. Morched, B. Gustavsen, and M. Tartibi, "A universal model for accurate calculation of electromagnetic transients on overhead lines and underground cables," *IEEE Transactions on Power Delivery*, vol. 14, no. 3, pp. 1032–1038, Jul. 1999.

[32] A. Tavighi, J. Martí, and J. A. G. Robles, "Comparison of the fdLine and ULM Frequency Dependent EMTP Line Models with a Reference Laplace Solution," in *International Power Systems Transients Conference (IPST)*, Cavtat, 2015.

[33] J. R. Marti and A. Tavighi, "Frequency-Dependent Multiconductor Transmission Line Model With Collocated Voltage and Current Propagation," *IEEE Transactions on Power Delivery*, vol. 33, no. 1, pp. 71–81, Feb. 2018.

[34] G. Ziegler, *Numerical distance protection*, 3rd ed., Siemens, Ed. Publicis Corporate Publishing, 2008.

[35] H. M. J. De Silva, A. Gole, and L. Wedepohl, "Accurate electromagnetic transient simulations of HVDC cables and overhead transmission lines," *International Conference on Power System Transients (IPST)*, vol. 2007, pp. 1–6, 2007.

[36] O. P. Hevia, "Alternative Transients Program - Comparison of transmission line models," *Revista Latinoamericana del ATP*, vol. 1, pp. 1–5, 1999.

[37] G. Song, X. Chu, S. Gao, X. Kang, Z. Jiao, and J. Suonan, "Novel Distance Protection Based on Distributed Parameter Model for Long-Distance Transmission Lines," *IEEE Transactions on Power Delivery*, vol. 28, no. 4, pp. 2116–2123, Oct. 2013.

[38] J. B. Xin, X. N. Lin, and Z. Q. Bo, "A New Single-Ended Fault Location Method Based on Bergeron Model," *Advanced Materials Research*, vol. 433-440, pp. 2939–2944, Jan. 2012.

[39] V. Cecchi, A. St. Leger, K. Miu, and C. Nwankpa, "Loading studies for power transmission line models in the presence of non-fundamental frequencies," *Summer Computer Simulation Conference 2007, SCSC'07, Part of the 2007 Summer Simulation Multiconference, SummerSim'07*, vol. 2, no. Figure 1, pp. 1373–1378, 2007.

[40] J.-M. Escané, *Réseaux d'énergie électrique. Modélisation: lignes, câbles*, Eyrolles, Ed. Paris, 1997.

[41] E. W. Weisstein. (2020). "Hyperbolic Cotangent," [Online]. Available: `https://mathworld.wolfram.com/HyperbolicCotangent.html`.

[42] R. L. Burden and J. D. Faires, *Numerical analysis*, 9th ed. Cengage Learning, 2010.

[43] W. J. Smolinski, "An Algorithm for Digital Impedance Calculation Using a Single PI Section Transmission Line Model," *IEEE Transactions on Power Apparatus and Systems*, vol. PAS-98, no. 5, pp. 1546–1551, Sep. 1979.

[44] M. Sachdev and R. Agarwal, "A technique for estimating transmission line fault locations from digital impedance relay measurements," *IEEE Transactions on Power Delivery*, vol. 3, no. 1, pp. 121–129, 1988.

[45] G. A. Asti, R. C. da Silva, S. Kurokawa, and E. C. M. da Costa, "Identification of transmission line parameters from temporal measurements of currents and voltages in their terminals: Influence oh the length line," in *2012 IEEE Power and Energy Society General Meeting*, IEEE, Jul. 2012, pp. 1–7.

[46] M. Wen, D. Chen, and X. Yin, "A novel fast distance relay for long transmission lines," *International Journal of Electrical Power & Energy Systems*, vol. 63, pp. 681–686, Dec. 2014.

[47] C. Radhakrishna Rao, H. Toutenburg, Shalabh, and C. Heumann, *Linear Models and Generalizations*, 3rd, ser. Springer Series in Statistics. Berlin, Heidelberg: Springer Berlin Heidelberg, 2008.

[48] D. M. Bates and D. G. Watts, *Nonlinear Regression Analysis and Its Applications*, 2nd. John Wiley & Sons, 1988.

[49] The MathWorks. (2020). "Decimate," [Online]. Available: `https://www.mathworks.com/help/signal/ref/decimate.html`.

[50] C. Weinstein, IEEE Acoustics, Speech, and S. P. S. D. S. P. Committee, *Programs for digital signal processing*. New York: IEEE Press, 1979.

[51] F. J. Taylor, *Digital Filters*, IEEE Serie. Hoboken, NJ, USA: John Wiley & Sons, Inc., Nov. 2011.

[52] S. Engelberg, "Time-limited Functions Are Not Band-limited," in *Digital Signal Processing*, London: Springer London, 2008, pp. 21–27.

[53] M. J. Thompson and D. L. Heidfeld, "Transmission line setting calculations - beyond the cookbook," in *2015 68th Annual Conference for Protective Relay Engineers*, IEEE, Mar. 2015, pp. 850–865.

[54] B. Kasztenny and D. Finney, "Fundamentals of Distance Protection," in *2008 61st Annual Conference for Protective Relay Engineers*, IEEE, Apr. 2008, pp. 1–34.

[55] D. K. Baissa and C. Rainey, "When BLUE is not best: non-normal errors and the linear model," *Political Science Research and Methods*, vol. 8, no. 1, pp. 136–148, Jan. 2020.

[56] N. J. Higham, *Accuracy and stability of numerical agorithms*, 2nd ed. Manchester: Siam, 2002.

[57] D. Lichtblau and E. W. Weisstein. (2020). "Condition Number," [Online]. Available: `https://mathworld.wolfram.com/ConditionNumber.html`.

[58] Y. Zhu and X. R. Li, "Recursive least squares with linear constraints," *Communications in information and systems*, vol. 7, no. 3, pp. 287–312, 2007.

[59] R. Johnstone, C. Johnson, R. Bitmead, and B. O. Anderson, "Exponential convergence of recursive least squares with exponential forgetting factor," in *1982 21st IEEE Conference on Decision and Control*, Orlando: IEEE, Dec. 1982, pp. 994–997.

[60] S. Haykin, "Method of Least-Squares," in *Adaptive Filter Theory*, 5th ed., Pearson, 2013, ch. 9, pp. 398–448.

[61] I. Tabus, "Advanced signal processing: Lecture 7 Least squares and RLS algorithms," Tampere University of Technology, Tech. Rep., 2012.

[62] M. S. Ahmad, O. Kukrer, and A. Hocanin, "The effect of the forgetting factor on the RI adaptive algorithm in system identification," in *ISSCS 2011 - International Symposium on Signals, Circuits and Systems*, IEEE, Jun. 2011, pp. 1–4.

[63] C. Paleologu, J. Benesty, and S. Ciochina, "A Robust Variable Forgetting Factor Recursive Least-Squares Algorithm for System Identification," *IEEE Signal Processing Letters*, vol. 15, no. February, pp. 597–600, 2008.

[64] P. Stoica and P. Åhgren, "Exact initialization of the recursive least-squares algorithm," *International Journal of Adaptive Control and Signal Processing*, vol. 16, no. 3, pp. 219–230, Apr. 2002.

[65] J. W. Osborne and E. Waters, "Four Assumptions of Multiple Regression That Researchers Should Always Test," *Practical Assessment, Research and Evaluation*, vol. 8, no. 2, pp. 1–5, 2002.

[66] A. Manero-Bastin. (2020). "7 Classical Assumptions of Ordinary Least Squares (OLS) Linear Regression," [Online]. Available: `https://www.datasciencecentral.com/profiles/blogs/7-classical-assumptions-of-ordinary-least-squares-ols-linear`.

[67] D. Cochrane and G. H. Orcutt, "Application of Least Squares Regression to Relationships Containing Auto-Correlated Error Terms," *Journal of the American Statistical Association*, vol. 44, no. 245, pp. 32–61, Mar. 1949.

[68] N. Beck and J. N. Katz, "What to do (and not to do) with Time-Series Cross-Section Data," *The American Political Science Review*, vol. 89, no. 3, pp. 634–647, 1995.

[69] S. A. van de Geer, "Least Squares Estimation," in *Encyclopedia of Statistics in Behavioral Science*, Brian S. Everitt & David C. Howell, Ed., vol. 2, Chichester, UK: John Wiley & Sons, Ltd, 2005, pp. 1041–1045.

[70] C. Zaiontz. (2020). "Robust Standard Errors," [Online]. Available: `http://www.real-statistics.com/multiple-regression/robust-standard-errors/`.

[71] S. Safi and A. White, "The Efficiency Of OLS In The Presence Of Auto-Correlated Disturbances In Regression Models," *Journal of Modern Applied Statistical Methods*, vol. 5, no. 1, pp. 107–117, May 2006.

[72] A. F. Hayes and L. Cai, "Using heteroskedasticity-consistent standard error estimators in OLS regression: An introduction and software implementation," *Behavior Research Methods*, vol. 39, no. 4, pp. 709–722, Nov. 2007.

[73] E. Clarke, *Circuit analysis of A-C power systems*, 1st ed. New York: John Wiley & Sons, Inc., 1943.

[74] F. Calero, "Mutual Impedance in Parallel Lines–Protective Relaying and Fault Location Considerations," in *34th Annual Western Protective Relay Conference*, Spokane, 2007, pp. 1–15.

[75] A. Apostolov, D. Tholomier, S. Sambasivan, and S. Richards, "Protection of Double Circuit Transmission Lines," in *2007 60th Annual Conference for Protective Relay Engineers*, IEEE, Mar. 2007, pp. 85–101.

[76] K. G. H. Mangunkusumo, A. A. Kusuma, and B. S. Munir, "A Case Study of Mutual Impedance Effect in Parallel Transmission Lines Under Maintenance Condition," in *2018 10th International Conference on Information Technology and Electrical Engineering (ICITEE)*, IEEE, Jul. 2018, pp. 192–195.

[77] Merlin Gerin, "Electrical network protection: protecion guide," Schneider Electric, Tech. Rep., 2003, pp. 1–73.

[78] N. Kondrath and M. Kazimierczuk, "Bandwidth of Current Transformers," *IEEE Transactions on Instrumentation and Measurement*, vol. 58, no. 6, pp. 2008–2016, Jun. 2009.

[79] R. Stewart and E. Pfann, "Oversampling and sigma-delta strategies for data conversion," *Electronics & Communication Engineering Journal*, vol. 10, no. 1, pp. 37–47, Feb. 1998.

[80] P. D. Saravanan and V. Jayaprakasan, "Design and Implementation of Efficient CIC Filter Structure for Decimation," *International Journal of Computer Applications*, vol. 65, pp. 1–7, 2013.

[81] The MathWorks. (2020). "FIR Filter Design," [Online]. Available: `https://nl.mathworks.com/help/signal/ug/fir-filter-design.html`.

[82] E. O. Schweitzer and D. Hou, "Filtering for protective relays," in *Communications, Computers and Power in the Modern Environment*, IEEE, 1993, pp. 15–23.

[83] Statistics How To. (2020). "T-Distribution Table," [Online]. Available: `https://www.statisticshowto.com/tables/t-distribution-table/`.

[84] R. Abboud, J. Bell, and B. Smyth, "Considerations and Benefits of Using Five Zones for Distance Protection," in *72nd Annual Georgia Tech Protective Relaying Conference*, 2018.

[85] J. Roberts, A. Guzman, and E. O. Schweitzer, "Z=V/I Does Not Make a Distance Relay," in *20th Annual Western Protective Relay Conference*, 1993, pp. 1–20.

[86] M. Eissa, "Ground Distance Relay Compensation Based on Fault Resistance Calculation," *IEEE Transactions on Power Delivery*, vol. 21, no. 4, pp. 1830–1835, Oct. 2006.

[87] D. Majambere and G. Fujita, "Impact of fault resistance on impedance relay: Adaptive Mho directional type scheme development using LabVIEW," in *IEEE Region 10 Annual International Conference, Proceedings/TENCON*, vol. 2017-Decem, IEEE, Nov. 2017, pp. 3006–3011.

[88] H. Shateri and S. Jamali, "Robustness of distance relay applied for distribution feeders with Mho characteristic against fault resistance," in *TENCON 2008 - 2008 IEEE Region 10 Conference*, IEEE, Nov. 2008, pp. 1–6.

[89] J. Roberts and A. Guzman, "Directional Element Design and Evaluation," in *21st Annual Western Protective Relay Conference*, 1994, pp. 1–21.

[90] K. Zimmerman and D. Costello, "Fundamentals and improvements for directional relays," in *2010 63rd Annual Conference for Protective Relay Engineers*, IEEE, Mar. 2010, pp. 1–12.

[91] E. O. Schweitzer, B. Kasztenny, and M. V. Mynam, "Performance of time-domain line protection elements on real-world faults," in *69th Annual Conference for Protective Relay Engineers, CPRE 2016*, IEEE, Apr. 2017, pp. 1–17.

[92] M. J. Thompson and A. Somani, "A tutorial on calculating source impedance ratios for determining line length," in *2015 68th Annual Conference for Protective Relay Engineers, CPRE 2015*, IEEE, Mar. 2015, pp. 833–841.

[93] B. Kasztenny, A. Guzmán, N. Fischer, M. V. Mynam, and D. Taylor, "Practical Setting Considerations for Protective Relays that Use Incremental Quantities and Traveling Waves," in *43rd Annual Western Protective Relay Conference*, 2016.

[94] A. R. Van C. Warrington, "Graphical Method for Estimating the Performance of Distance Relays During Faults and Power Swings," *Transactions of the American Institute of Electrical Engineers*, vol. 68, no. 1, pp. 608–621, Jul. 1949.

[95] E. Price and T. Einarsson, "The performance of faulted phase selectors used in transmission line distance applications," in *2008 61st Annual Conference for Protective Relay Engineers*, IEEE, Apr. 2008, pp. 484–490.

[96] B. Kasztenny, J. Mazereeuw, and B. Campbell, "Phase Selection for Single-Pole Tripping: Weak Infeed Conditions and Cross-Country Faults," in *27 th Annual Western Protective Relay Conference*, Spokane, 2000, pp. 1–19.

[97] G. Benmouyal and J. Mahseredjian, "A combined directional and faulted phase selector element based on incremental quantities," *IEEE Transactions on Power Delivery*, vol. 16, no. 4, pp. 478–484, 2001.

[98] R. M. Cheney, J. T. Thorne, and G. Hataway, "Distribution single-phase tripping and reclosing: Overcoming obstacles with programmable recloser controls," in *2009 Power Systems Conference*, IEEE, Mar. 2009, pp. 1–10.

[99] E. O. Schweitzer and B. Kasztenny, "Distance protection: Why have we started with a circle, does it matter, and what else is out there?" In *71st Annual Conference for Protective Relay Engineers, CPRE 2018*, vol. 2018-Janua, IEEE, Mar. 2018, pp. 1–19.

[100] G. Benmouyal and J. Roberts, "Superimposed Quantities: Their True Nature and Application in Relays," in *26th Annual Western Protective Relay Conference*, Pullman, WA USA, 1999, pp. 1–18.

[101] International Electrotechnical Commission. (2014). "Functional requirements for distance protection."

[102] Daqing Hou and J. Roberts, "Capacitive voltage transformer: transient overreach concerns and solutions for distance relaying," in *Proceedings of 1996 Canadian Conference on Electrical and Computer Engineering*, vol. 1, IEEE, 1996, pp. 119–125.

[103] D. Fernandes, W. Neves, and J. Vasconcelos, "Coupling capacitor voltage transformer: A model for electromagnetic transient studies," *Electric Power Systems Research*, vol. 77, no. 2, pp. 125–134, Feb. 2007.

[104] D. Costello and K. Zimmerman, "CVT transients revisited — Distance, directional overcurrent, and communications-assisted tripping concerns," in *2012 65th Annual Conference for Protective Relay Engineers*, IEEE, Apr. 2012, pp. 73–84.

[105] M. H. Zare, A. Mirzaei, and H. A. Abyaneh, "Improving capacitive voltage transformer response and its impact on distance relay performance," in *20th Iranian Conference on Electrical Engineering (ICEE2012)*, IEEE, May 2012, pp. 523–528.

[106] B. Kasztenny, D. Sharples, V. Asaro, and M. Pozzuoli, "Distance Relays and Capacitive Voltage Transformers — Balancing Speed and Transient Overreach," in *53rd Annual Conference for Protective Relay Engineers*, 2018.

[107] E. Nashawati, N. Fischer, B. Le, and D. Taylor, "Impacts of Shunt Reactors on Transmission Line Protection," in *38th Annual Western Protective Relay Conference*, 2013, pp. 1–16.

[108] S. Samineni, C. Labuschagne, and J. Pope, "Principles of shunt capacitor bank application and protection," in *2010 63rd Annual Conference for Protective Relay Engineers*, IEEE, Mar. 2010, pp. 1–14.

[109] X. Qi, M. Wen, X. Yin, Z. Zhang, J. Tang, and F. Cai, "A novel fast distance relay for series compensated transmission lines," *International Journal of Electrical Power & Energy Systems*, vol. 64, pp. 1–8, Jan. 2015.

List of publications

Conference papers

[1] N. Hoxha and J.-C. Maun, "Ultra-Fast Distance Protection Algorithm in Time-Domain Based on a Gamma Model of Line," in *Mediterranean Conference on Power Generation, Transmission, Distribution and Energy Conversion (MedPower 2018)*, Dubrovnik: Institution of Engineering and Technology, 2018, pp. 1–5.

[2] N. Hoxha and J.-C. Maun, "Ultra-fast Distance Protection Algorithm Based on a Gamma Transmission Line Model : Performances with Complex Power Networks," in *Protection, Automation & Control World Conference (PacWorld 2018)*, Sofia, 2018, pp. 1–14.